

Multivariate relative rate measurements of reactions  
between volatile organic compounds (VOCs)  
and atmospheric radicals

Jacob T. Shaw

Doctor of Philosophy

University of York

Chemistry

July 2018



# Abstract

Knowledge of the reactions between VOCs and atmospheric radicals and oxidants is fundamental to understanding atmospheric chemistry and the formation of air pollution in urban environments. This work describes the development of a new experimental technique for the simultaneous measurement of gas-phase rate coefficients for reactions between multiple VOCs and different atmospheric radicals. The technique is based on the traditional relative rate approach and succeeds in markedly increasing the rate of throughput of target reactions; an improvement necessary when considering the vast number of organic compounds observed in the atmosphere for which experimental oxidation data are not available. New rate coefficients are derived using a suite of the available kinetic literature as reference reactions to calibrate the results over a range of reactivity, thereby reducing the reliance on any single rate coefficient value.

This new multivariate method was applied to mixtures containing multiple VOCs with a range in functionalities and under different experimental conditions. Two different atmospherically relevant radicals were tested (OH and Cl) and the technique was adapted to allow for temperature controlled measurements.

Rate coefficients for the reactions of eight VOCs (1,2-, 1,3- and 1,4-diethylbenzene, *n*-pentylbenzene, 2-methylheptane, 2-methylnonane, ethylcyclohexane and 2,3-dimethylpent-1-ene) with OH at room temperature were derived for the first time. Rate coefficients for the reactions of 44 other VOCs with OH were also assessed concurrently with the derivation of these eight new results. A rate coefficient for the reaction between 2-methylheptane and Cl was measured for the first time, alongside the measurement of rate coefficients for the reactions of seven other VOCs with Cl.



# Table of contents

Abstract	iii
Table of contents	v
List of tables	xi
List of figures	xv
Acknowledgements	xxxii
Author's declaration	xxxv
<b>Chapter 1: Introduction</b>	<b>17</b>
1.1 Preface	35
1.2 Atmospheric composition	36
1.2.1 The troposphere	36
1.2.2 Organic compounds	36
1.2.2.1 Alkanes	38
1.2.2.2 Alkenes	39
1.2.2.3 Aromatics	43
1.2.3 Atmospheric oxidants	47
1.2.4 The HO <sub>x</sub> /NO <sub>x</sub> cycle	49
1.3 VOC oxidation chemistry	50
1.3.1 Chemical kinetics	50
1.3.2 Reactions with alkanes	51
1.3.2.1 Mechanism and products of alkane + OH reactions	53
1.3.2.2 The temperature dependence of alkane + OH reactions	55
1.3.3 Reactions with alkenes	56

1.3.3.1 Mechanism and products of alkene + OH reactions	58
1.3.4 Reactions with aromatic compounds	59
1.3.4.1 Mechanism and products of aromatic VOC + OH reactions	60
1.3.4.2 The temperature dependence of aromatic VOC + OH reactions	62
1.3.5 OH reactivity	62
1.4 Measuring gas-phase rate coefficients	64
1.4.1 Absolute methods	64
1.4.1.1 Discharge and stopped flow	64
1.4.1.2 Flash photolysis	65
1.4.1.3 Detection techniques	66
1.4.2 The relative rate method	67
1.4.2.1 OH relative rate methods	68
References	70
<b>Chapter 2: The multivariate relative rate technique overview</b>	93
2.1 The basic technique	94
2.1.1 Reactor characterisation	95
2.1.1.1 Reactor flow conditions	98
2.1.2 Lamp and lamp housing	99
2.1.3 Mass flow controllers	101
2.1.4 Gas sampling	101
2.1.5 Gas chromatography	101
2.1.5.1 The equilibrium theory of separation	102
2.1.5.2 The GC system	104
2.1.6 Mass spectrometry	104
2.1.6.1 Time-of-flight (ToF) mass spectrometry	105
2.1.6.3 The MS system	106
2.1.7 Synthetic gas mixtures	106
2.1.8 Experiment design	107

2.1.8.1 Internal standards	110
2.1.9 Literature <i>k</i> values	112
2.1.9.1 A note on errors	114
2.1.10 Data analysis and error propagation	115
2.2 Modifications to the basic technique	117
2.2.1 The HO <sub>2</sub> problem and the NO solution	117
2.2.1.1 Equipment set up	120
2.2.2 Kinetic studies of VOC + Cl reactions	121
2.2.2.1 Generation of Cl	122
2.2.2.2 Literature Cl rate coefficients	124
2.2.3 Temperature-dependent measurements	125
2.2.3.1 Temperature measurements	126
References	128
<b>Chapter 3: Kinetic studies of alkene + OH reactions</b>	<b>131</b>
3.1 Results and discussion	132
3.1.1 Monoterpene mixture 1	132
3.1.1.1 Typical chromatogram data	134
3.1.1.2 Typical peak area data	135
3.1.1.3 Relative rate plots	136
3.1.1.4 Calculation of rate coefficients	141
3.1.1.5 Comparisons to the literature	141
3.1.1.6 Comparisons to structure-activity relationships (SARs)	143
3.1.1.7 Control experiments	146
3.1.1.8 Products of the VOC + OH reactions	147
3.1.2 Monoterpene mixture 2	150
3.1.2.1 Relative rate plots	151
3.1.2.2 Calculation of rate coefficients	153
3.1.2.3 Comparisons to structure-activity relationships	156

3.1.3 Alkenes mixture	158
3.1.3.1 Typical chromatogram data	159
3.1.3.2 Relative rate plots	161
3.1.3.3 Calculation of rate coefficients	161
3.1.3.4 Comparisons to the literature	163
3.1.3.4 Determination of a new rate coefficient for the 2,3-dimethylpent-1-ene + OH reaction	166
3.1.3.5 Products of the VOC + OH reactions	167
3.2 Numerical simulations	168
3.2.1 Estimating OH concentration	168
3.2.1.1 Simulating OH concentration	169
3.2.1.2 Comparisons to similar systems	171
3.2.2 Understanding the observed curved relationship	172
3.2.2.1 Mathematical proof	173
3.2.2.2 Kinetic modelling	176
3.2.3 Simulating product formation	179
3.3.3.2 Isoprene	180
3.2.3.1 Xylenes	182
3.3.3.3 Monoterpenes	184
3.3.3.4 Summary	186
Conclusions	187
References	188
<b>Chapter 4: Kinetic studies of aromatic VOC + OH reactions</b>	195
4.1 Results and discussion	196
4.1.1 Small aromatic VOCs mixture	196
4.1.1.1 Typical chromatogram data	197
4.1.1.2 Relative rate plots	199
4.1.1.3 Calculation of rate coefficients	203

4.1.1.4	Determination of a new rate coefficient for the <i>n</i> -pentylbenzene + OH reaction	205
4.1.1.5	Comparison to SARs	206
4.1.2	Large aromatic VOCs mixture	209
4.1.2.1	Typical chromatogram data	211
4.1.2.2	Relative rate plots	212
4.1.2.3	Calculation of rate coefficients	215
4.1.2.4	Calculation of new rate coefficients	216
4.1.2.5	Comparison to SARs	217
4.2	Numerical simulations	219
4.2.1	Understanding the fate of the OH-aromatic adduct	219
4.2.1.1	Simulating the decomposition of the OH-aromatic adducts	221
4.2.1.2	Summary	227
4.2.2	Simulating the impact of NO	228
4.2.2.1	Impact on [pOH]	230
4.2.2.2	Impact on [HO <sub>2</sub> ]	231
4.2.2.3	Impact on [sOH]	232
4.2.2.4	Impact on [NO] and [NO <sub>2</sub> ]	234
4.2.2.5	Impact on pOH sinks	235
4.2.2.6	Impact on sOH sinks	236
4.2.2.7	Impact on VOCs	237
	Conclusions	238
	References	239
	<b>Chapter 5: Kinetic studies of alkane oxidation reactions</b>	<b>243</b>
5.1	Temperature-dependent alkane + OH reactions	244
5.1.1	Alkane mixture	244
5.1.2	Room temperature measurements	245
5.1.3	Elevated temperature measurements	248
5.1.4	Arrhenius expressions	250

5.1.4.1 OH + 2,2,3-trimethylbutane	250
5.1.4.2 OH + <i>n</i> -octane, OH + <i>n</i> -nonane and OH + <i>n</i> -decane	252
5.1.4.3 OH + cycloheptane and OH + cyclooctane	254
5.1.4.4 OH + 2-methylpentane and OH + 3-methylpentane	254
5.1.4.5 OH + <i>n</i> -undecane	258
5.1.4.6 OH + 2-methylheptane	258
5.1.4.7 OH + 2-methylnonane	260
5.1.4.8 OH + ethylcyclohexane	260
5.1.4.9 Summary	262
5.2 Alkanes + Cl reaction rate coefficient measurements	264
5.2.1 Control experiments	266
5.2.1.1 Cl <sub>2</sub> chromatogram	267
5.2.1.2 Potential losses of VOCs due to Cl <sub>2</sub>	268
5.2.2 Cl mixture 1	272
5.2.2.1 Typical chromatogram data	273
5.2.2.2 Relative rate plots	274
5.2.2.3 Calculation of rate coefficients	277
5.2.2.4 Comparisons to the literature	277
5.2.3 Cl mixture 2	278
5.2.3.1 Relative rate plots	279
5.2.3.2 Calculation of rate coefficients	281
5.2.3.4 Comparisons to the literature	281
5.2.3.3 Determination of a new rate coefficient for the 2-methylheptane + Cl reaction	282
5.2.4 Numerical simulations	284
5.2.4.1 Estimated Cl concentration and Cl <sub>2</sub> to Cl conversion	284
Conclusions	286
References	287
<b>Concluding remarks</b>	<b>291</b>

# List of tables

**Table 1.1** POCP values for various aromatic VOCs, as calculated using the MCM v3 (Jenkin et al., 2003). The precision in the POCP is expected to be  $\pm 2$  POCP units. 46

**Table 1.2** Estimated lifetimes of various alkanes due to reaction with OH (at 298 K), using  $k$  values provided in Atkinson (2003) and a 24-hour average [OH] of  $1 \times 10^6$  molecule  $\text{cm}^{-3}$ . The lifetimes of various alkanes due to reaction with  $\text{NO}_3$  (at 298 K) are also provided, using  $k$  values from Atkinson and Arey (2003) and an approximate night-time [ $\text{NO}_3$ ] of 90 pptv.  $k$  values for reaction with Cl were taken from various sources which are noted in the Table footer. The concentration of Cl used was  $10^3$  molecules  $\text{cm}^{-3}$ . 52

**Table 1.3** Estimated lifetimes of various alkenes due to reaction with OH (at 298 K), using  $k$  values provided in Atkinson and Arey (2003) and a 24-hour average [OH] of  $1 \times 10^6$  molecule  $\text{cm}^{-3}$ . The lifetimes of various alkenes due to reaction with  $\text{O}_3$  and  $\text{NO}_3$  (at 298 K) are also provided.  $k$  values were taken from Atkinson and Arey (2003) and the concentrations of  $\text{O}_3$  and  $\text{NO}_3$  used were 30 ppbv and 90 pptv respectively.  $k$  values for reaction with Cl were taken from various sources which are noted in the Table footer. The concentration of Cl used was  $10^3$  molecules  $\text{cm}^{-3}$ . 57

**Table 1.4** Estimated lifetimes of various aromatic VOCs due to reaction with OH (at 298 K), using  $k$  values provided in Atkinson and Arey (2003) and a 24-hour average [OH] of  $1 \times 10^6$  molecule  $\text{cm}^{-3}$ . The lifetimes of various aromatic VOCs due to reaction with  $\text{NO}_3$  (at 298 K) are also provided, using  $k$  values from Atkinson and Arey (2003) and an approximate night-time [ $\text{NO}_3$ ] of 90 pptv. Some values for  $k_{\text{NO}_3}$  are not provided in Atkinson and Arey (2003) and therefore corresponding approximate  $\tau_{\text{NO}_3}$  values are not included here. 60

**Table 3.1** List of VOCs, in descending order of evaluated literature  $k$  value, in monoterpenes mixture 1 along with their evaluated literature  $k$  value, reference and number of measurements found in the literature at the time of writing. 133

<b>Table 3.2</b> List of VOCs, in descending order of evaluated literature <i>k</i> value, in monoterpenes mixture 1 along with their range of depletions due to reaction with OH, measured <i>k</i> value and evaluated literature <i>k</i> value.	141
<b>Table 3.3</b> List of VOCs, in descending order of evaluated literature <i>k</i> value, in monoterpenes mixture 1 along with their SAR derived <i>k</i> values, experimentally measured <i>k</i> value and evaluated literature <i>k</i> value.	145
<b>Table 3.4</b> List of VOCs, in descending order of evaluated literature <i>k</i> value, in monoterpenes mixture 2 along with their evaluated literature <i>k</i> value, reference and number of measurements found in the literature at the time of writing.	150
<b>Table 3.5</b> List of VOCs, in descending order of evaluated literature <i>k</i> value, in monoterpenes mixture 2 along with their range of depletions due to reaction with OH, measured <i>k</i> value for both linear regression and three-parameter exponential analysis, and evaluated literature <i>k</i> value.	154
<b>Table 3.6</b> List of VOCs, in descending order of evaluated literature <i>k</i> value, in monoterpenes mixture 2 along with their SAR derived <i>k</i> values, experimentally measured <i>k</i> value and evaluated literature <i>k</i> value.	157
<b>Table 3.7</b> List of VOCs, in descending order of evaluated literature <i>k</i> value, in the alkenes mixture along with their evaluated literature <i>k</i> value, reference and number of measurements found in the literature at the time of writing.	158
<b>Table 3.8</b> List of VOCs, in descending order of evaluated literature <i>k</i> value, in the alkenes mixture along with their range of depletions due to reaction with OH, measured <i>k</i> value and evaluated literature <i>k</i> value.	161
<b>Table 3.9</b> List of reactions in kinetic simulations for modelling the OH concentration for monoterpenes mixture 1.	170
<b>Table 3.10</b> List of reactions in kinetic simulations for modelling the OH concentration for the alkenes mixture.	171
<b>Table 3.11</b> Summary of the conditions resulting in observed curvature in the depletion factor vs rate coefficient relationship during multivariate relative rate experiments.	172

<b>Table 4.1</b> List of VOCs, in descending order of evaluated literature $k$ value, in the small aromatic VOCs mixture along with their evaluated literature $k$ value, reference and the number of measurements found in the literature at the time of writing.	197
<b>Table 4.2</b> List of VOCs, in descending order of evaluated literature $k$ value, in the small aromatics mixture along with their measured $k$ value at each concentration of NO, average (weighted to the errors) measured $k$ value and evaluated literature $k$ value.	204
<b>Table 4.3</b> List of VOCs, in descending order of evaluated literature $k$ value, in the small aromatics mixture along with their SAR derived $k$ values, average experimentally measured $k$ value and evaluated literature $k$ value.	206
<b>Table 4.4</b> List of VOCs, in descending order of evaluated literature $k$ value, in the large aromatic mixture, along with their evaluated literature rate coefficient, reference and the number of measurements found in the literature at the time of writing.	210
<b>Table 4.5</b> List of VOCs, in descending order of evaluated literature $k$ value, in the large aromatics mixture along with their range of depletion due to reaction with OH, measured $k$ value and evaluated literature $k$ value.	215
<b>Table 4.6</b> Recommended $k$ values for the reactions between OH and the diethylbenzene stereoisomers, given the uncertainty in their measured values.	216
<b>Table 4.7</b> List of VOCs, in descending order of evaluated literature $k$ value, in the large aromatics mixture along with their SAR derived $k$ values, average experimentally measured $k$ value and evaluated literature $k$ value.	217
<b>Table 4.8</b> Different simulation scenarios.	221
<b>Table 4.9</b> List of HO <sub>x</sub> /NO <sub>x</sub> reactions included in the numerical simulation testing the impact of NO on the oxidation of aromatic VOCs.	228
<b>Table 4.10</b> List of the nine different [VOC] and [NO] scenarios simulated.	229
<b>Table 5.1</b> List of VOCs, in descending order of evaluated literature $k$ (298 K) value, in the alkane mixture along with their evaluated literature $k$ (298 K) value, recommended Arrhenius expression (where available), reference and the number of experimental studies found in the literature at the time of writing.	246

<b>Table 5.2</b> List of VOCs, in descending order of evaluated literature $k$ (298 K) value, in the alkanes mixture along with their measured $k$ (297 K) value and evaluated literature $k$ (298 K) value.	248
<b>Table 5.3</b> List of temperatures at which relative rate experiments were conducted on the alkanes mixture. The estimated $OH_{exp}$ , as derived from the weighted linear regressions for the relative rate plots, are provided, along with the $R^2$ value and the number of reference compounds used at each temperature.	249
<b>Table 5.4</b> Summary of Arrhenius parameters derived from this work alongside those recommended in Atkinson (2003).	262
<b>Table 5.5</b> List of compounds identified in the TICs obtained with and without $Cl_2$ in the presence of the large aromatics mixture (see Figure 5.16). Compounds which are underlined were present in the large aromatics mixture (see Chapter 4 Section 4.1.2).	271
<b>Table 5.6</b> List of VOCs, in descending order of evaluated literature $k$ value, in Cl mixture 1 along with their literature $k$ value used as a reference and the total number of measurements found in the literature at the time of writing.	272
<b>Table 5.7</b> List of VOCs, in descending order of literature $k$ value, in Cl mixture 1 along with their range of depletion due to reaction with Cl, measured $k$ value and literature $k$ value used as a reference.	277
<b>Table 5.8</b> List of VOCs, in descending order of literature $k$ value, in Cl mixture 2 along with their literature $k$ value used as a reference and the total number of measurements found in the literature at the time of writing.	278
<b>Table 5.9</b> List of VOCs, in descending order of literature $k$ value, in Cl mixture 2 along with their range of depletion due to reaction with Cl, measured $k$ value and literature $k$ value used as a reference.	281
<b>Table 6.1</b> Summary of all measured rate coefficients for VOC + OH reactions from all mixtures.	295

# List of figures

- Figure 1.1** The chemical structures of some conjugated alkenes including isoprene and the monoterpenes;  $\beta$ -ocimene, myrcene,  $\alpha$ -phellandrene,  $\beta$ -phellandrene and  $\alpha$ -terpinene. 40
- Figure 1.2** The chemical structures of some non-conjugated monocyclic alkenes including the monoterpenes;  $\gamma$ -terpinene, limonene and terpinolene 40
- Figure 1.3** The chemical structures of some non-conjugated bicyclic alkenes including the monoterpenes;  $\beta$ -pinene,  $\alpha$ -pinene, 3-carene and camphene. 41
- Figure 1.4** The chemical structures of some mono-substituted aromatic VOCs, including; toluene, ethylbenzene, *n*-propylbenzene, *i*-propylbenzene, *n*-butylbenzene, *t*-butylbenzene and *n*-pentylbenzene. 43
- Figure 1.5** The chemical structures of some di-substituted aromatic VOCs, including; *o*- and *m*-xylene, 2-, 3- and 4-ethyltoluene and 1,2-, 1,3- and 1,4-diethylbenzene. 44
- Figure 1.6** The chemical structures of some tri- and tetra-substituted aromatic VOCs, including; 1,2,3-, 1,2,4- and 1,3,5-trimethylbenzene and 1,2,3,5- and 1,2,4,5-tetramethylbenzene. 45
- Figure 1.7** Schematic showing the HO<sub>x</sub>/NO<sub>x</sub> cycle and some of the species involved in the chemical production and destruction of ozone in the troposphere. 49
- Figure 1.8** Schematic showing the anticipated reaction pathways resulting from the initial reaction between an alkane (denoted by RH) and OH, as initiated by H-atom abstraction. Adapted from Atkinson et al. (2008). 54
- Figure 1.9** Schematic showing the anticipated reaction pathways resulting from the initial reaction between an alkene (denoted by R<sub>2</sub>C=CR<sub>2</sub>) and OH, as initiated by OH addition to the carbon-carbon double bond. Adapted from Atkinson and Arey (2003). 58

**Figure 1.10** Schematic showing the anticipated reaction pathways resulting from the initial reaction between an aromatic VOC and OH, as initiated by OH addition to the aromatic structure.

61

**Figure 2.1** Brief flow schematic of experiment concept. All parts of the schematic will be outlined in more detail in the following section.

98

**Figure 2.2** Schematic of the flow reactor used for mixing of gas-phase reactants. All measurements are shown in mm. Humidified N<sub>2</sub> enters the reactor at the far right of the schematic via 1/4" tubing. The VOCs are injected into the reactor perpendicular to the gas flow via four radial holes in the central sliding 1/8" injector. The position of this injector was optimised to provide maximum exposure of VOCs to OH radicals with minimum exposure to the VUV light (Cryer, 2016). The typical residence time of VOCs inside the reactor after injection under normal flow conditions was approximately 4 s, with the oxidation chemistry expected to occur in under 0.5 s.

97

Figure 2.3 Typical relative intensities of the emission lines from the Hg/Ar Pen-Ray lamp source (adapted from [http://pas.ce.wsu.edu/CE415/PenRay\\_lamp\\_spectra.pdf](http://pas.ce.wsu.edu/CE415/PenRay_lamp_spectra.pdf)).

100

**Figure 2.4** Diffuse reflectance spectroscopy (DRS) recorded spectrum of the emission output from the Hg/Ar lamp between 190 and 650 nm. The spectrum is recorded as discrete bands, rather than lines, which match relatively closely to the typical intensity spectrum in Figure 2.2. The band at 184.5 nm was not observed as this was not recorded under vacuum.

100

**Figure 2.5** Schematic of the OH reactor configuration used. Key to abbreviations: CIA8 = air server and canister interface accessory; GC = gas chromatograph; MFC = mass flow controller; TOF-MS = time-of-flight mass spectrometer; TDU = thermal desorption unit. The flow rate through MFC 1 was stepped from 200 sccm through to 1000 sccm in 200 sccm intervals. The combined flow rate through MFC 1 and MFC 2 was kept constant at 1000 sccm. The flow rate through MFC 3, and hence through the H<sub>2</sub>O bubbler, was set to 2000 sccm resulting in a total flow through the reactor of 3000 sccm. See Figure 2.1 for a more comprehensive schematic of the reactor design.

108

**Figure 2.6** The process undertaken to find literature reference *k* values for VOC + OH reactions.

113

**Figure 2.7** The estimated OH reactivity towards HO<sub>2</sub> and VOCs for four different VOC mixtures measured as part of this work. Values are provided in units of s<sup>-1</sup>. The total OH reactivity for each of the four mixtures was approximately 140, 72, 36 and 32 s<sup>-1</sup>, for the monoterpenes, aromatics 2, aromatics 1 and alkanes mixtures respectively. All values were calculated using the evaluated reference literature *k* values for the VOCs (please refer to the later chapters). 119

**Figure 2.8** Schematic showing the equipment set up for experiments on aromatic VOCs. Key to abbreviations: CIA8 = air server and canister interface accessory, GC = gas chromatograph, MFC = mass flow controller, TDU = thermal desorption unit, TOF-MS = time-of-flight mass-spectrometer. See Figure 2.1 for a more comprehensive schematic of the reactor design. 120

**Figure 2.9** Experiment set up for the measurement of relative rate coefficients between VOCs and Cl radicals. Key to abbreviations: CIA8 = air server and canister interface accessory, GC = gas chromatograph, MFC = mass flow controller, TDU = thermal desorption unit, TOF-MS = time-of-flight mass-spectrometer. See Figure 2.1 for a more comprehensive schematic of the reactor design. 121

**Figure 2.10** Diffuse reflectance spectroscopy (DRS) recorded spectra of the emission output from the phosphor-coated Hg lamp (red) and the Hg/Ar lamp (black) between 190 and 650 nm. The Hg-Ar emission bands centred around 254 nm and 300 nm were not present in the phosphor-coated spectrum, and were instead replaced by a large band centred around approximately 330 nm. 123

**Figure 2.11** The flow reactor, with heating block, used for mixing of gas-phase reactants and measurement of temperature-dependent rate coefficients. All measurements are shown in mm. Humidified N<sub>2</sub> entered the reactor at the far right of the schematic via 1/4 " tubing. The VOCs were injected into the reactor perpendicular to the gas flow via the central sliding 1/8 " injector. The position of this injector was optimised to provide maximum exposure of VOCs to OH radicals with minimum exposure to the VUV light (Cryer, 2016). The heating block was controlled, and the temperature of the reactor maintained, by a PID controller. 125

**Figure 2.12** The flow reactor, with heating block, used for mixing of gas-phase reactants and measurement of temperature-dependent rate coefficients. All measurements are shown in mm. The heating block was controlled, and the temperature of the reactor maintained, by a PID controller. The positions of two thermocouples, T1 and T2, used for the control of temperature and measurement of gas temperature are also shown. 126

**Figure 2.13** Temperature of the reactor gas, at different PID settings and different positions within the reactor (relative to the point of VOC injection) as measured by the Type K mineral insulated thermocouple. 127

**Figure 3.1** Typical total ion chromatogram (TIC) sections obtained for monoterpenes mixture 1 with the lamp turned off (blue) and the lamp turned on (black). Greater differences in peak areas were observed for VOCs which have a larger rate coefficient value for their reaction with OH. Evaluated literature rate coefficients (in units of  $10^{-12} \text{ cm}^3 \text{ molecule}^{-1} \text{ s}^{-1}$ ) for these VOC + OH reactions were: *o*-xylene, 13 ( $\pm 3$ ); *m*-xylene, 23 ( $\pm 4$ );  $\alpha$ -pinene, 53 ( $^{+22}_{-15}$ );  $\beta$ -pinene, 79 ( $\pm 20$ ); camphene, 53 ( $\pm 11$ ); myrcene, 209 ( $\pm 42$ ) (see Table 3.1). 134

**Figure 3.2** Peak area data for isoprene in monoterpenes mixture 1. The five different estimated OH reactivities (of 50, 110, 180, 240 and  $290 \text{ s}^{-1}$ ) are shown in different colours. Only eight samples (four 'lamp on', four 'lamp off') were taken at an OH reactivity of  $50 \text{ s}^{-1}$  whilst 12 samples (six 'lamp on', six 'lamp off') were taken at all other OH reactivities. 135

**Figure 3.3** Relative rate plot for monoterpenes mixture 1 with an OH reactivity of  $240 \text{ s}^{-1}$ , at 295 K. Compounds with a reference rate coefficient for reaction with OH were plotted using evaluated literature values as references. Error bars on the y-axis, equal to one standard error, were calculated by combining the standard error in peak areas for six lamp-off and six lamp-on samples. Error bars on the x-axis were typically large (approximately  $\pm 20\text{-}30\%$ ) and accounted for deviations from the trend for all VOCs. A weighted (to the uncertainty in the y-values) linear fit was used to generate the slope, with a value of  $OH_{exp} = 1.06 (\pm 0.07) \times 10^9 \text{ molecules cm}^{-3} \text{ s}$  and  $R^2 = 0.965$ . The VOCs can be identified as follows; 1, *o*-xylene; 2, *m*-xylene; 3,  $\alpha$ -pinene; 4,  $\beta$ -pinene; 5, 3-carene; 6, isoprene; 7, limonene; 8,  $\gamma$ -terpinene; 9, myrcene; 10,  $\beta$ -ocimene. 137

**Figure 3.4** Relative rate plots for monoterpenes mixture 1 with OH reactivities of 110, 180, 240 and  $290 \text{ s}^{-1}$ . The  $R^2$  values for the weighted linear fits were 0.964, 0.941, 0.965 and 0.949 respectively. The values of  $OH_{exp}$  were  $1.44 (\pm 0.09)$ ,  $1.25 (\pm 0.10)$ ,  $1.06 (\pm 0.07)$  and  $1.27 (\pm 0.10) \times 10^9 \text{ molecules cm}^{-3} \text{ s}$  respectively. Error bars on the x-axis are not shown for reasons of clarity. 138

**Figure 3.5** Relative rate plot for monoterpenes mixture 1 with an OH reactivity of  $50 \text{ s}^{-1}$ , at 295 K. Compounds with a reference rate coefficient for reaction with OH were plotted using literature values. Error bars on the y-axis, equal to one standard error, were calculated by combining the standard error in peak areas for four lamp-off and four lamp-on samples. Error bars on the x-axis

are not displayed for reasons of clarity but were typically large (approximately  $\pm 20\text{-}30\%$ ) and accounted for deviations from the line. The black dashed line shows the relationship observed when the OH reactivity of the mixture was low, modelled by a three-parameter exponential curve (see Section 3.2.2). The VOCs can be identified as follows; 1, *o*-xylene; 2, *m*-xylene; 3,  $\alpha$ -pinene; 4,  $\beta$ -pinene; 5, 3-carene; 6, isoprene; 7, limonene; 8,  $\gamma$ -terpinene; 9, myrcene; 10,  $\beta$ -ocimene. 140

**Figure 3.6** Comparison of two SARs for the estimation of rate coefficients for the reactions between alkenes and OH, alongside the experimental results derived in this work (green) and the recommended literature values (black). The transparent bars are equivalent to the anticipated errors on the SAR derived *k* values; 15% for Peeters et al. (2007) and 40% for Jenkin et al. (2018). 145

**Figure 3.7** Relative rate plot for monoterpenes mixture 1 with no OH production, at 295 K. Compounds with a reference rate coefficient for reaction with OH were plotted using literature values. Error bars on the y-axis, equal to one standard error, were calculated by combining the standard error in peak areas for six lamp-off and six lamp-on samples. Error bars on the x-axis are not displayed for reasons of clarity but were typically large. The VOCs can be identified as follows; 1, *o*-xylene; 2, *m*-xylene; 3,  $\alpha$ -pinene; 4,  $\beta$ -pinene; 5, 3-carene; 6, isoprene; 7, limonene; 8,  $\gamma$ -terpinene; 9, myrcene; 10,  $\beta$ -ocimene. 146

**Figure 3.8** Typical total ion chromatograms (TICs) sections obtained for monoterpenes mixture 1 with the lamp turned off (blue) and the lamp turned on (black). Two peaks were identified here (methacrolein and methyl vinyl ketone) which were not present when the lamp was off but were when the lamp is on, leading to the conclusion that they are products of VOC + OH reactions. 147

**Figure 3.9** Relative rate plot for monoterpenes mixture 2 with an OH reactivity of  $265\text{ s}^{-1}$ , at 295 K. Compounds with a reference rate coefficient for reaction with OH were plotted using evaluated literature values as references. Error bars on the y-axis, equal to one standard error, were calculated by combining the standard error in peak areas for six lamp-off and six lamp-on samples. Error bars on the x-axis were typically large (approximately  $\pm 20\text{-}30\%$ ). A weighted (to the uncertainty in the y-values) linear fit was used to generate the slope, with a value of  $OH_{exp} = 0.6 (\pm 0.06) \times 10^9\text{ molecules cm}^{-3}\text{ s}$  and  $R^2 = 0.893$ . A three-parameter exponential relationship (Eq. 3.1) was used to generate the curve, with  $R^2 = 0.904$ . The VOCs can be identified as follows; 1, *m*-xylene; 2, 1,2,4-trimethylbenzene; 3,  $\alpha$ -pinene; 4, camphene; 5,  $\beta$ -pinene; 6, isoprene; 7, limonene; 8,  $\gamma$ -terpinene; 9,  $\beta$ -phellandrene; 10, terpinolene; 11,  $\alpha$ -phellandrene; 12,  $\alpha$ -terpinene. 152

**Figure 3.10** Relative rate plots for monoterpenes mixture 2 with OH reactivities of 73, 170, 265, 360 and 434 s<sup>-1</sup>. Two relationships between depletion and literature *k* value were modelled; a weighted linear regression (black) and a three-parameter exponential relationship (red; Eq. 3.1). The R<sup>2</sup> values for the weighted linear fits were 0.759, 0.858, 0.893, 0.777 and 0.839 respectively. The values of *OH<sub>exp</sub>* were 0.70 (± 0.12), 0.6 (± 0.07), 0.6 (± 0.06), 0.3 (± 0.05) and 0.4 (± 0.05) × 10<sup>9</sup> molecules cm<sup>-3</sup> s respectively. The R<sup>2</sup> values for the three-parameter exponential relationships were 0.933, 0.934, 0.904, 0.779 and 0.926 respectively. Error bars on the x-axis are not shown for reasons of clarity. 153

**Figure 3.11** Comparison of two SARs for the estimation of rate coefficients for the reactions between alkenes and OH, alongside the experimental results derived in this work (green) and the recommended literature values (black). The transparent bars are equivalent to the anticipated errors on the SAR derived *k* values; 15% for Peeters et al. (2007) and 40% for Jenkin et al. (2018). 157

**Figure 3.12** Typical total ion chromatogram (TIC) sections obtained for the alkenes mixture with the lamp turned off (blue) and the lamp turned on (black). Greater differences in peak areas were observed for VOCs which have a larger rate coefficient value for their reaction with OH. Evaluated literature rate coefficients (in units of 10<sup>-12</sup> cm<sup>3</sup> molecule<sup>-1</sup> s<sup>-1</sup>) for the VOC + OH reactions are: 1-hexene, 37 (± 11); 2,3-dimethylpentene, N/A; cyclohexene, 68 (± 17); 1-heptene, 40 (± 12) (see Table 3.7). 159

**Figure 3.13** TIC section and extracted ion chromatogram sections (EICs) at *m/z* 56 (red) and *m/z* 67 (blue) demonstrating the versatility of using ToF-MS as a detector in this method. 160

**Figure 3.14** Relative rate plot for the alkenes mixture with an OH reactivity of 30 s<sup>-1</sup>, at 295 K. Compounds with a reference rate coefficient for reaction with OH were plotted using evaluated reference values. Error bars on the y-axis, equal to one standard error, were calculated by combining the standard error in peak areas for six lamp-off samples and six lamp-on samples. Error bars on the x-axis were typically large (approximately ± 20-30%) and accounted for deviations from the trend for all VOCs. A weighted (to the uncertainty in the y-axis) linear fit was used to generate the slope with a value of *OH<sub>exp</sub>* = 1.8 (± 0.1) × 10<sup>9</sup> molecules cm<sup>-3</sup> s and R<sup>2</sup> of 0.95. Data for 2,3-dimethylpent-1-ene (A), which had no literature *k* value, was not used in the calculation of the fit. The VOCs can be identified as follows: 1, 1-hexene; 2, 1-heptene; 3, 1-octene; 4, 1-nonene; 5, α-pinene; 6, cyclopentene; 7, cyclohexene; 8, cycloheptene; 9, β-pinene; 10, isoprene. 1624

**Figure 3.15** Experimentally derived (data points) and predicted SAR derived (lines)  $k$  values for the homologous series of cycloalkene + OH reactions. Data from this study are shown in green and were in agreement with both previous experimentally measured values and with theoretical predictions. Errors are only shown for this work and not for the other experimental literature values. 164

**Figure 3.16** Experimentally derived (data points) and predicted SAR derived (lines)  $k$  values for the homologous series of 1-alkene + OH reactions. Data from this study are shown in green and were in good agreement with both previous experimentally measured values and with theoretical predictions. 165

**Figure 3.17** Simulated relative rate plot for monoterpenes mixture 1 with an OH reactivity of  $50 \text{ s}^{-1}$ . Three different theoretical sections of the reactor were simulated separately, with each section containing 1/3 [VOC] and exposed to different [OH] of  $1.0 \times 10^9$ ,  $5.0 \times 10^9$  and  $2.5 \times 10^{11}$  molecules  $\text{cm}^{-3}$ . 177

**Figure 3.18** Simulated relative rate plot for monoterpenes mixture 1 with an OH reactivity of  $50 \text{ s}^{-1}$ . The final concentrations of the VOCs in each of the simulated sections (Figure 3.17) were summed prior to the calculation of the depletion factor. The resulting relationship was clearly curved in a similar manner to that observed during experiment (Figure 3.5). The slope was plotted up to a depletion factor value of 0.4, to demonstrate that a linear relationship could be assumed up to that value for simplification. 177

**Figure 3.19** Simulated relative rate plot for monoterpenes mixture 1 with an OH reactivity of  $290 \text{ s}^{-1}$ . The final concentrations of the VOCs in each of the simulated sections were summed prior to the calculation of the depletion factor. The resulting relationship wasn't strictly linear but can be assumed to be. 178

**Figure 3.20** Time series showing the simulated changes in concentrations of OH,  $\text{HO}_2$ , isoprene and the isoprene oxidation products, total ISOPOO, total ISOPOOH and total IEPOX. 181

**Figure 3.21** Simulated distribution of products resulting from the OH-initiated oxidation of isoprene. Please refer to the MCM (Jenkin et al., 1997; Saunders et al., 2003; <http://mcm.leeds.ac.uk/MCM>; accessed 14/02/2018) for product structures. 181

**Figure 3.22** Simulated distribution of products resulting from the OH-initiated oxidation of *m*-xylene. Please refer to the MCM (Jenkin et al., 1997; Saunders et al., 2003; <http://mcm.leeds.ac.uk/MCM>; accessed 14/02/2018) for product structures. 182

- Figure 3.23** Simulated distribution of products resulting from the OH-initiated oxidation of *o*-xylene. Please refer to the MCM (Jenkin et al., 1997; Saunders et al., 2003; <http://mcm.leeds.ac.uk/MCM>; accessed 14/02/2018) for product structures. 183
- Figure 3.24** Simulated distribution of products resulting from the OH-initiated oxidation of  $\alpha$ -pinene. Please refer to the MCM (Jenkin et al., 1997; Saunders et al., 2003; <http://mcm.leeds.ac.uk/MCM>; accessed 14/02/2018) for product structures. 184
- Figure 3.25** Simulated distribution of products resulting from the OH-initiated oxidation of  $\beta$ -pinene. Please refer to the MCM (Jenkin et al., 1997; Saunders et al., 2003; <http://mcm.leeds.ac.uk/MCM>; accessed 14/02/2018) for product structures. 185
- Figure 3.26** Simulated distribution of products resulting from the OH-initiated oxidation of limonene. Please refer to the MCM (Jenkin et al., 1997; Saunders et al., 2003; <http://mcm.leeds.ac.uk/MCM>; accessed 14/02/2018) for product structures. 186
- Figure 4.1** Typical TIC sections obtained for the small aromatics mixture showing the peaks observed with the lamp off (blue) and the lamp on (black). The peaks were identified as: a, ethylbenzene; b, *m*-xylene; c, *o*-xylene; d, isopropylbenzene; e, *n*-propylbenzene; f, 3-ethyltoluene; g, 4-ethyltoluene; h, 2-ethyltoluene. 200
- Figure 4.2** TIC sections for the small aromatics mixture showing the peaks observed for *n*-pentylbenzene with the lamp turned off (blue) and the lamp turned on (black). 199
- Figure 4.3** Relative rate plot for the small aromatic VOCs mixture with an OH reactivity of approximately  $18 \text{ s}^{-1}$ , at 295 K. Compounds with a reference rate coefficient for reaction with OH were plotted using evaluated literature values as references. Error bars on the y-axis, equal to one standard error, were calculated by combining the standard error in peak areas for six lamp-off samples and six lamp-on samples. Error bars on the x-axis were typically large (approximately  $\pm 20\text{-}30\%$ ) and accounted for deviations from the trend for most VOCs. A weighted (to the uncertainty in the y-axis) linear fit was used to generate the slope with a value of  $OH_{exp} = 5.5 (\pm 0.6) \times 10^9 \text{ molecules cm}^{-3}$  and  $R^2$  of 0.899. Data for *n*-pentylbenzene (A), which had no literature  $k$  value, was not used in the calculation of the fit. The VOCs can be identified as follows: 1, *t*-butylbenzene; 2, toluene; 3, *n*-propylbenzene; 4, isopropylbenzene; 5, ethylbenzene; 6, 2-ethyltoluene; 7, 4-ethyltoluene; 8, *o*-xylene; 9, 3-ethyltoluene; 10, *m*-xylene. 200

**Figure 4.4** Relative rate plot for the small aromatic VOCs mixture with an OH reactivity of approximately  $18 \text{ s}^{-1}$  measured with 20 ppb NO, at 295 K. Compounds with a reference rate coefficient for reaction with OH were plotted using evaluated literature values as references. Error bars on the y-axis, equal to one standard error, were calculated by combining the standard error in peak areas for six lamp-off samples and six lamp-on samples. Error bars on the x-axis were typically large (approximately  $\pm 20\text{-}30\%$ ) and accounted for deviations from the trend for most VOCs. A weighted (to the uncertainty in the y-axis) linear fit was used to generate the slope with a value of  $OH_{exp} = 6.9 (\pm 0.9) \times 10^9 \text{ molecules cm}^{-3}$  and  $R^2$  of 0.853. Data for *n*-pentylbenzene (A), which had no literature *k* value, was not used in the calculation of the fit. The VOCs can be identified as follows: 1, *t*-butylbenzene; 2, toluene; 3, *n*-propylbenzene; 4, isopropylbenzene; 5, ethylbenzene; 6, 2-ethyltoluene; 7, 4-ethyltoluene; 8, *o*-xylene; 9, 3-ethyltoluene; 10, *m*-xylene.

201

**Figure 4.5** Relative rate plot for the small aromatic VOCs mixture with an OH reactivity of approximately  $18 \text{ s}^{-1}$  measured with 40 ppb NO, at 295 K. Compounds with a reference rate coefficient for reaction with OH were plotted using evaluated literature values as references. Error bars on the y-axis, equal to one standard error, were calculated by combining the standard error in peak areas for six lamp-off samples and six lamp-on samples. Error bars on the x-axis were typically large (approximately  $\pm 20\text{-}30\%$ ) and accounted for deviations from the trend for most VOCs. A weighted (to the uncertainty in the y-axis) linear fit was used to generate the slope with a value of  $OH_{exp} = 7.5 (\pm 0.8) \times 10^9 \text{ molecules cm}^{-3}$  and  $R^2$  of 0.909. Data for *n*-pentylbenzene (A), which had no literature *k* value, was not used in the calculation of the fit. The VOCs can be identified as follows: 1, *t*-butylbenzene; 2, toluene; 3, *n*-propylbenzene; 4, isopropylbenzene; 5, ethylbenzene; 6, 2-ethyltoluene; 7, 4-ethyltoluene; 8, *o*-xylene; 9, 3-ethyltoluene; 10, *m*-xylene.

202

**Figure 4.6** Relative rate plots for the small aromatics mixture with an OH reactivity of  $18 \text{ s}^{-1}$ , at 295 K. Different concentrations of NO in the reactor are shown by the different coloured data.  $OH_{exp}$ , calculated from the weighted linear regressions, increased with increasing [NO].

203

**Figure 4.7** Comparison of two different SAR methods (Kwok and Atkinson (1995), blue; Jenkin et al. (2018), red) for the prediction of rate coefficients for the reactions between aromatic VOCs and OH, alongside the experimental results derived in this work (green) and the recommended literature values (black).

207

**Figure 4.8** Typical TIC sections obtained for the large aromatics mixture showing the peaks observed with the lamp off (blue) and the lamp on (black). The peaks were identified as: a, *m*-

xylene; b, *o*-xylene; c,  $\alpha$ -pinene; d, 1,3,5-trimethylbenzene; e,  $\beta$ -pinene; f, 1,2,4-trimethylbenzene; g, 1,2,3-trimethylbenzene; h, 1,3-diethylbenzene; i, 1,4-diethylbenzene; j, 1,2-diethylbenzene. 211

**Figure 4.9** Relative rate plot for the large aromatics mixture with an OH reactivity of approximately  $48 \text{ s}^{-1}$ , at 295 K. Compounds with a reference rate coefficient for reaction with OH were plotted using evaluated reference values. Error bars on the y-axis, equal to one standard error, were calculated by combining the standard error in peak areas for eight lamp-off and eight lamp-on samples. Error bars on the x-axis were typically large (approximately  $\pm 20\text{-}30\%$ ) and accounted for deviations from the trend for all VOCs. A weighted (to the uncertainty in the y-values) linear fit was used to generate the slope, with a value of  $OH_{exp} = 1.8 (\pm 0.1) \times 10^9$  molecules  $\text{cm}^{-3} \text{ s}$  and  $R^2 = 0.980$ . Data for 1,2-, 1,3- and 1,4-diethylbenzene, which had no literature  $k$  values for their reaction with OH, were not used in the calculation of the fit. The VOCs can be identified as follows: 1, *o*-xylene; 2, *m*-xylene; 3, 1,2,4-trimethylbenzene; 4, 1,2,3-trimethylbenzene; 5,  $\alpha$ -pinene; 6, 1,2,4,5-tetramethylbenzene; 7, 1,3,5-trimethylbenzene; 8, 1,2,3,5-tetramethylbenzene; 9,  $\beta$ -pinene; 10, isoprene. 213

**Figure 4.10** Relative rate plots for the large aromatic VOCs mixture with OH reactivities of 21, 48, 75, 101 and  $123 \text{ s}^{-1}$ . The  $R^2$  for the weighted linear fits were 0.958, 0.980, 0.907, 0.967 and 0.829 respectively. The values of  $OH_{exp}$  were  $2.3 (\pm 0.1)$ ,  $1.8 (\pm 0.1)$ ,  $1.2 (\pm 0.2)$ ,  $1.0 (\pm 0.1)$  and  $0.7 (\pm 0.1) \times 10^9$  molecules  $\text{cm}^{-3} \text{ s}$  respectively. 214

**Figure 4.11** Comparison of two different SAR methods (Kwok and Atkinson (1995), blue; Jenkin et al. (2018), red) for the prediction of rate coefficients for the reaction between aromatic VOCs and OH, alongside the experimental results derived in this work (green) and the recommended literature values (black). 218

**Figure 4.12** Schematic showing the proposed decay of the OH-aromatic adduct back to the original aromatic reactant and OH. Other potential OH-aromatic adduct reactions are also shown. Schematic adapted from Newland et al., 2017. 219

**Figure 4.13** Simulated relative rate plot for the four aromatic VOCs incorporated in the numerical simulations under different modelling scenarios at 300 K. From left to right the points can be identified as; benzene, toluene, *p*-xylene and *m*-xylene. The adjusted  $R^2$  values for the linear fits were: Model A, 1.00; Model B, 0.173; Model C, 0.981. 222

**Figure 4.14** Simulated relative rate plot for the four aromatic VOCs incorporated in the kinetic simulations under different modelling scenarios at 350 K. From left to right the points can be

identified as; benzene, toluene, *p*-xylene and *m*-xylene. The adjusted R<sup>2</sup> values for the linear fits were: Model A, 1.00; Model B, 0.187; Model C, 0.771. 223

**Figure 4.15** Comparison of the impact that different concentrations of O<sub>2</sub> had on the simulated relative rate plots for four aromatic VOCs at 300 K. The R<sup>2</sup> values were 0.856, 0.981 and 1.00 for [O<sub>2</sub>] = 10<sup>15</sup>, 10<sup>16</sup> and 10<sup>17</sup> molecules cm<sup>-3</sup> respectively. 224

**Figure 4.16** Simulated relative rate plot for the four aromatic VOCs at 350 K. Rather than plotting depletion factor against *k*, as in typical relative rate plots, the depletion factor was plotted against the ratio of *k* to *k<sub>d</sub>*, to account for the thermal back-decomposition of the aromatic-OH adducts. The adjusted R<sup>2</sup> value for the linear regression was equal to 1.00 showing that aromatic VOC depletions at higher temperatures are proportional to this ratio. 225

**Figure 4.17** Model C simulated depletion factor at 350 K for four aromatic VOCs plotted against a different parameter to the normal relative rate plots. Here, simulated depletion factor was plotted against the ratio between the forwards rate coefficient for the reaction forming the OH-aromatic adduct and the rate coefficient for the decay of the OH-aromatic, or  $k \times k_{O_2} / k_d$ . The adjusted R<sup>2</sup> value for the linear regression was equal to 1.00. 226

**Figure 4.18** Simulated impact of different initial concentrations of NO on the concentration of *pOH* over time. The concentration of *pOH* decreased more rapidly with an increased concentration of NO. 230

**Figure 4.19** Simulated impact of different initial concentrations of NO on the concentration of HO<sub>2</sub> over time. The concentration of HO<sub>2</sub> decreased more rapidly with increasing concentration of NO and was reduced to a concentration of less than 1000 molecules cm<sup>-3</sup> within 3 s with a NO concentration of 70 ppb. 231

**Figure 4.20** Simulated impact of different initial concentrations of NO on the concentration of secondary OH (*sOH*) over time. *sOH* was not produced when NO wasn't present in the reactor. When NO was added to the reactor, *sOH* was generated rapidly, peaking at approximately 2 × 10<sup>10</sup> molecules cm<sup>-3</sup> with 70 ppb NO. The concentration of *sOH* then decreased with time, due to reactions with VOCs, HO<sub>2</sub>, NO and NO<sub>2</sub>. 232

**Figure 4.21** Simulated impact of different initial concentrations of NO on the total *sOH* produced over time. *sOH* was not produced when NO wasn't present in the reactor. 233

**Figure 4.22** Simulated impact of different initial concentrations of NO on the NO and NO<sub>2</sub> concentrations over time. 234

**Figure 4.23** Simulated impact of different initial concentrations of NO on the sinks for *pOH*; reaction with HO<sub>2</sub>, reaction with primary VOCs, reaction with NO, reaction with NO<sub>2</sub> and reaction with secondary VOCs (sVOCs). 235

**Figure 4.24** Simulated impact of different initial concentrations of NO on the sinks for *sOH*; reaction with HO<sub>2</sub>, reaction with primary VOCs, reaction with NO, reaction with NO<sub>2</sub> and reaction with secondary VOCs (sVOCs). 236

**Figure 4.25** Simulated impact of different initial concentrations of NO on the VOC sinks. 237

**Figure 5.1** Relative rate plot for the alkane mixture with an OH reactivity of 4.3 s<sup>-1</sup>, at 295 K. Compounds with a reference rate coefficient were plotted using evaluated literature values. Error bars on the y-axis, equal to one standard error, were calculated by combining the standard error in peak errors for six lamp-off and six lamp-on samples. Error bars on the x-axis were typically large (approximately ± 20-30 %) and accounted for deviations from the lines for all VOCs. A weighted (to the uncertainty in the y-values) linear fit was used to generate the slope, with a value of  $OH_{exp} = 3.8 (\pm 0.2) \times 10^9$  molecules cm<sup>-3</sup> and  $R^2 = 0.971$ . Data for 2-methylheptane, 2-methylnonane and ethylcyclohexane, which had no literature *k* values, were not used in the calculation of the fit, The VOCs can be identified as follows; 1, 2,2,3-trimethylbutane; 2, 2-methylpentane; 3, 3-methylpentane; 4, *n*-octane; 5, *n*-nonane; 6, *n*-decane; 7, *n*-undecane; 8, cycloheptane; 9, cyclooctane. 247

**Figure 5.2** Arrhenius plot showing the observed temperature dependence of the rate coefficient for the reaction between 2,2,3-trimethylbutane and OH. Rate coefficients derived as part of this work are shown alongside the available literature. Two Arrhenius expressions are also shown; one derived in this work (black) and the other as recommended by Atkinson, 2003 (red). 251

**Figure 5.3** Arrhenius plot showing the observed temperature dependence of the rate coefficient for the reaction between *n*-octane and OH. Rate coefficients derived as part of this work are shown alongside the available literature. Two Arrhenius expressions are also shown; one derived in this work (black) and the other as recommended by Atkinson, 2003 (red). 251

**Figure 5.4** Arrhenius plot showing the observed temperature dependence of the rate coefficient for the reaction between *n*-nonane and OH. Rate coefficients derived as part of this work are shown alongside the available literature. Two Arrhenius expressions are also shown; one derived in this work (black) and the other as recommended by Atkinson, 2003 (red). 253

**Figure 5.5** Arrhenius plot showing the observed temperature dependence of the rate coefficient for the reaction between *n*-decane and OH. Rate coefficients derived as part of this work are shown alongside the available literature. Two Arrhenius expressions are also shown; one derived in this work (black) and the other as recommended by Atkinson, 2003 (red). 253

**Figure 5.6** Arrhenius plot showing the observed temperature dependence of the rate coefficient for the reaction between cycloheptane and OH. Rate coefficients derived as part of this work are shown alongside the available literature. Two Arrhenius expressions are also shown; one derived in this work (black) and the other as recommended by Atkinson, 2003 (red). 256

**Figure 5.7** Arrhenius plot showing the observed temperature dependence of the rate coefficient for the reaction between cyclooctane and OH. Rate coefficients derived as part of this work are shown alongside the available literature. Two Arrhenius expressions are also shown; one derived in this work (black) and the other as recommended by Atkinson, 2003 (red). 256

**Figure 5.8** Arrhenius plot showing the observed temperature dependence of the rate coefficient for the reaction between 2-methylpentane and OH. Rate coefficients derived as part of this work are shown alongside the available literature. The Arrhenius expression derived in this work is also shown. 257

**Figure 5.9** Arrhenius plot showing the observed temperature dependence of the rate coefficient for the reaction between 3-methylpentane and OH. Rate coefficients derived as part of this work are shown alongside the available literature. The Arrhenius expression derived in this work is also shown. 257

**Figure 5.10** Arrhenius plot showing the observed temperature dependence of the rate coefficient for the reaction between *n*-undecane and OH. Rate coefficients derived as part of this work are shown alongside the available literature. The Arrhenius expression derived in this work is also shown. 259

**Figure 5.11** Arrhenius plot showing the observed temperature dependence of the rate coefficient for the reaction between 2-methylheptane and OH. Rate coefficients derived as part of this work

are shown alongside the available literature. The Arrhenius expression derived in this work is also shown. 259

**Figure 5.12** Arrhenius plot showing the observed temperature dependence of the rate coefficient for the reaction between 2-methylnonane and OH. The Arrhenius expression derived in this work is also shown. 261

**Figure 5.13** Arrhenius plot showing the observed temperature dependence of the rate coefficient for the reaction between ethylcyclohexane and OH. Rate coefficients derived as part of this work are shown alongside the available literature. The Arrhenius expression derived in this work is also shown. 261

**Figure 5.14**  $k_{Cl}$  values plotted against  $k_{OH}$  value for multiple VOC reactions. Linear and branched alkanes are shown in yellow and green respectively. Linear alkenes are shown in red, branched and cyclic alkenes are in purple and biogenic compounds (comprising mainly monoterpenes) are in blue. Aromatic VOCs are shown in black. 265

**Figure 5.15** TIC observed for a flow of  $Cl_2$  (0.3 ppm) in  $N_2$  injected into the reactor. The peaks were identified as molecular chlorine ( $Cl_2$ ), acetyl chloride ( $CH_3COCl$ ), acetic acid ( $CH_3COOH$ ), carbon tetrachloride ( $CCl_4$ ) and chloroacetyl chloride ( $CH_2ClCOCl$ ). 268

**Figure 5.16** TICs for the large aromatics mixture with  $Cl_2$  (red; 66 ppm) and without  $Cl_2$  (blue) in the reactor. See Table 5.5 for a list of peak identities. 269

**Figure 5.17** Typical TIC sections obtained for Cl mixture 1 with the lamp turned off (blue) and the lamp turned on (black). Greater differences in peak areas were observed for VOCs which have a larger rate coefficient for their reaction with Cl. Literature rate coefficients (in units of  $10^{-12} \text{ cm}^3 \text{ molecule}^{-1} \text{ s}^{-1}$ ) for these alkane + OH reactions are: *n*-nonane, 453 ( $\pm 28$ ); cyclooctane, 457 ( $\pm 15$ ) (see Table 5.6). 273

**Figure 5.18** Relative rate plot for Cl mixture 1 with a Cl reactivity of  $23 \text{ s}^{-1}$  and  $Cl_2$  (60 ppm) injected into the reactor, at 295 K. Compounds with a reference rate coefficient for reaction with Cl were plotted using literature values as references. Error bars on the y-axis, equal to one standard error, were calculated by combining the standard error in peak areas for four lamp-off and four lamp-on samples. Error bars on the x-axis were typically large and accounted for deviations from the trend for all VOCs. A weighted (to the uncertainty in the y-values) linear fit was used to generate the slope, with a value of  $Cl_{exp} = 0.5 (\pm 0.04) \times 10^9 \text{ molecules cm}^{-3} \text{ s}$  and  $R^2 =$

0.96. The VOCs can be identified as follows; 1, 2-methylpentane; 2, *n*-hexane; 3, *n*-octane; 4, *n*-nonane; 5, cyclooctane. 275

**Figure 5.19** Relative rate plots for Cl mixture 1 with a Cl reactivity of  $23 \text{ s}^{-1}$  and estimated  $[\text{Cl}_2]$  of 30, 33, 67 and 100 ppm. The  $R^2$  values for the weighted linear fits were 0.83, 0.69, 0.09 and 0.91 respectively. The values of  $Cl_{exp}$  were  $1.0 (\pm 0.2)$ ,  $0.4 (\pm 0.2)$ ,  $0.14 (\pm 0.12)$  and  $0.6 (\pm 0.1) \times 10^9$  molecules  $\text{cm}^{-3} \text{ s}$  respectively. Error bars on the x-axis are not shown for reasons of clarity. 276

**Figure 5.20** Relative rate plots for Cl mixture 2 with a Cl reactivity of  $27 \text{ s}^{-1}$  and estimated  $[\text{Cl}_2]$  of 50, 75, 100 and 150 ppm. The  $R^2$  values for the weighted linear fits were 0.54, 0.76, 0.93 and 0.21 respectively. The values of  $Cl_{exp}$  were  $0.3 (\pm 0.1)$ ,  $0.5 (\pm 0.1)$ ,  $0.7 (\pm 0.1)$  and  $0.2 (\pm 0.1) \times 10^9$  molecules  $\text{cm}^{-3} \text{ s}$  respectively. Error bars on the x-axis are not shown for reasons of clarity. 279

**Figure 5.21** Relative rate plot for Cl mixture 2 with a Cl reactivity of  $27 \text{ s}^{-1}$  and  $\text{Cl}_2$  (300 ppm) injected into the reactor, at 295 K. Compounds with a reference rate coefficient for reaction with Cl were plotted using literature values as references. Error bars on the y-axis, equal to one standard error, were calculated by combining the standard error in peak areas for four lamp-off and four lamp-on samples. Error bars on the x-axis were typically large and accounted for deviations from the trend for all VOCs. A weighted (to the uncertainty in the y-values) linear fit was used to generate the slope, with a value of  $Cl_{exp} = 1.1 (\pm 0.1) \times 10^9$  molecules  $\text{cm}^{-3} \text{ s}$  and  $R^2 = 0.97$ . The VOCs can be identified as follows; 1, toluene; 2, ethylbenzene; 3, 2-methylpentane; 4, *n*-octane; 5, *n*-nonane; 6, cyclooctane. 280

**Figure 5.22** Experimentally derived (data points) and predicted SAR derived (lines)  $k$  values for the homologous series of 2-methylalkane + Cl reactions. Data from this study are shown in green and were in good agreement with both previous experimentally measured values and theoretical predictions. 283

**Figure 5.23** The estimated concentrations of Cl radicals resulting from the photolysis of different concentrations of  $\text{Cl}_2$  injected into the reactor. 285



# Acknowledgements

Firstly, I would like to say a big thank you to Dr. Terry Dillon who has been an excellent supervisor throughout this whole process, providing indispensable advice regarding experiments, results and writing and also a great deal of support in terms of my development as a scientist. I would also like to share my appreciation for all those that have worked within the Dillon group over the past few years – I hope as the eldest PhD student in the group I was able to pass on my own good advice.

In addition to this I would like to thank all at the Wolfson Atmospheric Chemistry Group. It has been an incredible experience working with you all over the past four years (five if you count my Masters project). Big thanks must go to Martyn Ward, Jim Hopkins, Rich Lidster and Steve Andrews who all provided crucial assistance in both setting up and maintaining equipment and helping to fix things when everything seemed to go wrong. Thanks must also go to Shalini Punjabi, Rachel Dunmore and Kelly Pereira, with whom I shared many moments of vented frustration in the office. I would also like to mention any and all who attended the semi-regular (more so at certain points) Friday night drinking sessions; James Lee, Marv Shaw, Stuart Young, Stuart Grange, Andrew Rickard, and many others. Thanks also to Stefan Swift for the riveting stories which kept many of us entertained. Finally, I'd like to say a massive thanks to Shani Garraway, without whom this PhD would have been far more difficult to complete. Thanks for watching all the animal videos with me and good luck with your teaching in the future; I know you'll be fantastic.

I'd also like to show a massive amount of appreciation for the University of York Swimming and Water Polo Club. UYSWC has been a major part of my university life and I really can't express in words how much this club, and the people within it, have helped me complete this PhD. Thanks for all the training, the competing, the drinking, the laughing, the dancing, the tour-ing; thanks for the stupid sets we did (the Gatorade set, the Olympic set, playing charades etc.); thanks for the stupid games we played at BUCs; thanks for all the nights out and forcing me to wear stupid fancy dress even in my old age as a postgrad. There are far, far too many of you to mention individually (I could almost write another thesis about you all), but a few honourable mentions; Chris Unsworth (I followed in his footsteps), Bill Timpany, Danny Martland (sorry I was always injured

and I was the worst person to have to coach), Fiona Whiting (also part of the Dillon group and following in my footsteps!) and Nisha Desai (who's been vital in helping me cope with the writing process).

This ends soon I promise.

I'd also like to acknowledge all my friends from home. It is incredible that we remain this close even after leaving school so many years ago and I fully believe that is down to the remarkable people that you have all become over the past decade. You can finally all stop mocking me for still being at Uni after you all graduated years ago (although you're all actually jealous). The two stags that I have recently been on were an excellent distraction from thesis writing and I look forward to the many other great events that we have planned for the future. Special thanks must go to some of my longest friends; Nick Hodgkinson and Connor McCormack (I beat you to Dr.) in particular, but also Nathan Hoyle, Dean Matthews and Sam Burton, whom I have known since Longmoor. Paul Phillips you'll be upset if I don't mention you so here you go.

Some huge thanks must go to my long-term house mate, Marc Dickinson. Firstly, congratulations on completing your own PhD. I think it's fair to say that we shared a lot of the frustrations and tribulations that coincide with completing a PhD together but we also shared in the exciting moments when everything eventually fell into place. Oh, and thanks for completing all my games!

Finally, and this is a big finally, I'd like to thank my family (and my pets; Ducky, Petri and Spike). To my sister, Katie, you have been an absolutely incredible source of inspiration; not only are you one of the strongest and bravest people I know, but you are also the best sister I could hope for. I know it's not always been easy for you, but your perseverance and your natural inclination to keep going and not give up are now showing just how talented you are. I am super proud of who you are as a person now and look forward to watching you with every success in the future. To my Mum, firstly, thanks for all the help with writing. Despite protesting that you don't understand a word of what I've written, you still always manage to find something to correct! And to my Dad, thanks for all the bad jokes, and for being a constant source of excellent encouragement all the way through. To the both of you, thanks also for being the incredible parents that you are; I would not be the person I am today without your constant advice (read: nagging), your constant support and your general belief in me. Thank you for giving me the sense of wonderment at the world around me, the sense of exploration and discovery, and the sense of creativity that I think has been profoundly important for me reaching this point.

I think that's it. Now to the "fun" bit...

# Declaration

The work described in this thesis is the original work undertaken by the author, Jacob T. Shaw, at the University of York over the period 2014-2018. Except where stated, all of the work contained within this thesis represents the original contribution of the author. Some elements of the research in this thesis have been published previously in journals; where items were published alongside collaborators, the author of this thesis is solely responsible for the work presented here. Published work which relates to the work in this thesis can be found in Shaw et al. (2018) (<https://doi.org/10.5194/acp-18-4039-2018>).

This work has not previously been presented for an award at this, or any other, University. All sources are acknowledged as references.



# Chapter 1

## Introduction

### 1.1 Preface

Earth's atmosphere can be subdivided into five principle layers; the troposphere, the stratosphere, the mesosphere, the thermosphere and the exosphere. Each of these layers differ in terms of the physical processes that occur within them, and the interactions that they have with other systems. The atmosphere is a vastly complex mixture, one of the most complex known to man, which undergoes an incredible amount of physical and chemical processes over a wide variety of timescales, from chemical reactions occurring in nanoseconds, to climatic deviations occurring over millennia and longer.

Section 1.2 will cover some of the vast range of different chemical compounds that exist within the atmosphere, identifying their sources and also their impacts on air quality, human health and climate change.

Sections 1.3 and 1.4 will introduce the field of gas-phase chemical kinetics, its importance and the tools and techniques used to both experimentally measure, and theoretically estimate, the chemical processes occurring in the air around us.

## 1.2 Atmospheric composition

### 1.2.1 The troposphere

It is well known that the Earth's atmosphere comprises mainly nitrogen (78%), oxygen (21%) and argon (0.9%), with the remaining 0.1% made up of what are known as trace gases. One tenth of one percent of the atmosphere may not sound like much, but it accounts for a staggering amount of chemical species, from highly reactive radicals, to complex volatile organic compounds (VOCs), to harmful pollutants such as NO and NO<sub>2</sub>, and even to less-volatile compounds, which can partition between the gas-phase and solid- or liquid-phases. This vast array of chemical compounds interacts in multiple ways, and it is the research of such interactions that is the subject of the field of atmospheric chemistry.

### 1.2.2 Organic compounds

Organic compounds, for the purpose of this work, refers to those molecules which contain carbon-hydrogen bonds. Hydrocarbons refer to those organic compounds which consist entirely of carbon-hydrogen bonds i.e. there are no heteroatoms such as oxygen or nitrogen. There are three general classes of hydrocarbons, as defined by the International Union of Pure and Applied Chemistry (IUPAC) in *Nomenclature of Organic Chemistry* (Favre and Powell, 2013):

1. Saturated hydrocarbons, which contain only single bonds and are 'saturated' with hydrogen. Saturated hydrocarbons include alkanes and cycloalkanes.
2. Unsaturated hydrocarbons, which contain one or more double bonds or triple bonds and are referred to as alkenes or alkynes respectively.
3. Aromatic hydrocarbons, which incorporate at least one aromatic ring within their structure. Aromatic compounds contain a conjugated system of delocalised  $\pi$  electrons.

Organic compounds mainly enter the atmosphere through interactions with the biosphere; the processes associated with the growth and decay of organisms emit much of the organic chemical matter observed in the atmosphere. Combustion of dead, or living, organic matter also results in the emission of organic species. Combustion is primarily viewed as anthropogenic in origin but natural combustion, such as that which occurs as a result of forest fires, dominates in some regions.

The number and scope of organic compounds identified and observed in the atmosphere has steadily increased since the 1950s, when research into the causes of air pollution became more prolific. Prior to this, methane and formaldehyde were known to be present, as evidenced in *Compendium of Meteorology* (Gleckauf, 1951). Haagen-Smit (1952) observed the presence of at least 15 different organic acids in Los Angeles smog samples collected on filters whilst, in the same year, Mader et al. (1952) demonstrated that hydrocarbon compounds constitute much of the organic matter in the atmosphere and that they are directly involved with aerosol formation and air pollution. Gas chromatography, which was developed in the early 1950s, allowed for the identification of various C<sub>2</sub>-C<sub>5</sub> hydrocarbons in the exhaust gases emitted by cars (Eggertsen and Nelsen, 1958) and by 1978 over 500 hydrocarbon compounds, along with many other organic species with different functional groups, were listed in *Chemical Compounds in the Atmosphere* (Graedel, 1978). By the late 2000s, Goldstein and Galbally (2007) postulated that between 10<sup>4</sup> and 10<sup>5</sup> different organic compounds had been observed in the atmosphere, and suggested that that value may in fact be only a small fraction of the total number actually present.

The difficulty in providing an exact number, or even an approximate number, of atmospheric organic compounds is multifaceted. For one, the number of possible isomers of a particular chemical increases exponentially with the number of carbon atoms. For example, C<sub>4</sub>H<sub>10</sub> (butane) has just two structural isomers; *n*-butane and *i*-butane. In comparison, C<sub>10</sub>H<sub>22</sub> (decane) has 75 possible structural combinations. The number of possible structures becomes hopelessly complex when accounting for the various functional groups that can also be incorporated into organic molecules: alcohols, amines, ethers, halides, thiols, aldehydes, ketones, esters, carboxylic acids, amides, to name but a few. Indeed, multifunctional compounds are important for atmospheric chemistry as they are often associated with the production of secondary organic aerosols (SOA).

The second difficulty lies in the fact that many of these compounds exist in the atmosphere as trace gases. The 0.1% of the atmosphere that is the subject of this section includes *all* of these species and hence they can be found in concentrations as small as parts per million (ppm), parts per billion (ppb), parts per trillion (ppt), and even lower. Whilst visualising one part per hundred (one percent) is relatively simple for most, conceptualising parts per trillion and parts per billion, and even parts per million, is quite difficult, due to the inherently large numbers involved. One part per million is therefore roughly equal to a single word in the entire English version of all seven Harry Potter novels, whilst one part per billion is roughly equal to 7.4 people out of the total human population of our planet. One part per trillion is even harder to visualise; it is roughly equal to just three trees of the estimated 3 trillion trees growing on Earth. And herein lies the

difficulty in observing many of the organic compounds that exist in the atmosphere; the instruments used for their detection need to be capable of finding, and detecting, those three trees in amongst the three trillion trees around them.

### 1.2.2.1 Alkanes

Alkanes are the simplest of hydrocarbon structures, possessing only carbon and hydrogen atoms and fully saturated bonds; that is, each carbon atom is bonded to four other atoms. Alkanes can be linear, branched or cyclic. Cycloalkanes can also be monocyclic or polycyclic. Methane ( $\text{CH}_4$ ) is the simplest alkane and is often the subject of news articles relating to atmospheric chemistry and climate change. This is due to its role as a greenhouse gas and the fact that its atmospheric concentration has been increasing steadily since the 1750s, accompanied by the increasing rate of industrialisation worldwide.

Alkanes were shown to make up approximately 50% of the composition of exhaust emissions in the early 1990s, with  $\text{C}_6$  and  $\text{C}_8$  alkanes making the greatest contribution to the alkane fraction (Hoekman, 1992). This value appears to fluctuate somewhat and is likely dependent on the fuel being burnt and the engine loading. More recently alkane contributions to exhaust emissions were measured to be approximately 40% from vehicles in China and Hong Kong (Guo et al., 2011; Cao et al., 2016) but could be up to approximately 90% when the engine loading is above 30% (Pereira et al., 2017). Indeed, the actual fraction of alkanes in evaporation from unburnt fuel appears to be much greater than 50%, to the extent that a single alkane, isopentane, is used as a marker for fuel evaporation (Zhang et al., 2013; Salameh et al., 2014). Larger, long chain alkanes ( $\text{C}_{12}$ - $\text{C}_{18}$ ), which are labelled as intermediate volatile organic compounds (IVOCs) to distinguish them from VOCs, have also been detected in engine exhaust, using proton-transfer reaction mass spectrometry (PTR-MS) (Erickson et al., 2014).

A study of non-methane hydrocarbon (NMHC) in three cities in Saudi Arabia found that  $\text{C}_2$ - $\text{C}_6$  alkanes made up 10 of the 20 most abundant compounds, with mean 24-hour mixing ratios between 1 and 14 ppbv (Barletta et al., 2017). These results were compared with datasets from Pakistan and Singapore, with measured 24-hour average mixing ratios generally an order of magnitude lower in Singapore but an order of magnitude greater in Lahore, Pakistan. Total alkane mixing ratios in Beijing, China were measured to be 9.5 ppbv but this value increased by a factor of five from clear days to those days characterised as having 'heavy haze' (Liu et al., 2017). There

was also a clearly observed diurnal variation in alkane concentration during clear days, but this became far less apparent on heavy haze days.

More long-term studies have found that C<sub>2</sub>-C<sub>3</sub> alkane concentrations (markers of natural gas leakage) had not changed appreciably in many French cities over a period of approximately a decade (Waked et al., 2016). Significant downward trends, of between 3% and 6% per year, were observed for C<sub>4</sub>-C<sub>5</sub> alkane concentrations (markers of evaporative emissions and vehicle emissions) across the same set of cities however.

Alkanes therefore represent an important class of atmospheric compounds. They are ubiquitous in urban areas due to their connection to vehicle emissions and natural gas burning. The oxidation of alkanes by OH is covered in Section 1.3.2.

### 1.2.2.2 Alkenes

Alkenes also contain primarily carbon and hydrogen atoms but are characterised as containing at least one carbon-carbon double bond. As for alkanes, they can be linear, branched or cyclic. The position of the double bond can also differ within isomers, which can have an impact on molecular properties.

Many of the alkenes detected in the atmosphere have biogenic sources; they are emitted by vegetation undergoing the various chemical processes necessary for life and growth. The flux of carbon from the biosphere is dominated by a single compound, 2-methyl-1,3-butadiene (C<sub>5</sub>H<sub>8</sub>), otherwise known as isoprene. Many of the other alkene VOCs observed in the atmosphere are formed of multiple units of isoprene and are known as isoprenoids. The most common of these in the atmosphere are the monoterpenes (C<sub>10</sub>H<sub>16</sub>) and the sesquiterpenes (C<sub>15</sub>H<sub>24</sub>). However, isoprenoids also include many common chemicals such as cholesterol, vitamin A and rubber and are responsible for many scents and fragrances. Isoprenoid compounds can be highly varied in structure, comprising conjugated alkenes (of which isoprene is an example), non-conjugated monocyclic alkenes and non-conjugated bicyclic alkenes, amongst others. Figure 1.1, Figure 1.2 and Figure 1.3 show the structures of some of the alkenes which feature prominently in this work.

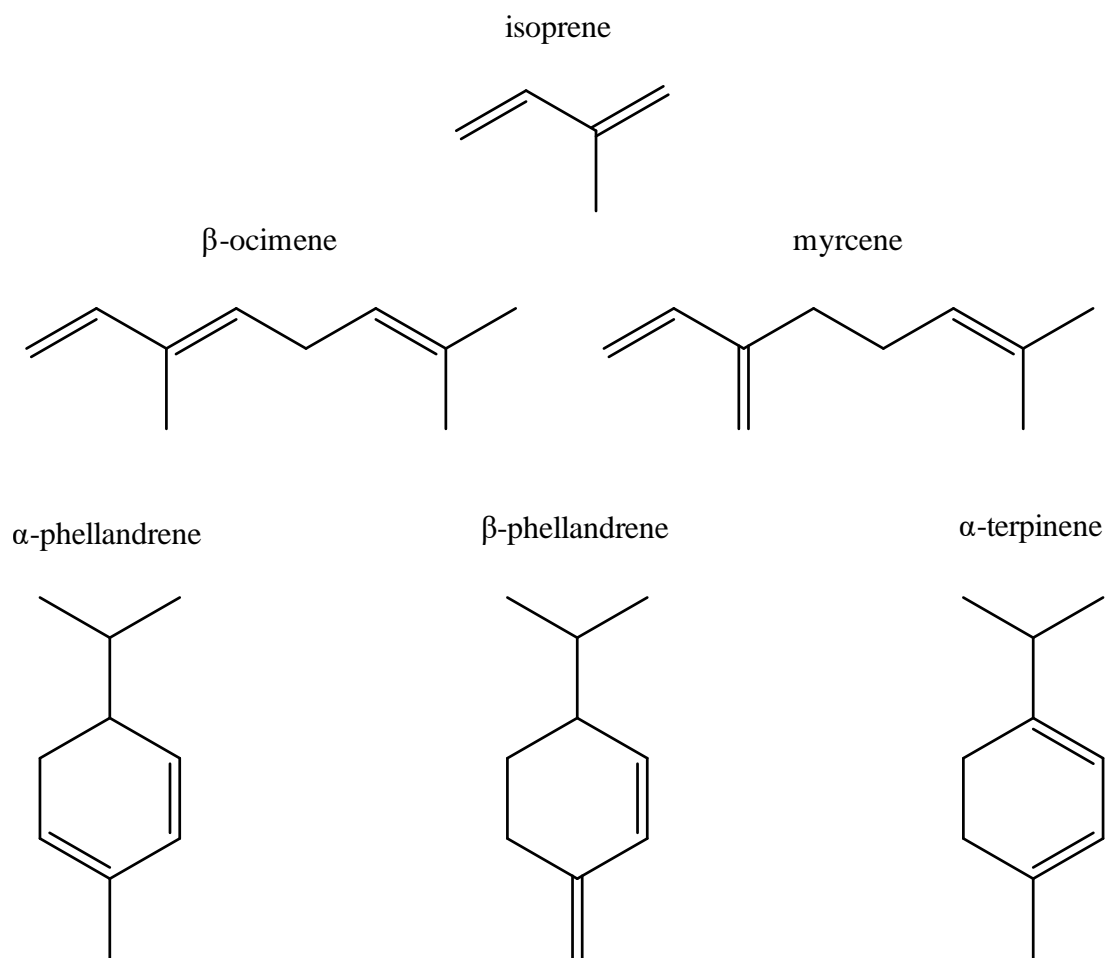


**Figure 1.1** The chemical structures of some conjugated alkenes including isoprene and the monoterpenes;  $\beta$ -ocimene, myrcene,  $\alpha$ -phellandrene,  $\beta$ -phellandrene and  $\alpha$ -terpinene.

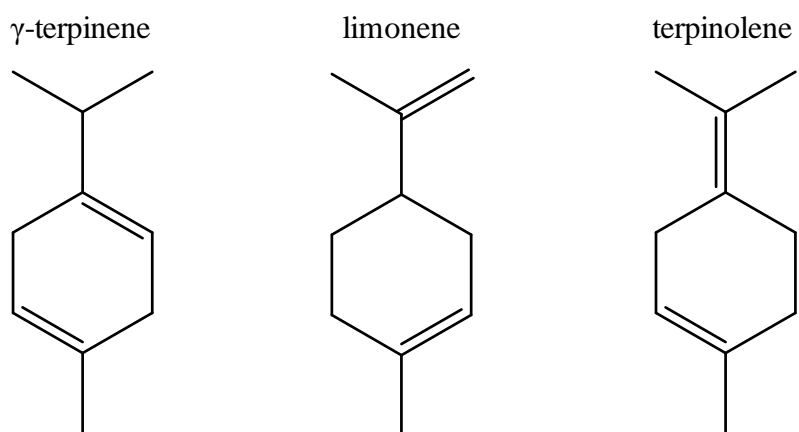


**Figure 1.2** The chemical structures of some non-conjugated monocyclic alkenes including the monoterpenes;  $\gamma$ -terpinene, limonene and terpinolene

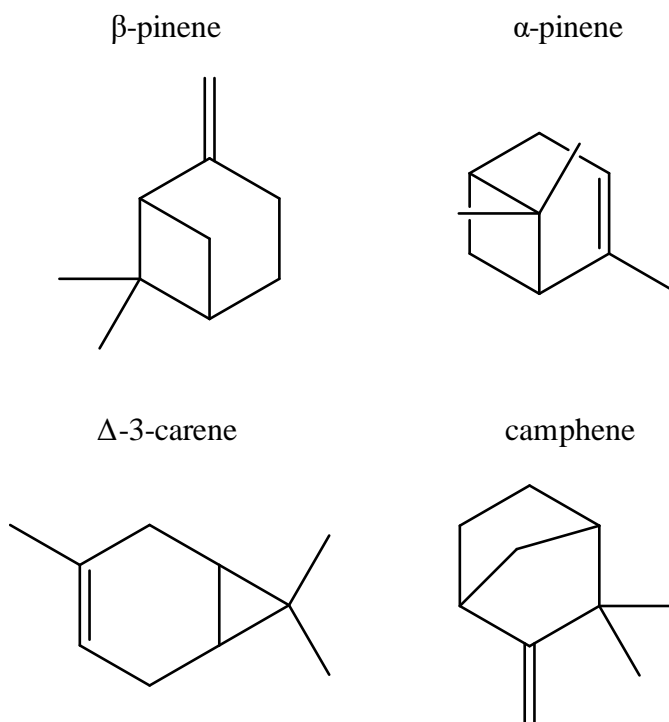


**Figure 1.3** The chemical structures of some non-conjugated bicyclic alkenes including the monoterpenes;  $\beta$ -pinene,  $\alpha$ -pinene, 3-carene and camphene.

The most recent estimates put the total flux of isoprene worldwide at approximately 500 Tg year<sup>-1</sup> (Guenther et al., 2012). This is estimated to be approximately half of the total budget of biogenic emissions, and of equal magnitude to the global methane flux. In plants, dimethylallyl pyrophosphate is converted into isoprene by an enzyme called isoprene synthase (Silver and Fall, 1991; Silver and Fall, 1995). A similar mechanism is also responsible for the synthesis of many higher order isoprenoids, including the monoterpenes and sesquiterpenes (Fuentes et al., 2000 and references therein). The synthesis of isoprene is closely linked to photosynthesis but the reason behind its production remains unverified. There is increasing evidence that many of the isoprenoid compounds are synthesised by plants as a response to stress (Vickers et al., 2009), although other possibilities have been presented (Rosenstiel et al., 2004; Sanadze, 2004; Magel et al., 2006). Once synthesised, isoprenoids do not accumulate within plants and are emitted to the atmosphere via the stomata.

Despite a total flux similar to that estimated for methane, an important greenhouse gas with average atmospheric concentrations of 1800 ppbv (Dlugokencky, 2018), the observed mixing ratios of isoprene in the atmosphere are on the order of 0 – 10 ppbv (von Kuhlmann et al., 2004). This is due to its extremely high reactivity, relative to that of methane (see Section 1.3.2 and Section 1.3.3).

The emissions of monoterpene species are hard to quantify due to their extremely high reactivity towards both OH and O<sub>3</sub>. Many laboratory studies have attempted to measure the emission factors ( $E_s$ ) for many isoprenoids using various open and closed systems (Tholl et al., 2006; Ortega and Helmig, 2008). However, these values are subject to significant uncertainties due in part to the variability in emission rates with time of day, environmental condition, plant stress and plant phenology, but also due to inherent difficulties within many of the sampling and measurement methods (Niinemets et al., 2011).

Measurements of atmospheric monoterpene concentrations have been made however. Three campaigns sampling 18 m above a boreal forest in Hyytiälä, Finland measured total monoterpene concentrations of between 100 and 300 pptv, of which 60% was accounted for by  $\alpha$ -pinene (Spanke et al., 2001). Recent measurements in the same location found  $\Delta$ -3-carene concentrations of between 5 pptv and 1.4 ppbv, (-)- $\alpha$ -pinene concentrations between 7 pptv and 0.5 ppbv, and (+)- $\alpha$ -pinene concentrations of between 9 pptv and 1.5 ppbv (Yassaa et al., 2012). A night-time maximum total monoterpene concentration of 2.9 ppbv was observed in a forested site in Northern Greece (Harrison et al., 2001). More recent measurements of isoprene and total monoterpenes were made in Borneo, in a tropical rainforest, with recorded mean mixing ratios of 1.3 and 0.18 ppbv respectively (Langford et al., 2010). This is far less than similar measurements made for other tropical rainforests, in for example, the Amazon, where isoprene and total monoterpene mixing ratios were on the order of approximately 1-10 and 0.1-3 ppbv respectively (e.g. Greenberg et al., 2004; Karl et al., 2007). Observable monoterpene concentrations are not limited to the terrestrial atmosphere however; recent measurements over oligotrophic waters in the Arctic and Atlantic oceans observed between 0.05 and 5 pptv of monoterpenes in the marine atmosphere (Hackenberg et al., 2017).

Alkenes therefore represent another important class of atmospheric compounds. They are ubiquitous throughout the world, due to their association with biomass. The oxidation of alkenes by OH is covered in Section 1.3.3.

### 1.2.2.3 Aromatics

Aromatic VOCs refer to those VOCs which contain an aryl group; a functional group in which the carbon structure contains delocalised  $\pi$ -electrons. The simplest aromatic VOC is benzene, which is a monocyclic structure, or monoaromatic hydrocarbon (MAH). Polycyclic, or polyaromatic hydrocarbons (PAH), are also prevalent in the atmosphere. These structures can be substituted by various functional groups. Alkyl groups, consisting of alkane-based hydrocarbon chains, are common aromatic substituents in the atmosphere. Figure 1.4, Figure 1.5 and Figure 1.6 show the chemical structures of some aromatic VOCs that are prominent in this work.

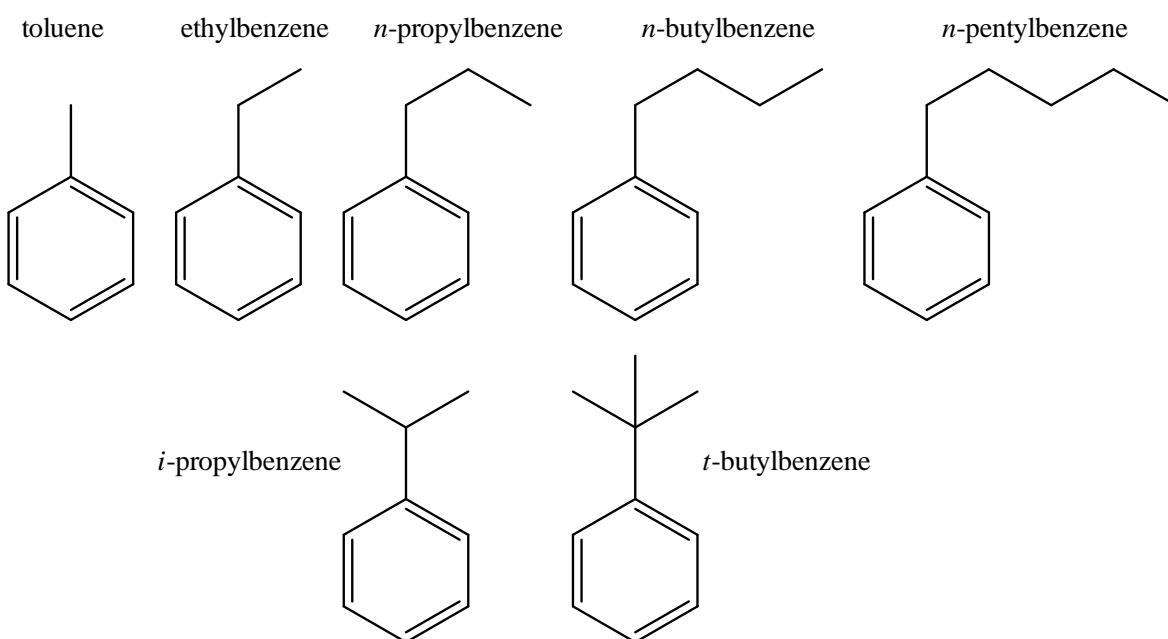


**Figure 1.4** The chemical structures of some mono-substituted aromatic VOCs, including; toluene, ethylbenzene, *n*-propylbenzene, *i*-propylbenzene, *n*-butylbenzene, *t*-butylbenzene and *n*-pentylbenzene.

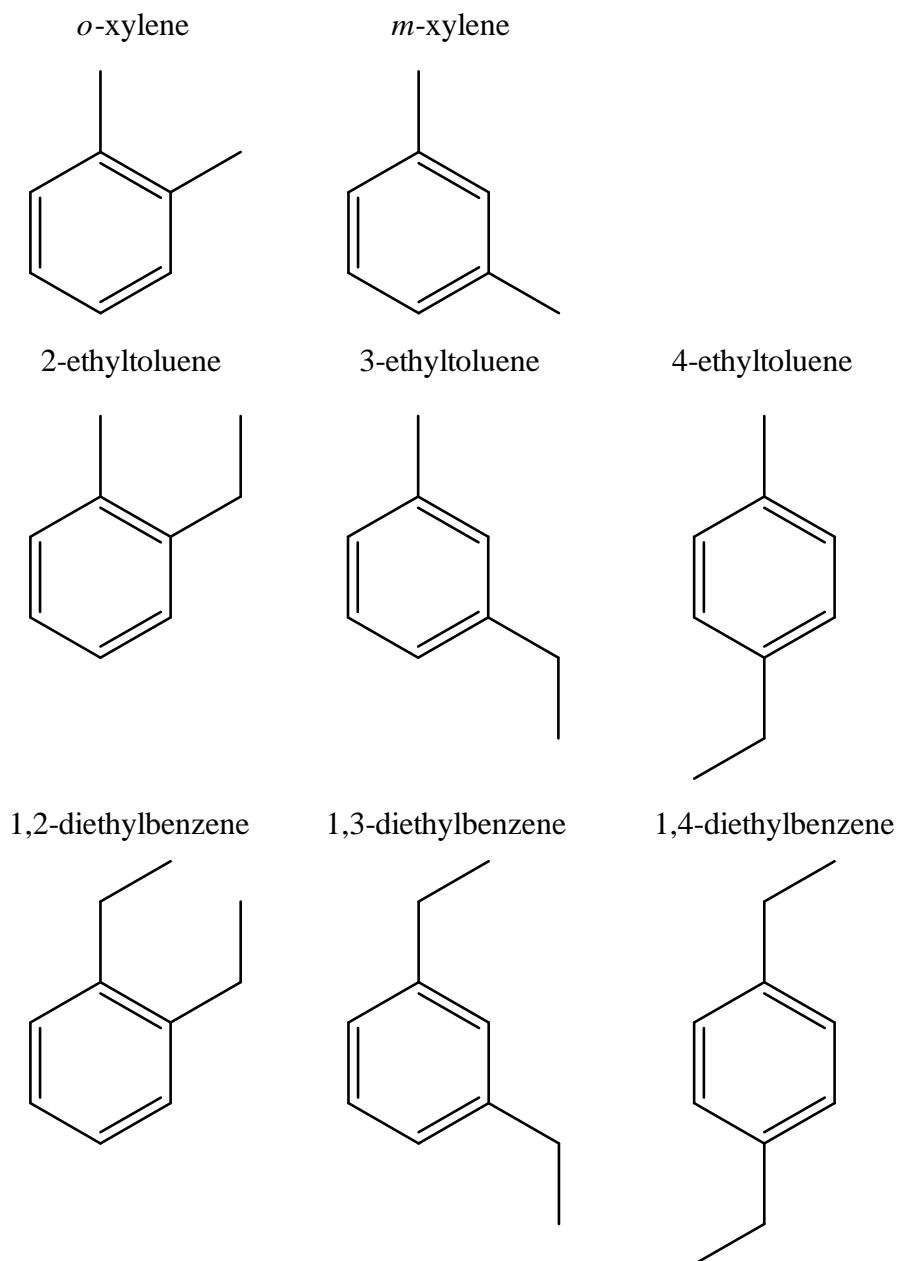


**Figure 1.5** The chemical structures of some di-substituted aromatic VOCs, including; *o*- and *m*-xylene, 2-, 3- and 4-ethyltoluene and 1,2-, 1,3- and 1,4-diethylbenzene.

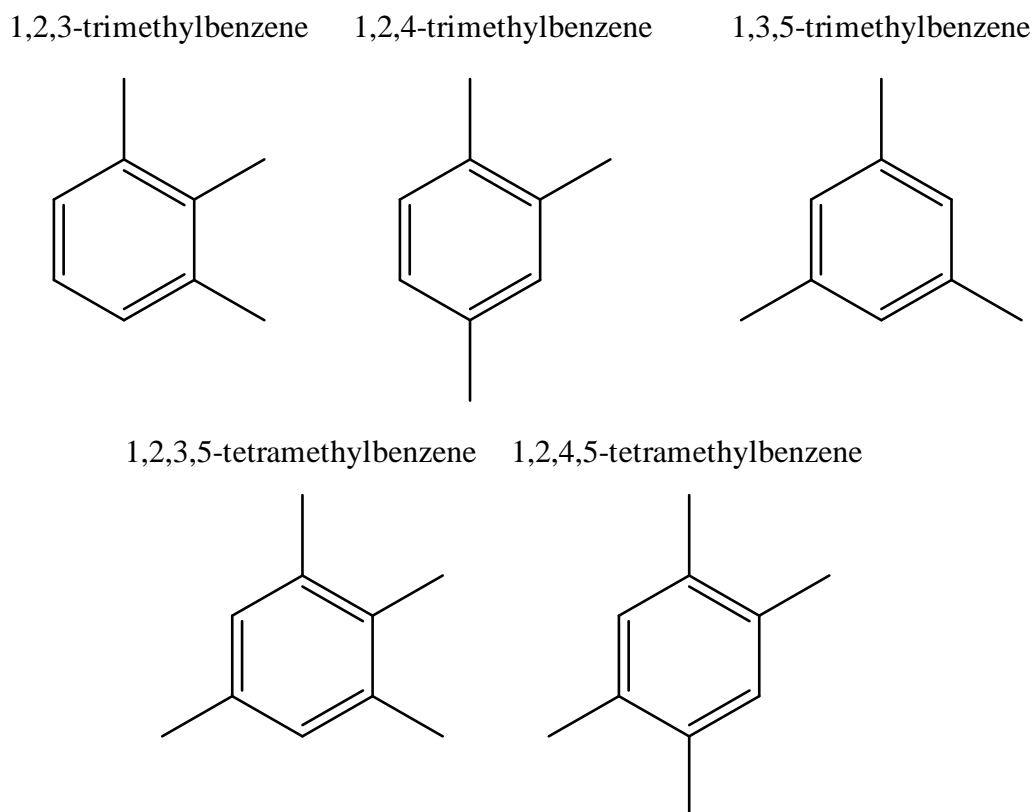


**Figure 1.6** The chemical structures of some tri- and tetra-substituted aromatic VOCs, including; 1,2,3-, 1,2,4- and 1,3,5-trimethylbenzene and 1,2,3,5- and 1,2,4,5-tetramethylbenzene.

Aromatic VOCs can account for a large proportion of the non-methane hydrocarbon (NMHC) mass as at least 90 different MAHs and PAHs have been identified in diesel fuel (Hamilton and Lewis, 2003). Measurements of aromatic VOCs from light-duty gasoline in China, showed that they accounted for up to 33% of the mass (Guo et al., 2011; Cao et al., 2016). The total concentration of five aromatic compounds at six urban sites in Mumbai was measured to be approximately 27 ( $\pm$  8) ppbv (Pandit et al., 2011). Similar concentrations, of up to approximately 30 ppbv for 11 aromatic compounds, were measured at six sites associated with the petrochemical industry in Yokohama City (Tiwari et al., 2010). Diurnal profiles for  $C_4$  substituted monoaromatics recorded in London, showed a winter-time peak of almost 500 ppbv, associated with traffic pollution (Dunmore et al., 2015). Many techniques struggle to quantify heavy monoaromatic VOC loadings; toluene-equivalent mixing ratios may therefore provide adequate prediction of the additional aromatic content of the atmosphere (Lidster et al., 2014). Toluene-equivalency values account for the aromatic species' concentration relative to toluene and rate of reaction with an atmospheric oxidant and are calculated through Eq. 1.1.

$$[EQ_{Tol}] = [X] \frac{k_{OH+X}}{k_{OH+Tol}} \quad \text{Eq. 1.1}$$

Values for the photochemical ozone creation potential (POCP) for different aromatic species have been calculated for 18 aromatic species (Jenkin et al., 2003), and are presented in Table 1.1.

POCPs describe the relative capability for an organic compound to produce ozone over north-west Europe (Derwent and Jenkin, 1991; Saunders et al., 2003). They are defined relative to ethene, which is given a POCP of 100. The values presented here were calculated using MCM v3. Monosubstituted aromatic species have lower POCP values than the di- and tri-substituted aromatics. Di- and tri-substituted aromatics therefore have POCP values which are comparable to those calculated for many alkenes, meaning that they are some of the species with the greatest potential for forming ozone (Saunders et al., 2003).

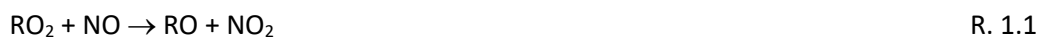
**Table 1.1** POCP values for various aromatic VOCs, as calculated using the MCM v3 (Jenkin et al., 2003). The precision in the POCP is expected to be  $\pm 2$  POCP units.

Name	Photochemical ozone creation potential	$k_{OH} / 10^{-12} \text{ cm}^3 \text{ molecule}^{-1} \text{ s}^{-1}$	Reference
1,2,4-trimethylbenzene	113	$33 \pm 8$	Calvert et al., 2002
1,2,3-trimethylbenzene	108.2	$33 \pm 8$	Calvert et al., 2002
1,3,5-trimethylbenzene	106.2	$57 \pm 11$	Calvert et al., 2002
ethene (reference)	100	$7.8 \left( \begin{smallmatrix} +7.8 \\ -3.9 \end{smallmatrix} \right)$	Atkinson et al., 2006
<i>m</i> -xylene	85.6	$23 \pm 3$	Calvert et al., 2002
<i>o</i> -xylene	84.1	$13 \pm 3$	Calvert et al., 2002
3-ethyltoluene	74	$19 \pm 7$	Calvert et al., 2002
4-ethyltoluene	73.2	$12 \pm 4$	Calvert et al., 2002
2-ethyltoluene	69.4	$12 \pm 4$	Calvert et al., 2002
ethylbenzene	52.5	$7.0 \pm 2$	Calvert et al., 2002
toluene	51	$5.6 \left( \begin{smallmatrix} +1.5 \\ -1.2 \end{smallmatrix} \right)$	Atkinson et al., 2006
<i>n</i> -propylbenzene	42.7	$5.8 \pm 1.5$	Calvert et al., 2002
<i>i</i> -propylbenzene	35.3	$6.3 \pm 2$	Calvert et al., 2002
benzene	20.3	$1.2 \left( \begin{smallmatrix} +0.3 \\ -0.3 \end{smallmatrix} \right)$	Atkinson et al., 2006

### 1.2.3 Atmospheric oxidants

The chemical transformation of molecules into other molecules in the atmosphere is generally initiated by oxidants and/or radical species. Of these, the hydroxyl radical (OH), is the primary oxidant with other major oxidants including ozone (O<sub>3</sub>), the nitrate radical (NO<sub>3</sub>) and the chlorine radical (Cl). NO<sub>3</sub> is an important radical for night time oxidation whilst Cl is thought to be the major oxidant in the marine boundary layer for certain chemical species.

O<sub>3</sub> is transported from the stratosphere, where there is a high concentration, into the troposphere by eddy diffusion (Roelofs and Lelieveld, 1997; Lelieveld and Dentener, 2000; Collins et al., 2003). An additional source of O<sub>3</sub> results from the interaction of VOCs, in the form of RO<sub>2</sub>, and nitrogen oxides (NO<sub>x</sub>) in the presence of sunlight (R. 1.1 through to R. 1.4).



O<sub>3</sub> is destroyed in photochemical cycles via reactions with VOCs. The net balance of production and destruction results in approximate mixing ratios at “clean” sites (low NO<sub>x</sub>) at ground level of up to 10-40 ppbv, whereas in regions associated with urban air pollution (high NO<sub>x</sub>), the mixing ratios can often exceed 100 ppbv.

Tropospheric ozone, no matter the concentration, is extremely important to the chemistry of the atmosphere as its photolysis results in the production of OH, via the O(<sup>1</sup>D) atom (R. 1.5 and R. 1.7). The excited O(<sup>1</sup>D) atom may also deactivate to ground state oxygen through interaction with a neutral molecule such as N<sub>2</sub> or O<sub>2</sub> (R. 1.6).



The above mechanism relies on photolysis and therefore is only applicable to day-time hours. The photolysis of  $\text{NO}_2$  (R. 1.3) results in the formation of  $\text{O}_3$ , which is itself photolysed during the production of the two OH radicals in R. 1.5, R. 1.6 and R. 1.7. Therefore, two photons (of  $\lambda \leq 400$  nm) are capable of producing two OH, which is essential to the chemistry of the troposphere.

The reactions between alkenes and  $\text{O}_3$ , which result in the formation of a carbonyl and a “Criegee intermediate”, can also yield OH (Kroll et al., 2001; Siese et al., 2001). This route for the formation of OH is independent of photolysis and is therefore likely a major night-time source (Paulson and Orlando, 1996), as well as being significant in the winter months at higher latitudes (Harrison et al., 2006). As the rate of ozonolysis of alkenes increases with increasing temperature (Johnson and Marston, 2008), OH production from Criegee intermediates is thought to be more important at the equator, where up to 13% of all OH radicals in forest regions may be formed in this way (Khan et al., 2018).

The reaction between NO and  $\text{O}_3$  leads to the formation of the nitrate radical,  $\text{NO}_3$ , via the formation of  $\text{NO}_2$  (R. 1.8 and R. 1.9).  $\text{NO}_3$  photolyses rapidly during the day, with an approximate lifetime of just 5 s, and is therefore much more important at night.



$\text{NO}_3$  radicals react with  $\text{NO}_2$  and establish an equilibrium with  $\text{N}_2\text{O}_5$  (R. 1.10). In the presence of inorganic chloride containing aerosol, such as sea spray, reactive uptake of  $\text{N}_2\text{O}_5$  onto the aerosol surface can result in the formation of nitryl chloride ( $\text{ClNO}_2$ ; R. 1.11; Finlayson-Pitts et al., 1989; Behnke et al., 1997; Schweitzer et al., 1998; Stewart et al., 2004; Thornton and Abbatt, 2005; Bertram and Thornton, 2009).



$\text{ClNO}_2$  is an efficient photolytic precursor for atomic chlorine with an atmospheric lifetime of less than a few hours after sunrise (R. 1.12; Furlan et al., 2000; Ghosh et al., 2012; Phillips et al., 2012).



### 1.2.4 The HO<sub>x</sub>/NO<sub>x</sub> cycle

Many of the species present in the atmosphere are involved in chemical cycles which result in the chemical production and destruction of ozone. One such way of representing these chemical cycles is through the HO<sub>x</sub>/NO<sub>x</sub> cycle, shown in Figure 1.7. HO<sub>x</sub> (which includes OH and HO<sub>2</sub>) and NO<sub>x</sub> (NO and NO<sub>2</sub>) are intrinsically involved in the photochemical production and destruction of ozone, through the oxidation of VOCs, denoted by RH. Here, the chemical reaction between OH and VOCs is simplified, as simple H-atom abstraction resulting in the production of H<sub>2</sub>O does not always occur, especially for unsaturated or aromatic VOCs. The chemical oxidation of different VOCs is explored below.

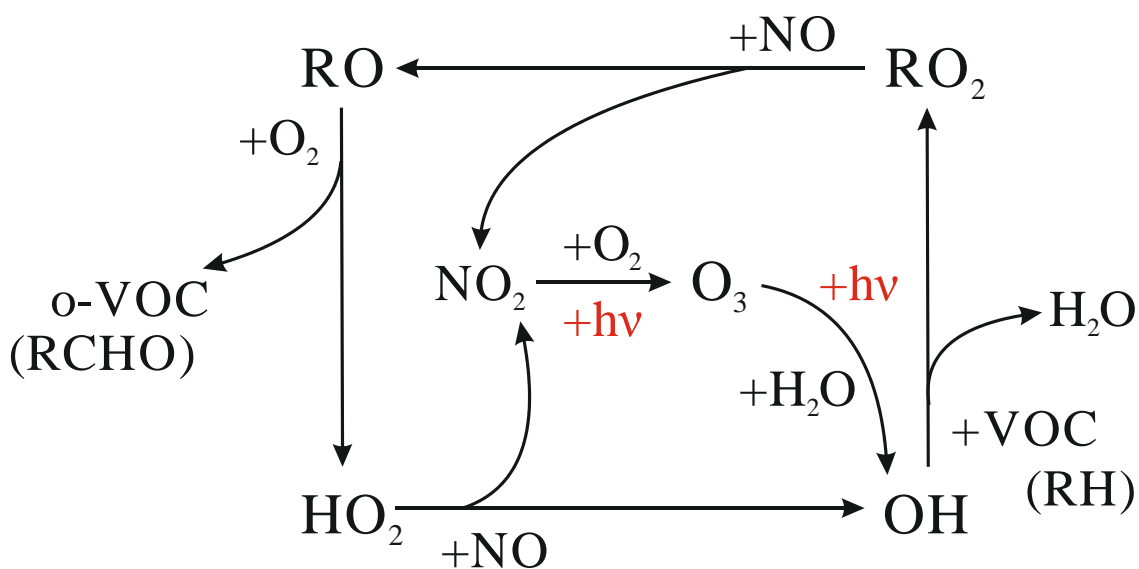


**Figure 1.7** Schematic showing the HO<sub>x</sub>/NO<sub>x</sub> cycle and some of the species involved in the chemical production and destruction of ozone in the troposphere.

## 1.3 VOC oxidation chemistry

Almost all VOC oxidation is initiated by the hydroxyl radical (OH). O<sub>3</sub> as an oxidant is relevant for unsaturated compounds and NO<sub>3</sub> is the primary night-time oxidant. The chlorine radical has gained more widespread attention as an oxidant recently, mainly due to the detection of chlorine radical precursors in mid-continental regions, far removed from marine and coastal environments which were originally thought to be the predominant locations for chlorine based chemical reactions (Osthoff et al., 2008; Thornton et al., 2010; Phillips et al., 2012; Riedel et al., 2012; Tham et al., 2014; Baker et al., 2016).

### 1.3.1 Chemical kinetics

Before reviewing the various oxidation schemes for the interaction between different functionalised VOCs and OH, it is necessary to have an understanding of chemical kinetics. The study of chemical kinetics is fundamental to understanding chemical reactions. Different chemical reactions proceed at different rates. The reaction rate is equal to the rate of removal of the reactants and the rate of production of the products (Eq. 1.2). Many factors can influence the rate of reaction. Therefore, the reaction rate can be averaged over a period of time, or given as an instantaneous rate at a particular point in time, or an initial rate for the start of a certain reaction.

$$\text{rate} = -\frac{\Delta [\text{reactant}]}{\text{time}} = \frac{\Delta [\text{product}]}{\text{time}} \quad \text{Eq. 1.2}$$

The rate of a reaction is dependent on the concentration of the reactants. The dependence of the reaction rate on concentrations is given by rate laws. In general, the rate is proportional to the product of the concentrations of the reactants and some value, referred to as the rate coefficient ( $k$ ), as in Eq. 1.3. The values of  $x$ ,  $y$  and  $z$  in Eq. 1.3 relate to the orders of reaction with respect to the reactants  $A$ ,  $B$  and  $C$ ; the values do not necessarily reflect the stoichiometry of the reaction. The overall reaction order is equal to the sum of  $x$ ,  $y$  and  $z$ . The rate coefficient ( $k$ ) is often referred to as the rate constant but is generally dependent on temperature and, for many reactions in the gas-phase, pressure. Hence, the term rate coefficient and not rate constant will be used throughout this work.

$$\text{rate} = k[A]^x[B]^y[C]^z \quad \text{Eq. 1.3}$$

Consider the reaction R. 1.10, where  $A$  is the reactant and  $k$  is the rate coefficient.



The concentration of A ( $[A]$ ) can be monitored over time. If the order of the reaction is  $n$ , then the differential rate law is given by Eq. 1.4. This expression can be integrated to form the integrated rate law, which provides a relationship between the concentration of the reactants and time. The form of the integrated rate law differs depending on the order of the reaction ( $n$ ). For a first order reaction, the integrated rate law is given by Eq. 1.5, and for a second order reaction, the integrated rate law is given by Eq. 1.6.

$$\frac{d[A]}{dt} = k[A]^n \quad \text{Eq. 1.4}$$

$$\ln\left(\frac{[A]_t}{[A]_0}\right) = -kt \quad \text{Eq. 1.5}$$

$$\frac{1}{[A]} = kt + \frac{1}{[A]_0} \quad \text{Eq. 1.6}$$

### 1.3.2 Reactions with alkanes

Alkanes are an important class of VOCs in that they are ubiquitous in urban areas largely due to their making up a large fraction of vehicle exhaust emissions (see Section 1.2.2.1). They react predominantly with OH and, to a lesser extent Cl and NO<sub>3</sub>, but have almost no interaction with O<sub>3</sub>. The reaction between OH and small alkanes is relatively slow when compared with reactions between other VOCs and OH. The kinetics of the reactions between OH and many alkanes have been measured across many studies. The reactions between OH and alkanes with fewer than four carbon atoms ( $< C_4$ ) are included in the evaluations by IUPAC (Atkinson et al., 2006; <http://iupac.pole-ether.fr/index.html>). A much broader review, encompassing over 50 alkanes with up to 16 carbon atoms and a diverse range of linear, branched and cyclic structures, is provided in Atkinson (2003). As may be expected, the number of studies on the reactions between alkanes and OH decreases with increasing number of carbon atoms. Smaller  $\leq C_5$  alkanes (methane, ethane, propane, *n*-butane, 2-methylpropane, *n*-pentane) benefit from multiple studies utilising a range of both absolute and relative rate methods across a large range in temperature. The extent of data for  $\geq C_6$  alkanes is far smaller, with studies often limited to room temperature and to the relative rate method.

The estimated lifetimes of some alkanes due to reaction with the OH radical (at  $T = 298 \text{ K}$ ) are provided in Table 1.2 using rate coefficients provided in Atkinson (2003) and a 24-hour average

[OH] of  $1 \times 10^6$  molecule  $\text{cm}^{-3}$  (Krol et al., 1998). These values range from periods of approximately 1 day for *n*-decane to 10 days for propane. The lifetime due to reaction with  $\text{O}_3$  is negligible for alkanes. The lifetime due to reaction with the  $\text{NO}_3$  radical is also provided in Table 1.2, using an approximate average  $\text{NO}_3$  concentration of 90 pptv as measured at night in Great Britain (Alliwell and Jones, 1998). This value for night-time  $[\text{NO}_3]$  is highly variable, however, and is entirely dependent on geographic location, with measurements of  $[\text{NO}_3]$  ranging between a few pptv in forest and marine environments to maxima of almost 1 ppbv in polluted regions (Brown and Stutz, 2012).

**Table 1.2** Estimated lifetimes of various alkanes due to reaction with OH (at 298 K), using  $k$  values provided in Atkinson (2003) and a 24-hour average [OH] of  $1 \times 10^6$  molecule  $\text{cm}^{-3}$ . The lifetimes of various alkanes due to reaction with  $\text{NO}_3$  (at 298 K) are also provided, using  $k$  values from Atkinson and Arey (2003) and an approximate night-time  $[\text{NO}_3]$  of 90 pptv.  $k$  values for reaction with Cl were taken from various sources which are noted in the Table footer. The concentration of Cl used was  $10^3$  molecules  $\text{cm}^{-3}$ .

Name	Approximate $\tau_{\text{OH}}$ / days	Approximate $\tau_{\text{NO}_3}$ / days	Approximate $\tau_{\text{Cl}}$ / days
methane	1800	5200	100000 <sup>a</sup>
ethane	47	500	200 <sup>a</sup>
propane	11	75	83 <sup>a</sup>
<i>n</i> -butane	4.9	110	56 <sup>a</sup>
<i>n</i> -pentane	3.1	60	46 <sup>b</sup>
2,2,3-trimethylbutane	3.0	22	65 <sup>c</sup>
cyclopentane	2.3		
<i>n</i> -hexane	2.2	48	38 <sup>b</sup>
<i>n</i> -heptane	1.7	35	34 <sup>b</sup>
cyclohexane	1.7	37	
<i>n</i> -octane	1.4	28	29 <sup>c</sup>
<i>n</i> -nonane	1.2	23	27 <sup>c</sup>
<i>n</i> -decane	1.1	19	24 <sup>c</sup>
<i>n</i> -undecane	0.9		
cycloheptane	0.9		27 <sup>d</sup>
cyclooctane	0.9		25 <sup>d</sup>

<sup>a</sup> Atkinson et al., 2006    <sup>b</sup> Atkinson and Aschmann, 1985    <sup>c</sup> Aschmann and Atkinson, 1995

<sup>d</sup> Aschmann and Atkinson, 2013

### 1.3.2.1 Mechanism and products of alkane + OH reactions

The initial reaction between radical oxidants and alkanes involves H-atom abstraction from the C-H bonds. This reaction forms an alkyl radical ( $R^{\bullet}$ ) which reacts rapidly with  $O_2$  to form an alkyl peroxy radical ( $RO_2^{\bullet}$ ). At this point, the  $RO_2^{\bullet}$  can undergo a number of reactions leading to the formation of alkyl peroxy nitrates, alkyl nitrates, carbonyls, alcohols and hydroperoxides, as shown in Figure 1.8. Larger alkoxy radicals ( $RO^{\bullet}$ ), produced from larger alkanes, are able to undergo isomerisation via a 1,5-hydrogen shift through a six-membered cyclic transition state (Atkinson et al., 1995; Eberhard et al., 1995). The reactions which occur depend on the environment and the chemical species present and may not always involve homogeneous gas-phase interactions (Atkinson et al., 2008).

For the  $C_7$  and higher carbon-number *n*-alkanes, the major products are 1,4-hydroxynitrates and 1,4-hydroxycarbonyls (Arey et al., 2001; Riesen et al., 2005). For branched alkanes, the rate of decomposition rivals that of isomerisation, leading to primarily carbonyl type products (Atkinson, 1997).

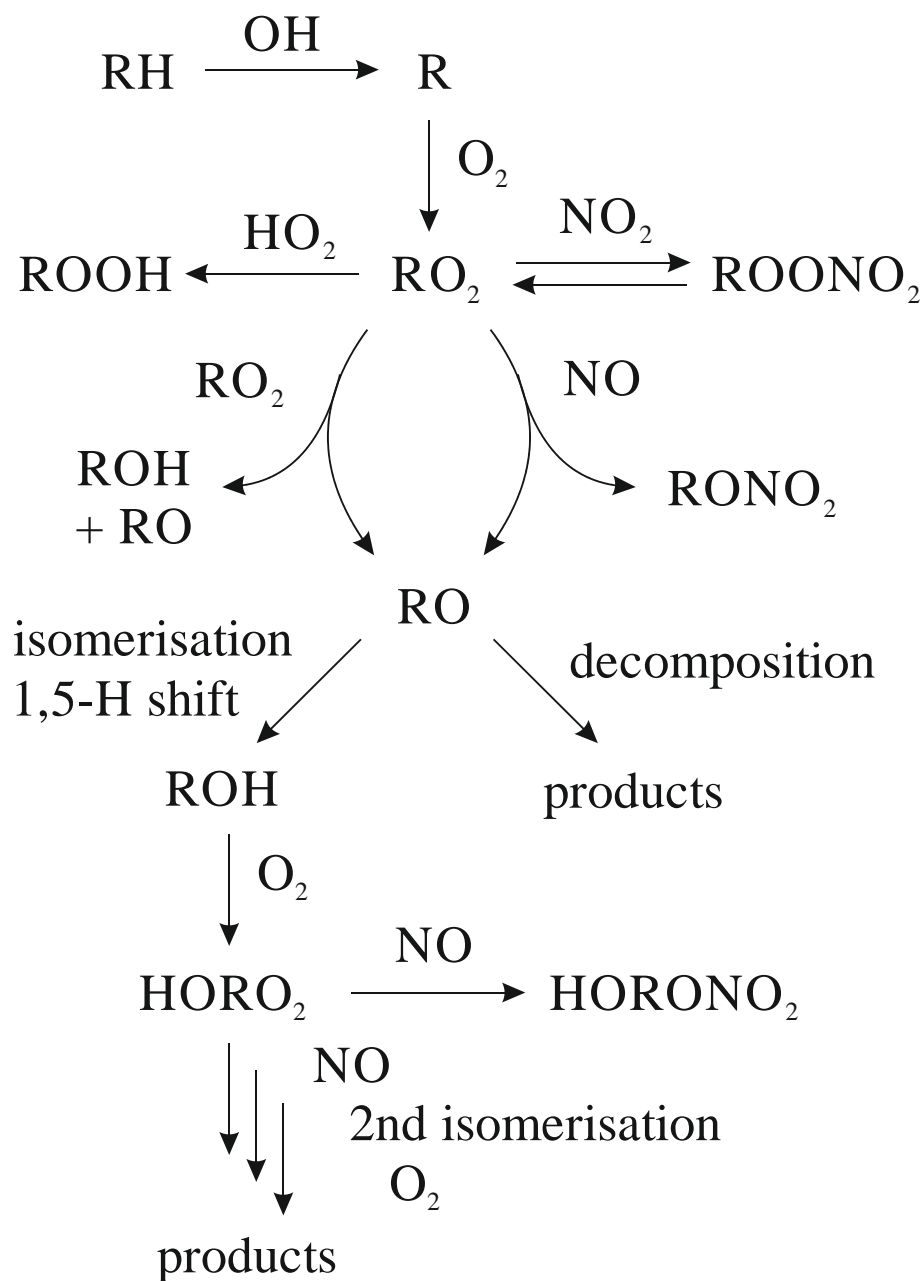


**Figure 1.8** Schematic showing the anticipated reaction pathways resulting from the initial reaction between an alkane (denoted by RH) and OH, as initiated by H-atom abstraction. Adapted from Atkinson et al. (2008).

1,4-hydroxycarbonyls themselves can isomerise to form dihydrofurans (Baker et al., 2005; Holt et al., 2005). Larger alkanes form alkyl-substituted dihydrofurans, which are highly reactive towards OH, NO<sub>3</sub> and O<sub>3</sub> (Martin et al., 2002). These reactions form carbonylestere, a major precursor to secondary organic aerosol (SOA) resulting from alkane oxidation (Lim and Ziemann, 2005). SOA yield increases linearly, from a value of 4% for C<sub>8</sub> to 90% for C<sub>17</sub> *n*-alkanes, with the majority of the SOA resulting from second- and third-generation products (Jordan et al., 2008).

Cyclic alkanes are known to yield more SOA than linear alkanes (Lim and Ziemann, 2009; Ziemann, 2011; Tkacik et al., 2012; Yee et al., 2013). Polycyclic alkanes, containing multiple connected rings, were not found to produce higher yields of SOA than monocyclic alkanes, despite being able to undergo multiple ring opening reactions (Hunter et al., 2014). Rather, unbranched, cyclic structures were found to yield high SOA, due to ring opening preventing fragmentation, followed by efficient functionalisation after reaction with O<sub>2</sub>.

### 1.3.2.2 The temperature dependence of alkane + OH reactions

All bimolecular rate coefficients exhibit some temperature dependency over a sufficiently large range. For example, all values must tend towards zero as the temperature approaches absolute zero (0 K, -273.15 °C). The Arrhenius expression relates the rate coefficient for a particular reaction to temperature (Eq. 1.7).

$$k = Ae^{\frac{-E_a}{RT}} \quad \text{Eq. 1.7}$$

*A* is referred to as the pre-exponential factor and is constant for a chemical reaction. In collision theory, *A* is given by the frequency of collisions which have the correct orientation for reaction to occur. *E<sub>a</sub>* is the activation energy, or the energy barrier which must be overcome for reaction to occur. A reaction which shows positive Arrhenius behaviour (*k* increases with *T*) must tend towards a collision limit at sufficiently high temperature. However, many reactions exhibit complex behaviour; they show both positive and negative temperature dependency across different temperature ranges and therefore have turning points on their Arrhenius plots.

A recent study on the kinetics of the OH radical with large chain > C<sub>10</sub> alkanes found that the rate coefficients for these reactions increase with temperature above 277 K, but are negatively dependent on temperature below 277 K (Phan and Li, 2017). This is in contrast to *n*-alkanes with carbon numbers < C<sub>10</sub>, for which the negative temperature dependent phenomenon is not observed. Phan and Li postulate that complexing of the longer-chain alkanes with water molecules causes structural distortions, weakening the C-H bonds in the -CH<sub>2</sub>- groups and allowing for easier hydrogen abstraction at low temperatures.

Temperature also has a substantial impact on the product yields and overall reactivity of the photochemical system initiated by alkane + OH reactions. Yields of alkyl nitrates and ketones decrease with increasing temperature, whilst yields of aldehydes increase with increasing temperature (Altshuller, 1991).

### 1.3.3 Reactions with alkenes

The oxidation of alkenes, excluding isoprene, in the atmosphere is generally dominated by reaction with  $O_3$ , although this does vary to some extent with structure, altitude and temperature. Despite the predomination of  $O_3$ , the reactions between alkenes and OH are relatively fast when compared with those between alkanes and OH. As for alkanes + OH, the reactions between OH and alkenes with fewer than four carbon atoms ( $< C_4$ ) are included in the evaluations by IUPAC (Atkinson et al., 2006; <http://iupac.pole-ether.fr/index.html>). A much broader evaluation, encompassing over 60 alkenes with up to 10 carbon atoms and a diverse range of linear, branched and cyclic structures, is also provided by Atkinson and Arey (2003).

The estimated lifetimes of some alkenes due to reaction with the OH radical (at 298 K) are provided in Table 1.3 using rate coefficients provided in Atkinson and Arey (2003) and a 24-hour average [OH] of  $1 \times 10^6$  molecule  $cm^{-3}$  (Krol et al., 1998). These values range from periods of approximately 1.6 hours for  $\gamma$ -terpinene to 11 hours for propene. Analogous lifetimes due to reaction with  $O_3$  and  $NO_3$  are also provided in Table 1.3. The concentration used for the calculation of  $\tau_{O_3}$  was 30 ppbv; a rough, modern day annual average ozone concentration in Northern Hemisphere (Vingarzan, 2004). The concentration used for the calculation of  $\tau_{NO_3}$  was the same as that used in the alkane estimations, of 90 pptv (Alliwell and Jones, 1998).

**Table 1.3** Estimated lifetimes of various alkenes due to reaction with OH (at 298 K), using  $k$  values provided in Atkinson and Arey (2003) and a 24-hour average [OH] of  $1 \times 10^6$  molecule  $\text{cm}^{-3}$ . The lifetimes of various alkenes due to reaction with  $\text{O}_3$ ,  $\text{NO}_3$  and Cl (at 298 K) are also provided.  $k$  values for reactions with  $\text{O}_3$  and  $\text{NO}_3$  were taken from Atkinson and Arey (2003) and the concentrations of  $\text{O}_3$  and  $\text{NO}_3$  used were 30 ppbv and 90 pptv respectively.  $k$  values for reaction with Cl were taken from various sources which are noted in the Table footer. The concentration of Cl used was  $10^3$  molecules  $\text{cm}^{-3}$ .

Name	Approximate $\tau_{\text{OH}}$ / hours	Approximate $\tau_{\text{O}_3}$ / hours	Approximate $\tau_{\text{NO}_3}$ / hours	Approximate $\tau_{\text{Cl}}$ / hours
ethene	33	240	600	2800 <sup>a</sup>
1,2-butadiene	11			
propene	11	37	13	1000 <sup>a</sup>
1-butene	8.9	39	9.3	800 <sup>b</sup>
1-pentene	8.9	36	8.4	700 <sup>b</sup>
1,2-pentadiene	7.8			
1-hexene	7.5	33	7.0	700 <sup>c</sup>
1-heptene	6.9	31	6.3	600 <sup>c</sup>
$\alpha$ -pinene	5.3	4.5	0.02	600 <sup>d</sup>
cyclopentene	4.2	0.7	0.3	800 <sup>e</sup>
cyclohexene	4.1	4.6	0.3	700 <sup>e</sup>
cycloheptene	3.8	1.5	0.3	500 <sup>e</sup>
$\beta$ -pinene	3.7	25	0.05	500 <sup>d</sup>
1,3,5-cycloheptatriene	2.9	7.0	0.1	
isoprene	2.8	30	0.2	500 <sup>d</sup>
limonene	1.7	1.8	0.01	400 <sup>d</sup>
$\gamma$ -terpinene	1.6	2.7	0.004	

<sup>a</sup> Atkinson et al., 2006    <sup>b</sup> Ezell et al., 2002    <sup>c</sup> Walavalkar et al., 2013

<sup>d</sup> Finlayson-Pitts et al., 1999    <sup>e</sup> Sharma et al., 2010



Whilst small 1,2-hydroxyalkoxy radicals are thought to primarily undergo decomposition, larger radicals can isomerise via a six-membered transition state (Eberhard et al., 1995; Kwok et al., 1996), much like in the case for the alkoxy radicals in Figure 1.8. However, in the case of monoterpenes, the cyclic structure may mean that this is not always possible (Calogirou et al., 1999).

The reaction of alkenes with OH is in direct competition with the reaction of alkenes with O<sub>3</sub>. Although the rate coefficients for alkene + O<sub>3</sub> reactions are generally much smaller than those for alkene + OH reactions (e.g. Calogirou et al., 1999; Atkinson and Arey, 2003), the concentration of O<sub>3</sub> is generally many orders of magnitude greater than that for OH (see Section 1.2.3). Despite this, oxidation of isoprene by OH is estimated to account for approximately 85% of the fate of tropospheric isoprene during the day (Paulot et al., 2012).

### 1.3.4 Reactions with aromatic compounds

Aromatic VOCs are generally more reactive towards OH than alkanes but less reactive than alkenes. The rate at which different aromatic compounds react with OH is largely dependent on the substituent groups attached to the ring. Electron donating groups, such as alkyl groups, provide a lower barrier for attack onto the delocalised  $\pi$ -electron system, promoting reaction. In contrast, electron withdrawing groups, such as halogens, reduce the reactivity of the aromatic system, inhibiting reaction with OH.

Rate coefficients for the reactions between many aromatics and OH are available in the IUPAC database (Atkinson et al., 2006; <http://iupac.pole-ether.fr/index.html>). However, the majority of the included reactions involve oxygenated or nitrogenated aromatic species, such as cresol and hydroxybenzene. Only two non-oxygenated or non-nitrogenated aromatic species are present; benzene, and toluene, the simplest alkyl substituted aromatic structure. As for the alkenes, a much broader evaluation of aromatic + OH rate coefficients was provided in Atkinson and Arey (2003).

Table 1.4 provides estimated atmospheric lifetimes for some alkyl-substituted monoaromatic hydrocarbons. The values vary from an approximate atmospheric lifetime for benzene of almost 10 days, to those for more highly substituted aromatics of just a few hours. Reaction with ozone is largely unimportant for aromatic compounds but reaction with NO<sub>3</sub> may be of importance at night-time;  $\tau_{\text{NO}_3}$  values are therefore also provided in Table 1.4 for comparison.

**Table 1.4** Estimated lifetimes of various aromatic VOCs due to reaction with OH (at 298 K), using  $k$  values provided in Atkinson and Arey (2003) and a 24-hour average [OH] of  $1 \times 10^6$  molecule  $\text{cm}^{-3}$ . The lifetimes of various aromatic VOCs due to reaction with  $\text{NO}_3$  (at 298 K) are also provided, using  $k$  values from Atkinson and Arey (2003) and an approximate night-time  $[\text{NO}_3]$  of 90 pptv. Some values for  $k_{\text{NO}_3}$  were not provided in Atkinson and Arey (2003) and therefore corresponding approximate  $\tau_{\text{NO}_3}$  values are not included here.

Name	Approximate $\tau_{\text{OH}}$ / days	Approximate $\tau_{\text{NO}_3}$ / days
benzene	9.5	174
<i>t</i> -butylbenzene	2.6	
toluene	2.1	75
<i>n</i> -propylbenzene	2.0	
isopropylbenzene	1.8	8.7
ethylbenzene	1.7	6.1
4-ethyltoluene	1.0	
2-ethyltoluene	1.0	13
<i>o</i> -xylene	0.9	10
<i>p</i> -xylene	0.8	
3-ethyltoluene	0.6	20
<i>m</i> -xylene	0.5	2.9
1,2,4-trimethylbenzene	0.4	2.8
1,2,3-trimethylbenzene	0.4	5.9
1,3,5-trimethylbenzene	0.2	
hexamethylbenzene	0.10	

#### 1.3.4.1 Mechanism and products of aromatic VOC + OH reactions

There are three main pathways that occur during the reaction between an aromatic VOC and OH.

1. Reaction at the aromatic ring through OH addition onto a carbon atom.
2. Reaction at the substituent group(s) via H-atom abstraction by OH.
3. Reaction at the substituent group(s) via OH addition onto any carbon-carbon double bonds present.

Figure 1.10 shows the main anticipated reactions resulting from OH addition to the aromatic ring, resulting in the formation of an OH-aromatic adduct.

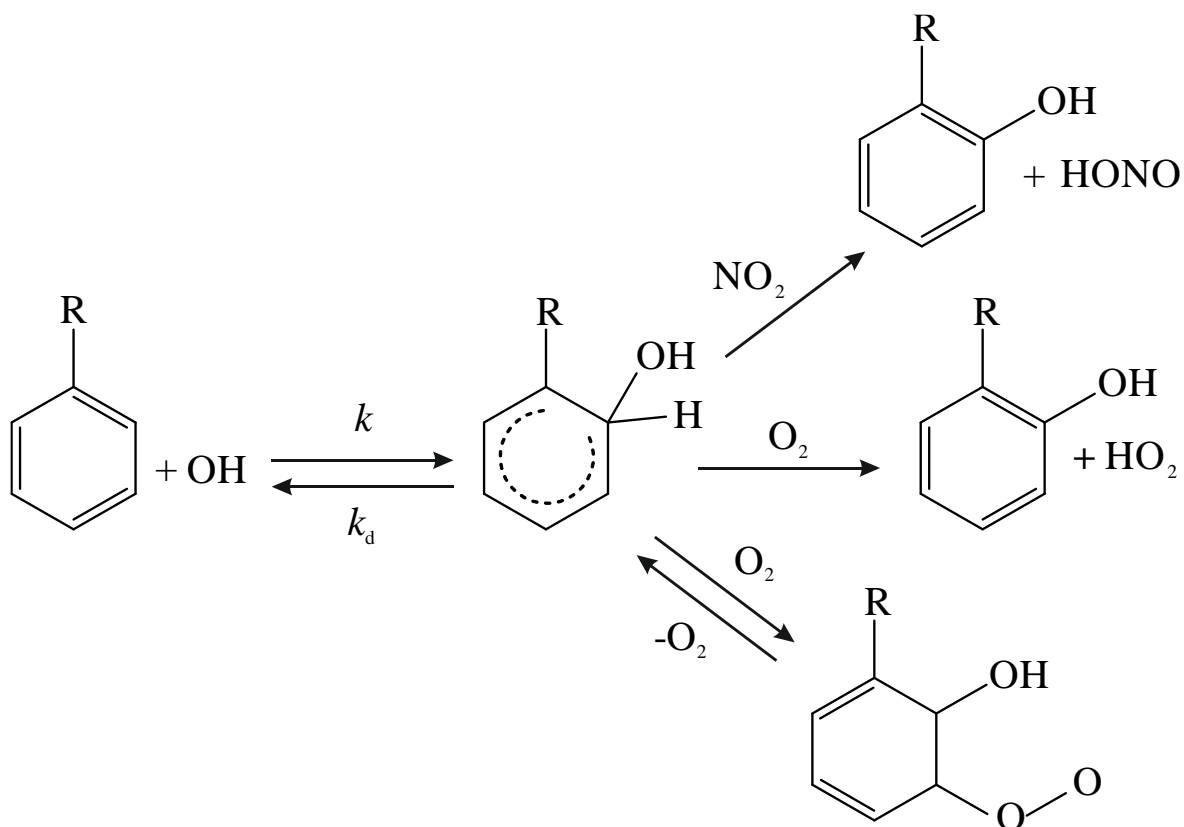


**Figure 1.10** Schematic showing the anticipated reaction pathways resulting from the initial reaction between an aromatic VOC and OH, as initiated by OH addition to the aromatic structure.

For benzene, and the methyl- and ethyl- substituted aromatics, the pathway involving OH addition to the ring is dominant at room temperature, accounting for over 90% of the OH reaction. The product of the OH addition to the ring is a hydroxyalkylcyclohexadienyl radical, or OH-aromatic adduct, which typically reacts with either O<sub>2</sub> or NO<sub>2</sub> in the atmosphere. For the OH-benzene, OH-toluene and OH-xylene adducts, this reaction with O<sub>2</sub> has rate coefficients between  $2\text{--}8 \times 10^{-16} \text{ cm}^3 \text{ molecule}^{-1} \text{ s}^{-1}$  (Bohn and Zetzsch, 1999; Bohn, 2001) and is understood to be irreversible. The rate coefficients for the reaction of OH-benzene, OH-toluene and OH-xylene with NO<sub>2</sub> are on the order of  $3 \times 10^{-11} \text{ cm}^3 \text{ molecule}^{-1} \text{ s}^{-1}$  (Knispel et al., 1990; Koch et al., 1994). The ratio of the O<sub>2</sub>:NO<sub>2</sub> rate coefficients is such that the OH-aromatic adducts will react almost exclusively with O<sub>2</sub> in the atmosphere, except perhaps in the most extreme of environments.

The H-atom abstraction process, of minor importance for benzene and the methyl- and ethyl- substituted aromatics, leads to the formation of benzyl or alkylbenzyl radicals. These react in a similar manner to alkyl radicals (see Sect. 1.3.2), forming benzaldehyde or alkylbenzaldehydes in the process.

Meta-substituted aromatics, such as *m*-xylene, are thought to react quicker than ortho- or para-substituted aromatics due to enhanced electrophilic addition of OH (Ravishankara et al., 1978; Nicovich et al., 1981). *m*-substitution leads to the formation of a resonance stabilised tertiary radical addition product (Mehta et al., 2009).

#### 1.3.4.2 The temperature dependence of aromatic VOC + OH reactions

Arrhenius plots for the reactions between aromatic VOCs and OH tend to exhibit complex behaviour. When plotted over a large range in temperature, two distinct regions are visible. Generally, below 350 K, the rate coefficient for these reactions show little change with temperature. However, at temperatures of approximately 400 K, the rate coefficients rapidly increase with increasing temperature.

It is thought that the OH-aromatic adduct undergoes thermal decomposition at temperatures greater than 325 K. The decomposition rates of some OH-aromatic adducts have been calculated. For the OH-benzene adduct, the recommended thermal decomposition rate constant is approximately  $3.4 \text{ s}^{-1}$  at 298 K (Atkinson, 1989). This means that H-atom abstraction from the substituent group becomes the dominant pathway for aromatic VOC + OH reactions at elevated temperatures.

The atmospheric lifetime of the OH-aromatic adduct is predicted to be approximately 0.3 s at 298 K (Atkinson and Arey, 2003). This rapidly decreases with increasing temperature, to an approximate lifetime of just 20  $\mu\text{s}$  at 450 K.

#### 1.3.5 OH reactivity

The OH reactivity is a measure of the total OH reactivity sink which may be useful for evaluating the contribution of VOCs to atmospheric chemistry. It is equal to the inverse of the lifetime of the OH radical and varies greatly depending on total VOC loading, from milliseconds urban areas to tens of seconds in clean air (Yang et al., 2016). The total OH reactivity ( $k_{OH}$ ) can be calculated using Eq. 1.8 and is equal to the sum of the concentrations of OH reactants ( $[X]$ ) multiplied by their rate coefficients for reaction with OH ( $k_X$ ).

$$k_{OH} = k_{CO}[CO] + k_{NO}[NO] + k_{NO_2}[NO_2] + k_{SO_2}[SO_2] + k_{O_3}[O_3] + \sum_i^n k_{VOC_i}[VOC_i] + \dots$$

Eq. 1.8

OH reactivity can be measured by monitoring the OH decay rate with laser induced fluorescence (e.g. Kovacs and Brune, 2001; Hansen et al., 2015) or by using the comparative reactivity method, in which a compound is used as a reference substance and measured using proton-transfer reaction mass-spectrometry (PTR-MS) or GC methods (e.g. Sinha et al., 2008; Nölscher et al., 2012).

Many field campaigns measuring total OH reactivity have identified a significant mismatch between measured results and modelled or calculated results (see Yang et al., 2016 and references therein). In urban environments, this discrepancy can range from less than 30% to greater than 50%, depending on season and geographic location. Calculated OH reactivity for forested areas also show extensive underestimations compared to measurements. This is referred to as the so-called 'missing reactivity'. It is generally attributed to organic species, and is thought to be caused by unmeasured and unidentified primary emissions and secondary oxidation products. Attempts to identify the causes of the missing reactivity have been made (e.g. Kato et al., 2011).

## 1.4 Measuring gas-phase rate coefficients

Almost all experimental VOC + OH kinetic data used for atmospheric science have been measured in controlled laboratory conditions. An array of different techniques exists for the measurement of gas-phase rate coefficients. These techniques can be broadly categorised as being either absolute measurements, in which the rate coefficient values are obtained by monitoring reactant concentrations directly, or as relative rate, in which the depletion in one VOC is measured relative to that of another with a known rate coefficient. The following sections will describe and contrast a selection of the available methods for measuring gas-phase rate coefficients.

### 1.4.1 Absolute methods

There are various techniques for directly monitoring the rates of reaction and deriving rate coefficients. Many of these techniques employ expensive and complicated equipment such as laser systems and mass spectrometers. Absolute methods generally require the careful measurement of at least one reactant concentration ( $[A]$  and  $[B]$ ) as a function of time. Monitoring both reactants can enhance the accuracy of the rate coefficients obtained (Wollenhaupt et al., 2000; Dillon et al., 2012). The concentrations of these reactants are often low, requiring instrumentation with high sensitivity and good signal-to-noise ratios. Measurements are often time consuming, involving multiple repeats at various time intervals to derive rate coefficient values. For this reason, reaction rates are monitored individually, to avoid interferences with the detection of multiple species which can often have similar chemical properties.

#### 1.4.1.1 Discharge and stopped flow

These techniques employ flow reactors with a movable injector. Continuous flow techniques were first developed in the early 1920s to study the binding rate of carbon monoxide to haemoglobin (Hartridge and Roughton, 1923a; Hartridge and Roughton, 1923b). Stopped-flow techniques were developed somewhat later, finding application again in biological sciences (Chance, 1951; Gibson, 1954). Improvements of temporal resolution to a few microseconds were made using rapid-scanning ultraviolet/visible spectroscopy to aid in enzyme mechanism studies (Brzovic and Dunn, 1995). Stopped-flow techniques were used for the determination of many gas-phase rate coefficients, and elucidation of the mechanisms, for example for the reactions between ozone

and alkenes (Herron and Huie, 1974; Herron and Huie, 1977) and for the reactions between  $\text{NO}_3$  and alkenes (Biggs et al., 1991).

The time between the initiation of the reaction and the point of detection can be measured if the velocity of the gas flow is known. Reactions are generally performed under pseudo-first-order conditions (one of the reactants is in excess of the other) and hence the concentrations of the reactants decrease exponentially over time. A decay-profile of the reactant concentration at the point of detection as a function of the injector position can then be built, with the position of the injector proportional to reaction time.

One of the major limitations of flow techniques resides in the mixing of reactants. These techniques assume that all reactants are uniformly mixed immediately upon injection, but, even when using gases, mixing is not instantaneous. Uniform mixing will therefore only be achieved at some point downstream of the flow reactor, and this may be difficult to quantify and account for. This reliance on the mixing time of reactants generally limits these techniques to slow reactions ( $10^{15} - 10^{19} \text{ cm}^3 \text{ molecule}^{-1} \text{ s}^{-1}$ ; Biggs et al., 1991). However, operating the flows under lower pressures can alleviate this problem by reducing the mixing time.

Other potential complications can also arise from heterogeneous reactions in which the gas-phase molecules interact with the walls of the reactor. These interactions can sometimes catalyse the intended reaction, promote secondary reactions or contribute to the loss of reactant species.

#### 1.4.1.2 Flash photolysis

Flow systems are inhibited by their inability to instantaneously mix reactants together; this limits their applicability to slower chemical reactions. This issue may be overcome by using flash photolysis, in which reactant precursors are premixed before the reaction is initiated. The development of flash photolysis, which allows for extremely fast chemical reactions to be monitored, was awarded the Nobel Prize in Chemistry in 1967 (Porter, 1950). The technique has been used to study the gas-phase recombination of radicals (Trainor and von Rosenberg Jr., 1974) and to investigate the reactions of radicals with VOCs (e.g. Braun and Lenzi, 1967; Wallington and Kurylo, 1987; Dagaut et al., 1990).

Premixing may be done at any pressure so long as the reactant precursors are non-reactive. The reaction is initiated using a pulse of light to generate the reactive species, which are consequently monitored over time. The limiting factor for this method is the length of the pulse of light; if this is

longer than the reaction time, absolute measurements are impossible. However, using pulsed laser photolysis techniques, flash durations of nanoseconds ( $10^{-9}$  s) are routine and it is even possible to employ pulse durations on the timescale of femtoseconds ( $10^{-15}$  s; Wulff et al., 1997; Kawai and Nagamura, 1998).

### 1.4.1.3 Detection techniques

A number of different methods for the detection of reactants (or products) can be employed.

Resonance fluorescence (RF) is often used to measure atomic species, which are electronically excited using a microwave discharge source. As the electronically excited atoms return to the ground state they emit energy in the form of light, in a process known as fluorescence. This light can then be detected via a photomultiplier, with the extent of fluorescence proportional to the concentration of the atomic species. RF has been used in studies of reactions of H atoms (e.g. Clyne and Monkhouse, 1977), Cl atoms (e.g. Bemand and Clyne, 1975), atomic oxygen ( $O^3P$ ; e.g. Slanger and Black, 1970) and in early studies of OH radical reactions (e.g. Zellner and Lorenz, 1984). RF is, however, limited to studying reactions under low pressure and in the absence of  $O_2$ .

Laser induced fluorescence (LIF) uses a similar principle to resonance fluorescence but is especially applicable to molecular species rather than atomic species. Dye lasers can be used to tune the excitation source to match particular transitions for the detected species, hence offering greater specificity. LIF only provides a relative measure of concentration, however, not an absolute measure, as provided by absorption techniques, and therefore must be calibrated with a reference source of OH. LIF is now used for most OH reaction studies (e.g. Dillon et al., 2017) as it can be applied to reaction mixtures in air; LIF is also used as part of the fluorescence assay by gas expansion (FAGE) technique for the detection and measurement of OH in ambient air in the troposphere (e.g. Hard et al., 1984; Commane et al., 2010). LIF has been used in measurements of reactions of  $NO_3$  (e.g. Ravishankara and Mauldin III, 1985),  $O(^1D)$  (e.g. Ravishankara et al., 2002; Dillon et al., 2007) and BrO and IO (e.g. Ingham et al., 1999; Dillon et al., 2006)

Absorption spectroscopy can be used to observe fast reactions. Concentration and absorption are related via the Beer-Lambert Law. Absorption techniques not only provide a direct measure of concentration but they also provide a complete decay trace for each experiment which is handy for self-reactions. Absorption spectroscopy has been used for the determination of rate coefficients for reactions of  $O_3$  (e.g. Hastie et al., 1976), OH (e.g. Nizkorodov et al., 2000),  $RO_2$  (e.g.

Boyd et al., 2003), NO<sub>3</sub> (e.g. Hall et al., 1988) and IO, ClO and BrO (e.g. Bloss et al., 2001; Rowley et al., 2001).

Mass spectrometry (MS) has also been employed to measure the decay of chemical species within chemical reactions (e.g. Morris Jr. et al., 1971; Zhang et al., 2001). MS has advantages in that it can be used to monitor multiple chemicals simultaneously. The concentrations of radicals which are typically used for each of these detection systems does vary; for example, for OH detection using absorption the typical concentrations employed are between 10<sup>12</sup> and 10<sup>14</sup> molecules cm<sup>-3</sup> whereas RF and LIF employ concentrations of between 10<sup>9</sup> and 10<sup>12</sup> molecules cm<sup>-3</sup>.

## 1.4.2 The relative rate method

The relative rate method is an indirect technique for the monitoring of reaction rates and derivation of rate coefficients. Unlike the absolute methods, where the concentration of the radical species must be monitored, the relative rate method requires only monitoring of the VOC, which is often much simpler. Gas chromatography is often the detection method of choice for relative rate methods but Fourier-transform infrared spectroscopy (FTIR) absorption spectroscopy is also commonly employed.

The relative rate method can be illustrated by an example with two reactions. These reactions are monitored simultaneously and both involve OH radicals reacting with two different, but similar, alkanes (R. 1.11 and R. 1.12). One, a reference compound (RH) has a known rate coefficient for its reaction with OH, whilst the other, the target compound (SH) does not.



The concentration of both the reference and target alkanes are then measured as the reaction progresses. As the OH concentration, which does not need to be known, is constant for both alkanes, the rate laws for R. 1.11 and R. 1.12 can be combined:

$$\frac{d[\text{RH}]}{dt} = k_{\text{R}}[\text{OH}][\text{RH}] \quad \text{Eq. 1.9}$$

$$\ln \left( \frac{[\text{RH}]_t}{[\text{RH}]_0} \right) = k_{\text{R}}[\text{OH}]t \quad \text{Eq. 1.10}$$

$$\ln \left( \frac{[\text{RH}]_t}{[\text{RH}]_0} \right) = \frac{k_{\text{R}}}{k_{\text{S}}} \ln \left( \frac{[\text{SH}]_t}{[\text{SH}]_0} \right) \quad \text{Eq. 1.11}$$

A plot of  $\ln\left(\frac{[\text{RH}]_t}{[\text{RH}]_0}\right)$  against  $\ln\left(\frac{[\text{SH}]_t}{[\text{SH}]_0}\right)$  should then yield a straight line, with the slope equal to the ratio of the rate coefficients for the reference and target reactions. This allows for the determination of the rate coefficient for the reaction of the target alkane (SH) with OH, often at high precision with  $R^2$  values approaching 0.99 for the linear regressions.

An important assumption must be made when using the relative rate method; the compounds must be assumed to only react with OH and nothing else. If either of the compounds react differently with any other potential oxidants, this would cause interferences in the observed relative depletions. These interferences must therefore be accounted for.

The technique is also somewhat limited to using reference compounds for which rate coefficients for reaction are already well measured. Fortunately, the simplicity of calculating new rate coefficients using this technique means that adjustments to recommended values for reference rate coefficients can be carried forward, long after the original measurements have been made.

#### 1.4.2.1 OH relative rate methods

The relative rate method has been used extensively for investigating and determining rate coefficients for reactions between OH and many VOCs.

Both photolytic systems and non-photolytic systems have been employed for the generation of OH radicals. Early examples of photolytic OH production include; the photolysis of  $\text{H}_2\text{O}_2$  at 253.7 nm (e.g. Gorse and Volman, 1972), the photolysis of HONO (e.g. Cox, 1975; Niki et al., 1978), and the photolysis of  $\text{NO}_x$ -organic-air mixtures (e.g. Doyle et al., 1975; Wu et al., 1976; Darnall et al., 1978). Photolysis of HONO-NO-air and methyl nitrite-NO-air systems yield higher concentrations of OH radicals, of approximately  $10^7 - 10^8$  molecules  $\text{cm}^{-3}$  (Atkinson et al., 1981; Cox et al., 1981; Atkinson et al., 1982). More recent sources have also utilised the photolysis of  $\text{CH}_3\text{ONO}$  at  $> 300$  nm (Aschmann et al., 2013) or the photolysis of  $\text{O}_3$  in the presence of excess  $\text{H}_2\text{O}$  (Bernard et al., 2018; Guo et al., 2018) or  $\text{H}_2$  (Srinivasulu et al., 2018).

Non-photolytic sources of OH include; the  $\text{H}_2\text{O}_2$ - $\text{NO}_2$  reaction system (Campbell et al., 1976), the  $\text{N}_2\text{H}_4 + \text{O}_3$  reaction (Tuazon et al., 1983) and the thermal decomposition of  $\text{HO}_2\text{NO}_2$  (Barnes et al., 1982).

Relative rate studies have been performed to derive rate coefficients for OH reactions with many different functionalities, including; alkanes (e.g. Atkinson et al., 1982; Harris and Kerr, 1988;

Wilson et al., 2006), cycloalkanes (e.g. Singh et al., 2013), alkenes (e.g. Darnall et al., 1976; Atkinson and Aschmann, 1984; da Silva Barbosa et al., 2015), monoterpenes (e.g., Atkinson et al., 1986; Kim et al., 2011), sesquiterpenes (e.g. Shu and Atkinson, 1995), aromatic hydrocarbons (e.g. Atkinson and Aschmann, 1989; Kramp and Paulson, 1998; Aschmann et al., 2013), polycyclic aromatic hydrocarbons (e.g. Brubaker Jr. and Hites, 1998; Phouongphouang and Arey, 2002), aldehydes (e.g. Alvarado et al., 1998; Baker et al., 2004), ketones (e.g. Baker et al., 2005), ethers (e.g. Coeur-Tourneur et al., 2010; Lauraguais et al., 2015) and chlorinated hydrocarbons (e.g. Edney et al., 1986) amongst others.

## References

- Aliwell, S. R. and Jones, R. L.: Measurements of tropospheric NO<sub>3</sub> at midlatitude, *J. Geophys. Res.*, 103, 5719-5727, <https://doi.org/10.1029/97JD03119>, 1998.
- Altshuller, A. P.: Chemical reactions and transport of alkanes and their products in the troposphere, *J. Atmos. Chem.*, 12, 19-61, <https://doi.org/10.1007/BF00053933>, 1991.
- Alvarado, A., Arey, J. and Atkinson, R.: Kinetics of the gas-phase reactions of OH and NO<sub>3</sub> radicals and O<sub>3</sub> with the monoterpene reaction products pinonaldehyde, caronaldehyde, and sabinaketone, *J. Atmos. Chem.*, 31, 3, 281-297, <https://doi.org/10.1023/A:1006010915971>, 1998.
- Arey, J., Aschmann, S. M., Kwok, E. S. C. and Atkinson, R.: Alkyl nitrate, hydroxyalkyl nitrate and hydroxycarbonyl formation from the NO<sub>x</sub>-air photooxidations of C<sub>5</sub>-C<sub>8</sub> *n*-alkanes, *J. Phys. Chem. A*, 105, 1020-1027, <https://doi.org/10.1021/jp003292z>, 2001.
- Aschmann, S. M. and Atkinson, R.: Rate constants for the gas-phase reactions of alkanes with Cl atoms at 296 ± 2 K, *Int. J. Chem. Kinet.*, 27, 613-622, 1995.
- Aschmann, S. M. and Atkinson, R.: Rate constants for the reactions of Cl atoms with a series of C<sub>6</sub>-C<sub>10</sub> cycloalkanes and cycloketones at 297 ± 2 K, *Int. J. Chem. Kinet.*, 45, 52-58, <https://doi.org/10.1002/kin.20743>, 2013.
- Aschmann, S. M., Arey, J. and Atkinson, R.: Rate constants for the reactions of OH radicals with 1,2,4,5-tetramethylbenzene, pentamethylbenzene, 2,4,5-trimethylbenzaldehyde, 2,4,5-trimethylphenol, and 3-methyl-3-hexene-2,5-dione and products of OH + 1,2,4,5-tetramethylbenzene, *J. Phys. Chem. A*, 117, 12, 2556-2568, <https://doi.org/10.1021/jp400323n>, 2013.
- Atkinson, R., Carter, W. P. L., Winer, A. M. and Pitts Jr., J. N.: An experimental protocol for the determination of OH radical rate constants with organics using methyl nitrite photolysis as an OH radical source, *JAPCA J. Air Waste Ma.*, 31, 10, 1090-1092, <https://doi.org/10.1080/00022470.1981.10465331>, 1981.

- Atkinson, R., Aschmann, S. M., Winer, A. M. and Pitts Jr., J. N.: Rate constants for the reaction of OH radicals with a series of alkanes and alkenes at  $299 \pm 2$  K, *Int. J. Chem. Kinet.*, 14, 5, 507-516, <https://doi.org/10.1002/kin.550140508>, 1982.
- Atkinson, R. and Aschmann, S. M.: Rate constants for the reaction of OH radicals with a series of alkenes and dialkenes at  $295 \pm 1$  K, *Int. J. Chem. Kinet.*, 16, 1175-1186, <https://doi.org/10.1002/kin.550161002>, 1984.
- Atkinson, R. and Aschmann, S. M.: Kinetics of the gas phase reaction of Cl atoms with a series of organics at  $296 \pm 2$  K and atmospheric pressure, *Int. J. Chem. Kinet.*, 17, 33-41, 1985.
- Atkinson, R., Aschmann, S. M. and Pitts Jr., J. N.: Rate constants for the gas-phase reactions of the OH radical with a series of monoterpenes at  $294 \pm 1$  K, *Int. J. Chem. Kinet.*, 18, 3, 287-299, <https://doi.org/10.1002/kin.550180303>, 1986.
- Atkinson, R. and Aschmann, S. M.: Rate constants for the gas-phase reactions of the OH radical with a series of aromatic hydrocarbons at  $296 \pm 2$  K, *Int. J. Chem. Kinet.*, 21, 5, 355-365, <https://doi.org/10.1002/kin.550210506>, 1989.
- Atkinson, R., Kwok, E. S. C., Arey, J. and Aschmann, S. M.: Reactions of alkoxy radicals in the atmosphere, *Faraday Discuss.*, 100, 23-37, <https://doi.org/10.1039/FD9950000023>, 1995.
- Atkinson, R.: Atmospheric reactions of alkoxy and  $\beta$ -hydroalkoxy radicals, *Int. J. Chem. Kinet.*, 29, 99-111, [https://doi.org/10.1002/\(SICI\)1097-4601\(1997\)29:2<99::AID-KIN3>3.0.CO;2-F](https://doi.org/10.1002/(SICI)1097-4601(1997)29:2<99::AID-KIN3>3.0.CO;2-F), 1997.
- Atkinson, R.: Kinetics of the gas-phase reactions of OH radicals with alkanes and cycloalkanes, *Atmos. Chem. Phys.*, 3, 2233-2307, <https://doi.org/10.5194/acp-3-2233-2003>, 2003.
- Atkinson, R. and Arey, J.: Gas-phase tropospheric chemistry of biogenic volatile organic compounds: A review, *Atmos. Environ.*, 37, S197-S219, [https://doi.org/10.1016/S1352-2310\(03\)00391-1](https://doi.org/10.1016/S1352-2310(03)00391-1), 2003.
- Atkinson, R., Baulch, D. L., Cox, R. A., Crowley, J. N., Hampson, R. F., Hynes, R. G., Jenkin, M. E., Rossi, M. J., Troe, J. and IUPAC Subcommittee: Evaluated kinetic and photochemical data for atmospheric chemistry: Volume II – gas-phase reactions of organic species, *Atmos. Chem. Phys.*, 6, 3625-4055, <https://doi.org/10.5194/acp-6-3625-2006>, 2006.

- Atkinson, R., Arey, J. and Aschmann, S. M.: Atmospheric chemistry of alkanes: review and recent developments, *Atmos. Environ.*, 42, 5859-5871, <https://doi.org/10.1016/j.atmosenv.2007.08.040>, 2008.
- Baker, A. K., Sauvage, C., Thorenz, U. R., van Velthoven, P., Oram, D. E., Zahn, A., Brenninkmeijer, C. A. M. and Williams, J.: Evidence for strong, widespread chlorine radical chemistry associated with pollution outflow from continental Asia, *Sci. Rep.-UK*, 6, <https://doi.org/10.1038/srep36821>, 36821, 2016.
- Baker, J., Arey, J. and Atkinson, R.: Rate constants for the gas-phase reactions of OH radicals with a series of hydroxyaldehydes at  $296 \pm 2$  K, *J. Phys. Chem. A*, 108, 34, 7032-7037, <https://doi.org/10.1021/jp048979o>, 2004.
- Baker, J., Arey, J. and Atkinson, R.: Rate constants for the reactions of OH radicals with a series of 1,4-hydroxyketones, *J. Photoch. Photobio. A*, 176, 231-237, <https://doi.org/10.1016/j.jphotochem.2005.07.022>, 2005.
- Barletta, B., Simpson, I. J., Blake, N. J., Meinardi, S., Emmons, L. K., Aburizaiza, O. S., Siddique, A., Zeb, J., Yu, L. E., Khwaja, H. A., Farrukh, M. A. and Blake, D. R.: Characterisation of carbon monoxide, methane and nonmethane hydrocarbons in emerging cities of Saudi Arabia and Pakistan and in Singapore, *J. Atmos. Chem.*, 74, 1, 87-113, <https://doi.org/10.1007/s10874-01609343-7>, 2017.
- Barnes, I., Bastian, V., Becker, K. H., Fink, E. H. and Zabel, F.: Reactivity studies of organic substances towards hydroxyl radicals under atmospheric conditions, *Atmos. Environ.*, 16, 3, 545-550, [https://doi.org/10.1016/0004-6981\(82\)90163-9](https://doi.org/10.1016/0004-6981(82)90163-9), 1982.
- Behnke, W., George, C., Scheer, V. and Zetzsch, C.: Production and decay of ClNO<sub>2</sub> from the reaction of gaseous N<sub>2</sub>O<sub>5</sub> with NaCl solution: Bulk and aerosol experiments, *J. Geophys. Res.*, 102, D3, 3795-3804, <https://doi.org/10.1029/96JD03057>, 1997.
- Bemand, P. B. and Clyne, M. A. A.: Atomic resonance fluorescence spectrometry for rate constants of rapid bimolecular reactions. Part 4 – Chlorine atom fluorescence  $4s^{2,4}P - 3p^{5,2}P$ , *J. Chem. Soc. Faraday Trans. 2*, 71, 1132-1144, <https://doi.org/10.1039/F29757101132>, 1975.

- Benkelberg, H.-J., Böge, O., Seuwen, R. and Warneck, P.: Product distributions from the OH radical-induced oxidation of but-1-ene, methyl substituted but-1-enes and isoprene in NO<sub>x</sub>-free air, *Phys. Chem. Chem. Phys.*, 2, 4029-4039, <https://doi.org/10.1039/b002053m>, 2000.
- Bernard, F., Papanastasiou, D. K., Papadimitriou, V. C. and Burkholder, J. B. Temperature dependent rate coefficients for the gas-phase reaction of the OH radical with linear (L<sub>2</sub>, L<sub>3</sub>) and cyclic (D<sub>3</sub>, D<sub>4</sub>) permethylsiloxanes, *J. Phys. Chem. A*, 122, 4252-4264, <https://doi.org/10.1021/acs.jpca.8b01908>, 2018.
- Bertram, T. H. and Thornton, J. A.: Toward a general parameterisation of N<sub>2</sub>O<sub>5</sub> reactivity on aqueous particles: The competing effects of particle liquid water, nitrate and chloride, *Atmos. Chem. Phys.*, 9, 8351-8363, <https://doi.org/10.5194/acp-9-8351-2009>, 2009.
- Biggs, P., Boyd, A. A., Canosa-Mas, C. E., Joseph, D. M. and Wayne, R. P.: A discharge stopped-flow technique for time-resolved studies of slow radical reactions in the gas phase, *Meas. Sci. Technol.*, 2, 675-678, <https://doi.org/10.1088/0957-0233/2/7/017>, 1991.
- Bloss, W. J., Nickolaisen, S. L., Salawitch, R. J., Friedl, R. R. and Sander, S. P.: Kinetics of the ClO self-reaction and 210 nm absorption cross section of the ClO dimer, *J. Phys. Chem. A*, 105, 11226-11239, <https://doi.org/10.1021/jp012429y>, 2001.
- Bohn, B. and Zetzsch, C.: Gas-phase reaction of the OH-benzene adduct with O<sub>2</sub>: Reversibility and secondary formation of HO<sub>2</sub>, *Phys. Chem. Chem. Phys.*, 1, 5097-5107, <https://doi.org/10.1039/A904887A>, 1999.
- Bohn, B.: Formation of peroxy radicals from OH-toluene adducts and O<sub>2</sub>, *J. Phys. Chem. A*, 105, 6092-6101, <https://doi.org/10.1021/jp0033972>, 2001.
- Boyd, A. A., Flaud, P.-M., Daugey, N. and Lesclaux, R.: Rate constants for RO<sub>2</sub> + HO<sub>2</sub> reactions measured under a large excess of HO<sub>2</sub>, *J. Phys. Chem. A*, 107, 818-821, <https://doi.org/10.1021/jp026581r>, 2003.
- Braun, W. and Lenzi, M.: Resonance fluorescence method for kinetics of atomic reactions. Reactions of atomic hydrogen with olefins, *Discuss. Faraday Soc.*, 44, 252-262, <https://doi.org/10.1039/DF9674400252>, 1967.

- Brown, S. S. and Stutz, J.: Night-time radical observations and chemistry, *Chem. Soc. Rev.*, 41, 6405-6447, <https://doi.org/10.1039/c2cs35181a>, 2012.
- Brubaker Jr., W. W. and Hites, R. A.: OH reaction kinetics of polycyclic aromatic hydrocarbons and polychlorinated dibenzo-*p*-dioxins and dibenzofurans, *J. Phys. Chem. A*, 102, 915-921, <https://doi.org/10.1021/jp9721199>, 1998.
- Brzovic, P. S. and Dunn, M. F.: Rapid-scanning ultraviolet/visible spectroscopy applied in stopped-flow studies, *Method. Enzymol.*, 246, 168-201, [https://doi.org/10.1016/0076-6879\(95\)46010-1](https://doi.org/10.1016/0076-6879(95)46010-1), 1995.
- Calvert, J. G., Atkinson, R., Becker, K. H., Kamens, R. M., Seinfeld, J. H., Wallington, T. J. and Yarwood, G.: The mechanisms of atmospheric oxidation of aromatic hydrocarbons, Oxford University Press, New York, 2002.
- Campbell, I. M., Handy, B. J. and Kirby, R. M.: Gas phase chain reaction of  $\text{H}_2\text{O}_2 + \text{NO}_2 + \text{CO}$ , *J. Chem. Soc. Farad. T.* 1, 71, 867-874, <https://doi.org/10.1039/F1975100867>, 1975.
- Cao, X., Yao, Z., Shen, X., Ye, Y. and Jiang, X.: On-road emission characteristics of VOCs from light-duty gasoline vehicles in Beijing, China, *Atmos. Environ.*, 124, 146-155, <https://doi.org/10.1016/j.atmosenv.2015.06.19>, 2016.
- Chance, B.: Rapid and sensitive spectrophotometry III. A double beam apparatus, *Rev. Sci. Inst.*, 22, 634, <https://doi.org/10.1063/1.1746021>, 1951.
- Clyne, M. A. A. and Monkhouse, P. B.: Atomic resonance fluorescence for rate constants of rapid bimolecular reactions. Part 5 – Hydrogen atom reactions;  $\text{H} + \text{NO}_2$  and  $\text{H} + \text{O}_3$ , *J. Chem. Soc. Faraday Trans. 2*, 73, 298-309, <https://doi.org/10.1039/F29777300298>, 1977.
- Coeur-Tourneur, C., Cassez, A. and Wenger, J. C.: Rate coefficients for the gas-phase reaction of hydroxyl radicals with methoxyphenol (guaiacol) and related compounds, *J. Phys. Chem. A*, 114, 43, 11645-11650, <https://doi.org/10.1021/jp1071023>, 2010.
- Collins, W. J., Derwent, R. G., Garnier, B., Johnson, C. E., Sanderson, M. G. and Stevenson, D. S.: Effect of stratosphere troposphere exchange on the future tropospheric ozone trend, *J. Geophys. Res.*, 108, 8528, <https://doi.org/10.1029/2002JD002617>, 2003.

- Comman, R., Floquet, C. F. A., Ingham, T., Stone, D., Evans, M. J. and Heard, D. E.: Observations of OH and HO<sub>2</sub> radicals over West Africa, *Atmos. Chem. Phys.*, **10**, 8783-8801, <https://doi.org/10.5194/acp-10-8783-2010>, 2010.
- Cox, R. A.: The photolysis of nitrous acid in the presence of carbon monoxide and sulphur dioxide, *J. Photochem.*, **3**, 2, 291-304, [https://doi.org/10.1016/0047-2670\(74\)80038-9](https://doi.org/10.1016/0047-2670(74)80038-9), 1974.
- Cox, R. A., Patrick, K. A. and Chant, S. A.: Mechanism of atmospheric photooxidation of organic compounds. Reactions of alkoxy radicals in oxidation of *n*-butane and simple ketones, *Environ. Sci. Technol.*, **15**, 5, 587-592, <https://doi.org/10.1021/es00087a011>, 1981.
- da Silva Barbosa, T., Peirone, S., Barrera, J. A., Abrate, J. P., Lane, S. I., Arbilla, G. and Bauerfeldth, G. F.: Rate coefficients for the reaction of OH radicals with *cis*-3-hexene: an experimental and theoretical study, *Phys. Chem. Chem. Phys.*, **17**, 8714-8722, <https://doi.org/10.1039/C4CP05760K>, 2015.
- Dagaut, P., Liu, R., Wallington, T. J. and Kurylo, M. J.: Flash photolysis resonance fluorescence investigation of the gas-phase reactions of hydroxyl radicals with cyclic ethers, *J. Phys. Chem.*, **94**, 5, 1881-1883, <https://doi.org/10.1012/j100368a030>, 1990.
- Darnall, K. R., Winer, A. M., Lloyd, A. C. and Pitts Jr., J. N.: Relative rate constants for the reaction of OH radicals with selected C<sub>6</sub> and C<sub>7</sub> alkanes and alkenes at 305 ± 2 K, *Chem. Phys. Lett.*, **44**, 3, 415-418, [https://doi.org/10.1016/0009-2614\(76\)80695-1](https://doi.org/10.1016/0009-2614(76)80695-1), 1976.
- Darnall, K. R., Atkinson, R. and Pitts Jr., J. N.: Rate constants for the reaction of the hydroxyl radical with selected alkanes at 300 K, *J. Phys. Chem.*, **82**, 14, 1581-1584, <https://doi.org/10.1021/j100503a001>, 1978.
- Derwent, R. G. and Jenkin, M. E.: Hydrocarbons and the long-range transport of ozone and PAN across Europe, *Atmos. Environ.*, **25A**, 1661-1678, [https://doi.org/10.1016/0960-1686\(91\)90025-3](https://doi.org/10.1016/0960-1686(91)90025-3), 1991.
- Dillon, T. J., Karunanandan, R. and Crowley, J. N.: The reaction of IO with CH<sub>3</sub>SCH<sub>3</sub>: products and temperature dependent rate coefficients by laser induced fluorescence, *Phys. Chem. Chem. Phys.*, **8**, 847-855, <https://doi.org/10.1039/B514718B>, 2006.

- Dillon, T. J., Horowitz, A. and Crowley, J. N.: Absolute rate coefficients for the reactions of O(<sup>1</sup>D) with a series of *n*-alkanes, Chem. Phys. Lett., 443, <https://doi.org/10.1016/j.cplett.2007.06.044>, 2007.
- Dillon, T. J., Tucceri, M. E., Dulitz, K., Horowitz, A., Vereecken, L. and Crowley, J. N.: Reaction of hydroxyl radicals with C<sub>4</sub>H<sub>5</sub>N (pyrrole): Temperature and pressure dependent rate coefficients, J. Phys. Chem. A, 116, 24, 6051-6058, <https://doi.org/10.1021/jp211241x>, 2012.
- Dillon, T. J., Dulitz, K., Groß, C. B. M. and Crowley, J. N.: Temperature-dependent rate coefficients for the reactions of the hydroxyl radical with the atmospheric biogenics isoprene, alpha-pinene and delta-3-carene, Atmos. Chem. Phys., 17, 15137-15150, <https://doi.org/10.5194/acp-17-15137-2017>, 2017.
- Dlugokencky, E.: Trends in atmospheric methane, NOAA/ESRL, [www.esrl.noaa.gov/gmd/ccgg/trends\\_ch4/](http://www.esrl.noaa.gov/gmd/ccgg/trends_ch4/), accessed 10/05/2018, 2018.
- Doyle, G. J., Lloyd, A. C., Darnall, K. R., Winer, A. M., Pitts Jr., J. N.: Gas phase kinetic study of relative rates of reaction of selected aromatic compounds with hydroxyl radicals in an environmental chamber, Environ. Sci. Technol., 9, 3, 237-241, <https://doi.org/10.1021/es60101a002>, 1975.
- Dunmore, R. E., Hopkins, J. R., Lidster, R. T., Lee, J. D., Evans, M. J., Rickard, A. R., Lewis, A. C. and Hamilton, J. F.: Diesel-related hydrocarbons can dominate gas-phase reactive carbon in megacities, Atmos. Chem. Phys., 15, 9983-9996, <https://doi.org/10.5194/acp-15-9983-2015>, 2015.
- Eberhard, J., Müller, C., Stocker, D. W. and Kerr, J. A.: Isomerisation of alkoxy radicals under atmospheric conditions, Env. Sci. Technol., 29, 232-241, <https://doi.org/10.1021/es00001a600>, 1995.
- Edney, E. O., Kleindienst, T. E. and Corse, E. W.: Room temperature rate constants for the reaction of OH with selected chlorinated and oxygenated hydrocarbons, Int. J. Chem. Kinet., 18, 12, 1355-1371, <https://doi.org/10.1002/kin.550181207>, 1986.

- Eggertsen, F. T. and Nelsen, F. M.: Gas chromatographic analysis of engine exhaust and atmosphere; determination of C<sub>2</sub> to C<sub>5</sub> hydrocarbons, *Anal. Chem.*, 30, 6, 1040-1043, <https://doi.org/10.1021/ac60138a009>, 1958.
- Erickson, M. H., Gueneron, M. and Jobson, B. T.: Measuring long chain alkanes in diesel engine exhaust by thermal desorption PTR-MS, *Atmos. Meas. Tech.*, 7, 225-239, <https://doi.org/10.5194/amt-7-225-2014>, 2014.
- Ezell, M. J., Wang, W., Ezell, A. A., Soskin, G. and Finlayson-Pitts, B. J.: Kinetics of reactions of chlorine atoms with a series of alkenes at 1 atm and 298 K: structure and reactivity, *Phys. Chem. Chem. Phys.*, 4, 5318-5820, <https://doi.org/10.1039/b207529f>, 2002.
- Favre, H. A. and Powell, W. H.: *Nomenclature of Organic Chemistry: IUPAC Recommendations and Preferred Names*, IUPAC Chemical Nomenclature and Structure Representation Division, Royal Society of Chemistry, 2013.
- Finlayson-Pitts, B. J., Ezell, M. J. and Pitts Jr., J. N.: Formation of chemically active chlorine compounds by reactions of atmospheric NaCl particles with gaseous N<sub>2</sub>O<sub>5</sub> and ClONO<sub>2</sub>, *Nature*, 337, 241-244, <https://doi.org/10.1038/337241a0>, 1989.
- Finlayson-Pitts, B. J., Keoshian, C. J., Buehler, B. and Ezell, A. A.: Kinetics of reaction of chlorine atoms with some biogenic organics, *Int. J. Chem. Kinet.*, 31, 491-499, 1999.
- Fuentes, J. D., Lerdau, M., Atkinson, R., Baldocchi, D., Bottenheim, W., Ciccioli, P., Lamb, B., Geron, C., Gu, L., Guenther, A., Sharkey, T. D. and Stockwell, W.: Biogenic hydrocarbons in the atmospheric boundary layer: a review, *B. Am. Meteorol. Soc.*, 81, 7, 1537-1575, [https://doi.org/10.1175/1520-0477\(2000\)081<1537:BHITAB>2.3.CO;2](https://doi.org/10.1175/1520-0477(2000)081<1537:BHITAB>2.3.CO;2), 2000.
- Furlan, A., Haeberli, M. A. and Huber, J. R.: The 248 nm photodissociation of ClNO<sub>2</sub> studied by photofragment translational energy spectroscopy, *J. Phys. Chem. A*, 104, 45, 10392-10397, <https://doi.org/10.1021/jp000792j>, 2000.
- Ghosh, B., Papanastasiou, D. K., Talukdar, R. K., Roberts, J. M. and Burkholder, J. B.: Nitryl chloride (ClNO<sub>2</sub>): UV/Vis absorption spectrum between 210 and 296 K and O(<sup>3</sup>P) quantum yield at 193 and 248 nm, *J. Phys. Chem. A*, 116, 24, 5796-5805, <https://doi.org/10.1021/jp207389y>, 2012.

- Gibson, Q. H.: Stopped-flow apparatus for the study of rapid reactions, *Discuss. Faraday Soc.*, 17, 137-139, <https://doi.org/10.1039/DF9541700137>, 1954.
- Gleckauf, E.: Composition of the Atmosphere, in *Compendium of Meteorology*, Malone, T. F., American Meteorological Society, Boston, 1951.
- Goldstein, A. H. and Galbally, I. E.: Known and unexplored organic constituents in the Earth's atmosphere, *Env. Sci. Technol.*, 41, 5, 1514-1521, <https://doi.org/10.1021/es072476p>, 2007.
- Gorse, R. A. and Volman, D. H.: Photochemistry of the gaseous hydrogen peroxide-carbon monoxide system: Rate constants for hydroxyl radical reactions with hydrogen peroxide and isobutane by competitive kinetics, *J. Photochem.*, 1, 1, 1-10, [https://doi.org/10.1016/0047-2670\(72\)80001-7](https://doi.org/10.1016/0047-2670(72)80001-7), 1972.
- Graedel, T. E.: *Chemical Compounds in the Atmosphere*, Academic Press, New York, 1978.
- Greenberg, J. P., Guenther, A. B., Petron, G., Wiedinmyer, C., Vega, O., Gatti, L. V., Tota, J. and Fisch, G.: Biogenic VOC emissions from forested Amazonian landscapes, *Global Change Biol.*, 10, 651-662, <https://doi.org/10.1111/j.1365-2486.2004.00758.x>, 2004.
- Guenther, A., Jiang, X., Heald, C. L., Sakulyanontvittaya, T., Duhl, T., Emmons, L. K. and Wang, X.: The model of emissions of gases and aerosols from nature version 2.1 (MEGAN 2.1): An extended and updated framework for modelling biogenic emissions, *Geosci. Model. Dev.*, 5, 1471-1492, <https://doi.org/10.5194/gmd-5-1471-2012>, 2012.
- Guo, H., Zou, S., Tasia, W., Chan, L. and Blake, D. R.: Emission characteristics of non-methane hydrocarbons from private cars and taxis at different driving speeds in Hong Kong, *Atmos. Environ.*, 45, 2711-2721, <https://doi.org/10.1016/j.atmosenv.2011.02.053>, 2011.
- Guo, Q., Zhang, N., Uchimaru, T., Chen, L., Quan, H. and Mizukado, J.: Atmospheric chemistry of cyc-CF<sub>2</sub>CF<sub>2</sub>CF<sub>2</sub>CH=CH-: Kinetics, products, and mechanism of gas-phase reaction with OH radicals, and atmospheric implications, *Atmos. Environ.*, 179, 69-76, <https://doi.org/10.1016/j.atmosenv.2018.02.005>, 2018.
- Haagen-Smit, A. J.: Chemistry and physiology of Los Angeles Smog, *Ind. Eng. Chem.*, 44, 6, 1342-1346, <https://doi.org/10.1021/ie50510a045>, 1952.

- Hackenberg, S. C., Andrews, S. J., Airs, R. L., Arnold, S. R., Bouman, H. A., Cummings, D., Lewis, A. C., Minaeian, J. K., Reifel, K. M., Small, A., Tarran, G. A., Tilstone, G. H. and Carpenter, L. J.: Basin-scale observations of monoterpenes in the Arctic and Atlantic Oceans, *Environ. Sci. Technol.*, **S1**, 10449-10458, <https://doi.org/10.1021/acs.est.7b02240>, 2017.
- Hall, I. W., Wayne, R. P, Cox, R. A., Jenkin, M. E. and Hayman, G. D.: Kinetics of the reaction of NO<sub>3</sub> with HO<sub>2</sub>, *J. Phys. Chem.*, **92**, 5049-5054, <https://doi.org/10.1021/j100328a043>, 1988.
- Hamilton, J. F. and Lewis, A. C.: Monoaromatic complexity in urban air and gasoline assessed using comprehensive GC and fast GC-TOF/MS, *Atmos. Environ.*, **37**, 5, 589-602, [https://doi.org/10.1016/S1352-2310\(02\)00930-5](https://doi.org/10.1016/S1352-2310(02)00930-5), 2003.
- Hansen, R. F., Blocquet, M., Schoemaeker, C., Léonardis, T., Locoge, N., Fittschen, C., Hanoune, B., Stevens, P. S., Sinha, V. and Dusanter, S.: Intercomparison of the comparative reactivity method (CRM) and pump-probe technique for measuring total OH reactivity in an urban environment, *Atmos. Meas. Tech.*, **8**, 4243-4264, <https://doi.org/10.5194/amt-8-4243-2015>, 2015.
- Hard, T. M., O'Brien, R. J., Chan, C. Y. and Mehrabzadeh, A. A.: Tropospheric free radical determination by fluorescence assay with gas expansion, *Environ. Sci. Technol.*, **18**, 10, 767-777, <https://doi.org/10.1021/es00128a009>, 1984.
- Harris, S. J. and Kerr, J. A.: Relative rate measurements of some reactions of hydroxyl radicals with alkanes studied under atmospheric conditions, *Int. J. Chem. Kinet.*, **20**, 12, 939-955, <https://doi.org/10.1002/kin.550201203>, 1988.
- Harrison, D., Hunter, M. C., Lewis, A. C., Seakins, P. W., Bonsang, B., Gros, V., Kanakidou, M., Touaty, M., Kavouras, I., Mihalopoulos, N., Stehpanou, E., Alves, C., Nunes, T. and Pio, C.: Ambient isoprene and monoterpene concentration in a Greek fir (*Abies Borisii-regis*) forest. Reconciliation with emissions measurements and effects on measured OH concentrations, *Atmos. Environ.*, **35**, 27, 4699-4711, [https://doi.org/10.1016/S1352-2310\(01\)00091-7](https://doi.org/10.1016/S1352-2310(01)00091-7), 2001.
- Harrison, R. M., Yin, J., Tilling, R. M., Cai, X., Seakins, P. W., Hopkins, J. R., Lansley, D. L., Lewis, A. C., Hunter, M. C., Heard, D. E., Carpenter, L. J., Creasy, D. J., Lee, J. D., Pilling, M. J., Carslaw, N., Emmerson, K. M., Redington, A., Derwent, R. G., Ryall, D., Mills, G. and Penkett, S. A.: Measurement and modelling of air pollution: Overview of the PUMA

consortium project, *Sci. Total Environ.*, 360, 5-25,  
<https://doi.org/10.1016/j.scitotenv.2005.08.053>, 2006.

Hartridge, H. and Roughton, F. J. W.: A method of measuring the velocity of very rapid chemical reactions, *Proc. Roy. Soc. (A)*, 104, 376-394, <https://doi.org/10.1098/rspa.1923.0116>, 1923a.

Hartridge, H. and Roughton, F. J. W.: The velocity with which carbon monoxide displaces oxygen from combination with haemoglobin, *Proc. Roy. Soc. (B)*, 94, 336-367, <https://doi.org/10.1098/rspb.1923.0008>, 1923b.

Hastie, D. R., Freeman, C. G., McEwan, M. J. and Schiff, H. I.: The reactions of ozone with methyl and ethyl nitrites, *Int. J. Chem. Kinet.*, 8, 307-313, <https://doi.org/10.1002/kin.550080212>, 1976.

Herron, J. T. and Huie, R. E.: Rate constants for the reactions of ozone with ethene and propene, from 235 to 362 deg K, *J. Phys. Chem.*, 78, 21, 2085-2088, <https://doi.org/10.1021/j100614a004>, 1974.

Herron, J. T. and Huie, R. E.: Stopped flow studies of the mechanisms of ozone-alkene reactions in the gas phase. Ethylene., *J. Am. Chem. Soc.*, 99, 16, 5430-5435, <https://doi.org/10.1021/ja00458a033>, 1977.

Hoekman, S. K.: Speciated measurements and calculated reactivities of vehicle exhaust emissions from conventional and reformed gasolines, *Environ. Sci. Technol.*, 26, 1206-1216, <https://doi.org/10.1021/es50002a610>, 1992.

Holt, T., Atkinson, R. and Arey, J.: Effect of water vapour concentration on the conversion of a series of 1,4-hydroxycarbonyls to dihydrofurans, *J. Photoch. Photobio. A*, 176, 231-237, <https://doi.org/10.1016/j.jphotochem.2005.08.029>, 2005.

Hunter, J. F., Carrasquillo, A. J., Daumit, K. E. and Kroll, J. H.: Secondary organic aerosol formation from acyclic, monocyclic, and polycyclic alkanes, *Environ. Sci. Technol.*, 48, 10227-10234, <https://doi.org/10.1021/es502674s>, 2014.

Ingham, T., Bauer, D., Sander, R., Crutzen, P. J. and Crowley, J. N.: Kinetics and products of the reactions BrO + DMS and Br + DMS at 298 K, *J. Phys. Chem. A*, 103, 36, 7199-7209, <https://doi.org/10.1021/jp9905979>, 1999.

- Jenkin, M. E., Saunders, S. M., Wagner, V. and Pilling, M. J.: Protocol for the development of the Master Chemical Mechanism, MCM v3 (Part B): Tropospheric degradation of aromatic volatiles organic compounds, *Atmos. Chem. Phys.*, 3, 181-193, <https://doi.org/10.5194/acp-3-181-2003>, 2003.
- Johnson, D. and Marston, G.: The gas-phase ozonolysis of unsaturated volatile organic compounds in the troposphere, *Chem. Soc. Rev.*, 37, 699-716, <https://doi.org/10.1039/B704260B>, 2008.
- Jordan, C. E., Ziemann, P. J., Griffin, R. J., Lim, Y. B., Atkinson, R. and Arey, J.: Modelling SOA formation from OH reactions with C<sub>8</sub>-C<sub>17</sub> *n*-alkanes, *Atmos. Environ.*, 42, 8015-8026, <https://doi.org/10.1016/j.atmosenv.2008.06.017>, 2008.
- Karl, T., Guenter, A., Yokelson, R. J., Greenberg, J., Potosnak, M., Blake, D. R. and Artaxo, P.: The tropical forest and fire emissions experiment: Emission, chemistry and transport of biogenic volatile organic compounds in the lower atmosphere over Amazonia, *J. Geophys. Res.-Atmos.*, 112, D18302, <https://doi.org/10.1029/2007JD008539>, 2007.
- Kato, S., Sato, T. and Kaji, Y.: A method to estimate the contribution of unidentified VOCs to OH reactivity, *Atmos. Environ.*, 45, 31, 5531-5539, <https://doi.org/10.1016/j.atmosenv.2011.05.074>, 2011.
- Kawai, H. and Nagamura, T.: Ultrafast dynamics of photogenerated styrylpyridinyl radical and its dimer radical cation with styrylpyridinium cation studied by femtosecond laser flash photolysis, *J. Chem. Soc. Faraday Trans.*, 94, 3581-3586, <https://doi.org/10.1039/A806076B>, 1998.
- Khan, M. A. H., Percival, C. J., Caravan, R. L., Taatjes, C. A. and Shallcross, D. E.: Criegee intermediates and their impacts on the troposphere, *Environ. Sci-Proc. Imp.*, 20, 437-453, <https://doi.org/10.1039/C7EM00585G>, 2018.
- Kim, D., Stevens, P. S. and Hites, R. A.: Rate constants for the gas-phase reactions of OH and O<sub>3</sub> with β-ocimene, β-myrcene, and α- and β-farnesene as a function of temperature, *J. Phys. Chem. A*, 115, 4, 500-506, <https://doi.org/10.1021/jp111173s>, 2011.
- Knispel, R., Koch, R., Siese, M. and Zetzsch, C.: Adduct formation of OH radicals with benzene, toluene, and phenol and consecutive reactions of the adducts with NO<sub>x</sub> and O<sub>2</sub>, *Ber.*

Bunsen-Ges. Phys. Chem., 94, 1375-1379, <https://doi.org/10.1002/bbpc.199000036>, 1990.

Koch, R., Knispel, R., Siese, M. and Zetzsch, C.: Absolute rate constants and products of secondary steps in the atmospheric degradation of aromatics in *Proceedings of the 6<sup>th</sup> European Symposium on the Physico-Chemical Behaviour of Atmospheric Pollutants*, Angeletti G., Restilli G., Eds.: European Commission, Brussels, Belgium, 143-149, 1994.

Kovacs, T. A. and Brune, W. H.: Total OH loss rate measurement, *J. Atmos. Chem.*, 39, 2, 105-122, <https://doi.org/10.1023/A:1010614113786>, 2001.

Kramp, F. and Paulson, S. E.: On the uncertainties in the rate coefficients for OH reactions with hydrocarbons, and the rate coefficients of the 1,3,5-trimethylbenzene and *m*-xylene reactions with OH radicals in the gas phase, *J. Phys. Chem. A*, 102, 16, 2685-2690, <https://doi.org/10.1021/jp973289o>, 1998.

Krol M., van Leeuwen, P. J. and Lelieveld, J.: Global OH trend inferred from methylchloroform measurements, *J. Geophys. Res.*, 103, 10697-10711, <https://doi.org/10.1029/98JD00459>, 1998.

Kroll, J. H., Hanisco, T. F., Donahue, N. M., Demerjian, K. L. and Anderson, J. G.: Accurate, direct measurements of OH yields from gas-phase ozone-alkene reactions using an in-situ LIF instrument, *Geophys. Res. Lett.*, 28, 3863-3866, <https://doi.org/10.1029/2001GL013406>, 2001.

Kwok, E. S. C., Atkinson, R. and Arey, J.: Isomerisation of  $\beta$ -hydroxyalkyl radicals formed from the OH radical initiated reactions of C<sub>4</sub>-C<sub>8</sub> 1-alkenes, *Env. Sci. Technol.*, 30, 1048-1052, <https://doi.org/10.1021/es950584i>, 1996.

Lauraguais, A., Bejan, I., Barnes, I., Wiesen, P. and Coeur, C.: Rate coefficients for the gas-phase reactions of hydroxyl radicals with a series of methoxylated aromatic compounds, *J. Phys. Chem. A*, 119, 24, 6179-6187, <https://doi.org/10.1021/acs.jpca.5b03232>, 2015.

Langford, B., Misztal, P. K., Nemitz, E., Davison, B., Helfter, C., Pugh, T. A. M., MacKenzie, A. R., Lim, S. F. and Hewitt, C. N.: Fluxes and concentrations of volatile organic compounds from a South-East Asian tropical rainforest, *Atmos. Chem. Phys.*, 10, 8391-8412, <https://doi.org/10.5194/acp-10-8391-2010>, 2010.

- Lelieveld, J. and Dentener, F. J.: What controls tropospheric ozone?, *J. Geophys. Res.*, **105**, 3531-3551, <https://doi.org/10.1029/1999JD901011>, 2000.
- Lidster, R. T., Hamilton, J. F., Lee, J. D., Lewis, A. C., Hopkins, J. R., Punjabi, S., Rickard, A. R. and Young, J. C.: The impact of monoaromatic hydrocarbons on OH reactivity in the coastal UK boundary layer and free troposphere, *Atmos. Chem. Phys.*, **14**, 6677-6693, <https://doi.org/10.5194/acp-14-6677-2014>, 2014.
- Lim, Y. B. and Ziemann, P. J.: Products and mechanism of secondary organic aerosol formation from reactions of *n*-alkanes with OH radicals in the presence of NO<sub>x</sub>, *Env. Sci. Technol.*, **39**, 9229-9236, <https://doi.org/10.1021/es051447g>, 2005.
- Lim, Y. B. and Ziemann, P. J.: Effects of molecular structure on aerosol yields from OH radical-initiated reactions of linear, branched, and cyclic alkanes in the presence of NO, *Environ. Sci. Technol.*, **43**, 2328-2334, <https://doi.org/10.1021/es803389s>, 2009.
- Liu, C., Ma, Z., Mu, Y., Liu, J., Zhang, C., Zhang, Y., Liu, P. and Zhang H.: The levels, variation characteristics, and sources of atmospheric non-methane hydrocarbon compounds during wintertime in Beijing, China, *Atmos. Chem. Phys.*, **17**, 10633-10649, <https://doi.org/10.5194/acp-17-10633-2017>, 2017.
- Mader, P. P., MacPhee, R. D., Lofberg, R. T. and Larson, G. P.: Composition of organic portion of atmospheric aerosols in the Los Angeles area, *Ind. Eng. Chem.*, **44**, 6, 1352-1355, <https://doi.org/10.1021/ie50510a047>, 1952.
- Magel, E., Mayrhofer, S., Müller, A., Zimmer, I., Hampf, R. and Schnitzler, J.-P.: Photosynthesis and substrate supply for isoprene biosynthesis in poplar leaves, *Atmos. Environ.*, **40**, 138-151, <https://doi.org/10.1016/j.atmosenv.2005.09.091>, 2006.
- Martin, P., Tuazon, E. C., Aschmann, S. M., Arey, J. and Atkinson, R.: Formation and atmospheric reactions of 4,5-dihydro-2-methylfuran, *J. Phys. Chem. A*, **106**, 11492-11501, <https://doi.org/10.1021/jp021499h>, 2002.
- Mehta, D., Nguyen, A., Montenegro, A. and Li, Z.: A kinetic study of the reaction of OH with xylenes using the relative rate/discharge flow/mass spectrometry technique, *J. Phys. Chem. A*, **113**, 46, 12942-12951, <https://doi.org/10.1021/jp905074j>, 2009.

- Molina, M. J. and Rowland, F. S.: Stratospheric sinks for chlorofluoromethanes: chlorine atom-catalysed destruction of ozone, *Nature*, 249, 810-812, <https://doi.org/10.1038/249810a0>, 1974.
- Morris Jr., E. D. and Niki, H.: Mass spectrometric study of the reaction of hydroxyl radical with formaldehyde, *J. Chem. Phys.*, 55, 1991-1992, <https://doi.org/10.1063/1.1676348>, 1971.
- Morris Jr., E. D., Stedman, D. H. and Niki, H.: Mass-spectrometric study of the reactions of the hydroxyl radical with ethylene, propylene, and acetaldehyde in a discharge-flow system, *J. Am. Chem. Soc.*, 93, 15, 3570-3572, <https://doi.org/10.1021/ja00744a004>, 1971.
- Nicovich, J. M., Thompson, R. L. and Ravishankara, A. R.: Kinetics of the reactions of the hydroxyl radical with xylenes, *J. Phys. Chem.*, 84, 20, 2913-2916, <https://doi.org/10.1021/j150620a012>, 1981.
- Niinemets, Ü, Kuhn, U., Harley, P C., Staudt, M., Arneith, A., Cescatti, A., Ciccioli, P., Copolovici, L., Geron, C., Guenther, A., Kesselmeier, J., Lerchau, M. T., Monson, R. K. and Peñuelas, J.: Estimations of isoprenoid emission capacity from enclosure studies: measurements, data processing, quality and standardised measurement protocols, *Biogeosciences*, 8, 2209-2246, <https://doi.org/10.5194/bg-8-2209-2011>, 2011.
- Niki, H., Maker, P. D., Savage, C. M. and Breitenbach, L. P.: Relative rate constants for the reaction of hydroxyl radical with aldehydes, *J. Phys. Chem.*, 82, 2, 132-134, <https://doi.org/10.1021/j100491a002>, 1978.
- Nizkorodov, S. A., Harper, W. W., Blackmon, B. W. and Nesbitt, D. J.: Temperature dependent kinetics of the OH/HO<sub>2</sub>/O<sub>3</sub> chain reaction by time-resolved IR laser absorption spectroscopy, *J. Phys. Chem. A*, 104, 17, 3964-3973, <https://doi.org/10.1021/jp9934984>, 2000.
- Nölscher, A. C., Sinha, V., Bockisch, S., Klüpfel, T. and Williams, J.: Total OH reactivity measurements using a new fast Gas Chromatographic Photo-Ionisation Detector (GC-PID), *Atmos. Meas. Tech.*, 5, 2981-2992, <https://doi.org/10.5194/amt-5-2981-2012>, 2012.
- Ortega, J. and Helmig, D.: Approaches for quantifying reactive and low-volatility biogenic organic compound emissions by vegetation enclosure techniques – Part A, *Chemosphere*, 72, 343-364, <https://doi.org/10.1016/j.chemosphere.2007.11.020>, 2008.

- Osthoff, H. D., Roberts, J. M., Ravishankara, A. R., Williams, E. J., Lerner, B. M., Sommariva, R., Bates, T. S., Coffman, D., Quinn, P. K., Dibb, J. E., Stark, H., Burkholder, J. B., Talukdar, R. K., Meagher, J., Fehsenfeld, F. C. and Brown, S. S.: High levels of nitryl chloride in the polluted subtropical marine boundary layer, *Nat. Geosci.*, **1**, 324-328, <https://doi.org/10.1038/ngeo177>, 2008.
- Pandit, G. G., Sahu, S. K. and Puranik, V. D.: Distribution and source apportionment of atmospheric non-methane hydrocarbons in Mumbai, India, *Atmos. Pollut. Res.*, **2**, 231-236, <https://doi.org/10.5094/APR.2011.029>, 2011.
- Paulot, F., Henze, D. K. and Wennberg, P. O.: Impact of the isoprene photochemical cascade on tropical ozone, *Atmos. Chem. Phys.*, **12**, 1307-1325, <https://doi.org/10.5194/acp-12-1307-2012>, 2012.
- Paulson, S. E. and Orlando, J. J.: The reactions of ozone with alkenes, an important source of HO<sub>x</sub> in the boundary layer, *Geophys. Res. Lett.*, **23**, 3727-3730, <https://doi.org/10.1029/96GL03477>, 1996.
- Pereira, K. L., Dunmore, R., Whitehead, J., Rami Alfarra, M., Allan, J. D., Alam, M. S., Harrison, R. M., McFiggans, G. and Hamilton, J. F.: The effect of varying engine conditions on unregulated VOC diesel exhaust emissions, *Atmos. Chem. Phys. Discuss.*, <https://doi.org/10.5194/acp-2017-603>, in review, 2017.
- Phan, M. and Li, Z.: Kinetics study of the reactions of OH with *n*-undecane and *n*-dodecane using the RR/DF/MS technique, *J. Phys. Chem. A.*, **121**, 3647-3654, <https://doi.org/10.1021/acs.jpca.7b01512>, 2017.
- Phillips, G. J., Tang, M. J., Thieser, J., Brickwedde, B., Schuster, G., Bohn, B., Lelieveld, J. and Crowley, J. N.: Significant concentrations of nitryl chloride observed in rural continental Europe associated with the influence of sea salt chloride and anthropogenic emissions, *Geophys. Res. Lett.*, **39**, L10811, <https://doi.org/10.1029/2012GL051912>, 2012.
- Phouongphouang, P. T. and Arey, J.: Rate constants for the gas-phase reactions of a series of alkylnaphthalenes with the OH radical, *Environ. Sci. Technol.*, **36**, 9, 1947-1952, <https://doi.org/10.1021/es011434c>, 2002.

- Porter, G.: Flash photolysis and spectroscopy. A new method for the study of free radical reactions, *P. Roy. Soc. Lond. A Mat.*, 200, 284-300, <https://doi.org/10.1098/rspa.1950.0018>, 1950.
- Ravishankara, A. R., Wagner, S., Fischer, S., Smith, G., Schiff, R., Watson, R. T., Tesi, G. and Davis, D. D.: A kinetics study of the reactions of OH with several aromatic and olefinic compounds, *Int. J. Chem. Kinet.*, 10, 783-804, <https://doi.org/10.1002/kin.550100802>, 1978.
- Ravishankara, A. R. and Mauldin III, R. L.: Absolute rate coefficient for the reaction of nitrogen trioxide (NO<sub>3</sub>) with *trans*-2-butene, *J. Phys. Chem.*, 89, 14, 3144-3147, <https://doi.org/10.1021/j100260a038>, 1985.
- Ravishankara, A. R., Dunlea, E. J., Blitz, M. A., Dillon, T. J., Heard, D. E., Pilling, M. J., Strekowski, R. S., Nicovich, J. M. and Wine, P. H.: Redetermination of the rate coefficient for the reaction of O(<sup>1</sup>D) with N<sub>2</sub>, *Geophys. Res. Lett.*, 29, 15, 1745, <https://doi.org/10.1029/2002GL014850>, 2002.
- Reisen, F., Aschmann, S. M., Atkinson, R. and Arey, J.: 1,4-hydroxycarbonyl products of the OH radical initiated reactions of C<sub>5</sub>-C<sub>8</sub> *n*-alkanes in the presence of NO, *Env. Sci. Technol.*, 39, 4447-4453, <https://doi.org/10.1021/es0483589>, 2005.
- Riedel, T. P., Bertram, T. H., Crisp, T. A., Williams, E. J., Lerner, B. M., Vlasenko, A., Li, S.-M., Gilman, J., de Gouw, J., Bon, D. M., Wagner, N. L., Brown, S. S. and Thornton, J. A.: Nitryl chloride and molecular chlorine in the coastal marine boundary layer, *Environ. Sci. Technol.*, 46, 19, 10463-10470, <https://doi.org/10.1021/es204632r>, 2012.
- Roelofs, G.-J. and Lelieveld, J.: Model study of the influence of cross-tropopause O<sub>3</sub> transports on tropospheric O<sub>3</sub> levels, *Tellus B*, 49, 38-55, <https://doi.org/10.3402/tellusb.v49i1.15949>, 1997.
- Rosenstiel, T. N., Ebbets, A. L., Khatri, W. C., Fall, R. and Monson, R. K.: Induction of poplar leaf nitrate reductase: a test of extrachloroplastic control of isoprene emission rate, *Plant. Biol. (Stuttg)*, 6, 12-21, <https://doi.org/10.1055/s-2003-44722>, 2004.
- Rowley, D. M., Bloss, W. J., Cox, R. A. and Jones, R. L.: Kinetics and products of the IO + BrO reaction, *J. Phys. Chem. A*, 105, 33, 7855-7864, <https://doi.org/10.1021/jp004494y>, 2001.

- Ruppert, L. and Becker, K. H.: A product study of the OH radical-initiated oxidation of isoprene: formation of C<sub>5</sub>-unsaturated diols, *Atmos. Environ.*, **34**, 1529-1542, [https://doi.org/10.1016/S1352-2310\(99\)00408-2](https://doi.org/10.1016/S1352-2310(99)00408-2), 2000.
- Salameh, T., Afif, C., Sauvage, S., Borbon, A. and Locoge, N.: Speciation of non-methane hydrocarbons (NMHCs) from anthropogenic sources in Beirut, Lebanon, *Environ. Sci. Pollut. R.*, **21**, 10867-10877, <https://doi.org/10.1007/s11356-014-2978-5>, 2014.
- Sanadze, G. A.: Biogenic isoprene (a review), *Russ. J. Plant. Physiol.*, **51**, 729-741, <https://doi.org/10.1023/B:RUPP.0000047821.63354.a4>, 2004.
- Saunders, S. M., Jenkin, M. E., Derwent, R.G. and Pilling, M. J.: Protocol for the development of the Master Chemical Mechanism, MCM v3 (Part A): Tropospheric degradation of non-aromatic volatile organic compounds, *Atmos. Chem. Phys.*, **3**, 161-180, <https://doi.org/10.5194/acp-3-161-2003>, 2003.
- Schweitzer, F., Mirabel, P. and George, C.: Multiphase chemistry of N<sub>2</sub>O<sub>5</sub>, ClNO<sub>2</sub>, and BrNO<sub>2</sub>, *J. Phys. Chem. A*, **102**, 22, 3942-3952, <https://doi.org/10.1021/jp980748s>, 1998.
- Sharma, A., Pushpa, A. A., Dhanya, S., Naik, P. D. and Bajaj, P. N.: *Int. J. Chem. Kinet.*, **42**, 2, 98-105, 2010.
- Shu, Y. and Atkinson, R.: Atmospheric lifetimes and fates of a series of sesquiterpenes, *J. Geophys. Res.*, **100**, 7275-7281, <https://doi.org/10.1021/95JD00368>, 1995.
- Siese, M., Becker, K. H., Brockmann, K. J., Geiger, H., Hofzumahaus, A., Holland, F., Mihelcic, D. and Wirtz, K.: Direct measurement of OH radicals from ozonolysis of selected alkenes: A EUPHORE simulation chamber study, *Env. Sci. Technol.*, **35**, 4660-4667, <https://doi.org/10.1021/es010150p>, 2001.
- Silver, G. M. and Fall, R.: Enzymatic synthesis of isoprene from dimethylallyl diphosphate in aspen leaf extracts, *Plant Physiol.*, **97**, 1588-1591, <https://doi.org/10.1104/pp.97.4.1588>, 1991.
- Silver, G. M. and Fall, R.: Characterisation of aspen isoprene synthase, an enzyme responsible for leaf isoprene emission to the atmosphere, *J. Biol. Chem.*, **270**, 13010-13016, <https://doi.org/10.1074/jbc.270.22.13010>, 1995.

- Singh, S., Fatima de Leon, M. and Li, Z.: Kinetics study of the reaction of OH radicals with C<sub>5</sub>-C<sub>8</sub> cycloalkanes at 240-340 K using the relative rate/discharge flow/mass spectrometry technique, *J. Phys. Chem. A*, 117, 42, 10863-10872, <https://doi.org/10.1021/jp406923d>, 2013.
- Sinha, V., Williams, J., Crowley, J. N. and Lelieveld, J.: The Comparative Reactivity Method – a new tool to measure total OH reactivity in ambient air, *Atmos. Chem. Phys.*, 8, 2213-2227, <https://doi.org/10.5194/acp-8-2213-2008>, 2008.
- Slanger, T. G. and Black, G.: Reaction rate measurements of O(<sup>3</sup>P) atoms by resonance fluorescence. II O(<sup>3</sup>O)+CO+M→CO<sub>2</sub>+M; M=He, Ar, N<sub>2</sub>, *J. Chem. Phys.*, 53, 3722, <https://doi.org/10.1063/1.1674554>, 1970.
- Spanke, J., Rannik, Ü, Forkel, R., Nigge, W. and Hoffman, T.: Emission fluxes and atmospheric degradation of monoterpenes above a boreal forest: field measurements and modelling, *Tellus B*, 53, 4, 406-422, <https://doi.org/10.1034/j.1600-0889.2001.530407.x>, 2001.
- Srinivasulu, G., Bunkan, A. J. C., Amedro, D. and Crowley, J. N.: Absolute and relative-rate measurement of the rate coefficient for reaction of perfluoro ethyl vinyl ether (C<sub>2</sub>F<sub>5</sub>OCF=CF<sub>2</sub>) with OH, *Phys. Chem. Chem. Phys.*, 20, 3761-3767, <https://doi.org/10.1039/c7cp08056e>, 2018.
- Stewart, D. J., Griffiths, P. T. and Cox, R. A.: Reactive uptake coefficients for heterogeneous reaction of N<sub>2</sub>O<sub>5</sub> with submicron aerosols of NaCl and natural sea salt, *Atmos. Chem. Phys.*, 4, 1381-1338, <https://doi.org/10.5194/acp-4-1381-2004>, 2004.
- Tham, Y. J., Yan, C., Xue, L., Zha, Q., Wang, X. and Wang, T.: Presence of high nitryl chloride in Asian coastal environment and its impact on atmospheric photochemistry, *Chinese Sci. Bull.*, 59, 4, 356-359, <https://doi.org/10.1007/s11434-013-0063-y>, 2014.
- Tholl, D., Boland, W., Hansel, A., Loretor, F., Roses, U. S. R. and Schnitzler, J.-P.: Practical approaches to plant volatile analysis, *Plant J.*, 45, 540-560, <https://doi.org/10.1111/j.1365-313X.2005.02612.x>, 2006.
- Thornton, J. A. and Abbatt, J. P. D.: N<sub>2</sub>O<sub>5</sub> reaction of submicron sea salt aerosol: Kinetics, products, and the effect of surface active organics, *J. Phys. Chem. A*, 109, 44, 10004-10012, <https://doi.org/10.1021/jp054183t>, 2005.

- Thornton, J. A., Kercher, J. P., Riedel, T. P., Wagner, N. L., Cozic, J., Holloway, J. S., Dubé, W. P., Wolfe, G. M., Quinn, P. K., Middlebrook, A. M., Alexander, B. and Brown, S. S.: A large atomic chlorine source inferred from mid-continental reactive nitrogen chemistry, *Nature*, 464, 271-274, <https://doi.org/10.1038/nature08905>, 2010.
- Tiwari, V., Hanai, Y. and Masunaga, S.: Ambient levels of volatile organic compounds in the vicinity of petrochemical industrial area of Yokohama, Japan, *Air Qual. Atmos. Health*, 3, 65-75, <https://doi.org/10.1007/s11869-009-0052-0>, 2010.
- Tkacik, D. S., Presto, A. A., Donahue, N. M. and Robinson, A. L.: Secondary organic aerosol formation from intermediate-volatility organic compounds: Cyclic, linear, and branched alkanes, *Environ. Sci. Technol.*, 46, 8773-8781, <https://doi.org/10.1021/es301112c>, 2012.
- Trainor, D. W. and von Rosenberg Jr, C. W.: Flash photolysis study of the gas phase recombination of hydroxyl radicals, *J. Chem. Phys.*, 61, 1010, <https://doi.org/10.1063/1.1681968>, 1974.
- Tuazon, E. C., Carter, W. P. L., Atkinson, R. and Pitts Jr., J. N.: The gas-phase reaction of hydrazine and ozone: A non-photolytic source of OH radicals for measurement of relative OH radical rate constants, *Int. J. Chem. Kinet.*, 15, 7, 619-629, <https://doi.org/10.1002/kin.550150704>, 1983.
- Vickers, C. E., Gershenzon, J., Lerdau, M. T. and Loreto, F.: A unified mechanism of action for volatile isoprenoids in plant abiotic stress, *Nat. Chem. Biol.*, 5, 5, 283-291, <https://doi.org/10.1038/nchembio.158>, 2009.
- Vingarzan, R.: A review of surface ozone background levels and trends, *Atmos. Environ.*, 38, 21, 3431-3442, <https://doi.org/10.1016/j.atmosenv.2004.03.030>, 2004.
- von Kuhlmann, R., Lawrence, M. G., Poschl, U. and Crutzen, P. J.: Sensitivities in global scale modelling of isoprene, *Atmos. Chem. Phys.*, 4, 1-17, <https://doi.org/10.5194/acp-4-1-2004>, 2004.
- Waked, A., Sauvage, S., Borbon, A., Gaudin, J., Pallares, C., Vagnot, M.-P., Léonardis, T. and Locoge, N.: Multi-year levels and trends of non-methane hydrocarbon concentrations observed in ambient air in France, *Atmos. Environ.*, 141, 263-275, <https://doi.org/10.1016/j.atmosenv.2016.06.059>, 2016.

- Walavalkar, M., Sharma, A., Alwe, H. D., Pushpa, K. K., Dhanya, S., Naik, P. D. and Bajaj, P. N.: Cl atom initiated oxidation of 1-alkenes under atmospheric conditions, *Atmos. Environ.*, 67, 93-100, <http://dx.doi.org/10.1016/j.atmosenv.2012.10.039>, 2013.
- Wallington, T. J. and Kurylo, M. J.: Flash photolysis resonance fluorescence investigation of the gas-phase reaction of OH radicals with a series of aliphatic ketones over the temperature range 240-440 K, *J. Phys. Chem.*, 91, 5050-5054, <https://doi.org/10.1021/j100303a033>, 1987.
- Wilson, E. W., Hamilton, W. A., Kennington, H. R., Evans, B. and Scott, N. W.: Measurement and estimation of rate constants for the reactions of hydroxyl radicals with several alkanes and cycloalkanes, *J. Phys. Chem. A*, 110, 10, 3593-3604, <https://doi.org/10.1021/jp055841c>, 2006.
- Wolff, M., Schotte, F., Naylor, G., Bourgeois, D., Moffat, K. and Mourou, G.: Time-resolved structures of macromolecules at the ESRF: Single-pulse Laue diffraction, stroboscopic data collection and femtosecond flash photolysis, *Nucl. Instrum. Meta. A*, 398, 69-84, [https://doi.org/10.1016/S0168-9002\(96\)01226-0](https://doi.org/10.1016/S0168-9002(96)01226-0), 1997.
- Wollenhaupt, M., Carl, S. A., Horowitz, A. and Crowley, J. N.: Rate coefficients for reaction of OH with acetone between 202 and 395 K, *J. Phys. Chem. A*, 104, 12, 2695-2705, <https://doi.org/10.1021/jp993738f>, 2000.
- Wu, C. H., Japar, S. M. and Niki, H.: Relative reactivities of HO-hydrocarbon reactions from smog reactor studies, *J. Environ. Sci. Health, Part A*, 11, 191-200, <https://doi.org/10.1080/10934527609385765>, 1976.
- Yang, Y., Shao, M., Wang, X., Nölscher, A. C., Kessel, S., Guenther, A. and Williams, J.: Towards a quantitative understanding of total OH reactivity: A review, *Atmos. Environ.*, 134, 147-161, <https://doi.org/10.1016/j.atmosenv.2016.03.010>, 2016.
- Yass, N., Song, W., Lelieveld, J., Vanhatalo, A., Bäck, J. and Williams, J.: Diel cycles of isoprenoids in the emissions of Norway spruce, four Scots pine chemotypes, and in Boreal forest ambient air during HUMPPA-COPEC-2010, *Atmos. Chem. Phys.*, 12, 7215-7229, <https://doi.org/10.5194/acp-12-7215-2012>, 2012.

- Yee, L. D., Craven, J. S., Loza, C. L., Schilling, K. A., Ng, N. L., Canagaratna, M. R., Ziemann, P. J., Flagan, R. C. and Seinfeld, J. H.: Effect of chemical structure on secondary organic aerosol formation from C<sub>12</sub> alkanes, *Atmos. Chem. Phys.*, **13**, 11121-11140, <https://doi.org/10.5194/acp-13-11121-2013>, 2013.
- Zellner, R. and Lorenz, K.: Laser photolysis/resonance fluorescence study of the rate constants for the reactions of OH radicals with C<sub>2</sub>H<sub>4</sub> and C<sub>3</sub>H<sub>6</sub>, *J. Phys. Chem.*, **88**, 5, 984-989, <https://doi.org/10.1021/j150649a028>, 1984.
- Zhang, D., Zhang, R., Church, C. and North, S. W.: Experimental study of hydroxyalkyl peroxy radicals from OH-initiated reactions of isoprene, *Chem. Phys. Lett.*, **343**, 49-54, [https://doi.org/10.1016/S0009-2614\(01\)00654-6](https://doi.org/10.1016/S0009-2614(01)00654-6), 2001.
- Zhang, Y., Wang, X., Zhang, Z., Lü, S., Shao, M., Lee, F. S. C. and Yu, J.: Species profiles and normalised reactivity of volatile organic compounds from gasoline evaporation in China, *Atmos. Environ.*, **79**, 110-118, <https://doi.org/10.1016/j.atmosenv.2013.06.029>, 2013.
- Ziemann, P. J.: Effects of molecular structure on the chemistry of aerosol formation from the OH-radical-initiated oxidation of alkanes and alkenes, *Int. Rev. Phys. Chem.*, **30**, 161-195, <https://doi.org/10.1080/0144235X.2010.550728>, 2011.



## Chapter 2

# The multivariate relative rate technique method

## 2 Overview

This chapter introduces the multivariate relative rate technique by characterising both the reactor design and the instrumentation used for the gas-phase VOC analysis. It describes the methods undertaken to measure gas-phase relative rate coefficients using this technique as well as outlines the procedures applied to process the data. This chapter also details the modifications made to the base technique that allowed for the measurement of rate coefficients for relatively slow VOC + OH reactions, for VOC + Cl reactions, and for temperature-dependent reactions.

## 2.1 The basic technique

The multivariate relative rate technique developed at the Wolfson Atmospheric Chemistry Laboratories, York, UK is of a conceptually simple design and is based on traditional relative rate experiments and “missing OH reactivity” experiments (Kato et al., 2011). For the measurements made in this work, gas-phase reactants were mixed together in a vessel, henceforth referred to as the ‘reactor’, and allowed to interact before being transferred to state-of-the-art instrumentation for analysis. The primary method of analysis employed throughout much of this work was gas-chromatography coupled to time-of-flight mass-spectrometry (GC-ToF-MS).

Figure 2.1 shows a brief schematic outlining the experimental concept. The following sections further describe in detail all the aspects of the experimental procedure; from the front end of the experiment to the analytical instrumentation used, along with their optimised settings, and the methods used to analyse the obtained data.

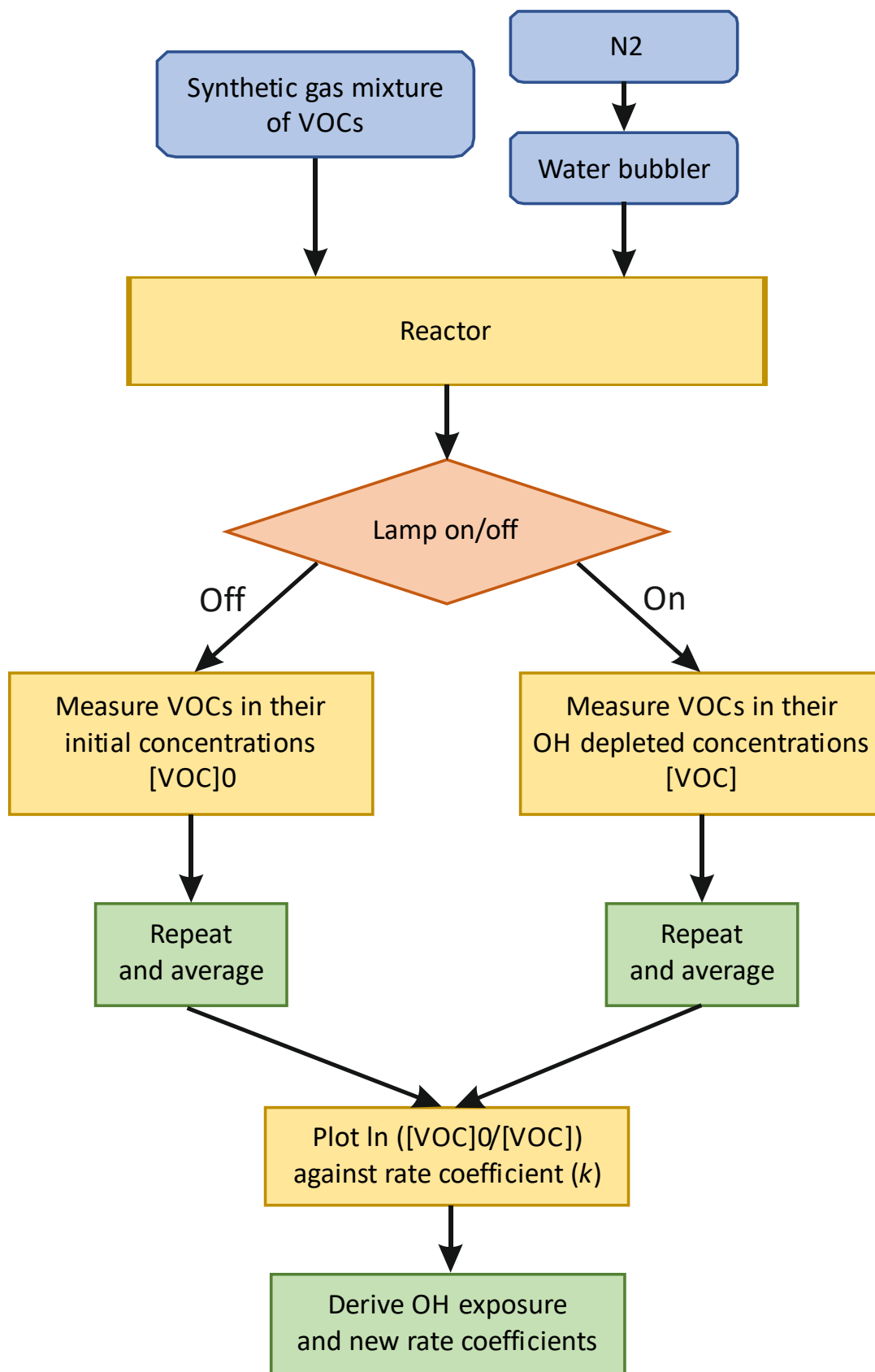


**Figure 2.1** Brief flow schematic of the experimental concept. All parts of the schematic will be outlined in more detail in the following section.

### 2.1.1 Reactor characterisation

The reactor comprised a single stainless-steel tube with approximate external dimensions of 470 × 25 × 25 mm and an internal volume of 250 cm<sup>3</sup>. A schematic of the reactor, designed at the University of Leeds, UK, is shown in Figure 2.2. A quartz window, positioned on the top face of the reactor, allowed collimated vacuum ultraviolet (VUV) light from a low-pressure Hg/Ar lamp (L.O.T., Pen-Ray<sup>®</sup>) to enter the reactor. N<sub>2</sub> (2000 standard cubic centimetres per minute (sccm)) was passed through a bubbler filled with high purity water (Fischer, Optima grade) and supplied to the reactor upstream of the quartz window via a mass flow controller (MKS Instruments). Gas-phase VOC reactants, in a flow of N<sub>2</sub> (1000 sccm), were introduced downstream of the quartz window via a stainless-steel injection tube with an external diameter of 3.2 mm. The injection tube was positioned so as to minimise the potential photolysis of the VOCs by VUV light but also maximise the exposure to the short-lived OH radical. This was done by varying the injector position and measuring the concentration of formaldehyde formed from methane oxidation (see Cryer, 2016). The optimised position for VOC injection was found to be approximately 150 mm downstream of the quartz window. The injector design ensured that VOCs were thoroughly mixed with the main flow within the reactor by passing the VOCs through an array of four holes which were radially distributed about the injection tube. The remainder of the reactor length allowed for ample reaction time for the gas-phase reactants at atmospheric pressure. When using a typical total flow rate of 3000 sccm through the reactor, the residence time of the organic mixture in the reactor was estimated to be approximately 4 s.

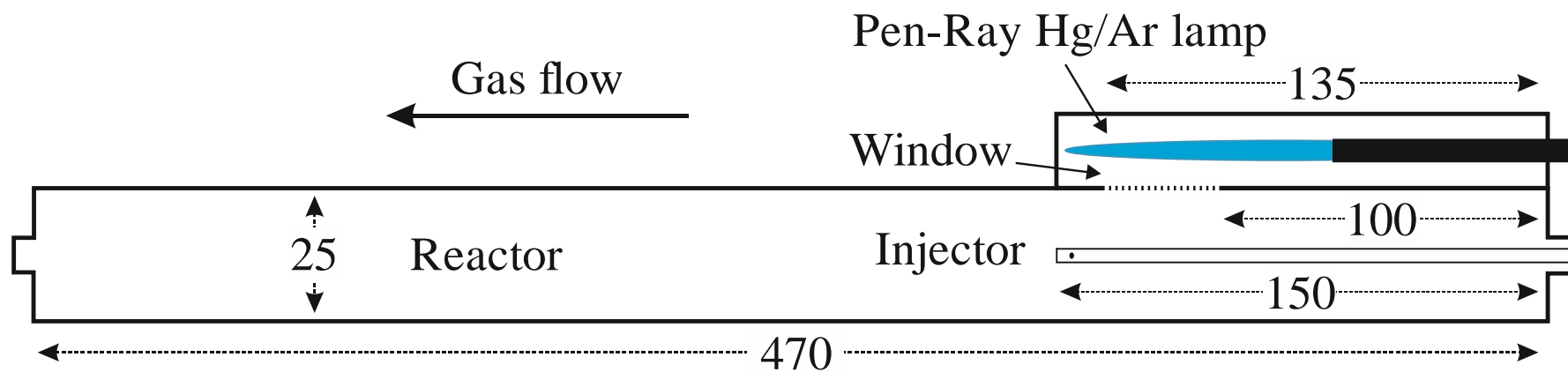


**Figure 2.2** Schematic of the flow reactor used for mixing of gas-phase reactants. All measurements are shown in mm. Humidified  $N_2$  enters the reactor at the far right of the schematic via 1/4" tubing. The VOCs are injected into the reactor perpendicular to the gas flow via four radial holes in the central sliding 1/8" injector. The position of this injector was optimised to provide maximum exposure of VOCs to OH radicals with minimum exposure to the VUV light (Cryer, 2016). The typical residence time of VOCs inside the reactor after injection under normal flow conditions was approximately 4 s, with the oxidation chemistry expected to occur in under 0.5 s.

### 2.1.1.1 Reactor flow conditions

The flow of a fluid through a pipe can be described as either laminar, in which the fluid flows in parallel layers with no disruption, or as turbulent, in which the flow is much more dynamic. Laminar flow is characterised as being slow whereas turbulent flow is typically chaotic and promotes mixing.

The Reynolds number ( $Re$ ) can be used to predict the type of flow through, for example, a cylindrical object such as the reactor (see Figure 2.2). A low Reynolds number ( $Re < 2300$ ) is indicative of laminar flow whilst higher numbers ( $Re > 4000$ ) suggest an increased degree of turbulence. The Reynolds number for a particular flow can be calculated using Eq. 2.1, where;  $\rho$  is the density of the fluid,  $u$  is the mean velocity of the fluid,  $\mu$  is the dynamic viscosity of the fluid,  $\nu$  is the kinematic viscosity of the fluid,  $Q$  is the volumetric flow rate,  $A$  is the cross-sectional area and  $D_H$  is the hydraulic diameter of the pipe (or reactor).  $D_H$  can be calculated using Eq. 2.2, where  $A$  is the cross-sectional area and  $P$  is the wetted perimeter. The wetted perimeter is the total area of the pipe in contact with the fluid. As the reactor contains gas, it can be assumed that the entire perimeter of the pipe is in contact with the fluid and hence  $D_H$  is equal to the internal area of the reactor walls.

$$Re = \frac{\rho u D_H}{\mu} = \frac{u D_H}{\nu} = \frac{Q D_H}{\nu A} \quad \text{Eq. 2.1}$$

$$D_H = \frac{4A}{P} \quad \text{Eq. 2.2}$$

The entrance length ( $L_e$ ) is another useful parameter used to characterise flows. The flow through a pipe usually takes some distance to fully establish itself; the distance that the fluid takes before establishing stable laminar, or continued turbulent, flow is termed the entrance length. This is calculated differently dependent on the type of flow ultimately established. For laminar flows, the entrance length is calculated using the Reynolds number and diameter of the pipe through Eq. 2.3, whilst for turbulent flows, the entrance length is calculated using Eq. 2.4.

$$L_e \sim 0.06 \times Re \times D \quad \text{Eq. 2.3}$$

$$L_e \sim 4.4 \times (Re)^{\frac{1}{6}} \times D \quad \text{Eq. 2.4}$$

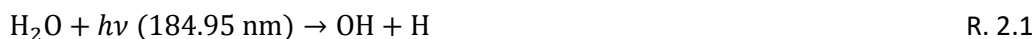
The primary flow of humidified  $N_2$  (equal to 2000 sccm) was calculated to have  $Re = 88$  with  $L_e = 0.1$  m. The flow after the VOCs were injected (equal to 3000 sccm) was calculated to have  $Re =$

132 with  $L_e = 0.2$  m. Clearly, for both cases,  $Re$  was much smaller than 2300, the threshold at which fluids are predicted to begin experiencing turbulence. Therefore, it is expected that laminar flow was established within the reactor. However, the calculated values of  $L_e$  were considerably high for the length of the reactor. Referring to Figure 2.2, it can be assumed that laminar flow was not fully established until approximately 0.35 m into the reactor, at which point it was likely that much of the chemistry had already taken place.

### 2.1.2 Lamp and lamp housing

The Hg/Ar lamp was positioned in either an aluminium or stainless-steel lamp housing on top of the reactor. A quartz window allowed for the VUV-light from the lamp to enter the reactor. A rubber seal placed between the housing and the reactor prevented the escape of gas around the quartz window. VUV light from the lamp entered the reactor through a section of multiple cylindrical steel tubes, each with a diameter of approximately 2 mm. This section ensured that the VUV light entering the reactor was collimated – that is, that all light that passed into the reactor entered in parallel. This served to minimise the light reflecting around the internal surfaces of the reactor which could have potentially caused interferences with any VOCs susceptible to photolysis further downstream.

Mercury lamps are a form of gas-discharge lamp that use vaporised mercury as a source of VUV emission. Figure 2.3 shows the emission spectrum and typical relative intensities for the Hg/Ar lamp in use in the experiment. Figure 2.4 shows the emission spectrum, recorded using diffuse reflectance spectroscopy (DRS), of the same lamp, between 190 and 650 nm. The primary UV and VUV peaks in the Hg emission line spectrum are at 184.5, 253.7 and 365.4 nm. The primary emission at 253.7 nm is of potential concern for the direct photolysis of VOCs. The emission at 184.5 nm, although not visible in Figure 2.3, can be used to photolyse  $H_2O$  into OH and H radicals (R. 2.1).



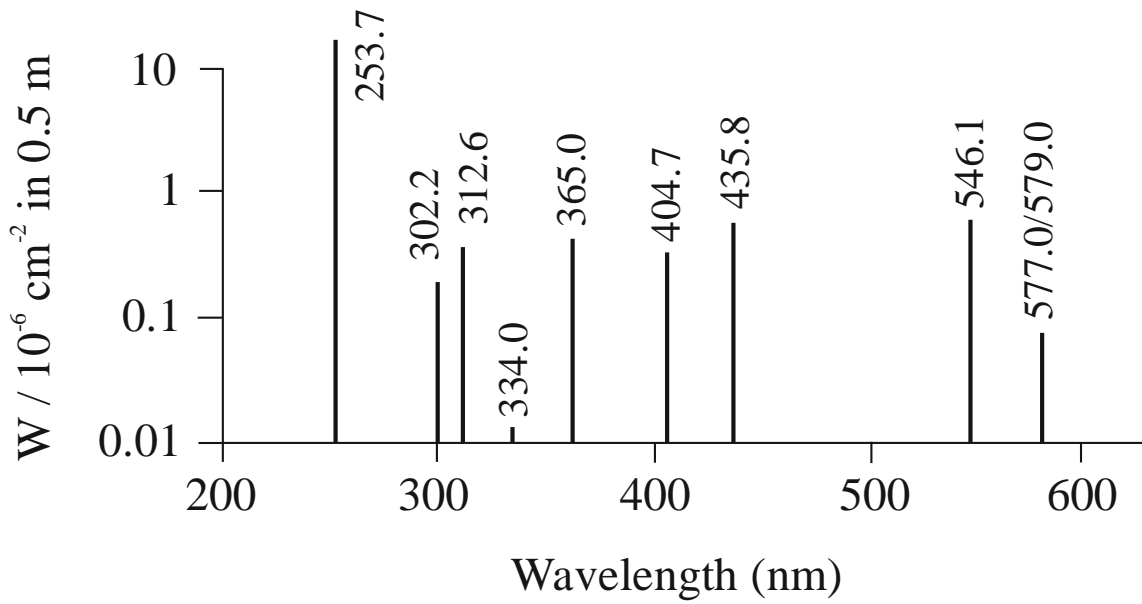


**Figure 2.3** Typical relative intensities of the emission lines from the Hg/Ar Pen-Ray lamp source (adapted from [http://pas.ce.wsu.edu/CE415/PenRay\\_lamp\\_spectra.pdf](http://pas.ce.wsu.edu/CE415/PenRay_lamp_spectra.pdf)).

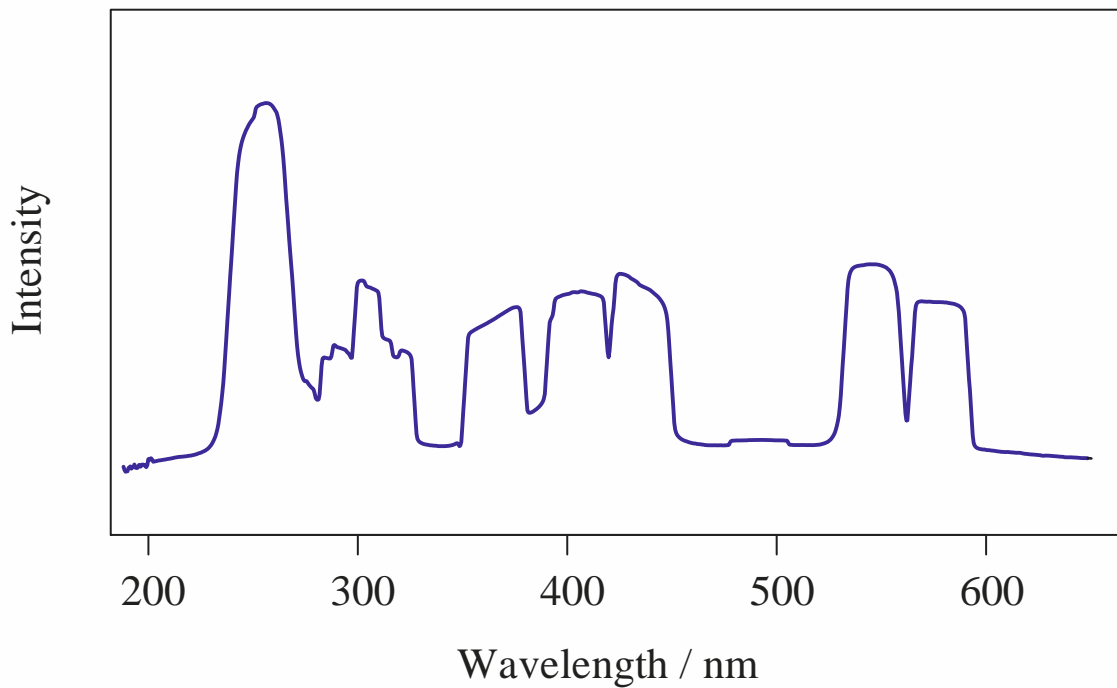


**Figure 2.4** Diffuse reflectance spectroscopy (DRS) recorded spectrum of the emission output from the Hg/Ar lamp between 190 and 650 nm. The spectrum is recorded as discrete bands, rather than lines, which match relatively closely to the typical intensity spectrum in Figure 2.3. The band at 184.5 nm was not observed as this was not recorded under vacuum.

### 2.1.3 Mass flow controllers

Mass flow controllers (MFCs) were used to regulate the flow of gas-phase reactants into the reactor. An MKS Instruments MFC controlled the flow of humidified N<sub>2</sub> at a consistent 2 slm (2000 sccm) at standard temperature and pressure (STP) into the reactor. Two Tylan MFCs controlled the flow of gas-phase VOCs and an additional diluting flow of dry N<sub>2</sub> into the reactor. The sum flow through these two MFCs was kept constant at 1 slm (1000 sccm). The Tylan MFCs were controlled automatically using the DAQFactory software package; changing the relative flow through each of the MFCs allowed for the concentration of VOCs into the reactor, and thereby the OH reactivity of the gas mixture, to be varied.

### 2.1.4 Gas sampling

VOCs were collected using a Unity 2 Thermal Desorption Unit (TDU) fitted with a Tenax TA sorbent trap and a Canister Interface Accessory (CIA) 8 Air Server attachment (Markes International). The system was pre-purged at a flow rate of 100 sccm for 10 minutes before sampling. During sampling, the trap was maintained below -20 °C and a sampling flow rate of 100 sccm used for one minute to give a total sample volume of 100 cm<sup>3</sup>. After sampling, the system lines and sorbent trap were purged with a carrier gas for three minutes at 100 sccm to eliminate oxygen from the system before desorption onto the gas chromatograph (GC) column. During the desorption process, the trap was rapidly heated to 250 °C and held for three minutes. All flow paths and sample lines were heated to 150 °C.

### 2.1.5 Gas chromatography

Gas chromatography is one of a suite of techniques that comes under the broad principle of chromatography. Chromatography is a common method for separating mixtures into their constituent components. It relies on the principle that different components within a mixture will have differing affinities to each of two phases. One of these phases is stationary, and aptly named the stationary phase, whilst the other moves in a defined direction, and is referred to as the mobile phase. As a component moves through this system, it will partition between the two phases; when interacting with the stationary phase the component is said to be 'retained', and when interacting with the mobile phase it is said to be unretained. The time a component spends retained on the stationary phase determines the time that the component elutes, or exits the

system. This time is known as the retention time ( $t_R$ ). Once eluted, the component can then be collected, or measured using a suitable detector.

In gas chromatography, the mobile phase is a gas. The gas is typically helium but nitrogen, argon or hydrogen are also commonly used. The stationary phase is film coated to the fused silica on the inner wall of a capillary column, through which the carrier gas flows. The choice of stationary phase material can have a large impact on the retention of analytes. Inert, or non-polar, columns interact with analytes physically, through Van der Waals forces. Hence, larger compounds with higher boiling points tend to have longer retention times. Polar columns add additional complexity to the interactions between the analyte and the stationary phase, with components possibly undergoing hydrogen bonding to the stationary phase, as well as other basic interactions. Separation is therefore based on the effects of these mechanisms. The strength of many of these interactions is largely dependent on temperature; therefore, GC columns are typically placed inside an oven, allowing for accurate temperature control, and hence control over the speed of analyte elution.

### 2.1.5.1 The equilibrium theory of separation

As an analyte moves through a column, it is in constant equilibrium between the mobile phase ( $A_M$ ) and the stationary phase ( $A_S$ ). The partition coefficient ( $K$ ) describes the equilibrium of the analyte between these two phases, and is equivalent to the ratio of the concentration, or mass, of the analyte in each of the two phases (Eq. 2.5 and 2.6).



$$K = \frac{C_S}{C_M} \quad \text{Eq. 2.6}$$

The capacity factor ( $k'$ ) is an experimental parameter used to describe the migration rates of analytes. It is related to the retention time of an analyte ( $t_R$ ) and the retention time of the mobile phase ( $t_M$ ) through Eq. 2.7.

$$k' = \frac{t_R - t_M}{t_M} \quad \text{Eq. 2.7}$$

For good separation to occur, each component must have a different capacity factor. The selectivity factor ( $\alpha$ ) is the ratio of the capacity factor for two different analytes. A large value of  $\alpha$  indicates good separation. For optimal separation, peaks should also be Gaussian in nature. For

this to be possible, band broadening, the process by which analyte molecules become spread out, must be limited.

It is possible to measure the efficiency of a column with respect to the separation of analytes. The theoretical plate model of chromatography visualises a column as divided into a large number of vertical layers, or plates. Analytes move through the column by transferring from one plate to the next. The number of plates ( $N$ ) is related to the efficiency and can be obtained by dividing the length of the column ( $L$ ) by the theoretical plate height ( $H$ ) (Eq. 2.8).

$$N = \frac{L}{H} \quad \text{Eq. 2.8}$$

The longer the column and the smaller the plates, the greater their number and the greater the efficiency of the column. The efficiency of an actual column can be estimated using the retention time of a chromatographic peak and its width at half height using Eq. 2.9.

$$N = 5.5 \left( \frac{t_R}{w_{1/2}} \right)^2 \quad \text{Eq. 2.9}$$

The van Deemter equation relates plate height to the linear velocity ( $\mu$ ) of the mobile phase through various parameters that control band broadening (Eq. 2.10). The eddy diffusion term ( $A$ ) describes the random paths that an analyte molecule can take through the stationary phase. In open tubular columns,  $A$  is equal to zero. The longitudinal diffusion ( $B$ ) describes the longitudinal spread of an analyte within the carrier gas. The mass transfer term ( $C$ ) considers the difficulty for an analyte to transfer between phases. The effects of longitudinal diffusion are reduced by increasing the velocity of the mobile phase, whilst the impacts of mass transfer are amplified by increasing velocity. This usually results in an optimum velocity for the mobile phase through a column.

$$H = A + \frac{B}{\mu} + C\mu \quad \text{Eq. 2.10}$$

Another measure of how well analytes are separated, which considers peak width, is provided by the resolution ( $R_S$ ). The resolution between two components, A and B, is given by Eq. 2.11, where  $w$  is the peak width. For adequate baseline separation, the resolution needs to be greater than 1.5.

$$R_S = \frac{2(t_{RA} - t_{RB})}{w_A + w_B} \quad \text{Eq. 2.11}$$

### 2.1.5.2 The GC system

The GC system used in this work was an Agilent 7890 (Agilent Technologies) fitted with a DB5-MS ultra-inert capillary column (60 m × 0.32 mm internal diameter (ID) × 1 µm film; Agilent Technologies). The temperature ramping of the GC oven was varied between synthetic gas mixtures to achieve optimum separation of the VOCs. The column head pressure was set to 50 psi (344 kPa) and operated in constant pressure mode using helium as the carrier gas. The GC method, along with the TDU settings, gave sample turn arounds of up to 25 minutes for more complicated mixtures, and up to 15 minutes for simpler mixtures.

### 2.1.6 Mass spectrometry

Mass spectrometry (MS) is an analytical technique used to separate and detect chemical species based on their mass to charge ratio ( $m/z$ ). MS requires molecules to be ionised before detection. Common methods of ionisation include: electron ionisation (EI), matrix assisted laser desorption ionisation (MALDI) and chemical ionisation (CI). Ionisation techniques can be 'hard' or 'soft'; this refers to the amount of energy transferred to the molecule during the ionisation process. Hard techniques transfer excess energy to the analyte, which can result in the fragmentation of the molecular structure. The extent of fragmentation, and the fragmentation ions formed as a result, depend on the extent of the excess energy. Fragmentation can provide information on the molecular structure of the analyte.

In electron ionisation, electrons are accelerated between a hot filament and an anode, encountering the vapourised analytes in the process. Electrons are typically removed from the analyte, as in R. 2.2, although electron capture (R. 2.3) is also possible but more unusual. As EI is a 'hard' ionisation technique, fragmentation occurs via the loss of either a neutral radical or charged species. The extent of fragmentation is often large which is both advantageous and disadvantageous: a large amount of fragmentation can assist with characterisation and identification but often comes at the expense of the loss of the molecular ion ( $M^+$ ) from the resulting mass spectrum.



In chemical ionisation, a reagent gas (such as methane, isobutane or ammonia) is ionised first, using a hot filament as in EI. The ionised reagent gas can then collide with the analytes, possibly transferring charge (usually in the form of a proton if using methane, CH<sub>4</sub>, as the reagent gas) in the process shown in R. 2.4.



In CI, therefore, the molecular weight of the analyte is easily obtained, although it is observed at one Dalton unit greater, due to the addition of the proton. However, very little fragmentation occurs which can make structural characterisation difficult.

Once ionised, analytes are separated by a mass analyser before detection. Mass analysers are typically operated under vacuum to minimise collisions between molecules. This is important as ions can decompose over time; fast transmission is therefore necessary for greater sensitivity. After mass separation, analytes are detected using simple detectors such as an electron multiplier, which counts the number of ions. Accurate identification of an analyte relies on high resolution measurements of an ion's mass. The resolving power,  $R$ , of a mass analyser reflects its ability to distinguish between two ions with a small mass difference (Eq. 2.12).

$$R = \frac{m}{\delta m} \quad \text{Eq. 2.12}$$

#### 2.1.6.1 Time-of-flight (ToF) mass spectrometry

In ToF-MS ionised analytes are accelerated in a flight tube using an electric field and allowed to drift to the reactor. Heavier ions move more slowly than lighter ions and hence have a longer 'time of flight'. The kinetic energy ( $E_k$ ) of a mass is given by Eq. 2.13.

$$E_k = \frac{1}{2}mv^2 \quad \text{Eq. 2.13}$$

Time-of-flight mass spectrometry offers advantages over flame ionisation detection, the more traditional detection method used after separation by gas chromatography. Firstly, there is considerable base line reduction and reduction in the signal-to-noise ratio. This can help with the detection of compounds at trace concentrations. Secondly, the mass spectrum produced during the elution of a compound can be compared to databases of mass spectra allowing for ease of identification of similar compounds. This is far more difficult when using GC-FID, where standards must generally be used to determine the order of elution for compounds with a similar number of

carbon atoms. Finally, mass spectrometry allows for co-eluting compounds to be considered and analysed separately, based on appropriate mass ion selection.

### 2.1.6.3 The MS system

The mass spectrometer coupled to the Agilent 7890 GC used in this work was a Markes International BenchTOF<sup>®</sup> time-of-flight mass spectrometer. The mass spectrometer was routinely calibrated and signal optimised. The air:water ratio within the flight tube was also regularly checked to ensure consistent operation. The MS was operated with the filament set to 1.60 V and a filament delay of 180 s. The delay was necessary for prolonging the lifetime of the detector. The first 3 min of elution through the GC was dominated by the most volatile gases, such as N<sub>2</sub> and any residual O<sub>2</sub>. These eluted in large quantities and would have resulted in large signals. The filament delay of 3 min was used to remove these signals from the recorded mass spectra whilst retaining the signal from the actual mixture components.

### 2.1.7 Synthetic gas mixtures

Ambient air, or “real air”, has previously been used as the gaseous matrix for the multivariate relative rate technique (Shaw et al., 2018). However, the use of ambient air resulted in a number of problems. These issues generally related to the complexity of the atmosphere; ambient air is a dynamic mixture which can vary hugely on both a temporal and spatial scale. This had to be considered when sampling the atmosphere for kinetic measurements as even small discrepancies in the initial VOC concentrations lead to major variations in the final results. A dual reactor system, in which one reactor was kept constantly dark, foregoing OH radical generation, was used in an attempt to account for atmospheric fluctuations. The system used for measuring rate coefficients using atmospheric sampling is described in Shaw et al. (2018) but is not used in this work.

Even after accounting for the erratic nature of the atmosphere, there are still many other problems associated with the use of ambient air as a gas matrix. For example, the number of identified VOCs can potentially be very large. This can lead to difficulties in separation using one dimensional gas chromatography and can also impact on peak resolution. The concentrations of individual VOCs can also be supremely low; even below the limit of detection for GC-ToF-MS. This can have a large impact on uncertainties, particularly if a VOC is depleted below the limit of detection after exposure to OH. Another problem concerns the potential interferences from multiple non-synthetic oxidants; ozone and endemic OH are likely to be present in ambient air,

particularly during the day, and these may perturb VOC concentrations in ways that can be difficult to account for.

One way of avoiding the problems associated with “real air” sampling was to prepare synthetic gas mixtures containing multiple VOCs. This not only simplified the gas matrix, by removing the likelihood of non-synthetic oxidant contaminants, but also allowed for the concentration of individual VOCs to be controlled.

Synthetic mixtures for this work were prepared by injecting a measured amount of undiluted liquid VOC into a 500 ml evacuated, double ended, stainless steel sample cylinder (Swagelok). This cylinder was then flushed into a pacified gas cylinder (10 L, Experis, Air Products) using N<sub>2</sub> (99.998 % purity). The gas cylinder could be pressurised with up to 100 bar N<sub>2</sub> to achieve the desired final mixing ratio for each VOC in the cylinder. Further dilutions were sometimes necessary for this, and these were accomplished by evacuating the cylinder to atmospheric pressure and then refilling with N<sub>2</sub> to the desired pressure.

### 2.1.8 Experiment design

Figure 2.5 shows the experimental setup for the measurement of multivariate gas-phase relative rate coefficients with OH. Humidified nitrogen was constantly supplied to the reactor throughout experiments. Injection of the synthetic gas mixture was triggered automatically when the GC was ready to begin collection of a new sample. Samples were alternated between light and dark; the Hg/Ar lamp was alternately switched on and off during the course of sampling. The VOC concentrations for a ‘lamp off’ sample were representative of the VOC mixing ratios within the synthetic mixture, albeit with increased dilution due to mixing with extra flows of N<sub>2</sub> upon entering the reaction chamber. A VOC measured from a dark sample was therefore said to be at its initial concentration ([VOC]<sub>0</sub>).

A ‘lamp on’ sample, in which the Hg/Ar lamp was used to photolyse H<sub>2</sub>O to form OH radicals (R. 2.1), gave VOC concentrations which were depleted when compared with the lamp-off concentration, due to the reaction between the VOCs and the radical oxidant. A VOC, measured from a ‘lamp on’ sample, was therefore said to be at its final concentration ([VOC]).

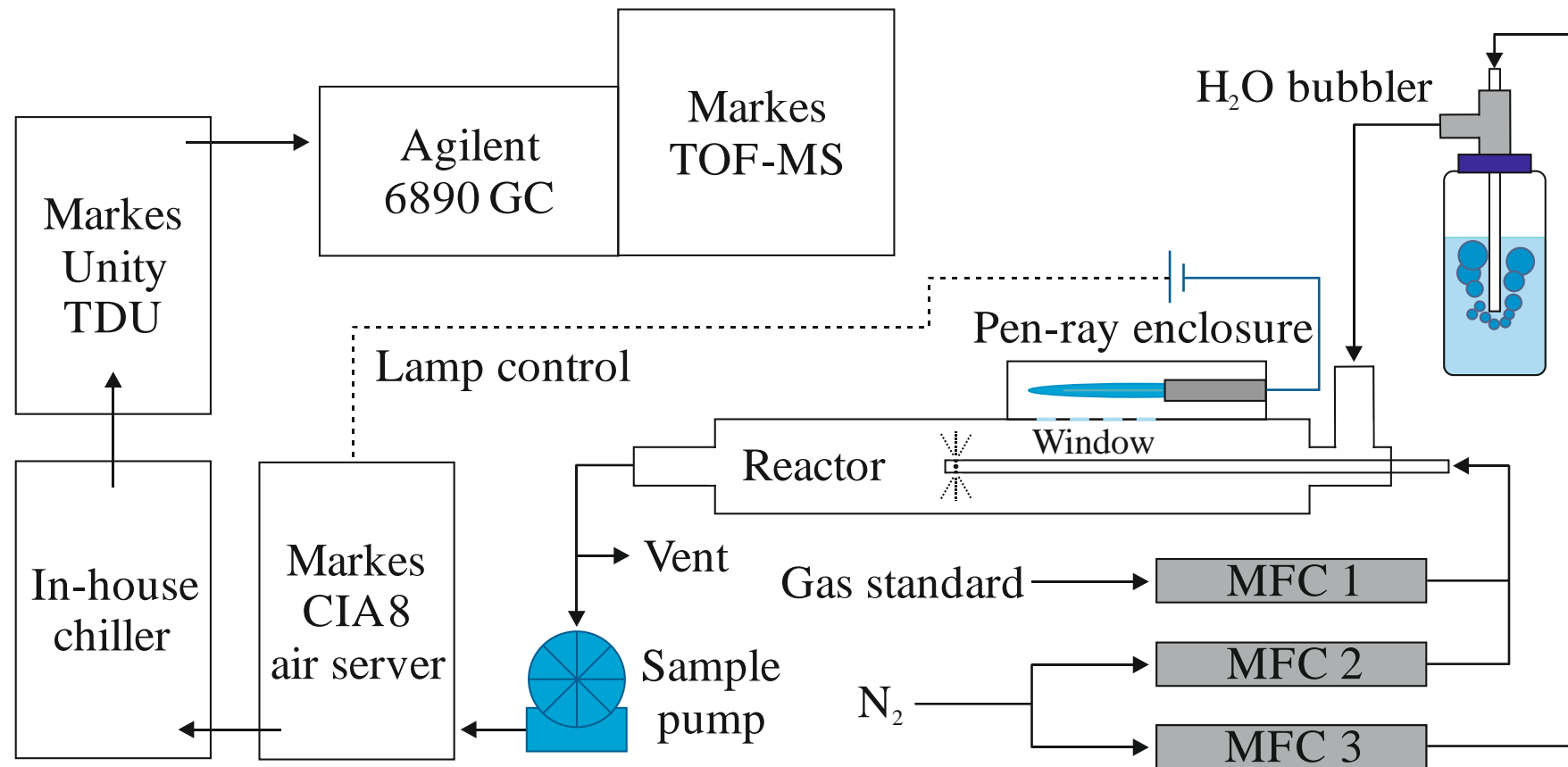


**Figure 2.5** Schematic of the OH reactor configuration used. Key to abbreviations: CIA8 = air server and canister interface accessory; GC = gas chromatograph; MFC = mass flow controller; TOF-MS = time-of-flight mass spectrometer; TDU = thermal desorption unit. The flow rate through MFC 1 was stepped from 200 sccm through to 1000 sccm in 200 sccm intervals. The combined flow rate through MFC 1 and MFC 2 was kept constant at 1000 sccm. The flow rate through MFC 3, and hence through the H<sub>2</sub>O bubbler, was set to 2000 sccm resulting in a total flow through the reactor of 3000 sccm. See Figure 2.2 for a more comprehensive schematic of the reactor design.

By alternating between light and dark reactor conditions over multiple sample runs, a set of observations comprising two populations of data ( $[\text{VOC}]_0$  and  $[\text{VOC}]$ ) for each VOC, was generated. For most reaction mixtures eight samples were collected with the reactor lamp switched off, and eight with the reactor lamp switched on. The lamp was alternated off and on across sample runs to remove the possibility of bias due to instrumental drift over time. For a description of how the GC-MS data for the “lamp-off” and “lamp-on” samples was analysed, please refer to Section 2.1.10.

The depletion in an individual VOC with a literature VOC + OH rate coefficient,  $k$ , was then evaluated using simple kinetic equations. Equations 2.14 to 2.16 demonstrate these kinetic equations using isoprene ( $\text{C}_5\text{H}_8$ ) as an example (R. 2.6). Eq. 2.14 shows the differential rate equation for the oxidation of isoprene by OH whilst Eq. 2.15 shows a rearrangement and a further integrated form of Eq. 2.14 respectively. These equations are analogous to Eq. 1.4 and Eq. 1.5 in Chapter 1 Section 1.3.1.



$$\frac{d[\text{C}_5\text{H}_8]}{dt} = -k_{\text{C}_5\text{H}_8} [\text{C}_5\text{H}_8][\text{OH}] \quad \text{Eq. 2.14}$$

$$\frac{d[\text{C}_5\text{H}_8]}{[\text{C}_5\text{H}_8]} = -k_{\text{C}_5\text{H}_8} [\text{OH}] dt \quad \text{Eq. 2.15}$$

$$\ln \left( \frac{[\text{C}_5\text{H}_8]_0}{[\text{C}_5\text{H}_8]} \right) = k_{\text{C}_5\text{H}_8} \int [\text{OH}] dt \quad \text{Eq. 2.16}$$

Equations 2.17 to 2.19 show a more general case for any VOC (R. 2.7).



$$\frac{d[\text{VOC}]}{dt} = -k[\text{VOC}][\text{OH}] \quad \text{Eq. 2.17}$$

$$\frac{d[\text{VOC}]}{[\text{VOC}]} = -k[\text{OH}] dt \quad \text{Eq. 2.18}$$

$$\ln \left( \frac{[\text{VOC}]_0}{[\text{VOC}]} \right) = k \int [\text{OH}] dt \quad \text{Eq. 2.19}$$

The depletion factor for a VOC due to its reaction with OH is represented by the term  $\ln \left( \frac{[\text{VOC}]_0}{[\text{VOC}]} \right)$ .

This is related to the rate coefficient for the reaction between the VOC and OH ( $k$ ) via Eq. 2.19.

The integral of the OH concentration over time ( $\int [\text{OH}] dt$ ) is known as the OH exposure ( $OH_{exp}$ ). This technique assumed that all VOCs in the reactor experienced identical exposure to OH owing to rapid homogenous mixing of the oxidant within the reactor. A proportional relationship between depletion factor ( $\ln\left(\frac{[\text{VOC}]_0}{[\text{VOC}]}\right)$ ) and  $k$  should therefore be observed for the range of VOCs, with the gradient of the slope equal to  $OH_{exp}$ . This derived relationship allowed for the calculation of previously unmeasured OH rate coefficients for VOC + OH reactions. All other VOC + OH reactions in the synthetic mixture therefore act as 'reference' reactions and any new rate coefficients are derived relative to each of these reference reactions. The use of multiple literature  $k$  values as reference values minimised the reliance on any single, possibly erroneous, literature value and also calibrated the system across a range of VOC reactivities.

This entire process was repeated multiple times using a different set of synthetic VOC mixture flow conditions to inject a different mixture OH reactivity into the reactor. Due to a constant OH reactivity towards the native  $\text{HO}_2$  in the reactor, the OH exposure of the mixture itself changed as the concentrations of the VOCs in the reactor varied. Hence, the analysis of VOC rate coefficients was performed individually for each OH reactivity of mixture injected into the reactor. Once VOC + OH rate coefficients had been calculated at each OH reactivity, final VOC + OH rate coefficients were derived by averaging across each of the individual values.

### 2.1.8.1 Internal standards

Internal standards are often used in analytical chemistry to correct for the loss of analytes during sampling and measurement which often varies across multiple repeats. Internal standards are typically chosen to be as similar as possible to the compound(s) of interest to maximise the likelihood that they are subjected to similar effects during sampling. In the case of this experiment, the diversity in the structural composition of the compounds in the mixtures meant that selecting a compound that was similar to all others was difficult. Instead, the internal standard used needed to be unaffected by exposure to OH, in order to account for variations in sampling conditions from 'lamp off' samples to 'lamp on' samples.

Few organic compounds are unreactive towards OH as they typically contain hydrogen atoms, which undergo H-atom abstraction by the oxidant. Organic compounds containing no hydrogen atoms do exist however; carbon tetrachloride ( $\text{CCl}_4$ ) is an example of such a compound.  $\text{CCl}_4$  is approximately a million times less reactive towards OH than most VOCs, with a recommended rate coefficient for reaction with OH of  $k < 1 \times 10^{-19} \text{ cm}^3 \text{ molecule}^{-1} \text{ s}^{-1}$  (Atkinson et al., 2006).

However,  $\text{CCl}_4$  is classed as a chlorofluorocarbon (CFC) and is therefore subject to significant regulations on its use. Many compounds which react relatively slowly with OH are also CFCs or hydrochlorofluorocarbons (HCFCs) and hence unsuitable for use as an internal standard.

Dichloromethane ( $\text{CH}_2\text{Cl}_2$ ) is a common solvent used in organic chemistry which is not classed as either a CFC or HCFC. Its recommended rate coefficient for reaction with OH is  $k = 1.0 \times 10^{-13} \text{ cm}^3 \text{ molecule}^{-1} \text{ s}^{-1}$ , at least an order of magnitude smaller than even the slowest reacting of aromatic VOCs. Dichloromethane (DCM) was therefore also included in VOC mixtures, with the intention of using it as an internal standard. Its small rate coefficient for reaction with OH meant that its depletion upon exposure to OH was negligible and therefore insignificant within the context of the experiments (simulated depletions of less than 1% for all mixtures). For this reason, its concentration for both 'lamp off' and 'lamp on' samples should be constant, providing consistent sampling conditions. Deviations in its concentration were therefore indicative of changes in the sampling conditions and not due to the presence of OH. These deviations were then corrected for with respect to the other VOCs.

The applicability of using DCM as an internal calibrant was examined by referring to the correlation in the peak areas between other VOCs and itself. For a compound to be used as a valid internal calibrant for another analyte, the peak areas should show good correlation i.e. samples with greater observed peak areas for the internal standard should show a similarly larger peak area for the other analyte. If a poor correlation were to be observed between the internal standard and another analyte, then it was unlikely to act as a useful internal calibrant for that species. Compounds that presented large  $R^2$  values for their correlation with DCM were therefore adjusted by normalising to the spread in the DCM peak areas. For the most part, this was limited to compounds which eluted within a few minutes of DCM.

### 2.1.9 Literature $k$ values

Some of the more common, or atmospherically relevant, VOCs benefit from having multiple measurements of their rate coefficient for reaction with OH available in the literature. Important reactions, such as that between isoprene and OH, have been measured using many different techniques and in many different laboratories and as such it can be difficult to choose a single value to use as the 'reference': the choice of different reference values can lead to slight variations in the results obtained at the end of an experiment, through minor adjustments to the calculated  $OH_{exp}$ . Fortunately, the International Union of Pure and Applied Chemistry (IUPAC) Task Group on Atmospheric Chemical Kinetic Data has put considerable effort into producing a set of evaluated rate coefficients for many important atmospheric reactions. The IUPAC database, which can be accessed online, provides recommended values for the reaction between OH and many short chain hydrocarbons, along with some of the more common monoterpenes and aromatic VOCs (Atkinson et al., 2006; <http://iupac.pole-ether.fr/>). These values are evaluated using a balance of literature data and are updated regularly. Hence, when selecting single values to use as references, this data was used as a matter of priority.

The IUPAC database is limited in scope, leaving the vast majority of larger, or less common atmospheric VOCs, without an evaluated  $k$  value. However, many VOC + OH reactions that do not appear in the IUPAC database have been reviewed and evaluated in Atkinson and Arey (2003). The database in their review paper is much more extensive than the IUPAC equivalent, but does not provide uncertainties, nor is it continually updated and hence does not account for measurements made since its publication. Much of the data in Atkinson and Arey (2003) was collated from the extensive evaluations of atmospheric oxidation of alkenes and aromatic hydrocarbons in Calvert et al. (2000, 2002). Roger Atkinson has also been personally involved with the measurements of many rate coefficients and is widely regarded as an expert in the field. Hence, it can be assumed that the majority of rate coefficients derived by his laboratory are internally consistent. Some  $k$  values in Atkinson and Arey (2003) were taken from a single measurement made using the traditional relative rate method. Some of the recommended  $k$  values for the reference VOC + OH reactions used in those experiments have changed since publication. In the case that a recommended  $k$  value in Atkinson and Arey (2003) was based on only a single experiment, this value was adjusted to account for changes to the recommended reference compound values made after publication.

In the few instances that a rate coefficient for a reaction between a certain VOC and OH neither appeared in the Atkinson and Arey (2003) database, nor had an Atkinson derived coefficient in the literature, any other experimental literature value was taken as a reference. In the case that there were multiple measurements of the same rate coefficient, an average of those values, weighted to the uncertainties, was used. Theoretical values for reaction rate coefficients were never used as reference values.

Figure 2.6 shows a flowchart illustrating this process.

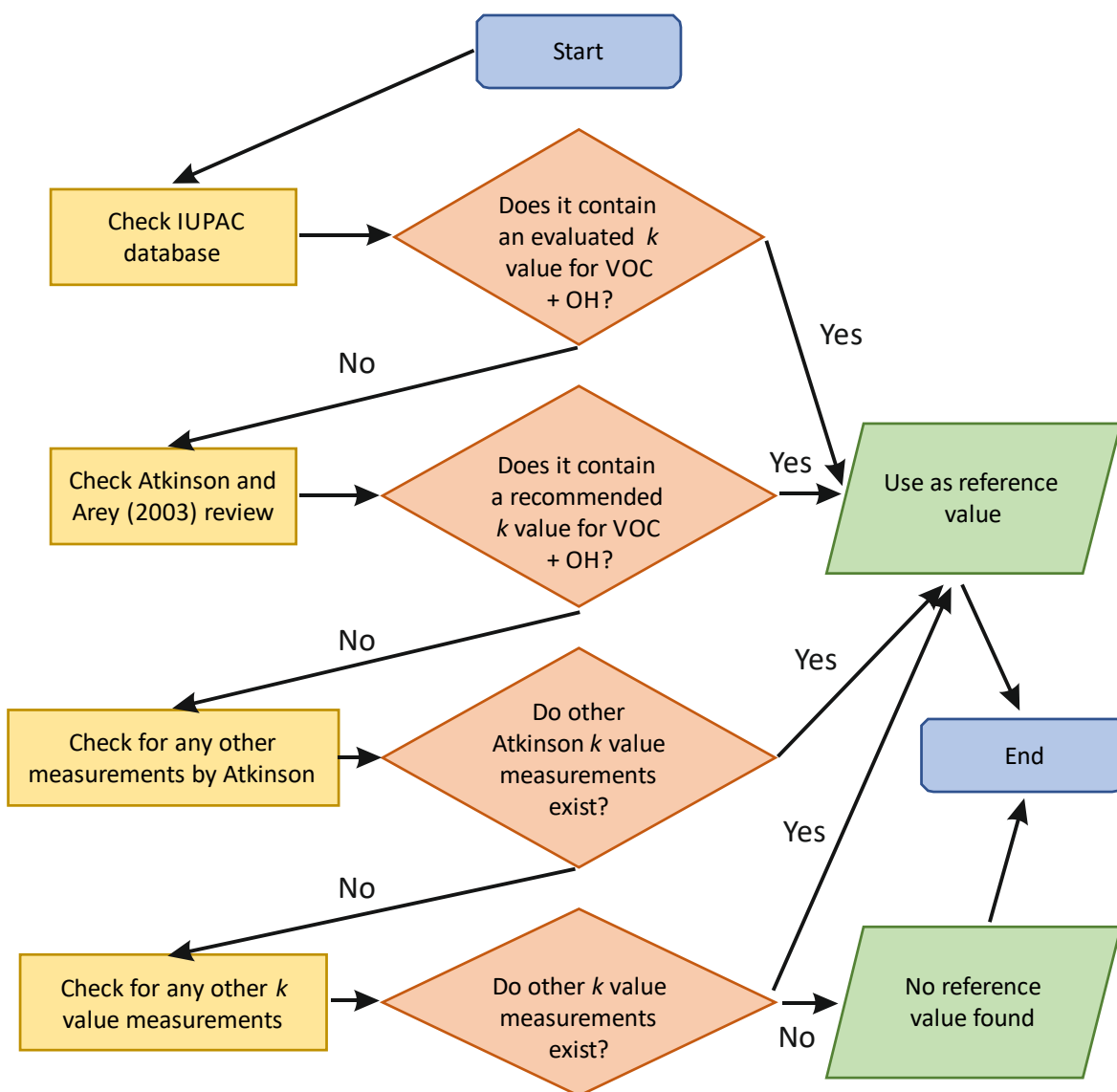


**Figure 2.6** The process undertaken to find literature reference  $k$  values for VOC + OH reactions.

### 2.1.9.1 A note on errors

The errors and uncertainties provided alongside many of the referenced literature rate coefficients in this work differ considerably. The errors in measured values often vary from symmetrical uncertainties of a few percent to much more substantial errors. For example, the relative rate measured rate coefficient for the 1-nonene + OH reaction, of  $43.2 \times 10^{-12} \text{ cm}^3 \text{ molecule}^{-1} \text{ s}^{-1}$ , provided by Aschmann and Atkinson (2008) has a very small uncertainty of  $0.5 \times 10^{-12} \text{ cm}^3 \text{ molecule}^{-1} \text{ s}^{-1}$ . On the other hand, the rate coefficient for the  $\beta$ -pinene + OH reaction, of  $93.5 (\pm 27.9) \times 10^{-12} \text{ cm}^3 \text{ molecule}^{-1} \text{ s}^{-1}$ , provided by Dash and Rajakumar (2013) has a much larger relative error, despite using a similar relative rate technique.

The uncertainties provided on the evaluated and recommended rate coefficients, taken from the Calvert et al. (2000, 2002) and Atkinson and Arey (2003) reviews, tend to reflect the greater uncertainties. This is often because the recommended values are the result of weighted averages of multiple individual measured values, and hence, somewhat arbitrarily large errors of  $\pm 20\%$  or greater are placed upon them.

Whilst the IUPAC recommended values also tend to be given large uncertainties, of more than 10%, the errors on their values are asymmetric. For example, the reliability in the recommended value for the isoprene + OH reaction, is given as a change in  $\log k$  ( $\Delta \log k$ ) =  $\pm 0.06$  at 298 K. This therefore converts to an asymmetrical error when calculated for the units used in this work.

### 2.1.10 Data analysis and error propagation

GC-MS data was analysed using automatic peak integration software (Agilent Technologies) using appropriate mass ion selection for each individual VOC. Mass ion selection allowed for the total separation of peaks in the case that two VOCs had co-eluted and had unique mass fragmentation ions.

There was considerable variation in the measured peak areas for some VOCs when sampling some OH reactivities, even after minor fluctuations in the volume sampled by the TDU were considered. Potentially anomalous peak areas were therefore removed using the MAD<sub>e</sub> method (Burke, 2001) before an average 'lamp off' value ([VOC]<sub>0</sub>) and 'lamp on' value ([VOC]) was calculated, along with an associated standard error for each ( $\sigma_{[VOC]_0}$  and  $\sigma_{[VOC]}$ ). This calculation was performed at each individual OH reactivity for a mixture. The depletion factor ( $\ln\left(\frac{[VOC]_0}{[VOC]}\right)$ ) was then calculated for each VOC, with the uncertainty in the depletion factor given by Eq. 2.20 and Eq. 2.21.

$$\frac{\sigma_{[VOC]_0}}{\frac{[VOC]_0}{[VOC]}} = \sqrt{\left(\frac{\sigma_{[VOC]_0}}{[VOC]_0}\right)^2 + \left(\frac{\sigma_{[VOC]}}{[VOC]}\right)^2} \quad \text{Eq. 2.20}$$

$$\sigma_{\ln\left(\frac{[VOC]_0}{[VOC]}\right)} = \left| \frac{d \ln\left(\frac{[VOC]_0}{[VOC]}\right)}{d\left(\frac{[VOC]_0}{[VOC]}\right)} \right| \sigma_{\frac{[VOC]_0}{[VOC]}} = \left| \frac{1}{\frac{[VOC]_0}{[VOC]}} \right| \sigma_{\frac{[VOC]_0}{[VOC]}} \quad \text{Eq. 2.21}$$

Once this process had been repeated for each of the VOCs, a relative rate plot at each OH reactivity was produced using all the depletion factors and the reference  $k$  values. Linear regression, weighted to the uncertainties in  $\ln\left(\frac{[VOC]_0}{[VOC]}\right)$ , but not to the uncertainties in the evaluated reference  $k$  values, was performed to find the  $OH_{exp}$  using Eq. 2.19. Weights for the linear fit were calculated the uncertainties in the depletion factors as given by Eq. 2.22.

$$w_i = \frac{1}{\sigma_i^2} \quad \text{Eq. 2.22}$$

The  $OH_{exp}$ , along with the depletion factors, was then used to estimate new rate coefficients for each of the VOCs at each OH reactivity using Eq. 2.23, with the uncertainty in  $k$  given as  $\sigma_k$  by Eq. 2.24.

$$k = \frac{\ln \frac{[VOC]_0}{[VOC]} - c}{OH_{exp}} \quad \text{Eq. 2.23}$$

$$\sigma_k = \frac{\frac{\sigma_{\ln \frac{[VOC]_0}{[VOC]} + \sigma_c}}{\ln \frac{[VOC]_0}{[VOC]} + c}}{OH_{exp}} + \frac{\sigma_{OH_{exp}}}{OH_{exp}} \quad \text{Eq. 2.24}$$

Finally, a single measured  $k$  value for each VOC + OH reaction was calculated by averaging the individual  $k$  values at each of the OH reactivities used, weighted to their respective uncertainties,  $\sigma_k$ . The errors quoted on every final  $k$  value in this work are equal to one standard deviation. These final values were then compared against both the reference evaluated values and other  $k$  values found in the wider literature. This allowed for an assessment of the reliability of the technique for reproducing existing reaction rate coefficients, and by extension, an assessment of the capability for estimating new rate coefficients.

## 2.2 Modifications to the basic technique

The experimental set up and techniques outlined above were applied to the majority of OH + VOC rate coefficient measurements. However, to fully realise the potential of this method for the measurement of gas-phase rate coefficients, it was deemed necessary to make some minor modifications and developments. The following section outlines the changes and developments initiated in order to allow for these measurements to be made.

### 2.2.1 The HO<sub>2</sub> problem and the NO solution

The generation of OH via the photolysis of H<sub>2</sub>O also results in the production of atomic hydrogen radicals (R. 2.8). It is expected that HO<sub>2</sub> is rapidly formed by the reaction between H-atoms and endemic O<sub>2</sub> which cannot be totally excluded from the reactor (R. 2.9). It can be assumed that H radicals react almost exclusively in this way, thereby producing HO<sub>2</sub> in similar concentrations to OH.



HO<sub>2</sub> is much less reactive towards VOCs than OH. Thus, it can be assumed that the observed depletions in the VOCs are almost entirely due to reaction with OH. However, OH and HO<sub>2</sub> may react together at a considerable rate (R. 2.10); HO<sub>2</sub> may therefore represent a significant OH sink within the reactor. In an ideal situation, OH would only react with the VOCs.



R. 2.10 has a recommended rate coefficient of  $k_3 = 1.1 \times 10^{-10} \text{ cm}^3 \text{ molecule}^{-1} \text{ s}^{-1}$  (Atkinson et al., 2006). Thus, this reaction may proceed at a rate fast enough to compete with the VOCs for OH. For the synthetic mixtures containing mainly monoterpenes and alkenes, described in Chapter 3, numerical simulations showed that this does not seem to be a problem. The reactions between these VOCs and OH have sufficiently large rate coefficients to compete with  $\text{HO}_2$  for OH. However, the rate coefficients for many aromatic species are between 1 and 2 orders of magnitude smaller than those for the unsaturated hydrocarbons. For mixtures containing mainly aromatic species, such as those described in Chapter 4, the  $\text{HO}_2$  reaction may largely outcompete the VOCs for OH, leading to negligible observable depletions in the measured peak areas for the VOCs.

This is illustrated in Figure 2.7 which shows the estimated OH reactivity towards  $\text{HO}_2$  and the VOCs in each of four different mixtures. As the concentration of  $\text{HO}_2$  is constant between mixtures, the OH reactivity towards it remains at approximately  $22 \text{ s}^{-1}$ . For the first monoterpenes mixture, the OH reactivity towards  $\text{HO}_2$  is only a fraction of the total OH reactivity. However, for mixtures comprising much slower reacting VOCs, this reactivity towards  $\text{HO}_2$  is much more dominant. For example,  $\text{HO}_2$  accounts for just 16 % of the OH reactivity for Monoterpenes 1 but 68 % for the alkanes mixture.

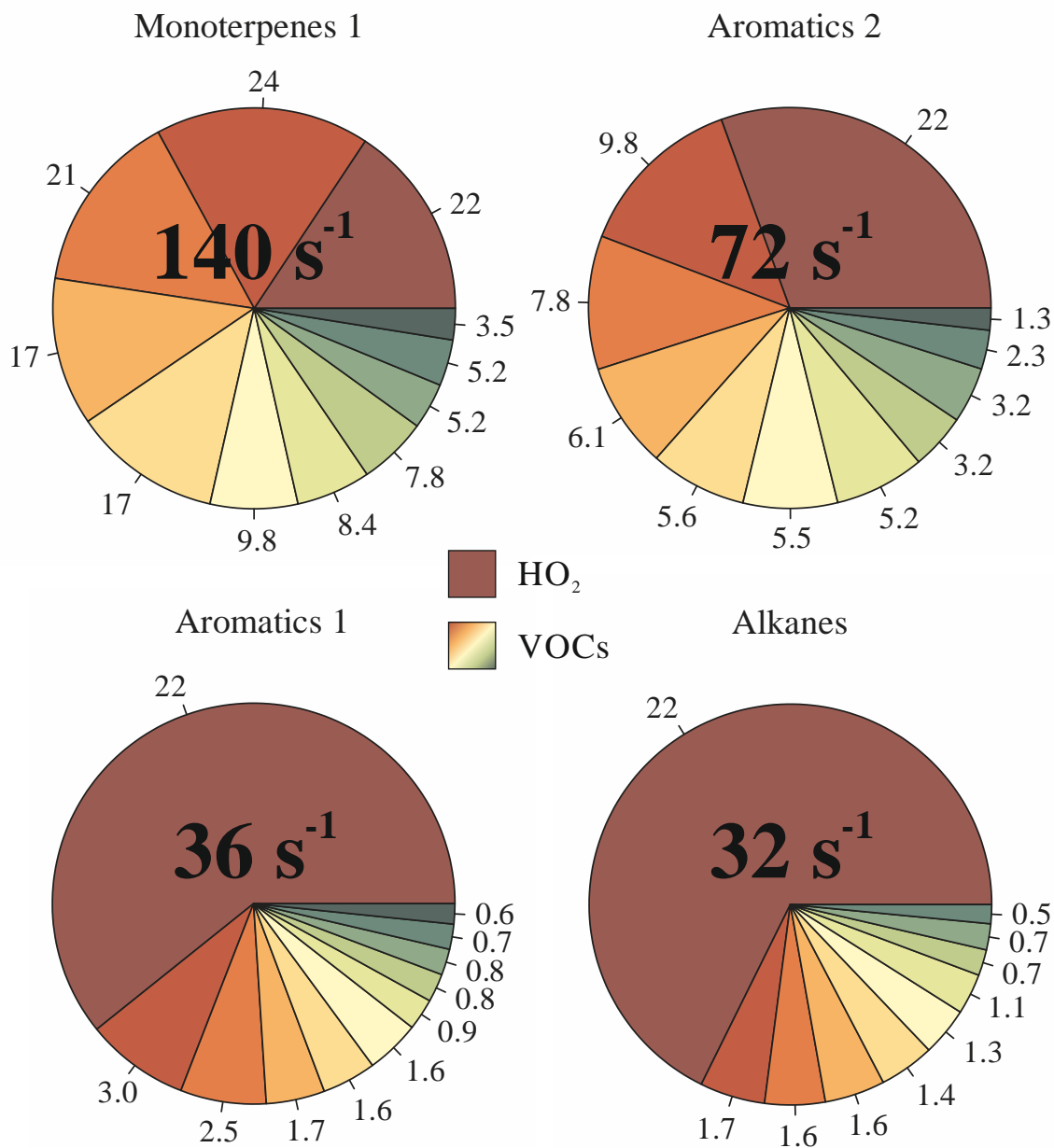


**Figure 2.7** The estimated OH reactivity towards HO<sub>2</sub> and VOCs for four different VOC mixtures measured as part of this work. Values are provided in units of s<sup>-1</sup>. The total OH reactivity for each of the four mixtures was approximately 140, 72, 36 and 32 s<sup>-1</sup>, for the monoterpenes, aromatics 2, aromatics 1 and alkanes mixtures respectively. All values were calculated using the evaluated reference literature *k* values for the VOCs (please refer to the following chapters).

Fortunately, the impacts of HO<sub>2</sub> may be mitigated via the addition of NO (R. 2.11). NO reacts with HO<sub>2</sub> with a recommended rate coefficient of  $k_4 = 8.5 \times 10^{-12} \text{ cm}^3 \text{ molecule}^{-1} \text{ s}^{-1}$  (Atkinson et al., 2006). Although this rate coefficient is quite small, by adding excess amounts of NO to the reactor it may be possible to significantly reduce the amount of OH reacting with HO<sub>2</sub>.



R. 2.11 also has an additional advantage in that it provides another source of OH, ultimately improving the efficiency of the original H<sub>2</sub>O photolysis in terms of the OH yield.

### 2.2.1.1 Equipment set up

Figure 2.8 shows how a cylinder containing 5 ppm NO was incorporated into the experimental set up. The NO inlet was added to the gas line containing humidified N<sub>2</sub> prior to it entering the reactor. An extra mass flow controller (MFC 4) was used so that the flow of NO could be varied between 0 and 200 sccm.

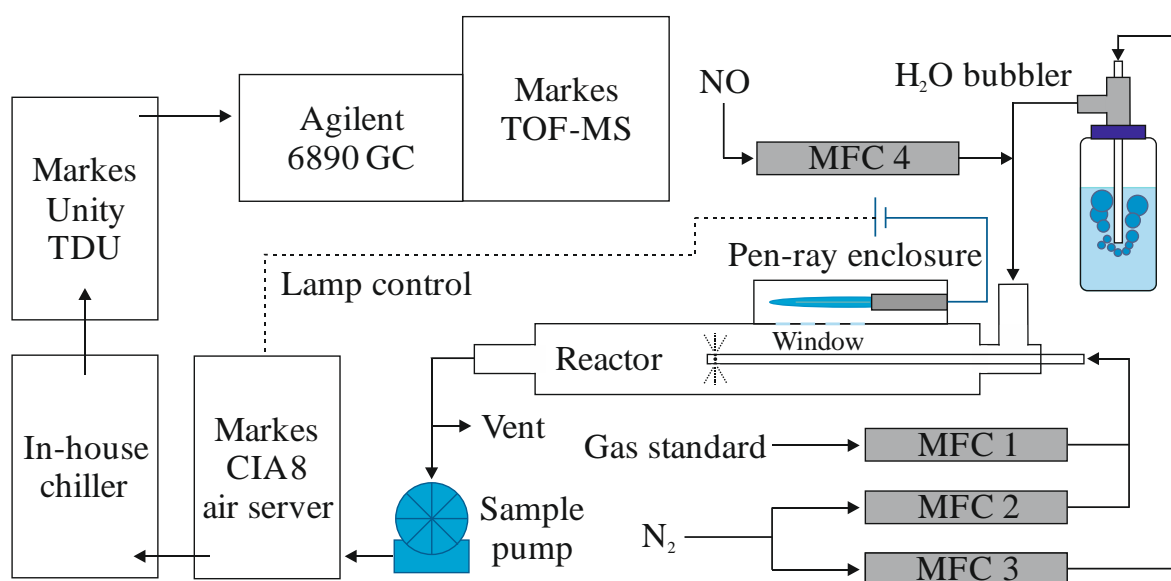


**Figure 2.8** Schematic showing the equipment set up for experiments on aromatic VOCs. Key to abbreviations: CIA8 = air server and canister interface accessory, GC = gas chromatograph, MFC = mass flow controller, TDU = thermal desorption unit, TOF-MS = time-of-flight mass-spectrometer. See Figure 2.2 for a more comprehensive schematic of the reactor design.

## 2.2.2 Kinetic studies of VOC + Cl reactions

Figure 2.9 shows the experimental set up for measuring VOC + Cl reaction rate coefficients. The main difference between the setup used for OH and that used for Cl was in the generation of the radical oxidant. The water bubbler, used as the precursor for OH radicals, was removed and replaced with a gas canister containing Cl<sub>2</sub> (see Section 2.2.2.1 for more information). The inclusion of a toxic gas (Cl<sub>2</sub>) meant that the system wasn't vented directly into the laboratory. Instead, a diaphragm pump was attached to the end of the reactor to remove any excess Cl<sub>2</sub> not photolysed by the lamp, or possibly formed by the recombination of Cl atoms. In order to prevent the pump from reducing the pressure within the reactor, it was attached in such a way as to act mainly on laboratory air.

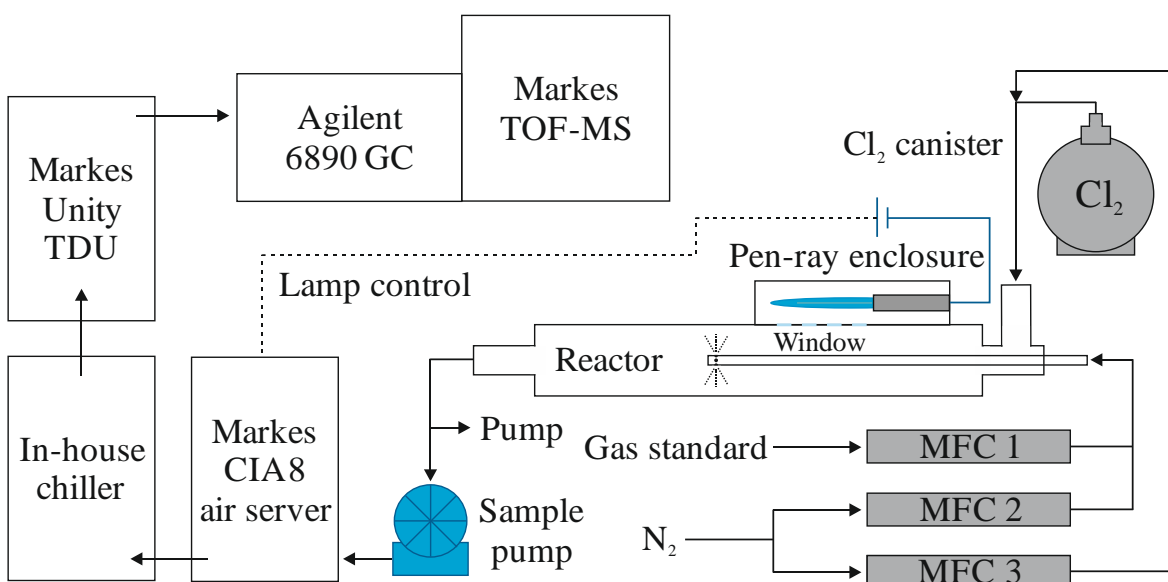


**Figure 2.9** Experiment set up for the measurement of relative rate coefficients between VOCs and Cl radicals. Key to abbreviations: CIA8 = air server and canister interface accessory, GC = gas chromatograph, MFC = mass flow controller, TDU = thermal desorption unit, TOF-MS = time-of-flight mass-spectrometer. See Figure 2.2 for a more comprehensive schematic of the reactor design.

The experiment design remained the same as that used for OH reaction measurements; samples were alternated between light (lamp on) and dark (lamp off) with a constant flow of Cl<sub>2</sub> through the reactor. The depletion in an individual VOC with a literature Cl + VOC rate coefficient,  $k$ , was evaluated by kinetic equations (Eqs. 2.25 to 2.27), using *n*-butane (C<sub>4</sub>H<sub>10</sub>) as an example (R. 2.12).



$$\frac{d[\text{C}_4\text{H}_{10}]}{dt} = -k_{\text{C}_4\text{H}_{10}} [\text{C}_4\text{H}_{10}] [\text{Cl}] \quad \text{Eq. 2.25}$$

$$\frac{d[\text{C}_4\text{H}_{10}]}{[\text{C}_4\text{H}_{10}]} = -k_{\text{C}_4\text{H}_{10}} [\text{Cl}] dt \quad \text{Eq. 2.26}$$

$$\ln \left( \frac{[\text{C}_4\text{H}_{10}]_0}{[\text{C}_4\text{H}_{10}]} \right) = k_{\text{C}_4\text{H}_{10}} \int [\text{Cl}] dt \quad \text{Eq. 2.27}$$

A more general case, for any VOC, is shown in Eqs. 2.28 to 2.30.



$$\frac{d[\text{VOC}]}{dt} = -k [\text{VOC}] [\text{Cl}] \quad \text{Eq. 2.28}$$

$$\frac{d[\text{VOC}]}{[\text{VOC}]} = -k [\text{Cl}] dt \quad \text{Eq. 2.29}$$

$$\ln \left( \frac{[\text{VOC}]_0}{[\text{VOC}]} \right) = k \int [\text{Cl}] dt \quad \text{Eq. 2.30}$$

The depletion in a VOC due to its reaction with Cl is represented by the depletion factor ( $\ln \left( \frac{[\text{VOC}]_0}{[\text{VOC}]} \right)$ ). Equation 2.30 relates the depletion factor in a particular VOC to the rate coefficient,  $k$ , for its reaction with Cl. The integral of the Cl concentration over time ( $\int [\text{Cl}] dt$ ) is known as the Cl exposure ( $Cl_{exp}$ ) and is analogous to the  $OH_{exp}$  discussed in Sect. 2.1.8. Assuming rapid mixing within the reactor, all VOC experienced consistent  $Cl_{exp}$ , which yielded a proportional relationship between VOC depletion factor and  $k$  value. As for the OH rate coefficient measurement experiments, this allowed for the estimation of new rate coefficients for those VOC without established  $k$  values.

### 2.2.2.1 Generation of Cl

Several precursor compounds were considered for use as photolytic sources of atomic chlorine. Most had high toxicity or produced other reactive intermediates as well as Cl. Oxalyl chloride ( $(\text{COCl})_2$ ) was recently identified as a potential clean source for chlorine atoms for kinetic studies due to its unreactive by-products, large UV absorption cross-section and low reactivity towards other radicals (Baklanov and Krasnoperov, 2001). However, it is extremely toxic and corrosive, having a short-term exposure limit (STEL) of 0.1 ppm. Phosgene ( $\text{COCl}_2$ ) was another potential

precursor considered, with a similar chemical composition to oxalyl chloride and similarly low reactivity towards radicals but much easier to handle. Its use as a chemical weapon during World War I, however, meant that it was a highly-regulated compound; phosgene is even more toxic than oxalyl chloride, with a STEL of just 0.06 ppm. Both  $(\text{COCl})_2$  and  $\text{COCl}_2$  are suitably photolysed at 254 nm, a key spectral band in the Hg/Ar lamp emission spectra (see Figure 2.4).

Molecular chlorine ( $\text{Cl}_2$ ) is a somewhat less toxic alternative. Its photodissociation, shown in R. 2.14, only produces atomic chlorine so there are no unwanted by-products and, whilst still toxic, it has a higher STEL of 0.5 ppm.  $\text{Cl}_2$  is not suitably photolysed at 254 nm but is at 330 nm.



A phosphor-coated Hg discharge lamp (Jelight) was used to photolyse  $\text{Cl}_2$  at 330 nm. The DRS measured emission spectrum from the phosphor-coated Hg lamp is shown in Figure 2.10, alongside the DRS measured emission spectrum for the original Hg/Ar lamp for comparison. The large bands centred at 254 nm in the non-coated lamp emission spectrum were not present in that for the phosphor-coated lamp. However, a large peak centred around 330 nm appears in the phosphor-coated emission spectrum, which was not present in the emission from the non-coated lamp.

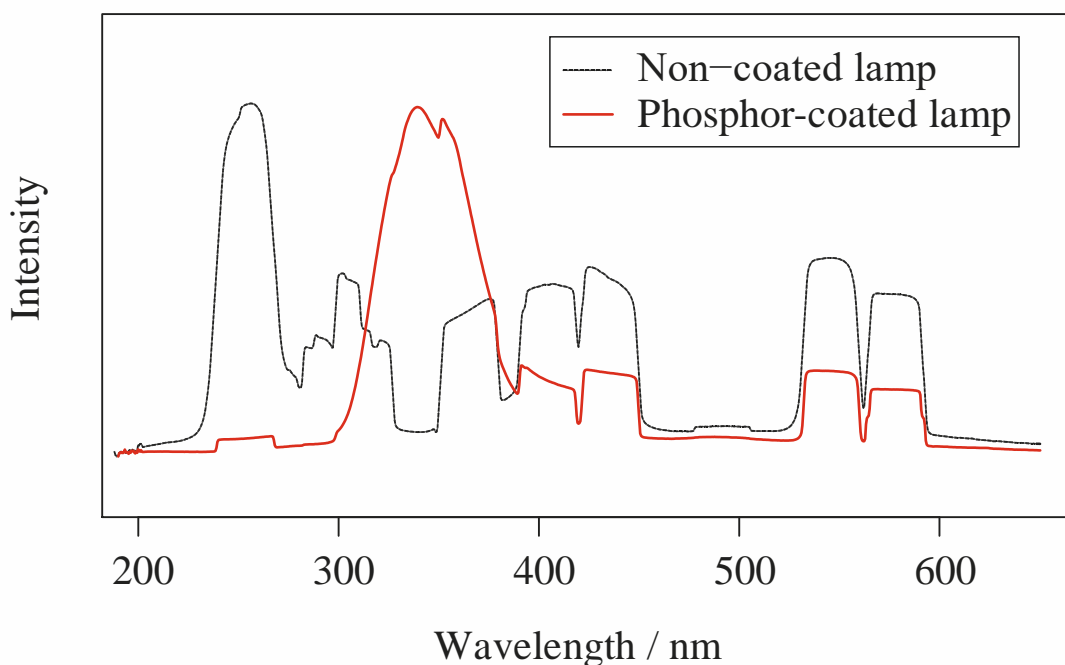


**Figure 2.10** Diffuse reflectance spectroscopy (DRS) recorded spectra of the emission output from the phosphor-coated Hg lamp (red) and the Hg/Ar lamp (black) between 190 and 650 nm. The Hg-Ar emission bands centred around 254 nm and 300 nm were not present in the phosphor-coated spectrum, and were instead replaced by a large band centred around approximately 330 nm.

Cl<sub>2</sub> (1-5 % in N<sub>2</sub>) was supplied to the reactor from a Silco Canister (Restek) via a MFC. The concentration of Cl<sub>2</sub> in the reactor, after dilution with further N<sub>2</sub>, was approximately 0.3-2 % depending on the initial Cl<sub>2</sub> concentration within the Silco Canister. Using a canister coupled to an MFC for the Cl precursor offered a significant advantage over using a water bubbler for the OH precursor. The major advantage resided in the ability to control the amount of Cl<sub>2</sub> entering the reactor, and thereby potentially control the amount of Cl generated via photolysis. The use of a water bubbler in the OH experiments removed this element of control, making it necessary to change the flows of the VOC mixtures into the reactor in order to alter the reactor conditions. For the Cl experiments, this wasn't necessary: the conditions could be altered by either changing the flow of Cl<sub>2</sub> into the reactor, or by changing the flow of VOC mixture into the reactor.

### 2.2.2.2 Literature Cl rate coefficients

Fewer *k* values were available in the literature for VOC + Cl reactions when compared with VOC + OH reactions. Whilst the IUPAC database does include reactions involving Cl, the number and scope of these is limited when compared with OH; there are approximately 70 reactions for Cl (mainly with oxygenated-VOCs) compared to 260 reactions for OH. The number of VOC + Cl reactions that could be measured using this set up (i.e. four or more carbon atoms) and that also appeared in the IUPAC database was also minimal; currently the IUPAC database only includes data for reactions between Cl and VOCs with up to four carbon atoms.

Additionally, unlike for OH + VOC reactions, for which extensive reviews exist (e.g. Calvert et al., 2000, 2002, 2011; Atkinson and Arey, 2003), very few reviews were available for Cl chemistry and few of those focused on rate coefficient evaluations (e.g. Faxon and Allen, 2013). In the absence of these reviews, Cl + VOC rate coefficients were evaluated individually prior to their use as reference values. This was generally trivial due to the limited number of replicate measurements. In the case that two or more measurements for a single VOC + Cl reaction were found, a literature reference value was chosen based on its likelihood of agreement with the rest of the dataset.

### 2.2.3 Temperature-dependent measurements

The rate coefficients for all gas-phase reactions are dependent on temperature. The rate coefficient for a particular reaction may increase or decrease with increasing temperature. It is therefore desirable to make temperature-dependent measurements of the rate coefficients for many VOC + OH reactions in order to better describe atmospheric oxidation processes.

An in-house built heating system with proportional-integral-derivative (PID) controller was installed onto the reactor to allow for careful and controlled heating of the reactor walls, and thereby the gas-phase reactants. It was deemed satisfactory to only heat the first 11 cm section after the point of injection due to the majority of the VOC + OH reactions taking place within the first second after mixing. Figure 2.11 shows a schematic of the reactor configuration with the heating block attached.

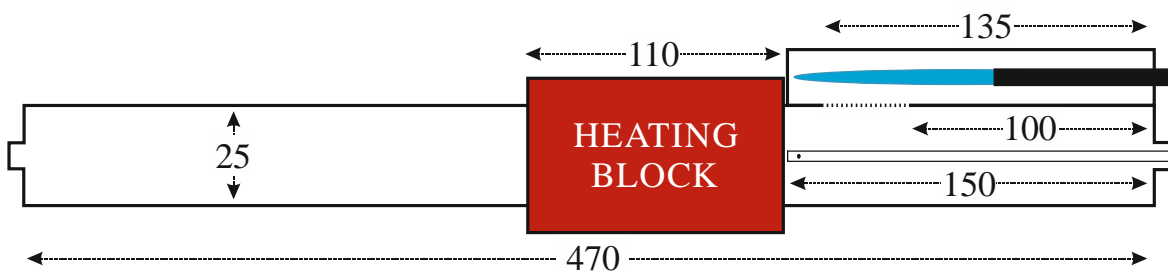


**Figure 2.11** The flow reactor, with heating block, used for mixing of gas-phase reactants and measurement of temperature-dependent rate coefficients. All measurements are shown in mm. Humidified N<sub>2</sub> entered the reactor at the far right of the schematic via 1/4" tubing. The VOCs were injected into the reactor perpendicular to the gas flow via the central sliding 1/8" injector. The position of this injector was optimised to provide maximum exposure of VOCs to OH radicals with minimum exposure to the VUV light (Cryer, 2016). The heating block was controlled, and the temperature of the reactor maintained, by a PID controller.

Two thermocouples were used to control and monitor the temperature of the reactor. The first (T1) was inserted between the heating block and the reactor walls and provided feedback to the PID controller which maintained the temperature setting. The second (T2) was a Type K mineral insulated thermocouple which was inserted into the reactor to measure the temperature of the gas. T2 was located approximately 20 mm downstream of the point of injection. The positions of both T1 and T2 are shown in Figure 2.12.

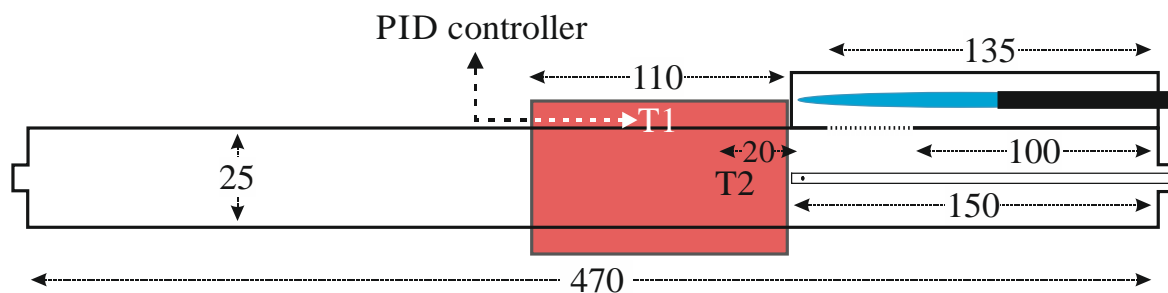


**Figure 2.12** The flow reactor, with heating block, used for mixing of gas-phase reactants and measurement of temperature-dependent rate coefficients. All measurements are shown in mm. The heating block was controlled, and the temperature of the reactor maintained, by a PID controller. The positions of two thermocouples, T1 and T2, used for the control of temperature and measurement of gas temperature are also shown.

### 2.2.3.1 Temperature measurements

By varying the position of T2 in the reactor, the temperature of the gas inside the reactor at different positions was measured. An optimal zone of stabilised temperature was found when the VOC injection position was moved 20 mm further into the reactor. This minor adjustment to the point of injection appeared to have minimal impact on OH exposure and provided only a small range in measured temperature over the length of the reactor in which the oxidation chemistry was thought to occur.

Figure 2.13 illustrates the measured temperature at different points within the reactor at three different PID temperature settings; 65, 95 and 130 °C. At each setting, the temperature increased rapidly from approximately 25 mm upstream of the point of injection to reach the desired temperature at the point of VOC injection. The measured temperature was then stable for at least the extent of the heating block (approximately 110 mm) downstream of the point.

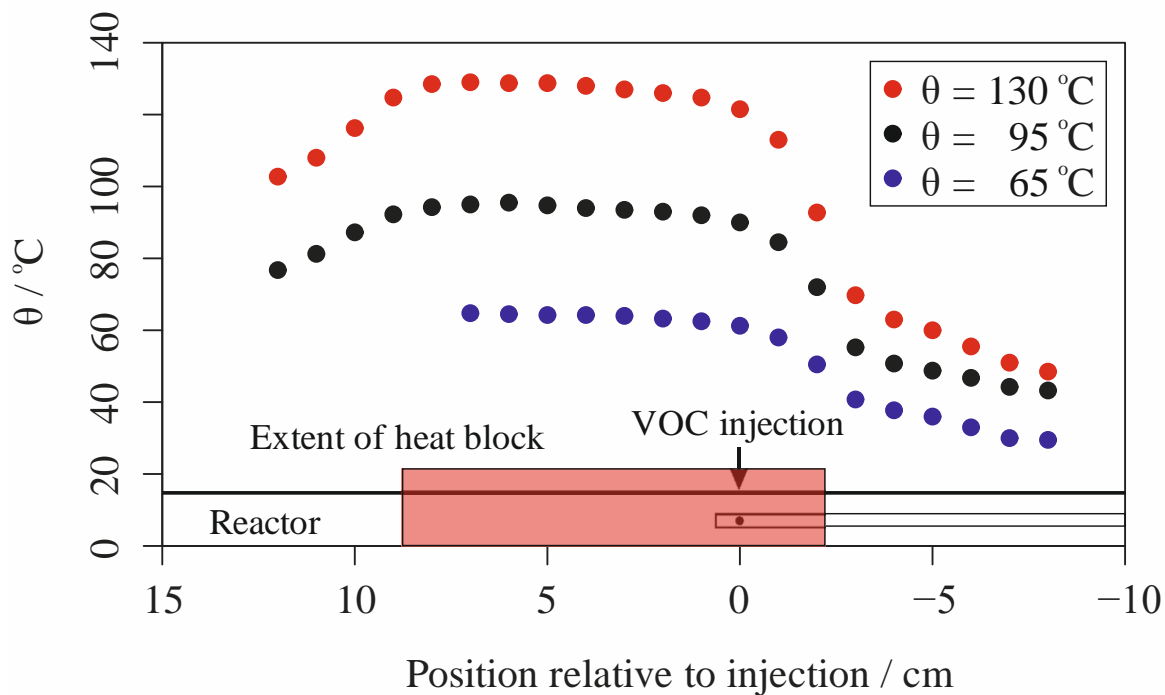


**Figure 2.13** Temperature of the reactor gas, at different PID settings and different positions within the reactor (relative to the point of VOC injection) as measured by the Type K mineral insulated thermocouple.

## References

- Aschmann, S. M. and Atkinson, R.: Rate constants for the gas-phase reactions of OH radicals with *E*-7-tetradecene, 2-methyl-1-tridecene and C<sub>7</sub>-C<sub>14</sub> 1-alkenes at 295 ± 1 K, *Phys. Chem. Chem. Phys.*, 10, 4159-4164, <https://doi.org/10.1039/B803527J>, 2008.
- Atkinson, R. and Arey, J.: Atmospheric degradation of volatile organic compounds, *Chem. Rev.*, 103, 4605-4638, doi:10.1021/cr0206420, 2003.
- Atkinson, R., Baulch, D. L., Cox, R. A., Crowley, J. N., Hampson, R. F., Hynes, R. G., Jenkin, M. E., Rossi, M. J. and Troe, J.: Evaluated kinetic and photochemical data for atmospheric chemistry: Volume II – gas phase reactions of organic species, *Atmos. Chem. Phys.*, 6, 3265-4055, 2006. Also found at <http://iupac.pole-ether.fr/>.
- Burke, S.: Missing values, outliers, robust statistics & non-parametric methods. LC.GC Europe Online Supplement, statistics and data analysis, 19-24, 1998.
- Calvert, J. G., Atkinson, R., Kerr, J. A., Madronich, S., Moortgat, G. K., Wallington, T. J. and Yarwood, G.: The mechanisms of atmospheric oxidation of the alkenes, Oxford University Press, New York, 2000.
- Calvert, J. G., Atkinson, R., Becker, K. H., Kamens, R. M., Seinfeld, J. H., Wallington, T. J. and Yarwood, G.: The mechanisms of atmospheric oxidation of aromatic hydrocarbons, Oxford University Press, New York, 2002.
- Cryer, D. R.: Measurements of hydroxyl radical reactivity and formaldehyde in the atmosphere, PhD thesis, University of Leeds, 2016.
- Dash, M. R. and Rajakumar, B.: Experimental and theoretical rate coefficients for the gas phase reaction of β-pinene with OH radical, *Atmos. Environ.*, 79, 161-171, <https://doi.org/10.1016/j.atmosenv.2013.05.039>, 2013.
- Faxon, C. B. and Allen, D. T.: Chlorine chemistry in urban atmospheres: A review, *Environ. Chem.*, 10, 221-223, <https://doi.org/10.1071.EN13026>, 2013.

Kato, S., Sato, T. and Kajii, Y.: A method to estimate the contribution of unidentified VOCs to OH reactivity, *Atmos. Environ.*, 45, 31, 5531-5539, <https://doi.org/10.1016/j.atmosenv.2011.05.074>, 2011.

Shaw, J. T., Lidster, R. T., Cryer, D. R., Ramirez, N., Whiting, F. C., Bousted, G. A., Whalley, L. K., Ingham, T., Rickard, A. R., Dunmore, R. E., Heard, D. E., Lewis, A. C., Carpenter, L. J., Hamilton, J. F. and Dillon, T. J.: A self-consistent, multivariate method for the determination of gas-phase rate coefficients applied to reactions of atmospheric VOCs and the hydroxyl radical, *Atmos. Chem. Phys.*, 18, 4039-4054, <https://doi.org/10.5194/acp-18-4039-2018>, 2018.



## Chapter 3

# Kinetic studies of alkene + OH reactions

### 3 Overview

This chapter describes the work undertaken to measure rate coefficients for the reactions between OH and various VOCs containing one or more carbon-carbon double bonds (please refer to Chapter 1 Sections 1.2.2.2 and 1.3.3 for more information on alkenes as VOCs). Three distinct synthetic mixtures, containing 24 different VOCs, were tested with the experimental setup described in Chapter 2. The results for these reactions were compared with the available literature to assess the applicability of this technique for the measurement of multiple relative rate coefficients simultaneously. Numerical simulations were also performed to broaden the understanding of the chemistry occurring within the reactor, and to validate the technique and the assumptions underpinning the analysis.

A new room temperature rate coefficient for the reaction between OH and 2,3-dimethylpent-1-ene is provided in Table 3.8.

## 3.1 Results and discussion

The following section outlines the results from multiple mixtures containing monoalkenes and dialkenes, many of which were monoterpenes with the chemical formula  $C_{10}H_{16}$ . Results from three different synthetic mixtures, measured at room temperature (approximately 295 K) are presented.

### 3.1.1 Monoterpene mixture 1

This mixture contained 11 VOCs, of which all had at least one  $k$  measurement, for their reaction with OH, available in the literature. Eight of the VOCs were monoterpenes ( $C_{10}H_{16}$ ), including; 3-carene,  $\alpha$ -pinene,  $\beta$ -ocimene,  $\beta$ -pinene, camphene,  $\gamma$ -terpinene, limonene, and myrcene (see Chapter 1 Section 1.2.2.2 for the structures of these compounds and others). The other three VOCs were isoprene and  $m$ - and  $o$ -xylene, which all benefited from having multiple  $k$  measurements in the literature and were therefore very suitable for use as reference compounds. The two xylenes are aromatic in nature and are not considered to be unsaturated VOCs. They were included as part of this mixture to broaden the range in rate coefficients measured and provide a calibration at a lower limit. Both  $m$ - and  $o$ -xylene also benefited from many literature measurements, so their reference  $k$  values had smaller relative uncertainties, unlike some of the other components of this mixture.

Table 3.1 gives a full list of the 11 VOCs in this mixture, along with the reference rate coefficient used for their reaction with OH and the number of measurements which could be found in the literature at the time of writing.

There was only a small range in  $k$  values across the VOCs for this mixture. The estimated total OH reactivity of this mixture at standard temperature and pressure (STP) was  $900\text{ s}^{-1}$ . This mixture was diluted with  $N_2$  in differing amounts to inject gaseous samples into the reactor with a range of OH reactivities approximately between 50 and  $300\text{ s}^{-1}$ .

**Table 3.1** List of VOCs, in descending order of evaluated literature  $k$  value, in monoterpenes mixture 1 along with their evaluated literature  $k$  value, reference and number of measurements found in the literature at the time of writing.

Name	Evaluated literature $k$ (298 K) / $10^{-12}$ cm <sup>3</sup> molecule <sup>-1</sup> s <sup>-1</sup>	Reference used	Number of literature measurements
$\beta$ -ocimene	245 $\pm$ 49	Atkinson and Arey, 2003	4
$\gamma$ -terpinene	170 ( $^{+44}_{-35}$ )	Atkinson et al., 2006	1
myrcene	209 $\pm$ 42	Atkinson and Arey, 2003	4
limonene	170 $\pm$ 51	Atkinson and Arey, 2003	5
isoprene	100 ( $^{+15}_{-13}$ )	Atkinson et al., 2006	25+
3-carene	85 $\pm$ 17	Atkinson and Arey, 2003	2
$\beta$ -pinene	79 $\pm$ 20	Atkinson and Arey, 2003	10
$\alpha$ -pinene	53 ( $^{+23}_{-19}$ )	Atkinson et al., 2006	9
camphene	53 $\pm$ 11	Atkinson and Arey, 2003	2
<i>m</i> -xylene	23 $\pm$ 4	Calvert et al., 2002	15
<i>o</i> -xylene	13 $\pm$ 3	Calvert et al., 2002	10

## 3.1.1.1 Typical chromatogram data

Figure 3.1 shows sections of typical total ion chromatograms (TIC) obtained for this mixture with the reactor lamp turned off (blue) and the reactor lamp turned on (black). There was a clear reduction in the observed concentrations of all the VOCs detected when the lamp was turned on (black), reflected in the reduction in the peak areas relative to the sample with the lamp turned off (blue). Using a TOF-MS provided clear advantages over FID, in that the background interference was reduced and the peaks were easily identified.

The peak assigned to camphene had a much smaller measured area than those for the other VOCs in this mixture. The size of the peak was indicative of a less-than-ideal concentration of camphene within the synthetic gas mixture. For this reason, the depletion factor results for camphene for this mixture were ignored.

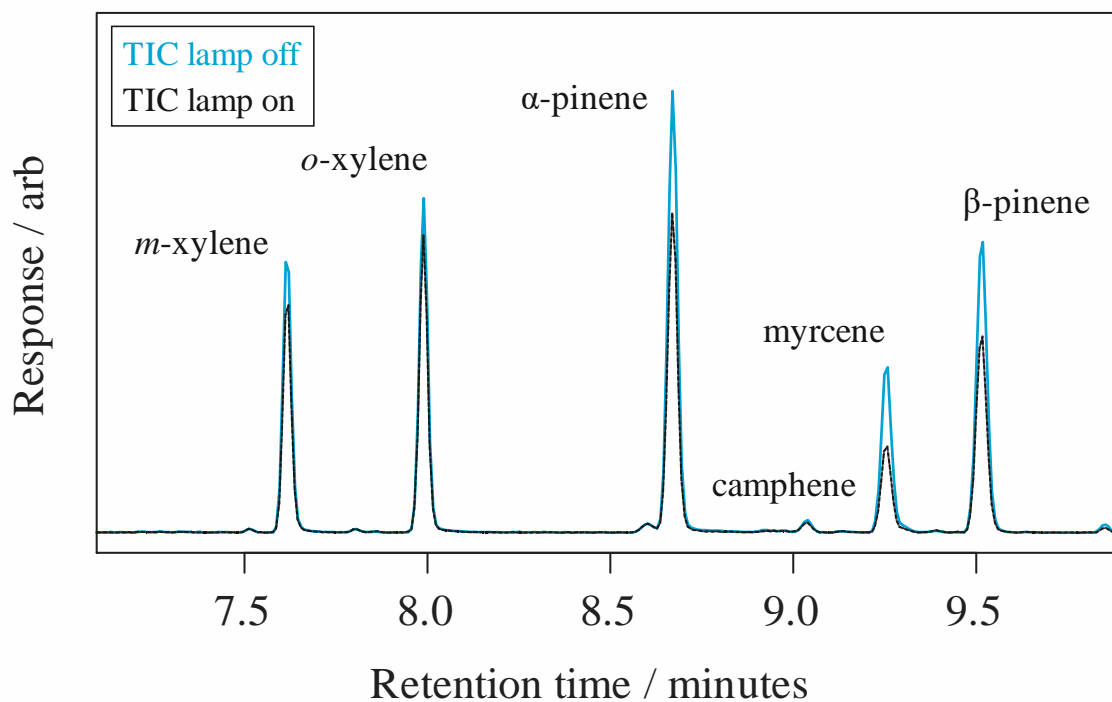


**Figure 3.1** Typical total ion chromatogram (TIC) sections obtained for monoterpenes mixture 1 with the lamp turned off (blue) and the lamp turned on (black). Greater differences in peak areas were observed for VOCs which have a larger rate coefficient value for their reaction with OH. Evaluated literature rate coefficients (in units of  $10^{-12} \text{ cm}^3 \text{ molecule}^{-1} \text{ s}^{-1}$ ) for these VOC + OH reactions were: *o*-xylene,  $13 (\pm 3)$ ; *m*-xylene,  $23 (\pm 4)$ ;  $\alpha$ -pinene,  $53 (\pm 22)$ ;  $\beta$ -pinene,  $79 (\pm 20)$ ; camphene,  $53 (\pm 11)$ ; myrcene,  $209 (\pm 42)$  (see Table 3.1).

## 3.1.1.2 Typical peak area data

Figure 3.2 shows a typical peak area plot for isoprene. The five different OH reactivities, relating to the different VOC flow regimes injected into the reactor, are shown in different colours. The alternating pattern between lamp-off and lamp-on samples is easily distinguished in the zigzagging nature of the data.

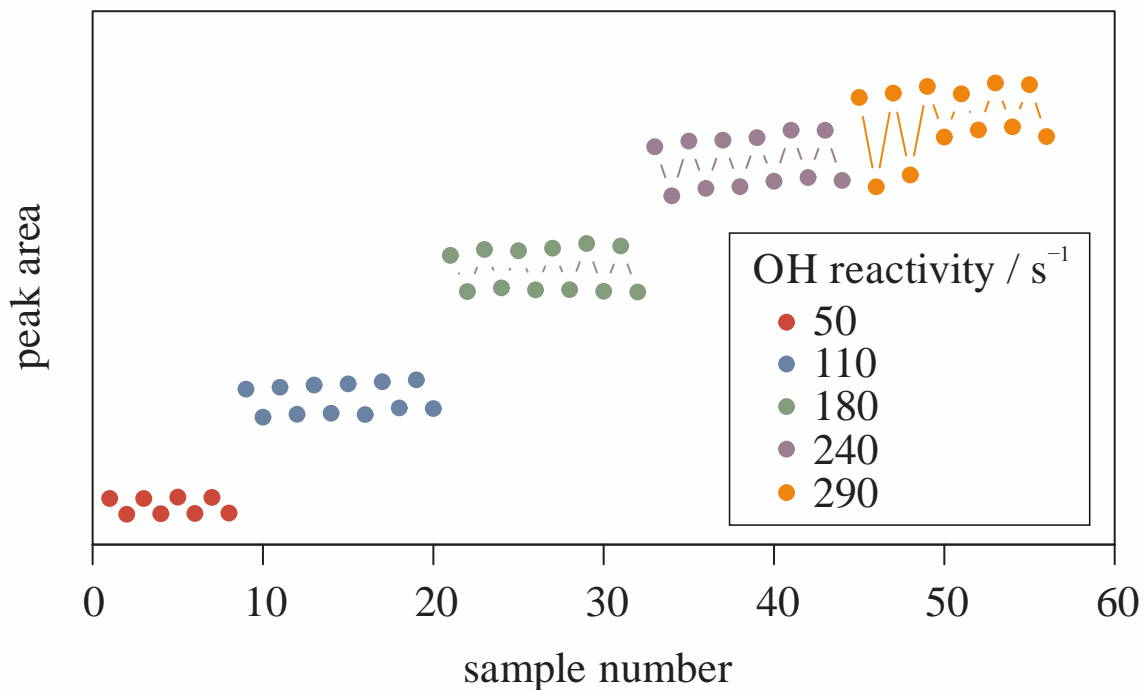
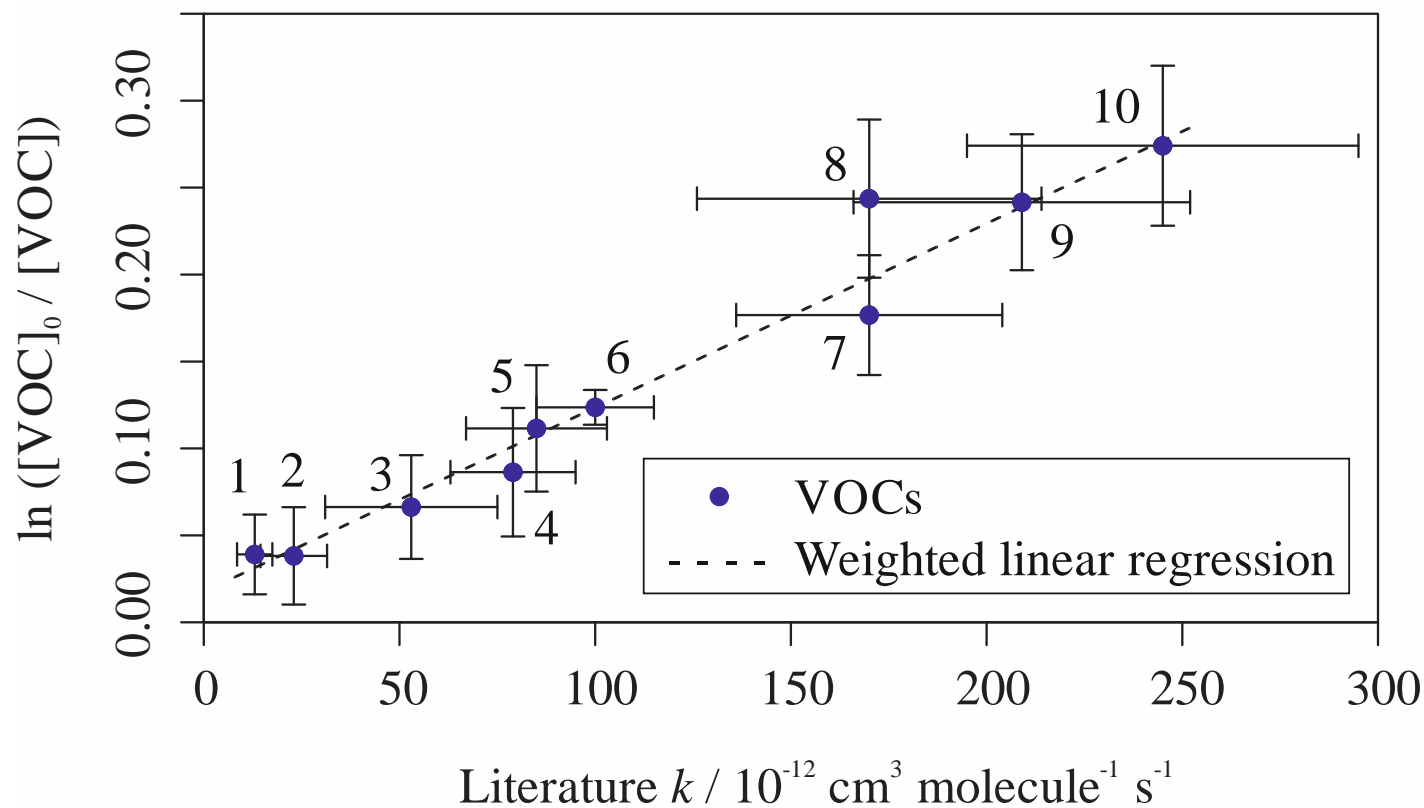


**Figure 3.2** Peak area data for isoprene in monoterpenes mixture 1. The five different estimated OH reactivities (of 50, 110, 180, 240 and 290 s<sup>-1</sup>) are shown in different colours. Only eight samples (four 'lamp on', four 'lamp off') were taken at an OH reactivity of 50 s<sup>-1</sup> whilst 12 samples (six 'lamp on', six 'lamp off') were taken at all other OH reactivities.

### 3.1.1.3 Relative rate plots

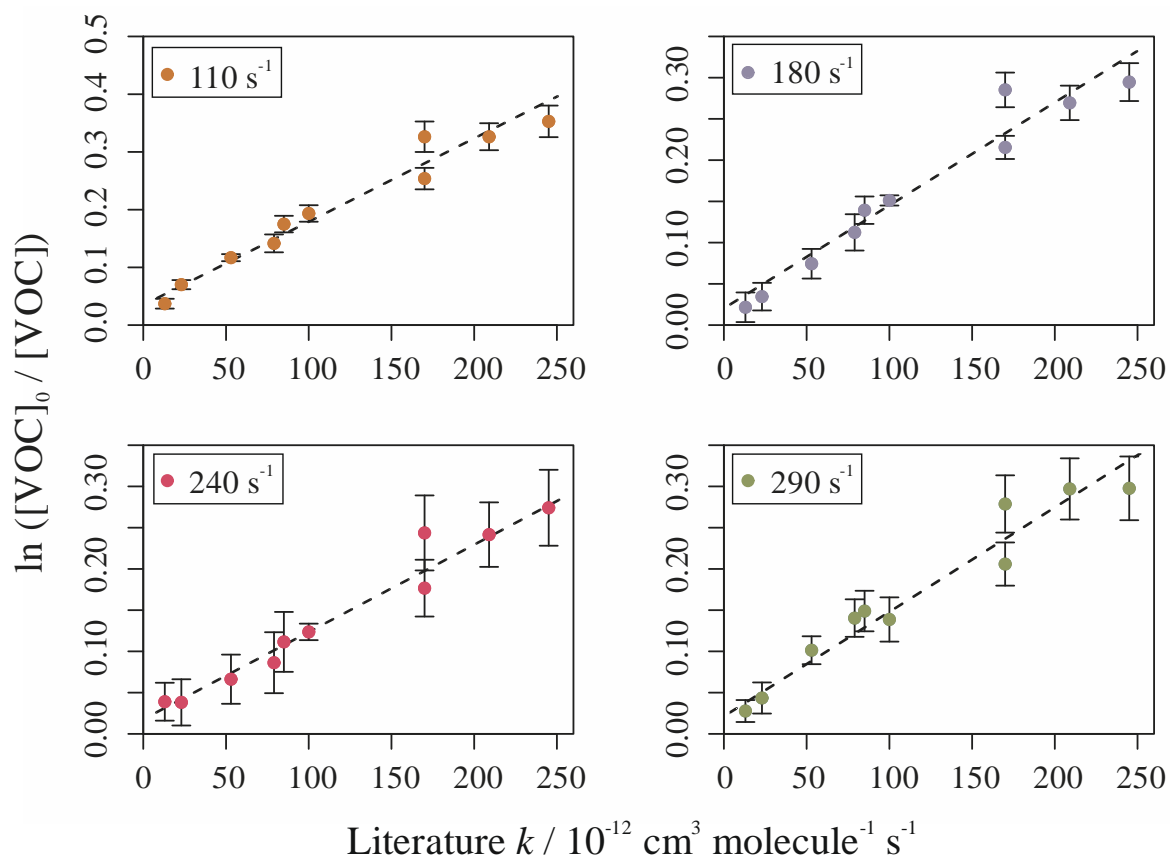
The depletion factor for each VOC ( $\ln \left( \frac{[\text{VOC}]_0}{[\text{VOC}]} \right)$ ) was plotted against the evaluated literature values using Eq. 2.19. Linear regression, weighted to the uncertainties in the depletion factors, was then used to find the  $OH_{exp}$  as per Chapter 2 Section 2.1.8.

Figure 3.3 shows the relative rate plot for monoterpenes mixture 1 with an OH reactivity of  $240 \text{ s}^{-1}$ . There was a clear linear correlation between depletion factor and rate coefficient. Despite Eq. 2.19 suggesting that a rate coefficient of zero should result in a depletion of zero, effectively forcing the intercept through the origin, a non-zero intercept as determined by the linear fit was found to be a more appropriate approximation of the trend. The  $OH_{exp}$  obtained using weighted linear regression had a value of  $(1.06 \pm 0.07) \times 10^9 \text{ molecules cm}^{-3} \text{ s}$ . The  $R^2$  value for the fit was equal to 0.965. The uncertainties in the literature  $k$  reference values were substantially large enough to account for the deviations of every data point from the linear trend.



**Figure 3.3** Relative rate plot for monoterpenes mixture 1 with an OH reactivity of  $240 \text{ s}^{-1}$ , at 295 K. Compounds with a reference rate coefficient for reaction with OH were plotted using evaluated literature values as references. Error bars on the y-axis, equal to one standard error, were calculated by combining the standard error in peak areas for six lamp-off and six lamp-on samples. Error bars on the x-axis were typically large (approximately  $\pm 20\text{-}30\%$ ) and accounted for deviations from the trend for all VOCs. A weighted (to the uncertainty in the y-values) linear fit was used to generate the slope, with a value of  $OH_{exp} = 1.06 (\pm 0.07) \times 10^9 \text{ molecules cm}^{-3} \text{ s}$  and  $R^2 = 0.965$ . The VOCs can be identified as follows; 1, *o*-xylene; 2, *m*-xylene; 3,  $\alpha$ -pinene; 4,  $\beta$ -pinene; 5, 3-carene; 6, isoprene; 7, limonene; 8,  $\gamma$ -terpinene; 9, myrcene; 10,  $\beta$ -ocimene.

A similar trend was observed for monoterpene mixture 1 with OH reactivities of 110, 180 and 290  $\text{s}^{-1}$  as shown in Figure 3.4. The OH exposures for these mixtures were  $1.44 (\pm 0.09)$ ,  $1.25 (\pm 0.10)$  and  $1.27 (\pm 0.10) \times 10^9$  molecules  $\text{cm}^{-3} \text{s}$  respectively. The  $R^2$  values for the linear regressions were 0.964, 0.941 and 0.949 respectively.  $OH_{exp}$  generally decreased with increasing OH reactivity. This correlates well with studies by Li et al. (2015) and Peng et al. (2015) who modelled a decrease in  $OH_{exp}$  with increasing OH reactivity.



**Figure 3.4** Relative rate plots for monoterpenes mixture 1 with OH reactivities of 110, 180, 240 and 290  $\text{s}^{-1}$ . The  $R^2$  values for the weighted linear fits were 0.964, 0.941, 0.965 and 0.949 respectively. The values of  $OH_{exp}$  were  $1.44 (\pm 0.09)$ ,  $1.25 (\pm 0.10)$ ,  $1.06 (\pm 0.07)$  and  $1.27 (\pm 0.10) \times 10^9$  molecules  $\text{cm}^{-3} \text{s}$  respectively. Error bars on the x-axis are not shown for reasons of clarity.

For this mixture with an OH reactivity of  $50 \text{ s}^{-1}$ , the experiment with the lowest concentration of VOCs injected into the reactor, the data displayed a different, non-linear relationship (Figure 3.5). It isn't immediately clear why this data is inconsistent with Eq. 2.19 but the non-linearity indicated that the OH exposure was not uniform across the range of VOCs. This was likely due to incomplete mixing within the flow reactor. Fortunately, the fact that the relationship between depletion and rate coefficient wasn't linear did not necessarily detract from the relative rate nature of the experiment: it was still possible to extract relative rate information if a reliable and consistent function was plotted through the observed data. The curved line in Figure 3.5 was plotted using a three-parameter exponential function (Eq. 3.1) and gave a relatively good fit through all the data with an  $R^2$  of 0.99. For more information regarding understanding the curved nature of the relationship observed for this plot, and other relative plots, please refer to Section 3.2.2.

$$y = e^{a + \frac{b}{x+c}} \quad \text{Eq. 3.1}$$

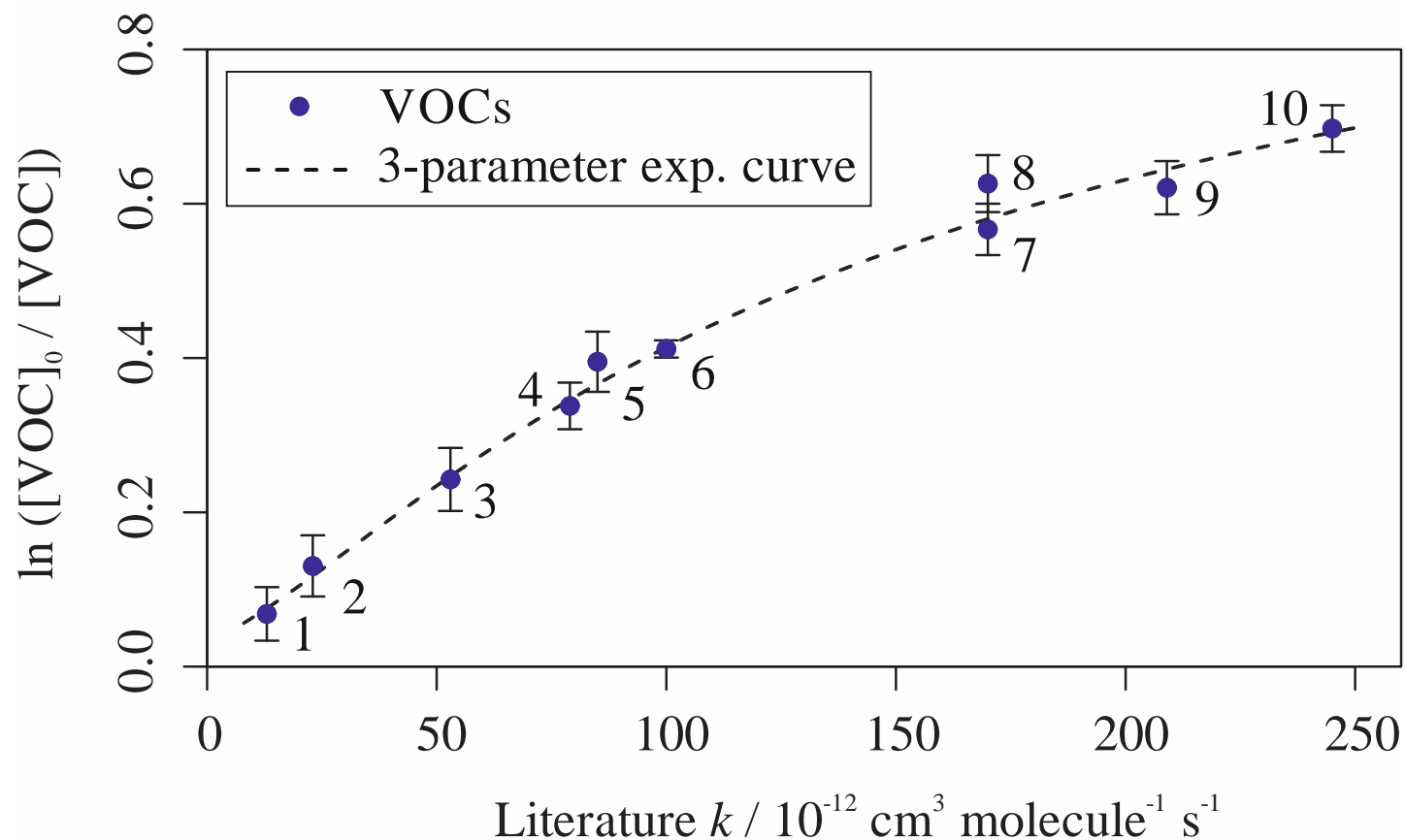


**Figure 3.5** Relative rate plot for monoterpenes mixture 1 with an OH reactivity of  $50 \text{ s}^{-1}$ , at 295 K. Compounds with a reference rate coefficient for reaction with OH were plotted using literature values. Error bars on the y-axis, equal to one standard error, were calculated by combining the standard error in peak areas for four lamp-off and four lamp-on samples. Error bars on the x-axis are not displayed for reasons of clarity but were typically large (approximately  $\pm 20\text{-}30\%$ ) and accounted for deviations from the line. The black dashed line shows the relationship observed when the OH reactivity of the mixture was low, modelled by a three-parameter exponential curve (see Section 3.2.2). The VOCs can be identified as follows; 1, *o*-xylene; 2, *m*-xylene; 3,  $\alpha$ -pinene; 4,  $\beta$ -pinene; 5, 3-carene; 6, isoprene; 7, limonene; 8,  $\gamma$ -terpinene; 9, myrcene; 10,  $\beta$ -ocimene.

### 3.1.1.4 Calculation of rate coefficients

It was possible to estimate rate coefficients for each VOC + OH reaction relative to all other VOC + OH reactions in the mixture using Eq. 2.19 and the OH exposures approximated using weighted linear regression. This was performed at each of the individual OH reactivities injected into the reactor. The value estimated from the lowest OH reactivity (Figure 3.5) was ignored, due to the non-linear relationship, resulting in four  $k$  values for each reaction, each with an associated  $1\sigma$  uncertainty. An average, weighted to the uncertainties, of these four values was then taken to yield a final, single rate coefficient for the reaction between each VOC and OH relative to each other (Table 3.2).

**Table 3.2** List of VOCs, in descending order of evaluated literature  $k$  value, in monoterpenes mixture 1 along with their range of depletions due to reaction with OH, measured  $k$  value and evaluated literature  $k$  value.

Name	Range of depletion / %	Measured $k$ (295 K) / $10^{-12} \text{ cm}^3 \text{ molecule}^{-1} \text{ s}^{-1}$	Evaluated literature $k$ / $10^{-12} \text{ cm}^3 \text{ molecule}^{-1} \text{ s}^{-1}$
$\beta$ -ocimene	27 - 70	$223 \pm 10$	$245 \pm 49$
$\gamma$ -terpinene	24 - 63	$207 \pm 6$	$170 (^{+44}_{-35})$
myrcene	24 - 62	$204 \pm 8$	$209 \pm 42$
limonene	18 - 57	$152 \pm 4$	$170 \pm 51$
isoprene	12 - 41	$104 \pm 6$	$100 (^{+15}_{-13})$
3-carene	11 - 40	$97 \pm 4$	$85 \pm 17$
$\beta$ -pinene	9 - 34	$78 \pm 11$	$79 \pm 20$
$\alpha$ -pinene	7 - 24	$56 \pm 6$	$53 (^{+22}_{-15})$
<i>m</i> -xylene	3 - 13	$22 \pm 6$	$23 \pm 4$
<i>o</i> -xylene	2 - 7	$5 \pm 7$	$13 \pm 3$

All of the measurements made using the multivariate relative rate technique were in good agreement with the evaluated literature values, within errors.

### 3.1.1.5 Comparisons to the literature

Whilst the final, measured rate coefficients for the 11 VOC + OH reactions were in good agreement with the reference literature  $k$  data set used (see Table 3.2), the wider literature contains many more examples of rate coefficient data for many of the compounds.

The measured result for the  $\alpha$ -pinene + OH reaction, of  $56 (\pm 6) \times 10^{-12} \text{ cm}^3 \text{ molecule}^{-1} \text{ s}^{-1}$ , was in excellent agreement with two recent measurements by Montenegro et al. (2012) and Dash et al. (2014), of  $53.3 (\pm 9.4)$  and  $53.3 (\pm 7.9) \times 10^{-12} \text{ cm}^3 \text{ molecule}^{-1} \text{ s}^{-1}$  respectively. There are instances

in the older literature of measurements greater than  $60 \times 10^{-12} \text{ cm}^3 \text{ molecule}^{-1} \text{ s}^{-1}$ , but these are not significantly different to that presented here due to the uncertainty given on the value measured in this work (Kleindienst et al., 1982; Chuong et al., 2002; Davis and Stevens, 2005).

Similarly, for the  $\beta$ -pinene + OH reaction, the measured value presented in this work, of  $78 (\pm 11) \times 10^{-12} \text{ cm}^3 \text{ molecule}^{-1} \text{ s}^{-1}$ , was in good agreement with much of the literature on the same reaction. Recent measurements by Montenegro et al. (2012) and Dash and Rajakumar (2013) were somewhat higher, at  $81.2 (\pm 14.1)$  and  $93.5 (\pm 28) \times 10^{-12} \text{ cm}^3 \text{ molecule}^{-1} \text{ s}^{-1}$  respectively but their large uncertainties meant that they were not significantly different to the value presented here.

The measurements for some of the other monoterpene + OH reactions were also in good agreement with recent literature results. Braure et al. (2014) provided a recently measured  $k$  value for the limonene + OH reaction of  $165 (\pm 25) \times 10^{-12} \text{ cm}^3 \text{ molecule}^{-1} \text{ s}^{-1}$  whilst Gaona-Colmán et al. (2016) gave a value for the  $\beta$ -ocimene + OH reaction of  $236 (\pm 54) \times 10^{-12} \text{ cm}^3 \text{ molecule}^{-1} \text{ s}^{-1}$ . Both were in good agreement with their equivalents in this work.

The most recent measurements of the myrcene + OH reaction, by Hites and Turner (2009) and Kim et al. (2011), were much larger than that presented here but do not differ significantly due to the very large uncertainties placed upon them. Their experimentally derived  $k$  values, of  $335 (\pm \frac{144}{101})$  and  $334 (\pm \frac{220}{132}) \times 10^{-12} \text{ cm}^3 \text{ molecule}^{-1} \text{ s}^{-1}$  for Hites and Turner (2009) and Kim et al. (2011) respectively, were over 50% larger than that measured using the multivariate relative rate technique in this work.

Isoprene is the most extensively studied VOC in the mixture, with over 25 measurements cited in the IUPAC evaluation. Our measured value, of  $104 (\pm 6) \times 10^{-12} \text{ cm}^3 \text{ molecule}^{-1} \text{ s}^{-1}$ , was not only in good agreement with recent relative rate measurements, of  $107 (\pm 3) \times 10^{-12} \text{ cm}^3 \text{ molecule}^{-1} \text{ s}^{-1}$ , but was also in good agreement with recent absolute measurements, of  $102 (\pm 9)$  and  $93 (\pm 4) \times 10^{-12} \text{ cm}^3 \text{ molecule}^{-1} \text{ s}^{-1}$ , (Poppe et al., 2007; Singh and Li, 2007; Dillon et al., 2017).

Measurements of two aromatic VOCs were also made as part of this study. The first, and faster reacting of the two,  $m$ -xylene, was estimated to have a  $k$  value of  $22 (\pm 6) \times 10^{-12} \text{ cm}^3 \text{ molecule}^{-1} \text{ s}^{-1}$ . This value was in good agreement with the more recent measurement of  $22.0 (\pm 2.7) \times 10^{-12} \text{ cm}^3 \text{ molecule}^{-1} \text{ s}^{-1}$  by Kramp and Paulson (1998), in which the OH +  $m$ -xylene reaction was measured using the relative rate method with 10 separate reference compounds.

The second aromatic VOC, *o*-xylene, was estimated to have an OH reaction rate coefficient of  $5 (\pm 7) \times 10^{-12} \text{ cm}^3 \text{ molecule}^{-1} \text{ s}^{-1}$ . This was over 50% smaller than the evaluated reference value, of  $13 (\pm 3) \times 10^{-12} \text{ cm}^3 \text{ molecule}^{-1} \text{ s}^{-1}$ . Our measurement for the *o*-xylene + OH reaction had a large uncertainty placed upon it, likely owing to it being the slowest reaction in this mixture. However, the large uncertainty does mean it was in fair agreement with much of the literature, in particular with measurements by Atkinson and Aschmann (1989), of  $12.2 (\pm 1.9) \times 10^{-12} \text{ cm}^3 \text{ molecule}^{-1} \text{ s}^{-1}$ .

### 3.1.1.6 Comparisons to structure-activity relationships (SARs)

SARs are often used to estimate rate coefficients (and other parameters) for those compounds which do not have experimentally determined values. SARs relate experimentally derived datasets to the structural properties of chemical species to provide a method of estimation which does not directly rely on experimentation. However, they require accurate and reliable kinetic information from a wide range of reactions to provide sensible predictions for the various rate coefficients and substituent factors needed (Calvert et al., 2002).

One such SAR, for the reaction between OH and alkenes, was provided by Peeters et al. (1999) and was subsequently updated in Peeters et al. (2007). These SARs rely on two hypotheses: firstly, that the overall rate coefficient for OH addition is the total of the rate coefficients for OH addition at each site, and secondly that the rate coefficient for OH addition at each site is determined by the substituent groups adjacent to that site. The SAR is based on experimentally derived  $k$  values for the reactions of nine alkenes and conjugated dienes with OH. Unlike other SARs for alkene + OH reactions, Peeters et al. (1999, 2007) excluded contributions from H-atom abstraction. This was largely due to it being generally insignificant when compared with OH addition to the carbon-carbon double bond.

A more recent SAR, by Jenkin et al. (2018), built upon the SAR provided by Peeters et al. (2007) but accounted for more recent reports of the increasing rate of addition with increasing alkene size for homologous series (Aschmann and Atkinson, 2008; Nishino et al., 2009). The SAR in Jenkin et al. (2018) also explicitly considered H-atom abstraction and therefore many values for calculating site specific OH addition parameters differed, albeit only marginally.

Figure 3.6 shows a comparison between the rate coefficients predicted using the SARs in Peeters et al. (1999, 2007) and Jenkin et al. (2018) and the alkenes measured experimentally as part of this mixture, alongside the literature evaluated rate coefficients (Table 3.3). The measured results were closer to the literature than the SARs for six of the eight alkenes and monoterpenes.

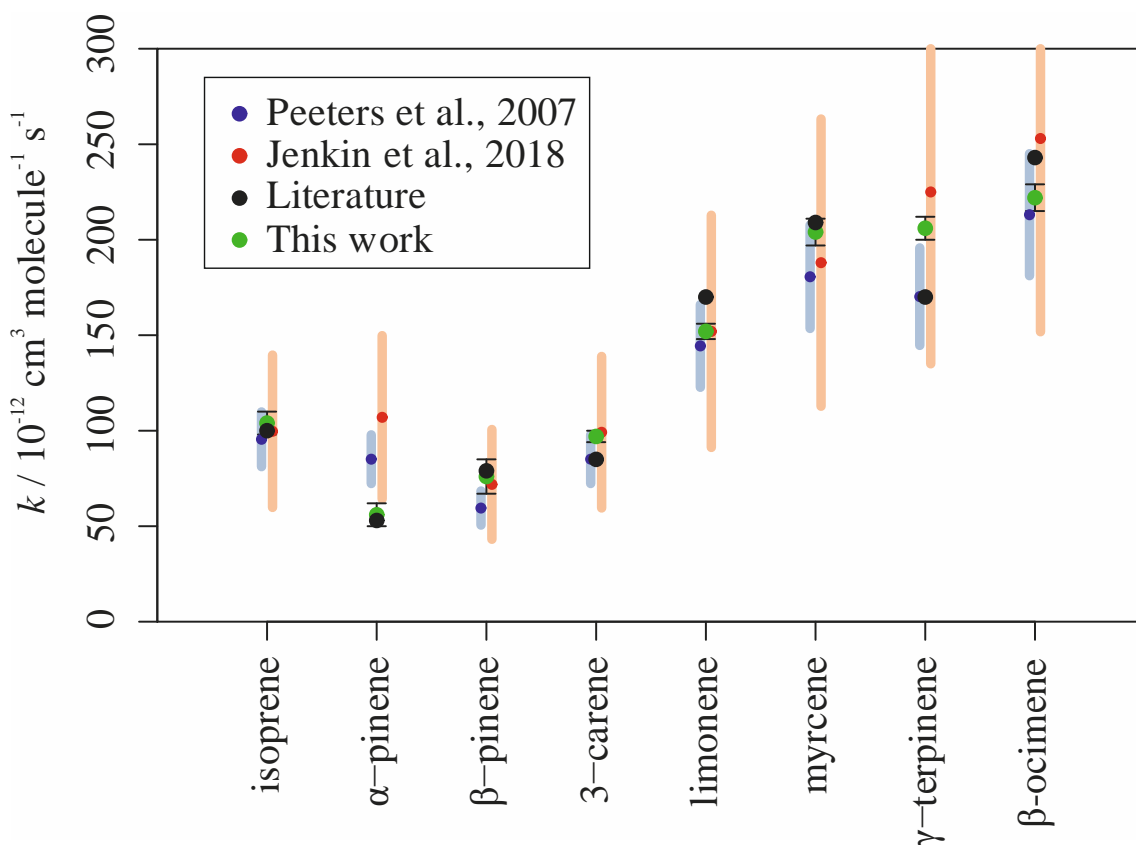
The large underprediction in the Peeters et al. (2007) SAR derived  $\beta$ -pinene + OH  $k$  value was understood to be due to the exclusion of H-atom abstraction contributions.  $\alpha$ -pinene had the largest deviation from its experimental  $k$  value; this was tentatively explained based on steric hindrance; the bridging group across the ring blocks OH addition to the double bond in the ring structure. This is less important for  $\beta$ -pinene, as the double bond is outside the ring. Despite some pitfalls in the predictions for some alkenes, the Peeters et al. (2007) SAR gave a better estimation than the multivariate relative rate technique for both 3-carene and  $\gamma$ -terpinene. However, the SAR also performed somewhat more poorly in predictions for the reactions of OH with the conjugated dienes, myrcene and  $\beta$ -ocimene.

The Jenkin et al. (2018) SAR performed considerably better than the Peeters et al. (2007) SAR for estimating the rate coefficient for the  $\beta$ -pinene + OH reaction. It did, however, overpredict that for the  $\alpha$ -pinene + OH reaction by a similar magnitude. The SAR derived rate coefficient for the 3-carene + OH reaction was in good agreement with the experimental result provided here, but both were somewhat greater than two previous literature measurements. The Jenkin et al. (2018) SAR performed much better when estimating rate coefficients for the conjugated diene + OH reactions, as illustrated by that for the  $\beta$ -ocimene + OH reaction.

Evidently, experimentally derived values are preferred to those which have been estimated through parameterisation. However, it appears that in the absence of a measured  $k$  value for an OH oxidation reaction involving an alkene, the SAR in Jenkin et al. (2018) provides a reasonably accurate estimate for many compounds. The limited scope of this work, in terms of the range and variability in olefinic structures used, makes it difficult to verify the SAR for more than just monoterpenes and simple alkenes.

**Table 3.3** List of VOCs, in descending order of evaluated literature  $k$  value, in monoterpenes mixture 1 along with their SAR derived  $k$  values, experimentally measured  $k$  value and evaluated literature  $k$  value.

Name	Rate coefficient for reaction with OH / $10^{-12} \text{ cm}^3 \text{ molecule}^{-1} \text{ s}^{-1}$			
	This work	Peeters et al. (2007) SAR	Jenkin et al. (2018) SAR	Evaluated literature
$\beta$ -ocimene	$223 \pm 10$	$213 \pm 32$	$253 \pm 101$	$245 \pm 49$
$\gamma$ -terpinene	$207 \pm 6$	$170 \pm 26$	$225 \pm 90$	$170 (^{+44}_{-35})$
myrcene	$204 \pm 8$	$181 \pm 27$	$188 \pm 75$	$209 \pm 42$
limonene	$152 \pm 4$	$144 \pm 22$	$152 \pm 61$	$170 \pm 51$
isoprene	$104 \pm 6$	$95.5 \pm 14$	$99.7 \pm 40$	$100 (^{+15}_{-13})$
3-carene	$97 \pm 4$	$85.1 \pm 13$	$99.2 \pm 40$	$85 \pm 17$
$\beta$ -pinene	$76 \pm 11$	$59.5 \pm 9$	$71.9 \pm 29$	$79 \pm 20$
$\alpha$ -pinene	$56 \pm 6$	$85.1 \pm 13$	$107 \pm 43$	$53 (^{+22}_{-15})$

**Figure 3.6** Comparison of two SARs for the estimation of rate coefficients for the reactions between alkenes and OH, alongside the experimental results derived in this work (green) and the recommended literature values (black). The transparent bars are equivalent to the anticipated errors on the SAR derived  $k$  values; 15% for Peeters et al. (2007) and 40% for Jenkin et al. (2018).

## 3.1.1.7 Control experiments

To ensure that any observed depletions in VOC concentration were due to reaction with OH, rather than by photochemistry initiated by the VUV lamp, dry (rather than humidified) nitrogen was used to inhibit the formation of OH radicals. The data was processed in exactly the same way as above. Figure 3.7 shows the result of this experiment with no anticipated OH radical production. The measured depletion factors were significantly smaller than those observed when OH was produced (see Figure 3.3) and many were considered to be approximately 0, within errors. The only exceptions to this were 3-carene and  $\gamma$ -terpinene; their depletion factors were both greater than 0 and their errors did not coincide with 0. This could suggest that they underwent some appreciable photochemistry within the reactor, especially  $\gamma$ -terpinene. There was also a linear trend observed between depletion factor and rate coefficient for reaction with OH. This may indicate that H<sub>2</sub>O was not entirely excluded from the reactor and that OH production still occurred, or that there was some other mechanism for OH production within the reactor. It may also be evidence that some photolysis did indeed occur, with the resultant radical products responsible for the increased chemistry and depletion factors.

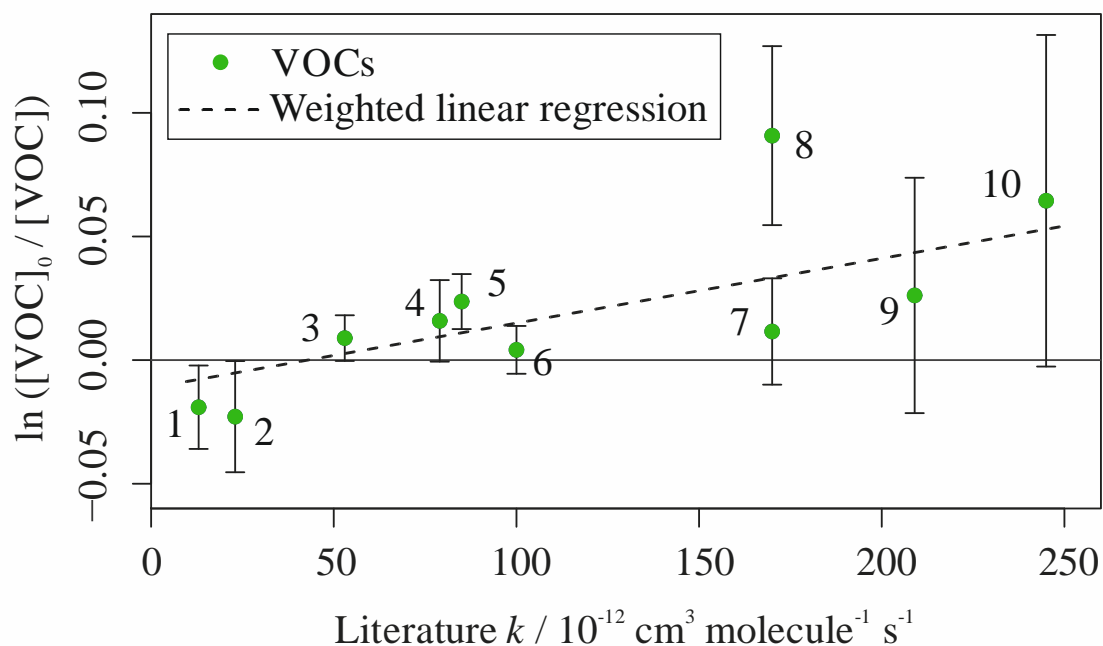


**Figure 3.7** Relative rate plot for monoterpenes mixture 1 with no OH production, at 295 K. Compounds with a reference rate coefficient for reaction with OH were plotted using literature values. Error bars on the y-axis, equal to one standard error, were calculated by combining the standard error in peak areas for six lamp-off and six lamp-on samples. Error bars on the x-axis are not displayed for reasons of clarity but were typically large. The VOCs can be identified as follows; 1, *o*-xylene; 2, *m*-xylene; 3,  $\alpha$ -pinene; 4,  $\beta$ -pinene; 5, 3-carene; 6, isoprene; 7, limonene; 8,  $\gamma$ -terpinene; 9, myrcene; 10,  $\beta$ -ocimene.

### 3.1.1.8 Products of the VOC + OH reactions

The depletions in the concentrations of the VOCs when the lamp was on compared with when the lamp was off can easily be distinguished on the TICs in Figure 3.1. It would therefore be expected that any products of the VOC + OH reactions would be just as easy to identify in the same chromatograms. The losses in VOCs, assuming full transfer of VOCs from liquid injection during the preparation stage to analysis, were between approximately 1 and 10 ppb, depending on the OH reactivity of the gas mixture. Hence, it would stand to reason that between 1 and 10 ppb of products would have been generated. Unfortunately, product peaks were not easily identified in the gas chromatography data. Two small, potential product peaks did exist and are shown in Figure 3.8. These peaks were identified as methacrolein and methyl vinyl ketone (MVK), both of which are isomers of  $C_4H_6O$ . Their presence in the lamp-on chromatogram but not the lamp-off chromatogram suggests that they were the products of the VOC + OH reactions.

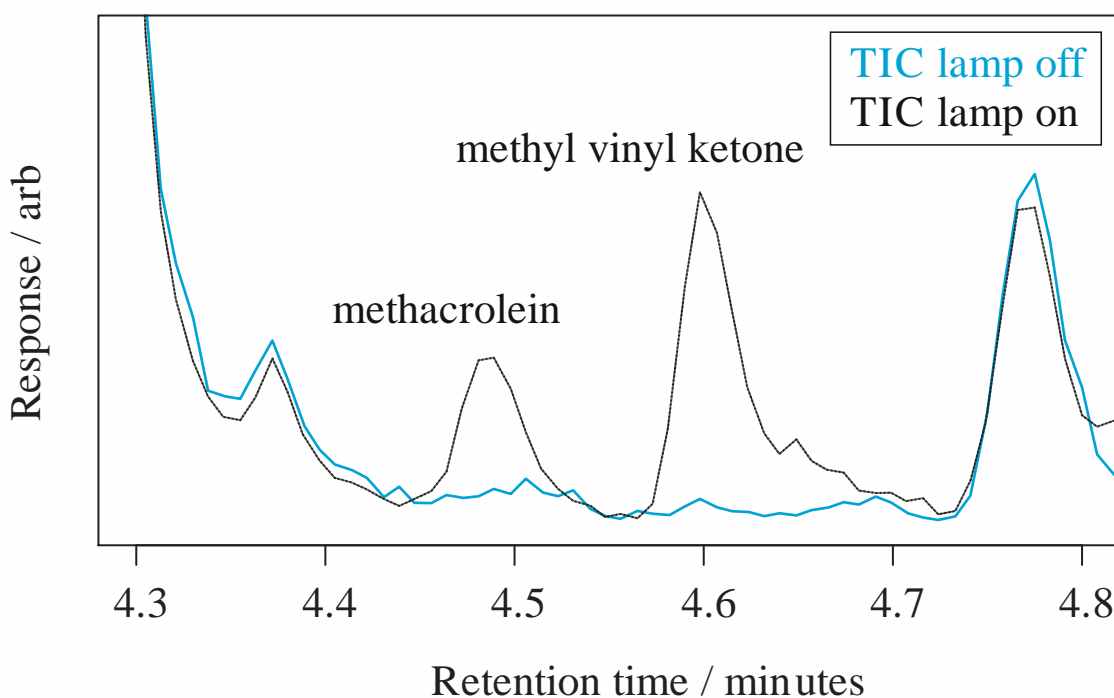
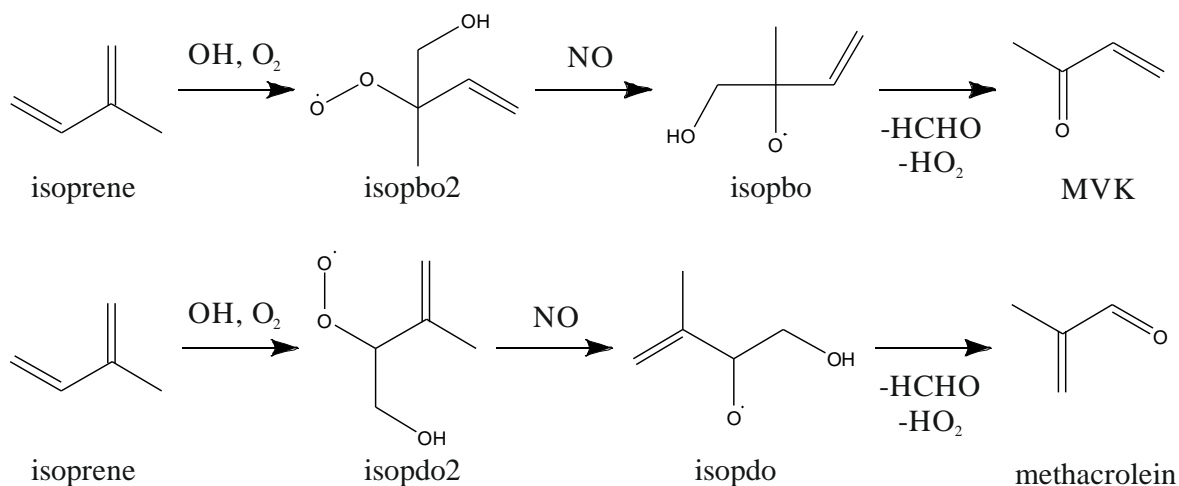


**Figure 3.8** Typical total ion chromatograms (TICs) sections obtained for monoterpenes mixture 1 with the lamp turned off (blue) and the lamp turned on (black). Two peaks were identified here (methacrolein and methyl vinyl ketone) which were not present when the lamp was off but were when the lamp is on, leading to the conclusion that they are products of VOC + OH reactions.

The Master Chemical Mechanism (MCM; Jenkin et al., 1997; Saunders et al., 2003; <http://mcm.leeds.ac.uk/MCM/>; accessed 14/02/2018) can be used to identify the potential precursors that lead to the products identified in Figure 3.8. MVK can be produced directly by the reaction of isoprene and O<sub>3</sub>, with a rate coefficient of approximately  $k = 1.3 \times 10^{-17} \text{ cm}^3 \text{ molecule}^{-1} \text{ s}^{-1}$  and branching ratio for its formation of 0.2. It seems unlikely that this was the major reaction that produced the MVK observed in Figure 3.8, owing to both the low anticipated concentration of O<sub>3</sub> in the reactor, and the exceptionally small rate coefficient for the reaction. However, there were other routes that produce MVK from the OH-initiated oxidation of isoprene in the MCM. One such route involved reaction with NO and is shown in Schematic 3.1.

Methacrolein can also be produced directly from the oxidation of isoprene by O<sub>3</sub>, albeit with a branching ratio slightly greater than that forming MVK, of 0.3. Once again, a route involving a primary reaction with OH and then further reaction with O<sub>2</sub> and NO was also available for the production of methacrolein from isoprene (Schematic 3.1).



**Schematic 3.1** Potential routes for the formation of methyl vinyl ketone (MVK) and methacrolein beginning with the oxidation of isoprene by OH. Compound names and reaction schemes were taken directly from the Master Chemical Mechanism (MCM; Jenkin et al., 1997; Saunders et al., 2003; <http://mcm.leeds.ac.uk/MCM/>; accessed 14/02/2018).

The MCM also contains detailed oxidation schemes for three of the monoterpenes that appeared in this mixture;  $\alpha$ -pinene,  $\beta$ -pinene and limonene. Neither MVK nor methacrolein were found in the oxidation schemes for either of  $\alpha$ - and  $\beta$ -pinene, although similar structures based on the MVK unit could be found. There were several routes for the formation of methacrolein from limonene, although it was difficult to identify the exact reactants required due to the complexity and size of the entire chemical scheme.

It is therefore likely that both MVK and methacrolein were products of the VOC + OH reactions for this mixture. However, analysis of the MCM suggests that other reactants were required for their eventual formation, such as  $O_3$  and NO. Whilst it isn't impossible that these reactants existed within the reactor, the potential for their presence would have minor consequences for the initial oxidation of the primary VOCs. The concentration of  $O_3$  at the end of the reactor had been previously measured to be on the order of 5 ppb (Shaw et al., 2018). This was far too low to have any consequences for the OH oxidation chemistry. Even if potentially large, but unlikely, concentrations of  $O_3$  were present in the reactor, of greater than 100 ppm, reactions with OH would still dominate for most of the VOCs.

### 3.1.2 Monoterpene mixture 2

This mixture contained 13 VOCs, of which all had at least one  $k$  measurement available in the literature. Nine of the VOCs were monoterpenes, including;  $\alpha$ - and  $\beta$ -phellandrene,  $\alpha$ - and  $\beta$ -pinene,  $\alpha$ -terpinene,  $\gamma$ -terpinene, camphene, limonene, and terpinolene. A sesquiterpene,  $\alpha$ -cedrene, was also included, along with isoprene,  $m$ -xylene and 1,2,4-trimethylbenzene.

Table 3.4 gives a full list of the 13 VOCs in this mixture, along with the reference rate coefficient used for their reaction with OH and the number of measurements which could be found in the literature at the time of writing. Although  $\alpha$ -cedrene was included as part of this mixture, it was not identified in the TIC recorded and hence its rate coefficient could not be evaluated.

There was a similar range in  $k$  values across the VOCs in this mixture, when compared with the range for the first monoterpenes mixture. The estimated total OH reactivity of this mixture at standard temperature and pressure (STP) was  $1300 \text{ s}^{-1}$ . This mixture was diluted with  $\text{N}_2$  in differing amounts to inject gaseous samples into the reactor with a range of OH reactivities approximately between 70 and  $400 \text{ s}^{-1}$ .

**Table 3.4** List of VOCs, in descending order of evaluated literature  $k$  value, in monoterpenes mixture 2 along with their evaluated literature  $k$  value, reference and number of measurements found in the literature at the time of writing.

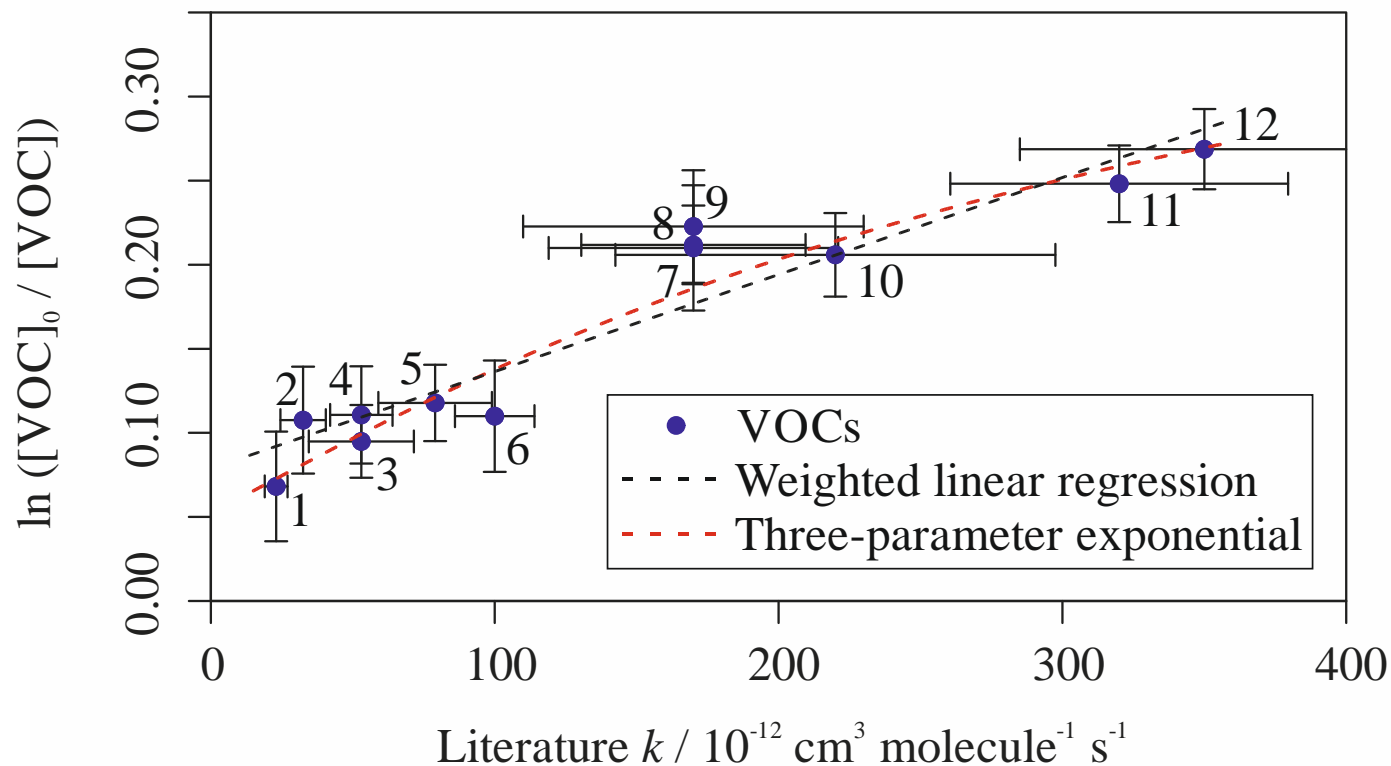
Name	Evaluated literature $k$ (298 K) / $10^{-12} \text{ cm}^3$ $\text{molecule}^{-1} \text{ s}^{-1}$	Reference used	Number of literature measurements
$\alpha$ -terpinene	350 ( $^{+71}_{-59}$ )	Atkinson et al., 2006	2
$\alpha$ -phellandrene	320 ( $^{+65}_{-54}$ )	Atkinson et al., 2006	2
Terpinolene	220 ( $^{+91}_{-64}$ )	Atkinson et al., 2006	1
$\beta$ -phellandrene	170 ( $^{+70}_{-50}$ )	Atkinson et al., 2006	1
$\gamma$ -terpinene	170 ( $^{+44}_{-35}$ )	Atkinson et al., 2006	1
Limonene	$170 \pm 51$	Atkinson and Arey, 2003	5
Isoprene	100 ( $^{+15}_{-13}$ )	Atkinson et al., 2006	25+
$\beta$ -pinene	$79 \pm 20$	Atkinson and Arey, 2003	10
$\alpha$ -cedrene	67 ( $^{+17}_{-14}$ )	Atkinson et al., 2006	1
$\alpha$ -pinene	53 ( $^{+23}_{-15}$ )	Atkinson et al., 2006	9
Camphene	$53 \pm 11$	Atkinson and Arey, 2003	2
1,2,4-trimethylbenzene	$33 \pm 8$	Atkinson and Arey, 2003	5
$m$ -xylene	$23 \pm 4$	Atkinson and Arey, 2003	15

### 3.1.2.1 Relative rate plots

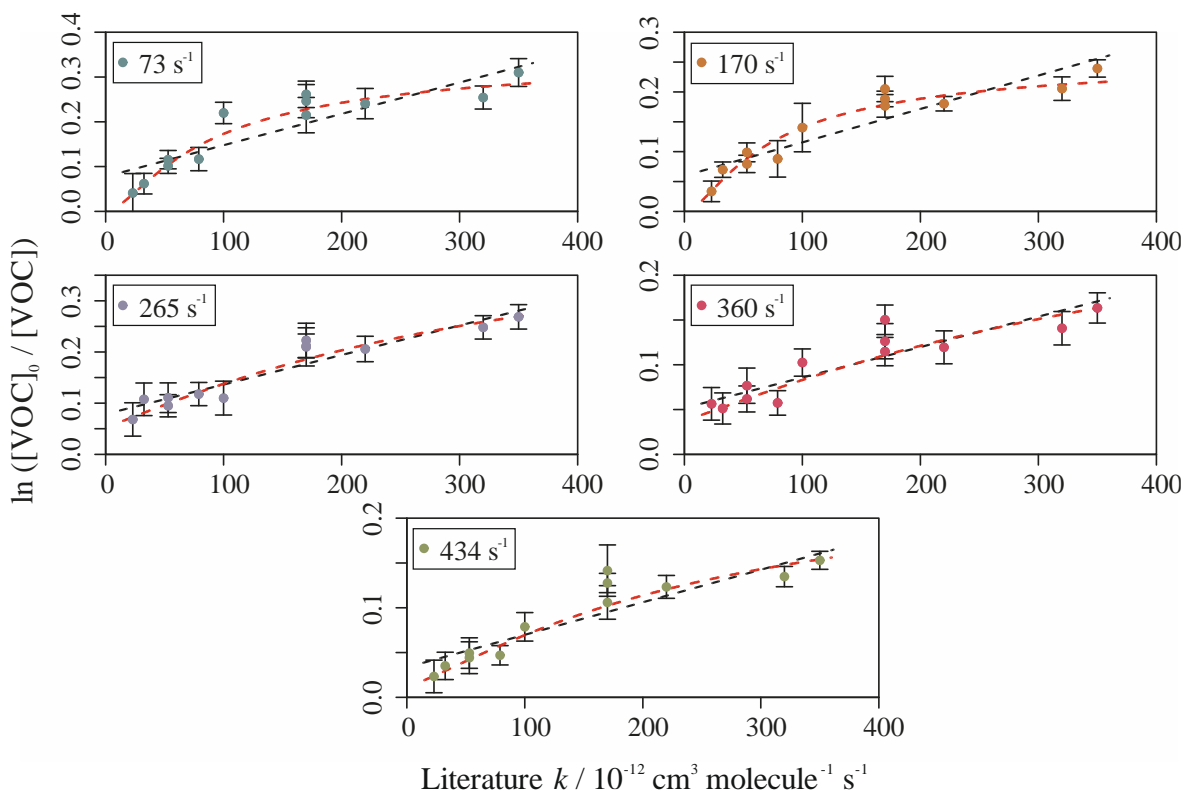
The relative rate plots for this mixture, obtained by plotting  $\ln\left(\frac{[\text{VOC}]_0}{[\text{VOC}]}\right)$  against evaluated literature  $k$  values, did not all show a linear trend. Rather, the depletion factors for the two lowest OH reactivities showed a more pronounced curved trend, much like that for the lowest OH reactivity for monoterpenes mixture 1 (see Figure 3.5).

Figure 3.9 shows a relative rate plot for this mixture with an OH reactivity of  $265\text{ s}^{-1}$ . There was a clear increase in depletion factor with increasing evaluated literature rate coefficient. Whilst the relationship at this OH reactivity was well modelled with a linear regression ( $R^2 = 0.893$ ), the same was not true for all the OH reactivities tested. Figure 3.10 shows the five relative rate plots for this mixture, with OH reactivities of 73, 170, 265, 360 and  $434\text{ s}^{-1}$ . Each individual plot is shown with both the linear relationship, as given by weighted linear regression (black), and the curved relationship, as modelled using the three-parameter exponential relationship given by Eq. 3.1.

It is quite clear that, for this mixture with the two lowest OH reactivities, the exponential relationship provided a much better estimation of the trend observed between depletion factor and  $k$  value. However, for this mixture with OH reactivities greater than  $170\text{ s}^{-1}$ , the curved relationship was much less pronounced and closely matched that given by the weighted linear regression. For more information regarding understanding the curved nature of this, and other relative plots, please refer to Section 3.2.2.



**Figure 3.9** Relative rate plot for monoterpenes mixture 2 with an OH reactivity of  $265 \text{ s}^{-1}$ , at 295 K. Compounds with a reference rate coefficient for reaction with OH were plotted using evaluated literature values as references. Error bars on the y-axis, equal to one standard error, were calculated by combining the standard error in peak areas for six lamp-off and six lamp-on samples. Error bars on the x-axis were typically large (approximately  $\pm 20\text{-}30\%$ ). A weighted (to the uncertainty in the y-values) linear fit was used to generate the slope, with a value of  $OH_{exp} = 0.6 (\pm 0.06) \times 10^9 \text{ molecules cm}^{-3} \text{ s}$  and  $R^2 = 0.893$ . A three-parameter exponential relationship (Eq. 3.1) was used to generate the curve, with  $R^2 = 0.904$ . The VOCs can be identified as follows; 1, *m*-xylene; 2, 1,2,4-trimethylbenzene; 3,  $\alpha$ -pinene; 4, camphene; 5,  $\beta$ -pinene; 6, isoprene; 7, limonene; 8,  $\gamma$ -terpinene; 9,  $\beta$ -phellandrene; 10, terpinolene; 11,  $\alpha$ -phellandrene; 12,  $\alpha$ -terpinene.



**Figure 3.10** Relative rate plots for monoterpenes mixture 2 with OH reactivities of 73, 170, 265, 360 and 434 s<sup>-1</sup>. Two relationships between depletion and literature  $k$  value were modelled; a weighted linear regression (black) and a three-parameter exponential relationship (red; Eq. 3.1). The R<sup>2</sup> values for the weighted linear fits were 0.759, 0.858, 0.893, 0.777 and 0.839 respectively. The values of  $OH_{exp}$  were 0.70 ( $\pm 0.12$ ), 0.6 ( $\pm 0.07$ ), 0.6 ( $\pm 0.06$ ), 0.3 ( $\pm 0.05$ ) and 0.4 ( $\pm 0.05$ )  $\times 10^9$  molecules cm<sup>-3</sup> s respectively. The R<sup>2</sup> values for the three-parameter exponential relationships were 0.933, 0.934, 0.904, 0.779 and 0.926 respectively. Error bars on the x-axis are not shown for reasons of clarity.

### 3.1.2.2 Calculation of rate coefficients

Using Eq. 2.19, and the relationships determined via either weighted linear regression or the three-parameter exponential, it was possible to estimate a rate coefficient for each of the VOC + OH reactions for this mixture relative to all the others at each OH reactivity. These five values, for each of the two different modelled relationships, were then averaged, weighted to the errors, to yield a single relative rate coefficient for each of the VOCs. These final values are given in Table 3.5.

**Table 3.5** List of VOCs, in descending order of evaluated literature  $k$  value, in monoterpenes mixture 2 along with their range of depletions due to reaction with OH, measured  $k$  value for both linear regression and three-parameter exponential analysis, and evaluated literature  $k$  value.

Name	Range of depletion / %	Linear regression measured $k / 10^{-12} \text{ cm}^3 \text{ molecule}^{-1} \text{ s}^{-1}$	Curve measured $k / 10^{-12} \text{ cm}^3 \text{ molecule}^{-1} \text{ s}^{-1}$	Evaluated literature $k / 10^{-12} \text{ cm}^3 \text{ molecule}^{-1} \text{ s}^{-1}$
$\alpha$ -terpinene	14 - 27	$327 \pm 4$	$348 \pm 22$	$350 (^{+71}_{-59})$
$\alpha$ -phellandrene	13 - 22	$273 \pm 18$	$269 \pm 21$	$320 (^{+65}_{-54})$
Terpinolene	12 - 21	$223 \pm 16$	$198 \pm 23$	$220 (^{+91}_{-64})$
$\beta$ -phellandrene	13 - 22	$260 \pm 20$	$270 \pm 30$	$170 (^{+70}_{-50})$
$\gamma$ -terpinene	12 - 22	$236 \pm 14$	$221 \pm 19$	$170 (^{+44}_{-35})$
Limonene	10 - 19	$206 \pm 16$	$176 \pm 19$	$170 \pm 51$
Isoprene	9 - 21	$138 \pm 56$	$119 \pm 36$	$100 (^{+15}_{-13})$
$\beta$ -pinene	5 - 11	$49 \pm 21$	$59 \pm 9$	$79 \pm 20$
$\alpha$ -pinene	4 - 10	$32 \pm 4$	$50 \pm 3$	$53 (^{+22}_{-16})$
Camphene	5 - 10	$61 \pm 11$	$61 \pm 5$	$53 \pm 11$
1,2,4-trimethylbenzene	4 - 5	$16 \pm 27$	$39 \pm 6$	$33 \pm 8$
<i>m</i> -xylene	1 - 4	$-21 \pm 27$	$23 \pm 4$	$23 \pm 4$

The two aromatic VOCs incorporated as part of this mixture were also the two VOCs with the smallest rate coefficients for reaction with OH. The result for *m*-xylene, which was also present in the first monoterpenes mixture, using linear regression was negative, due largely to the curved relationship between depletion factor and  $k$  value for the mixture at low OH reactivity. In a similar manner, many of the VOCs at the slower end of the reactivity scale (1,2,4-trimethylbenzene and  $\alpha$ - and  $\beta$ -pinene) show measured  $k$  values that were much smaller than the literature evaluated equivalents when using the weighted linear regression analysis. Using the three-parameter exponential analysis provided much better results for many of these compounds; the values for *m*-xylene, 1,2,4-trimethylbenzene and  $\alpha$ -pinene were all in excellent agreement with their evaluated literature values.

The results for the reaction between  $\beta$ -pinene and OH using both linear regression and the three-parameter exponential were substantially smaller than the evaluated literature coefficient and that measured in the first monoterpenes mixture, of  $78 (\pm 11) \times 10^{-12} \text{ cm}^3 \text{ molecule}^{-1} \text{ s}^{-1}$ . In contrast, those measured for the isoprene + OH reaction, were both much greater than the evaluated literature value and that measured in the first monoterpenes mixture, of  $104 (\pm 6) \times 10^{-12} \text{ cm}^3 \text{ molecule}^{-1} \text{ s}^{-1}$ . For both reactions, the curve measured values were in agreement with the evaluated literature value, within errors.

The rate coefficient for the limonene + OH reaction, measured using the three-parameter exponential was in excellent agreement with both the evaluated literature coefficient and that measured in the first monoterpenes mixture, of  $152 (\pm 4) \times 10^{-12} \text{ cm}^3 \text{ molecule}^{-1} \text{ s}^{-1}$ . The same was true for  $\gamma$ -terpinene, with a measurement of  $207 (\pm 6) \times 10^{-12} \text{ cm}^3 \text{ molecule}^{-1} \text{ s}^{-1}$  from the first monoterpenes mixture. On the other hand, the results for these two compounds using the linear regression analysis were much greater than the evaluated literature coefficient and those measured in monoterpenes mixture 1, demonstrating that the three-parameter exponential relationship was much more applicable for these compounds.

The four VOCs with the largest rate coefficients for reaction with OH were not included as part of monoterpenes mixture 1. For the reaction between  $\beta$ -phellandrene and OH, both the linear regression and the three-parameter exponential measured results were in excellent agreement with each other, but are approximately 50% larger than the evaluated literature rate coefficient. The opposite was true for  $\alpha$ -phellandrene, where the results from both linear regression and the exponential analysis were in good agreement but were much smaller than the literature value, by roughly 20%.

The result for the terpinolene + OH reaction using linear regression was in good agreement with the evaluated literature coefficient but the three-parameter exponential result was approximately 10% smaller. The results for the  $\alpha$ -terpinolene + OH reaction showed the opposite trend, with the three-parameter exponential measure rate coefficient in excellent agreement with the evaluated literature value whilst the linear regression measured rate coefficient was approximately 10% smaller.

To summarise, most of the results from this mixture were improved by using the three-parameter exponential model in Eq. 2.19. The improvement was most drastic for those VOCs at the lower end of the reactivity scale in this mixture; *m*-xylene, 1,2,4-trimethylbenzene and  $\alpha$ -pinene all showed significant improvement relative to the linear regression measured values for example.

### 3.1.2.3 Comparisons to structure-activity relationships

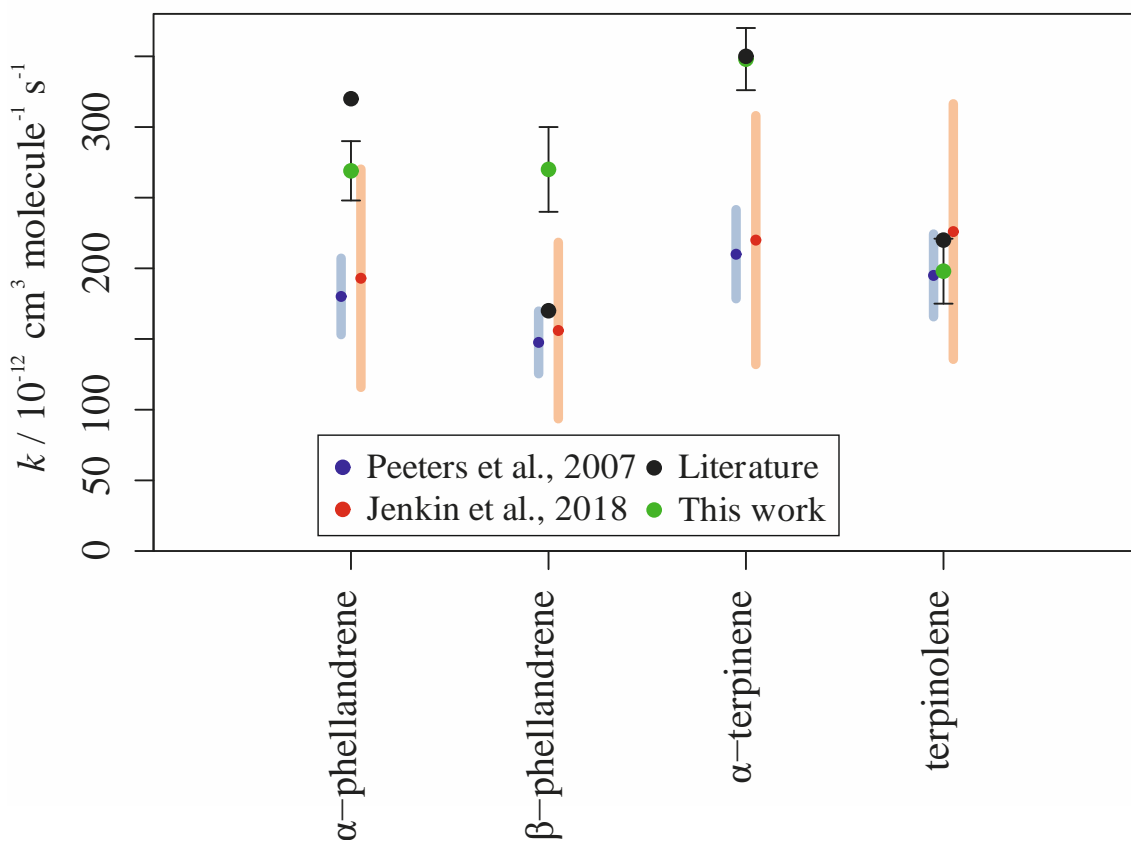
In the absence of multiple experimental rate coefficient measurements for the reactions of  $\alpha$ - and  $\beta$ -phellandrene,  $\alpha$ -terpinene and terpinolene with OH, SARs provide a necessary comparison for the experimental results in this work. As explained in Section 3.1.1.6, there are two SARs in the literature which provide estimates for the reactions between alkenes and dialkenes with OH. The SAR in Peeters et al. (2007) was shown to work relatively well, despite excluding contributions from H-atom abstraction by OH, but performed poorly with conjugated dienes. The more recent SAR, by Jenkin et al. (2018), generally provided slightly better estimations of alkene + OH rate coefficients, particularly for the conjugated dienes. This may be attributed to the explicit treatment of site specific H-atom abstraction rates.

Table 3.6 and Figure 3.11 provide the SAR estimated values alongside the measured values in this work, and the evaluated literature values, for the reactions of these four monoterpenes with OH. The Jenkin et al. (2018) SAR performed particularly well when estimating the rate coefficient for the reaction between terpinolene and OH. The Peeters et al. (2007) SAR also provided a good estimation for the same reaction, within errors. The measured value in this work was in excellent agreement with the Peeters et al. (2007) SAR.

The other three monoterpenes,  $\alpha$ - and  $\beta$ -phellandrene and  $\alpha$ -terpinene, are conjugated dienes. Both SARs predicted rate coefficients which were in excellent agreement with the evaluated literature value for the  $\beta$ -phellandrene + OH reaction. The measured value in this work for the same reaction was therefore in poor agreement with both the evaluated literature value and the SARs. However, the two SARs performed poorly when predicting the rate coefficients for the reactions of  $\alpha$ -phellandrene and  $\alpha$ -terpinene with OH. Unlike for  $\beta$ -phellandrene, the measured values in this work were much closer to the evaluated literature values than the SARs for the reactions of  $\alpha$ -phellandrene and  $\alpha$ -terpinene with OH.

**Table 3.6** List of VOCs, in descending order of evaluated literature  $k$  value, in monoterpenes mixture 2 along with their SAR derived  $k$  values, experimentally measured  $k$  value and evaluated literature  $k$  value.

Name	Rate coefficient for reaction with OH / $10^{-12} \text{ cm}^3 \text{ molecule}^{-1} \text{ s}^{-1}$			
	This work	Peeters et al. (2007) SAR	Jenkin et al. (2018) SAR	Evaluated literature
$\alpha$ -terpinene	$348 \pm 22$	$210 \pm 32$	$220 \pm 88$	$350 (^{+71}_{-59})$
$\alpha$ -phellandrene	$269 \pm 21$	$180 \pm 27$	$193 \pm 77$	$320 (^{+65}_{-54})$
terpinolene	$198 \pm 23$	$195 \pm 29$	$226 \pm 90$	$220 (^{+91}_{-64})$
$\beta$ -phellandrene	$270 \pm 30$	$148 \pm 22$	$156 \pm 63$	$170 (^{+70}_{-50})$

**Figure 3.11** Comparison of two SARs for the estimation of rate coefficients for the reactions between alkenes and OH, alongside the experimental results derived in this work (green) and the recommended literature values (black). The transparent bars are equivalent to the anticipated errors on the SAR derived  $k$  values; 15% for Peeters et al. (2007) and 40% for Jenkin et al. (2018).

### 3.1.3 Alkenes mixture

This mixture contained 11 VOCs, 10 of which had at least one  $k$  measurement available in the literature. 2,3-dimethylpent-1-ene, a branched 1-alkene, had no available literature rate coefficient for its reaction with OH at the time of writing. Four of the 11 VOCs were linear 1-alkenes and three were cyclic alkenes. The remaining three VOCs were isoprene and  $\alpha$ - and  $\beta$ -pinene, all of which contain unsaturated carbon-carbon double bonds. Table 3.7 gives a full list of the 11 VOCs, along with the reference rate coefficient used for their reaction with OH, their references and the number of available measurements in the literature at the time of writing.

The estimated total OH reactivity of this mixture at STP was  $480 \text{ s}^{-1}$ . After further dilution with  $\text{N}_2$ , the injected samples had a range in OH reactivity of approximately 25 to  $160 \text{ s}^{-1}$ .

**Table 3.7** List of VOCs, in descending order of evaluated literature  $k$  value, in the alkenes mixture along with their evaluated literature  $k$  value, reference and number of measurements found in the literature at the time of writing.

Name	Evaluated literature $k$ (298 K) / $10^{-12} \text{ cm}^3$ molecule $^{-1} \text{ s}^{-1}$	Reference used	Number of literature measurements
isoprene	$100 (^{+15}_{-13})$	Atkinson et al., 2006	25+
$\beta$ -pinene	$79 \pm 20$	Atkinson and Arey, 2003	10
cycloheptene	$74 \pm 10$	Atkinson and Arey, 2003	1
cyclohexene	$68 \pm 17$	Atkinson and Arey, 2003	9
cyclopentene	$67 \pm 23$	Atkinson and Arey, 2003	3
$\alpha$ -pinene	$53 (^{+22}_{-15})$	Atkinson et al., 2006	9
1-nonene	$43.2 \pm 0.5$	Aschmann and Atkinson, 2008	2
1-octene	$41.4 \pm 0.8$	Aschmann and Atkinson, 2008	2
1-heptene	$40 \pm 12$	Atkinson and Arey, 2003	2
1-hexene	$37 \pm 11$	Atkinson and Arey, 2003	2
2,3-dimethylpent-1-ene			0

## 3.1.3.1 Typical chromatogram data

A typical TIC for this mixture is shown in Figure 3.12. The blue line represents mixtures with the lamp turned off and the black line represents samples with the reactor lamp switched on. There was an observable difference in the peak areas of the detected VOCs with the lamp turned on.

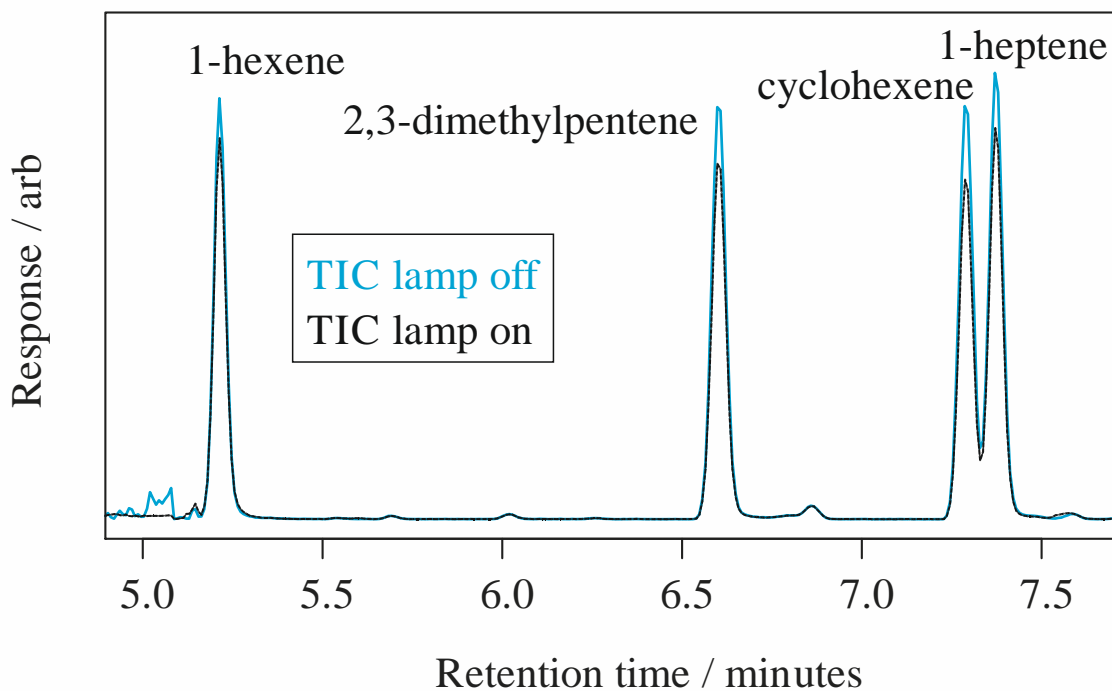


**Figure 3.12** Typical total ion chromatogram (TIC) sections obtained for the alkenes mixture with the lamp turned off (blue) and the lamp turned on (black). Greater differences in peak areas were observed for VOCs which have a larger rate coefficient value for their reaction with OH. Evaluated literature rate coefficients (in units of  $10^{-12} \text{ cm}^3 \text{ molecule}^{-1} \text{ s}^{-1}$ ) for the VOC + OH reactions are: 1-hexene,  $37 (\pm 11)$ ; 2,3-dimethylpentene, N/A; cyclohexene,  $68 (\pm 17)$ ; 1-heptene,  $40 (\pm 12)$  (see Table 3.7).

Figure 3.13 nicely demonstrates one of the advantages of using a ToF-MS as a detector over FID. Two VOCs (cyclohexene and 1-heptene) displayed similar retention times and were therefore poorly resolved. Despite this, they were analysed separately using an  $m/z$  of 56 for 1-heptene and an  $m/z$  of 67 for cyclohexene. This would not have been possible if using a different method of detection, such as FID.

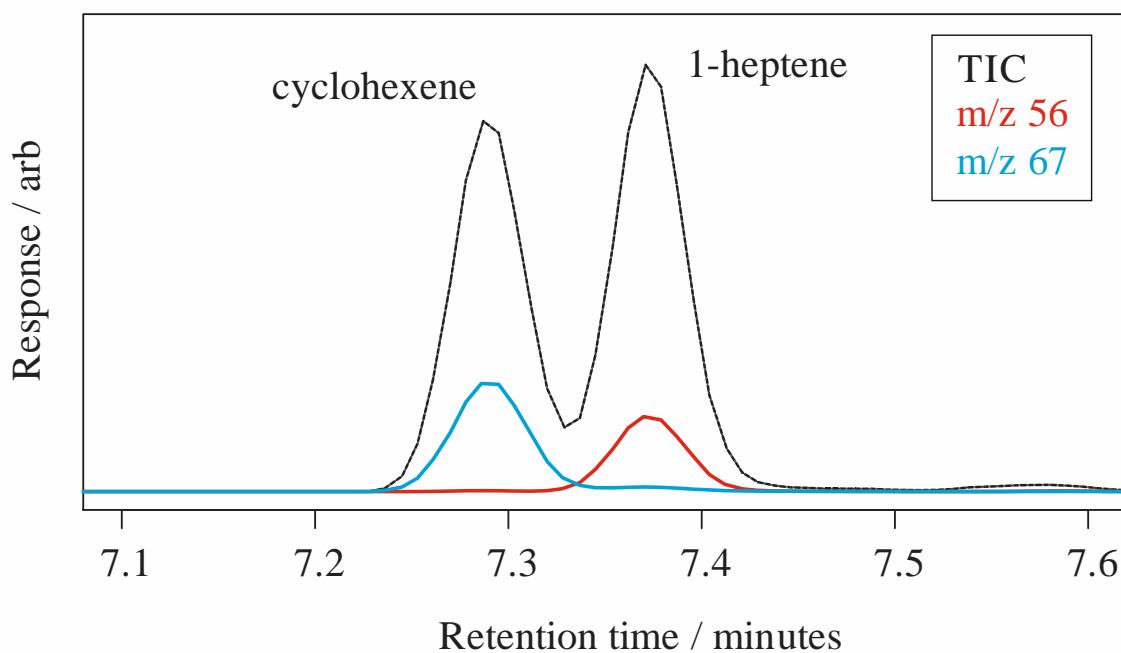


**Figure 3.13** TIC section and extracted ion chromatogram sections (EICs) at  $m/z$  56 (red) and  $m/z$  67 (blue) demonstrating the versatility of using ToF-MS as a detector in this method.

### 3.1.3.2 Relative rate plots

Figure 3.14 shows an example of a relative rate plot for this mixture with an OH reactivity of  $30 \text{ s}^{-1}$ . There was an obvious linear relationship between  $k$  value and depletion factor due to OH. The OH exposure for this sample was approximately  $1.8 (\pm 0.1) \times 10^9 \text{ molecules cm}^{-3} \text{ s}$  with  $R^2 = 0.95$ . A similar linear trend was observed for all the VOCs at each of the OH reactivities tested for this mixture. The measured  $OH_{exp}$  values were  $1.3 (\pm 0.3)$ ,  $1.2 (\pm 0.2)$ ,  $1.0 (\pm 0.2)$  and  $0.7 (\pm 0.2) \times 10^9 \text{ molecules cm}^{-3} \text{ s}$  for this mixture with OH reactivities of 60, 100, 130 and  $160 \text{ s}^{-1}$  respectively. The linear fits were generally good, with a possible slight decrease in  $R^2$  value with increasing OH reactivity ( $R^2$  values: 0.95, 0.69, 0.73, 0.84 and 0.69).

### 3.1.3.3 Calculation of rate coefficients

As demonstrated for the above mixtures, it was possible to estimate a  $k$  value for each of the components in this mixture, by averaging the results at each OH reactivity. These values are provided in Table 3.8 along with the literature reference  $k$  values. All measured values were in excellent agreement with the evaluated literature reference for the same reaction.

**Table 3.8** List of VOCs, in descending order of evaluated literature  $k$  value, in the alkenes mixture along with their range of depletions due to reaction with OH, measured  $k$  value and evaluated literature  $k$  value.

Name	Range of depletion / %	Measured $k$ (295 K) / $10^{-12} \text{ cm}^3 \text{ molecule}^{-1} \text{ s}^{-1}$	Evaluated literature $k$ / $10^{-12} \text{ cm}^3 \text{ molecule}^{-1} \text{ s}^{-1}$
isoprene	8 - 26	$103 \pm 5$	$100 (^{+15}_{-13})$
$\beta$ -pinene	5 - 21	$75 \pm 12$	$79 \pm 20$
cycloheptene	6 - 20	$74 \pm 10$	$74 \pm 10$
cyclohexene	6 - 20	$71 \pm 4$	$68 \pm 17$
cyclopentene	7 - 19	$69 \pm 9$	$67 \pm 23$
$\alpha$ -pinene	4 - 17	$53 \pm 4$	$53 (^{+22}_{-15})$
1-nonene	4 - 15	$41 \pm 3$	$43.2 \pm 0.5$
1-octene	4 - 15	$44 \pm 5$	$41.4 \pm 0.8$
1-heptene	3 - 13	$36 \pm 4$	$40 \pm 12$
1-hexene	2 - 15	$46 \pm 12$	$37 \pm 11$
2,3-dimethylpent-1-ene	5 - 17	$57 \pm 3$	

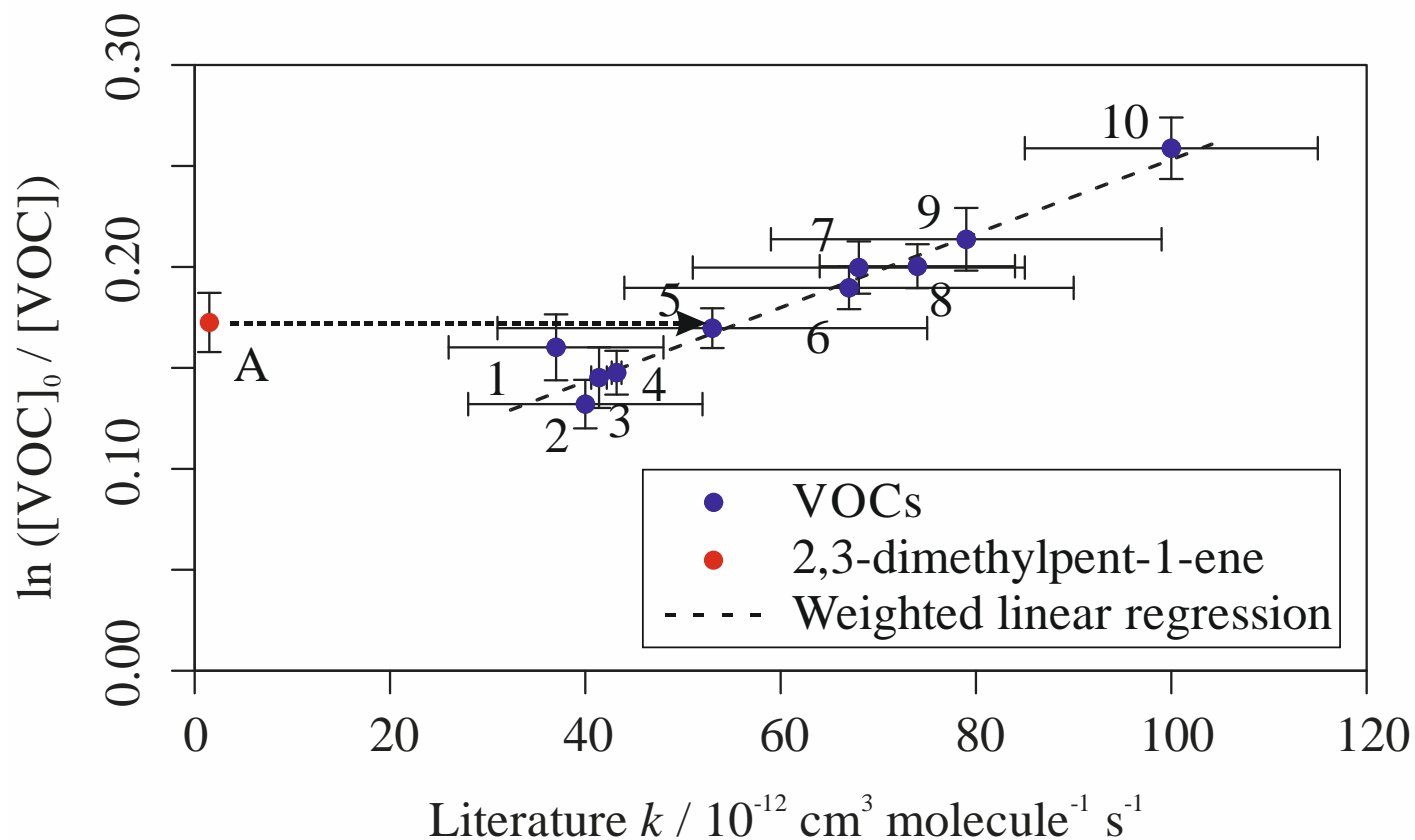


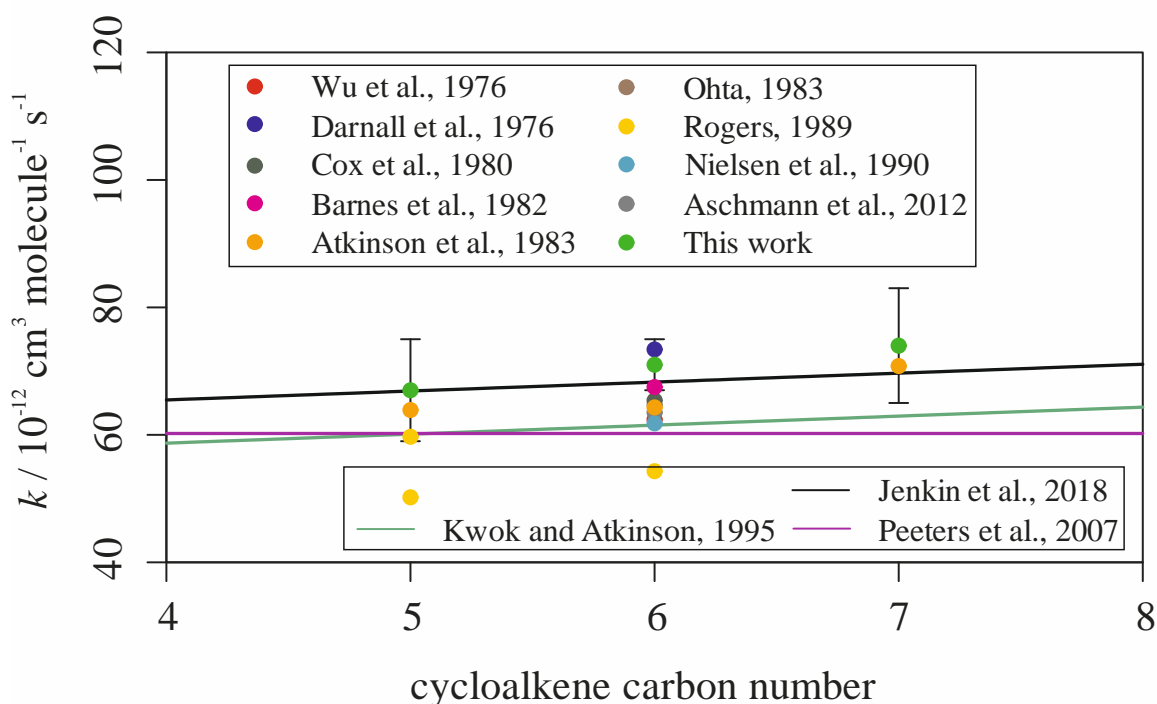
**Figure 3.14** Relative rate plot for the alkenes mixture with an OH reactivity of  $30 \text{ s}^{-1}$ , at 295 K. Compounds with a reference rate coefficient for reaction with OH were plotted using evaluated reference values. Error bars on the y-axis, equal to one standard error, were calculated by combining the standard error in peak areas for six lamp-off samples and six lamp-on samples. Error bars on the x-axis were typically large (approximately  $\pm 20\text{-}30\%$ ) and accounted for deviations from the trend for all VOCs. A weighted (to the uncertainty in the y-axis) linear fit was used to generate the slope with a value of  $OH_{exp} = 1.8 (\pm 0.1) \times 10^9 \text{ molecules cm}^{-3} \text{ s}$  and  $R^2$  of 0.95. Data for 2,3-dimethylpent-1-ene (A), which had no literature  $k$  value, was not used in the calculation of the fit. The VOCs can be identified as follows: 1, 1-hexene; 2, 1-heptene; 3, 1-octene; 4, 1-nonene; 5,  $\alpha$ -pinene; 6, cyclopentene; 7, cyclohexene; 8, cycloheptene; 9,  $\beta$ -pinene; 10, isoprene.

### 3.1.3.4 Comparisons to the literature

The measured value, of  $103 (\pm 5) \times 10^{-12} \text{ cm}^3 \text{ molecule}^{-1} \text{ s}^{-1}$ , for the isoprene + OH reaction was in good agreement with the recent literature. It was also in excellent agreement with that measured in monoterpenes mixture 1 for the same reaction, but in poor agreement with that from the second monoterpenes mixture. Similarly, the measurements of the  $\alpha$ - and  $\beta$ -pinene reactions with OH were in good agreement with the wider literature and with other measurements in this work (see Section 3.1.1.5 for more analysis).

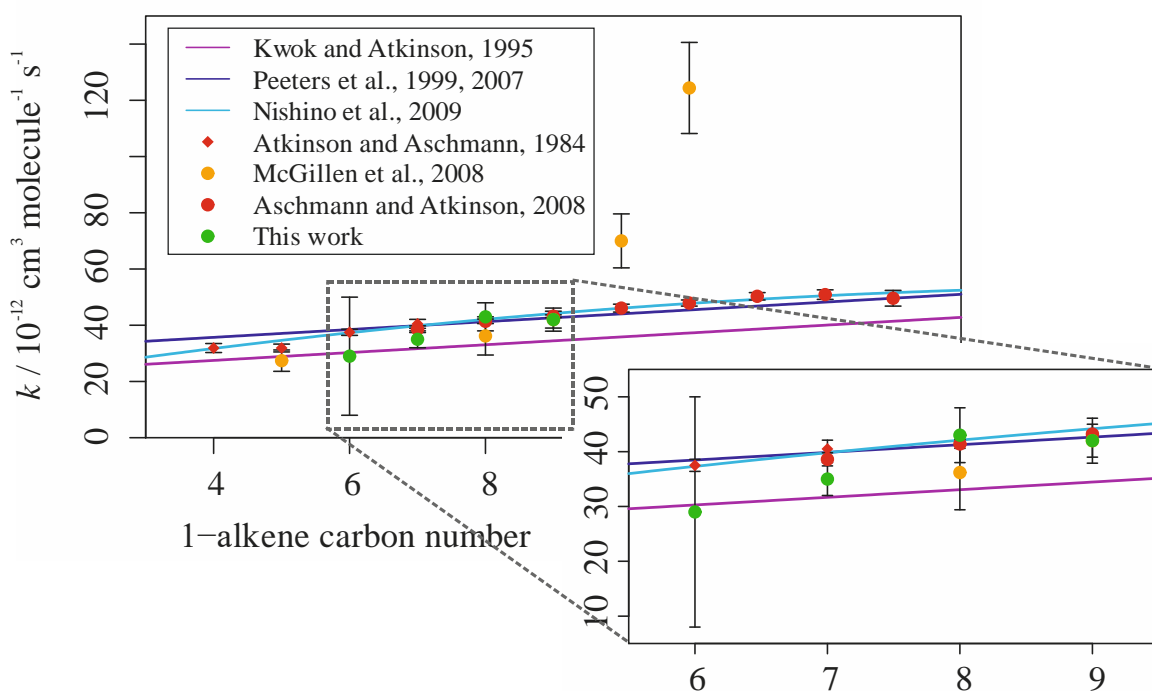
There were very few experimental measurements for cyclic alkene + OH reactions in the literature; most of the ones that did exist were for the cyclohexene + OH reaction. Figure 3.15 shows the literature measurements for the three cyclic alkenes; cyclopentene, cyclohexene and cycloheptene. There were nine measurements for cyclohexene but only three for cyclopentene and one for cycloheptene. The measured values in this work were generally greater than those in the literature, although the values were not adjusted to account for updates to the reference compound rate coefficient for relative rate studies. The majority of cyclohexene + OH  $k$  values were around  $63 \times 10^{-12} \text{ cm}^3 \text{ molecule}^{-1} \text{ s}^{-1}$  but there was a single value larger than that, of  $73.4 (\pm 14.7) \times 10^{-12} \text{ cm}^3 \text{ molecule}^{-1} \text{ s}^{-1}$ , albeit with a large uncertainty (Darnall et al., 1976).

Figure 3.15 also presents the trend in cyclic alkene + OH rate coefficients as predicted by three SARs (Kwok and Atkinson, 1995; Peeters et al., 1999, 2007; Jenkin et al., 2018). The SAR in Peeters et al., (1999, 2007) predicted no increase in rate coefficient with increasing size of ring whereas those by Kwok and Atkinson and Jenkin et al. predicted a marginal increase. This was largely due to the difference in method used for estimation. Peeters et al. (2007) did not include H-atom abstraction in their SAR; the rate coefficient was approximated using just the rate of addition to the double bond(s) and the impact of the substituent groups around it. They suggested that including an additional H abstraction term in their SAR would account for many residual errors between their predictions and experimental values but were hesitant to include one as the contemporary understanding of H-atom abstraction was 'too rudimentary'. Whilst the SAR in Kwok and Atkinson (1995) did include H-atom abstraction, it also tended to under-predict the rate coefficient for the reaction between cycloalkenes and OH. The SAR in Jenkin et al. (2018) performed much better; its estimations were in excellent agreement with both the literature values and the measurements made as part of this work.



**Figure 3.15** Experimentally derived (data points) and predicted SAR derived (lines)  $k$  values for the homologous series of cycloalkene + OH reactions. Data from this study are shown in green and were in agreement with both previous experimentally measured values and with theoretical predictions. Errors are only shown for this work and not for the other experimental literature values.

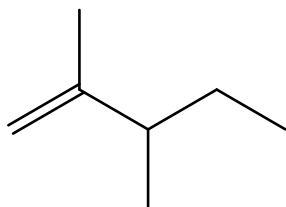
There were also very few experimental measurements for the 1-alkene + OH reactions in the literature. Figure 3.16 shows the measurements made using the multivariate relative rate technique alongside both literature experimental measurements and theoretical predictions of the rate coefficients using SARs. Figure 3.16 clearly demonstrates the predicted trend in 1-alkene + OH rate coefficients, as estimated by different SARs from Kwok and Atkinson (1995), Peeters et al. (1999, 2007) and Nishino et al. (2009). Each of these predicted a slight increase in the 1-alkene + OH reaction rate coefficient with increasing number of carbon atoms. The more recent SAR, developed by Jenkin et al. (2018), is not shown for the sake of clarity as it closely follows the trend estimated by the SAR in Peeters et al. (2007). The relationship provided by Nishino et al. (2009) gave the best agreement with the available experimental results. This was likely due to their SAR being limited to estimating rate coefficients for the 1-alkene and 2-methyl-1-alkene + OH reactions; in contrast, the other SARs were developed for multiple VOC functionalities. The experimental results in this work were in good agreement with the SAR estimations and were generally between the highest and lowest estimations. The experimental results for 1-octene and 1-nonene were also in excellent agreement with recent experimental measurements made by McGillen et al. (2007) of  $36.2 (\pm 6.8)$  and  $42.0 (\pm 4.1) \times 10^{-12} \text{ cm}^3 \text{ molecule}^{-1} \text{ s}^{-1}$  respectively.



**Figure 3.16** Experimentally derived (data points) and predicted SAR derived (lines)  $k$  values for the homologous series of 1-alkene + OH reactions. Data from this study are shown in green and were in good agreement with both previous experimentally measured values and with theoretical predictions.

### 3.1.3.4 Determination of a new rate coefficient for the 2,3-dimethylpent-1-ene + OH reaction

This mixture contained the compound 2,3-dimethylpent-1-ene, for which no literature rate measurements for its reaction with OH could be found at the time of writing. The structure of 2,3-dimethylpent-1-ene is shown in Schematic 3.2. This compound had been detected in the emissions from certain tomato variants cultivated in Portugal but was unlikely to contribute significantly to OH reactivity in the region (Figueira et al., 2014). The measured room temperature rate coefficient for the reaction of this compound with OH was  $k = 57 (\pm 3) \times 10^{-12} \text{ cm}^3 \text{ molecule}^{-1} \text{ s}^{-1}$ . Again, SARs were used to estimate a  $k$  value for this compound. Using the four different SARs found in Kwok and Atkinson (1995), Peeters et al. (1999, 2007), Nishino et al. (2009) and Jenkin et al. (2018), the rate coefficient for OH + 2,3-dimethylpent-1-ene was estimated as  $k = 55.0, 63.1, 59.3$  and  $62.4 \times 10^{-12} \text{ cm}^3 \text{ molecule}^{-1} \text{ s}^{-1}$  respectively. The experimental result for this compound was therefore in excellent agreement with two of these SAR predictions, and in relatively good agreement with the remaining two. The SAR by Peeters et al. (1999, 2007) did predict a slightly higher  $k$  value but this method also overpredicted the rate coefficients for similar branched non-conjugated alkenes, such as 3,3-dimethylbut-1-ene and 2,3-dimethylpent-2-ene. Due to the close proximity of the SAR predictions and the measured value, it is probable that this value is a very good approximation of the 2,3-dimethylpent-1-ene + OH rate coefficient.



2,3-dimethylpent-1-ene

**Schematic 3.2** Structure of 2,3-dimethylpent-1-ene.

### 3.1.3.5 Products of the VOC + OH reactions

Two small peaks were observed in the lamp-on gas chromatographs but not in the lamp-off chromatographs, suggesting that they were potentially the products of the VOC + OH reactions. As for the first monoterpenes mixture, the peaks were much smaller than the peaks for the primary VOCs. The peaks were identified as 2-methylfuran and 3-methylpentan-2-one.

Neither of these compounds were included in the MCM v3.3.1 (Jenkin et al., 1997; Saunders et al., 2003; <http://mcm.leeds.ac.uk/MCM>; accessed 14/02/2018) but compounds similar to 3-methylpentan-2-one were present, including; 2-pentanone (MPRK), 3-methylbutan-2-one (MIPK) and 4-methylpentan-2-one (MIBK). However, none of these compounds appeared in the detailed oxidation schemes for the monoalkenes that were represented in the MCM (1-pentene, 2-methylbut-1-ene, 1-hexene, 2-hexene, 2,3-dimethylbut-2-ene). Analysis of the MCM database suggests that aldehydes, not ketones, are a more likely product of both 1- and 2-alkene oxidation. Interestingly, the ketones mentioned above were produced as a result of alkane oxidation in the MCM.

Although 2-methylfuran did not appear in the MCM, it was identified in the emissions from biomass burning in the Mediterranean (Ciccioli et al., 2001). Not only was it positively identified, but it was also present in the highest concentration relative to the other non-oxygenated furan compounds identified in the same work.

## 3.2 Numerical simulations

Numerical simulations were used to complement the experimental studies and to further aid in the comprehension of the experimental results. Most of the simulations were performed using Kintecus V5.20 (Ianni, 2017; <http://kintecus.com/>).

### 3.2.1 Estimating OH concentration

An estimation of the concentration of OH in the reactor, whilst not necessary for deriving experimental  $k$  values, is of importance for simulating the reactions occurring within the reactor. Without the use of direct OH monitoring techniques such as laser induced fluorescence (LIF), it is impossible to experimentally measure the concentration of OH in the reactor. Instead, the OH concentration must be calculated, or derived from other parameters.

The OH concentration could have been estimated by calculating the photoproduction of OH from H<sub>2</sub>O under the VUV light from the Hg lamp (R. 3.1 and Eq. 3.2). However, in the absence of a measured H<sub>2</sub>O concentration (humidity) and lamp output ( $F$ , the actinic flux density), this was difficult.



$$\frac{d[\text{OH}]}{dt} = -J[\text{H}_2\text{O}] = \int \sigma_{\text{H}_2\text{O}}(\lambda)\phi_{\text{H}_2\text{O}}(\lambda)F(\lambda)d\lambda \times [\text{A}] \quad \text{Eq. 3.2}$$

Instead, the concentration of OH in the reactor was estimated by totalling the losses in each VOC. Four assumptions were necessary in order for this estimation to apply. Many of these assumptions also applied to the experimental procedure.

1. It was assumed that the OH within the reactor reacted entirely with the VOCs. This was unlikely to be entirely true, as the OH almost certainly reacted with itself, with HO<sub>2</sub> (a by-product of OH production) and with any products of the VOC + OH reactions. It was also likely that the OH interacted with the walls.
2. It was assumed that the VOCs within the reactor reacted entirely with OH i.e. that any observed losses in the VOCs were due to reaction with OH, and not due to reaction with O<sub>3</sub>, other oxidants, or due to photolysis.
3. It was assumed that the concentration of each VOC in the reactor was equal to that calculated from the injection of its liquid sample i.e. *all* the liquid compound entered the

gas cylinder during the creation of the gaseous mixture (see Chapter 2 Section 2.1.7). In most cases, the concentration of each compound was calculated to be 30 ppbv in the gas cylinder. This was unlikely to be entirely true, as some of the liquid compound injected into the cylinder was likely lost during transfer. However, without the use of external calibration, it was impossible to derive actual concentrations of each VOC from the measured peak areas. As outlined earlier, the GC data was used to derive relative concentrations of each species from lamp off to lamp on, not absolute concentrations.

4. The measured peak area for each VOC with the lamp off ( $[\text{VOC}]_0$ ) was assumed to be equal to the concentration of VOC anticipated to be in the reactor i.e. no losses occurred between the reactor and the analytical equipment. This is somewhat similar to the assumptions made for the actual experiment. However, for the experiment it was only assumed that any losses after the VOC + OH reactions occurred were consistent between lamp-off and lamp-on runs. In this case, the same assumption remained true but it was also assumed that no losses at all took place, in order that the measured peak area for lamp-off be equated to the estimated  $[\text{VOC}]$ .

For monoterpenes mixture 1, summing the losses in the VOC concentrations resulted in an average  $[\text{OH}] = 1.6 (\pm 0.5) \times 10^{11}$  molecules  $\text{cm}^{-3}$  over the different OH reactivities tested. For the alkenes mixture, the average  $[\text{OH}] = 0.9 (\pm 0.2) \times 10^{11}$  molecules  $\text{cm}^{-3}$ . These values were in agreement with each other, within errors.

### 3.2.1.1 Simulating OH concentration

The estimated OH concentration was further developed by attempting to account for OH losses to both  $\text{HO}_2$  and to OH itself. Kinetic simulations for both monoterpenes mixtures 1 and the alkenes mixture were performed in order to attempt to account for the other sinks of OH that were likely to occur within the reactor. The kinetic models for monoterpenes mixture 1 and the alkenes mixture included the reactions outlined in Table 3.9 and Table 3.10 respectively. In all cases, the VOC + OH reactions formed a non-reactive product, given the name VOC-A, and  $\text{H}_2\text{O}$ .  $\text{H}_2\text{O}$  was assumed to be unreactive towards OH. The rate coefficient values used for the models were the same as the evaluated literature rate coefficients, rather than the measured  $k$  values, described in Section 3.1.1.4 and Section 3.1.3.3. The initial  $[\text{OH}]$  differed for different iterations of the simulations, as did the initial  $[\text{HO}_2]$ , which was set to be equal to the initial  $[\text{OH}]$ , with the assumption that they would be produced in roughly equal amounts by the photolysis of  $\text{H}_2\text{O}$ .

The simulation for each mixture was first performed with the OH concentration estimated in Section 3.2.1 of  $1.6 (\pm 0.5)$  and  $0.9 (\pm 0.2) \times 10^{11}$  molecules  $\text{cm}^{-3}$  for monoterpenes mixture 1 and the alkenes mixture respectively. The modelled depletion for each VOC was then compared with the corresponding experimental depletion, and the initial [OH] adjusted accordingly; if the observed depletions were greater in the experiment than in the simulation, [OH] was increased and if the observed depletions were greater in the simulation than in the experiments, [OH] was decreased. This was repeated until the average ratio of modelled to measured depletion across the different VOCs was equal to 1.00 (to at least two significant figures).

This study resulted in an estimated initial [OH] of  $3.1 (\pm 1.0)$  and  $1.3 (\pm 0.2) \times 10^{11}$  molecules  $\text{cm}^{-3}$  for monoterpenes mixture 1 and the alkenes mixture respectively. Simulating the other OH sinks therefore resulted in a 94% increase in estimated [OH] for monoterpenes mixture 1 and a 44% increase for the alkenes mixture.

**Table 3.9** List of reactions in kinetic simulations for modelling the OH concentration for monoterpenes mixture 1.

Reaction	$k / 10^{-12} \text{ cm}^3 \text{ molecule}^{-1} \text{ s}^{-1}$
$\text{OH} + \text{OH} \rightarrow \text{H}_2\text{O} + \text{O}$	1.48
$\text{OH} + \text{OH} \rightarrow \text{H}_2\text{O}_2$	6.20
$\text{OH} + \text{HO}_2 \rightarrow \text{H}_2\text{O} + \text{O}_2$	110
$\text{HO}_2 + \text{HO}_2 \rightarrow \text{H}_2\text{O}_2 + \text{O}_2$	1.60
isoprene + OH $\rightarrow$ isopreneA + H <sub>2</sub> O	100
<i>m</i> xylene + OH $\rightarrow$ <i>m</i> xyleneA + H <sub>2</sub> O	23
<i>o</i> xylene + OH $\rightarrow$ <i>o</i> xyleneA + H <sub>2</sub> O	13
$\alpha$ pinene + OH $\rightarrow$ $\alpha$ pineneA + H <sub>2</sub> O	53
myrcene + OH $\rightarrow$ myrceneA + H <sub>2</sub> O	209
$\beta$ pinene + OH $\rightarrow$ $\beta$ pineneA + H <sub>2</sub> O	79
carene + OH $\rightarrow$ careneA + H <sub>2</sub> O	85
ocimene + OH $\rightarrow$ ocimeneA + H <sub>2</sub> O	245
limonene + OH $\rightarrow$ limoneneA + H <sub>2</sub> O	170
$\gamma$ terpinene + OH $\rightarrow$ $\gamma$ terpineneA + H <sub>2</sub> O	170

**Table 3.10** List of reactions in kinetic simulations for modelling the OH concentration for the alkenes mixture.

Reaction	$k / 10^{-12} \text{ cm}^3 \text{ molecule}^{-1} \text{ s}^{-1}$
$\text{OH} + \text{OH} \rightarrow \text{H}_2\text{O} + \text{O}$	1.48
$\text{OH} + \text{OH} \rightarrow \text{H}_2\text{O}_2$	6.20
$\text{OH} + \text{HO}_2 \rightarrow \text{H}_2\text{O} + \text{O}_2$	110
$\text{HO}_2 + \text{HO}_2 \rightarrow \text{H}_2\text{O}_2 + \text{O}_2$	1.60
isoprene + OH $\rightarrow$ isopreneA + H <sub>2</sub> O	100
cyclopentene + OH $\rightarrow$ cyclopentaneA + H <sub>2</sub> O	67
hexene + OH $\rightarrow$ hexeneA + H <sub>2</sub> O	37
dimethylpentene + OH $\rightarrow$ dimethylpenteneA + H <sub>2</sub> O	56
cyclohexene + OH $\rightarrow$ cyclohexeneA + H <sub>2</sub> O	68
heptene + OH $\rightarrow$ hepteneA + H <sub>2</sub> O	39
octene + OH $\rightarrow$ octeneA + H <sub>2</sub> O	39
cycloheptene + OH $\rightarrow$ cyclohepteneA + H <sub>2</sub> O	74
nonene + OH $\rightarrow$ noneneA + H <sub>2</sub> O	43
$\alpha$ pinene + OH $\rightarrow$ $\alpha$ pineneA + H <sub>2</sub> O	53
$\beta$ pinene + OH $\rightarrow$ $\beta$ pineneA + H <sub>2</sub> O	74

### 3.2.1.2 Comparisons to similar systems

The values estimated in this work were of a similar order of magnitude to those measured for a similar system (Cryer, 2016). The reaction of OH with methanol and subsequent detection of formaldehyde was used to measure the [OH] produced in a reactor with similar properties to that described here. The [OH] was measured to be approximately  $2.6 (\pm 1.5) \times 10^{10} \text{ molecules cm}^{-3}$ , almost an order of magnitude lower than that estimated for the reactor system in this work.

### 3.2.2 Understanding the observed curved relationship

It was generally expected that the relationship between depletion factor and rate coefficient would be linear, as derived in Equations 3.3 through to 3.5. The  $OH_{exp}$  is given by the gradient of the slope when plotting depletion factor against literature  $k$  value, and is equivalent to the integral of the OH concentration over time.

$$\frac{d[\text{VOC}]}{dt} = -k[\text{VOC}][\text{OH}] \quad \text{Eq. 3.3}$$

$$\frac{d[\text{VOC}]}{[\text{VOC}]} = -k[\text{OH}]dt \quad \text{Eq. 3.4}$$

$$\ln\left(\frac{[\text{VOC}]_0}{[\text{VOC}]}\right) = k \int [\text{OH}]dt \quad \text{Eq. 3.5}$$

However, in some cases, a curved relationship between depletion factor and  $k$  value was observed. This deviation from linearity appeared to occur at low OH reactivity, as was the case for monoterpenes mixture 1 and 2, or when the VOC mixture contained compounds with very large rate coefficients for reaction with OH. For monoterpenes mixture 1,  $\beta$ -ocimene had the largest rate coefficient for reaction with OH ( $245 (\pm 49) \times 10^{-12} \text{ cm}^3 \text{ molecule}^{-1} \text{ s}^{-1}$ ) and curvature was only evident at OH reactivities smaller than  $110 \text{ s}^{-1}$ . The exact threshold at which significant curvature began for this mixture is unknown; curvature was observed at an OH reactivity of  $50 \text{ s}^{-1}$  but not above  $110 \text{ s}^{-1}$ . For monoterpenes mixture 2, the largest VOC + OH rate coefficient was for  $\alpha$ -terpinene + OH ( $350 (\pm \frac{71}{59}) \times 10^{-12} \text{ cm}^3 \text{ molecule}^{-1} \text{ s}^{-1}$ ). Curvature was potentially observed for this mixture at all OH reactivities (70 to  $400 \text{ s}^{-1}$ ) but was much more obvious at the lower OH reactivities than at OH reactivities greater than  $265 \text{ s}^{-1}$ . In contrast, no curvature was observed for the alkenes mixture with OH reactivities between 25 and  $150 \text{ s}^{-1}$ . This information is summarised in Table 3.11.

**Table 3.11** Summary of the conditions resulting in observed curvature in the depletion factor vs rate coefficient relationship during multivariate relative rate experiments.

Mixture	Range in OH reactivity / $\text{s}^{-1}$	Largest rate coefficient / $10^{-12} \text{ cm}^3 \text{ molecule}^{-1} \text{ s}^{-1}$	Curvature observed?
Monoterpenes mixture 1	50 - 300	245 ( $\pm 49$ ) ( $\beta$ -ocimene)	Only at $50 \text{ s}^{-1}$
Monoterpenes mixture 2	70 - 400	350 ( $\pm \frac{71}{59}$ ) ( $\alpha$ -terpinene)	Yes
Alkenes	25 - 150	100 ( $\pm \frac{15}{13}$ ) (isoprene)	No

Clearly, a number of factors affected whether the observed relationship between depletion factor and rate coefficient was linear or not. Numerical simulations were undertaken to try and gain a greater understanding of what these factors may have been, and why they resulted in a non-linear relationship.

A non-linear relationship between depletion factor and rate coefficient suggests that the  $OH_{exp}$  was not uniform for all the VOCs in the mixture. Rather, the observed curved relationships suggest that  $OH_{exp}$  was greater for VOCs with smaller values of  $k$  than for those VOCs with larger values of  $k$ . As  $OH_{exp}$  is equivalent to the integral of the OH concentration over time, this means that either:

- Different VOCs were exposed to different concentrations of OH. For this to be the case, it must be assumed that OH within the reactor was poorly mixed.
- Different VOCs are exposed to the same concentration of OH, but for different lengths of time. For this to be the case, it must be assumed that the VOCs within the reactor were poorly mixed.
- Some combination of the above two cases.

### 3.2.2.1 Mathematical proof

A simple mathematical model was used to prove that a curved relationship for the multivariate relative rate technique was possible. In this mathematical model, the results from a two-component mixture, VOC A and VOC B (R. 3.2 and R. 3.3) are used. VOC A had a rate coefficient for reaction with OH equal to  $k$  whilst VOC B had a rate coefficient for reaction with OH equal to  $2k$ .



In the normal scenario, assuming that both VOCs were exposed to an equivalent concentration of OH, the results of the experiment are given by Equations 3.6 and 3.7 for VOC A and B respectively.

$$\ln\left(\frac{[A]_0}{[A]}\right) = k \int_0^t [\text{OH}]_t dt \quad \text{Eq. 3.6}$$

$$\ln\left(\frac{[B]_0}{[B]}\right) = 2k \int_0^t [\text{OH}]_t dt \quad \text{Eq. 3.7}$$

As, in this case, the  $OH_{exp}$  term is equal, we can substitute Eq. 3.6 into 3.7, generating Eq. 3.8.

Hence, the depletion factor for VOC A, with rate coefficient equal to  $k$ , is equal to half the depletion factor of VOC B, which has a rate coefficient of  $2k$ . This shows that the relationship between depletion factor and  $k$  is linear, provided that the  $OH_{exp}$  term is the same for both VOCs.

$$\ln\left(\frac{[B]_0}{[B]}\right) = 2 \ln\left(\frac{[A]_0}{[A]}\right) \quad \text{Eq. 3.8}$$

However, if we assume that VOCs A and B were exposed to two different OH concentrations,  $z_1$  and  $z_2$ , the relationship changes. We can assume that  $z_2$  was twice as large as  $z_1$  (Eq. 3.9) and can also divide each VOC's initial concentration ( $[A]$  and  $[B]$ ) equally into two parts, using Eq. 3.10 as an example for VOC A.

$$z_2 = 2z_1 \quad \text{Eq. 3.9}$$

$$\frac{[A]_0}{2} = [A]_u \quad \text{Eq. 3.10}$$

Now, one half of VOC A ( $[A]_u$ ) was depleted to some amount of A, given by a constant ( $\alpha$ ) by  $z_1$  (Eq. 3.11). The other half of VOC A ( $[A]_u$ ) was depleted to some other amount of A, given by a different constant ( $\beta$ ) by  $z_2$  (Eq. 3.12).

$$\ln\left(\frac{[A]_u}{\alpha[A]}\right) = k \int z \, dt \quad \text{Eq. 3.11}$$

$$\ln\left(\frac{[A]_u}{\beta[A]}\right) = k \int 2z \, dt = 2k \int z \, dt \quad \text{Eq. 3.12}$$

Taking an exponent of both Eq. 3.11 and Eq. 3.12, and then summing them together, to simulate the mixing of the two halves of  $[A]$ , results in Eq. 3.13.

$$\frac{[A]_u}{\alpha[A]} + \frac{[A]_u}{\beta[A]} = \frac{[A]_0}{[A](\alpha+\beta)} = e^{kz} + e^{2kz} \quad \text{Eq. 3.13}$$

This can be simplified using Eq. 3.14 and Eq. 3.15, resulting in Eq. 3.16.

$$r = e^{kz} \quad \text{Eq. 3.14}$$

$$e^{kz} + e^{2kz} = r + r^2 \quad \text{Eq. 3.15}$$

$$\ln\left(\frac{[A]_0}{[A](\alpha+\beta)}\right) = \ln(r + r^2) \quad \text{Eq. 3.16}$$

The same method can be applied to VOC B, which reacts with OH with a rate coefficient of  $2k$ .

This yields the following set of equations:

$$\frac{[B]_u}{\delta[B]} = e^{2kz} \quad \text{Eq. 3.17}$$

$$\frac{[B]_u}{\varepsilon[B]} = e^{4kz} \quad \text{Eq. 3.18}$$

$$\ln\left(\frac{[B]_0}{[B](\delta+\varepsilon)}\right) = \ln(r^2 + r^4) \quad \text{Eq. 3.19}$$

It is clear from Eq. 3.16 and Eq. 3.19 that the depletion factors for VOCs A and B are no longer related by a factor of 2, despite that being the relationship between their rate coefficients and the relationship that is observed when the  $OH_{exp}$  for the two VOCs is equivalent (as in Eq. 3.8). Instead the relationship between the depletion factors for VOCs A and B is rather more complicated, as demonstrated by the following set of equations.

$$\frac{[A]_0}{[A](\alpha+\beta)} = r + r^2 \quad \text{Eq. 3.20}$$

$$\frac{[B]_0}{[B](\delta+\varepsilon)} = r^2 + r^4 \quad \text{Eq. 3.21}$$

$$r + r^2 = p \quad \text{Eq. 3.22}$$

$$\frac{[A]_0}{[A](\alpha+\beta)} = p \quad \text{Eq. 3.23}$$

$$\frac{[B]_0}{[B](\delta+\varepsilon)} = p^2 - 2r^3 \quad \text{Eq. 3.24}$$

$$\frac{[B]_0}{[B](\delta+\varepsilon)} = \left(\frac{[A]_0}{[A](\alpha+\beta)}\right)^2 - 2r^3 \quad \text{Eq. 3.25}$$

$$\ln\left(\frac{[B]_0}{[B](\delta+\varepsilon)}\right) = \ln\left(\frac{\left(\frac{[A]_0}{[A](\alpha+\beta)}\right)^2}{2r^3}\right) = \ln\left(\frac{\left(\frac{[A]_0}{[A](\alpha+\beta)}\right)^2}{2e^{3kz}}\right) \quad \text{Eq. 3.26}$$

In conclusion, it was demonstrated mathematically that both linear and curved relationships between depletion factor and rate coefficient were possible. For a linear relationship to occur, VOCs must experience equivalent  $OH_{exp}$ , as would be the case if OH were well mixed. For a curved relationship to occur, VOCs must experience exposures to differing OH concentrations, as would be the case if OH were poorly mixed in the reactor. These mathematical equations also likely only apply for idealised scenarios where the initial VOC concentrations are similar.

### 3.2.2.2 Kinetic modelling

Simple kinetic simulations were conducted using Kintecus. The model incorporated the VOC + OH reaction for each VOC in monoterpenes mixture 1 and simple HO<sub>x</sub> chemistry (Table 3.9). The OH + VOC reactions produced non-reactive products, termed VOC-A, and H<sub>2</sub>O, which was also assumed to be non-reactive towards OH.

In order to simulate different mixing conditions, the reactor was split into three different theoretical sections in which:

1. One third of the [VOC] was exposed to a “low” [OH], of  $1.0 \times 10^9$  molecules cm<sup>-3</sup>.
2. One third of the [VOC] was exposed to a “high” [OH], of  $2.5 \times 10^{11}$  molecules cm<sup>-3</sup>.
3. One third of the [VOC] was exposed to an [OH] somewhere between the above two values, of  $5.0 \times 10^{10}$  molecules cm<sup>-3</sup>.

The average of these three values of [OH] was roughly  $1 \times 10^{11}$  molecules cm<sup>-3</sup>, similar to the best estimate of [OH] within the reactor (see Chapter 2 Section 2.3.1).

The depletion factors for each of these simulated sections were plotted separately, as in Figure 3.17. In each, case the relationship between depletion factor and rate coefficient was linear ( $R^2 = 1.0$ ), albeit with different values of  $OH_{exp}$  (slope). This was expected, as the model could not simulate deviations from the line and all VOCs were depleted exactly in proportion to their rate coefficients.

However, if the concentration of each VOC in each section was totalled before the depletion factor was calculated, the resulting plot against rate coefficient was curved, as shown in Figure 3.18. This plot is more representative of what would happen during the experiment; the three theoretical reactor sections would likely mix prior to sampling into the GC-MS, resulting in an observed depletion factor that was a result of the different depletions from each section. The modelled relationship in Figure 3.18 was roughly similar to the experimentally observed relationship shown in Figure 3.5. The slope in Figure 3.18 was plotted up to a depletion factor value of 0.4, to highlight that a linear relationship could be used with a good deal of agreement up to that point.

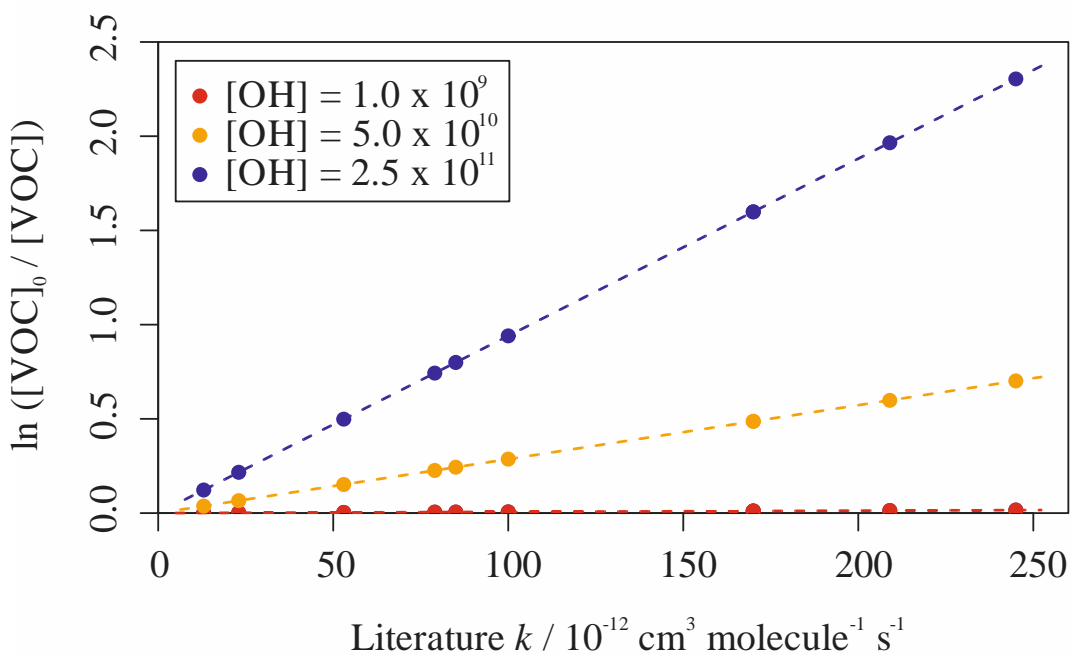


**Figure 3.17** Simulated relative rate plot for monoterpenes mixture 1 with an OH reactivity of  $50 \text{ s}^{-1}$ . Three different theoretical sections of the reactor were simulated separately, with each section containing 1/3 [VOC] and exposed to different [OH] of  $1.0 \times 10^9$ ,  $5.0 \times 10^9$  and  $2.5 \times 10^{11}$  molecules  $\text{cm}^{-3}$ .

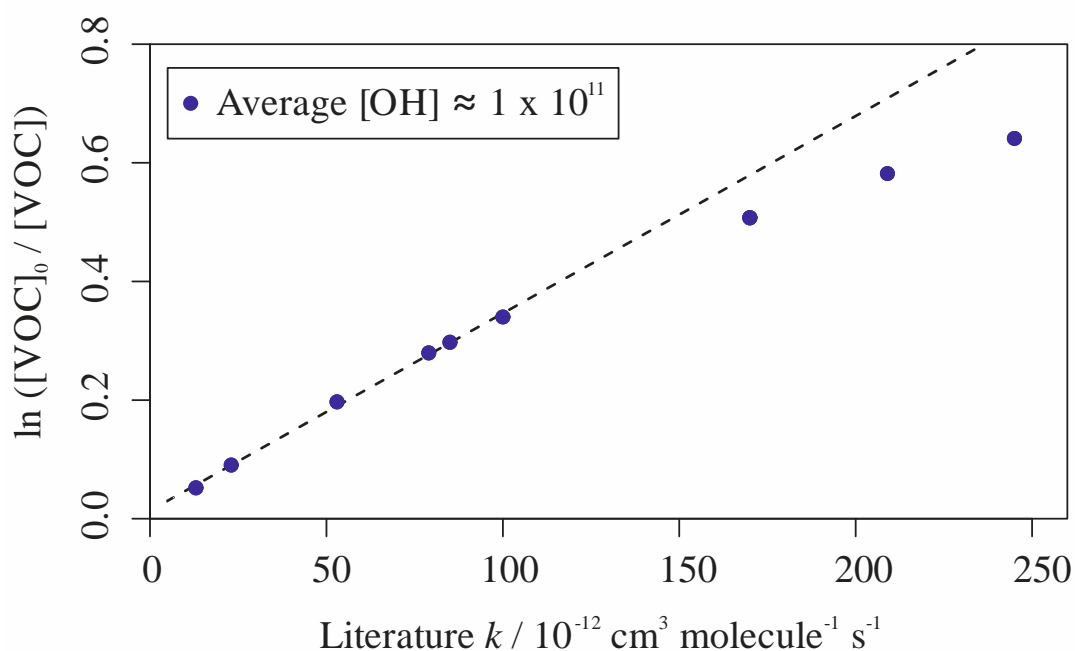


**Figure 3.18** Simulated relative rate plot for monoterpenes mixture 1 with an OH reactivity of  $50 \text{ s}^{-1}$ . The final concentrations of the VOCs in each of the simulated sections (Figure 3.17) were summed prior to the calculation of the depletion factor. The resulting relationship was clearly curved in a similar manner to that observed during experiment (Figure 3.5). The slope was plotted up to a depletion factor value of 0.4, to demonstrate that a linear relationship could be assumed up to that value for simplification.

Whilst curvature was observed experimentally at lower [VOC] (lower OH reactivity), it was less evident at higher [VOC] (greater OH reactivity). The same was also true in the simulations; Figure 3.19 shows the same simulation as that for above but for a mixture with an OH reactivity of  $290 \text{ s}^{-1}$ . As in Figure 3.18, the final concentrations of the VOCs from each section were totalled before calculation of the depletion factor. The resulting relationship was not exactly linear and would certainly not be noticeably curved within the experimental noise. It is worth noting that the depletion factor did not extend above 0.4, as was the case for OH reactivity =  $50 \text{ s}^{-1}$  for both experiment and for simulation.

Presumably, there is a continuum between a highly curved relationship at low OH reactivity, and a less highly curved relationship at higher OH reactivity. It therefore becomes increasingly more appropriate to model the relationship between depletion factor and  $k$  value with a linear weighted regression analysis with increasing OH reactivity. However, this does not apply to all the mixtures; the alkenes mixture was measured at lower OH reactivity than the monoterpenes mixtures but still had a linear relationship. The second monoterpenes mixture was also analysed at a higher OH reactivity than the first monoterpenes mixture and still had a curved relationship.

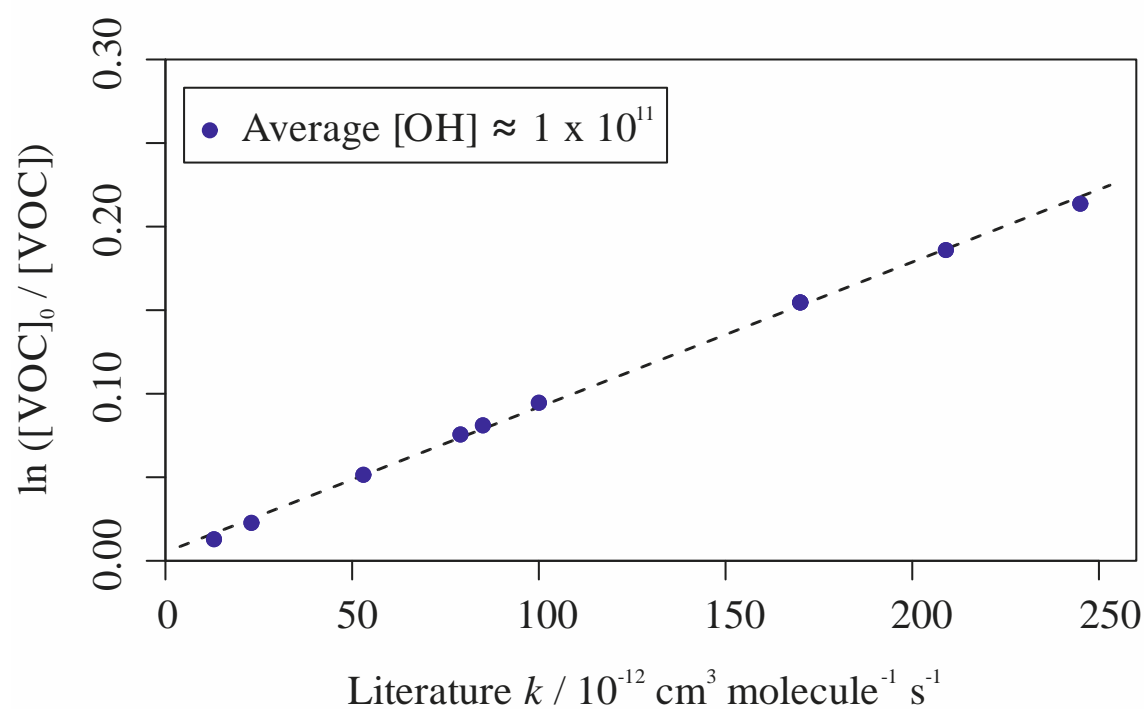


**Figure 3.19** Simulated relative rate plot for monoterpenes mixture 1 with an OH reactivity of  $290 \text{ s}^{-1}$ . The final concentrations of the VOCs in each of the simulated sections were summed prior to the calculation of the depletion factor. The resulting relationship wasn't strictly linear but can be assumed to be.

### 3.2.3 Simulating product formation

Despite large observed depletions in many of the VOC reactants, complementary increases in oxidation products were not observed experimentally. Sections 3.1.1.8 and 3.1.3.5 described the few species that were potentially observed as products of the VOC + OH reactions due to their detection during 'lamp-on' samples. These compounds included methyl vinyl ketone and methacrolein for monoterpenes mixture 1 and 2-methylfuran and 3-methylpentan-2-one for the alkenes mixture. The peak areas for those compounds were typically orders of magnitudes smaller than the measured peak areas for the reactant peaks, suggesting that a large amount of product formation was not accounted for by these observations.

Kinetic simulations, which included the reactions in Table 3.9 but with more comprehensive chemical oxidation schemes for the VOCs, were performed to predict the types of products that may be observed during experiments. The MCM (<http://mcm.leeds.ac.uk/MCM>) was used as a basis for these simulations, providing both the chemical schemes and the rate coefficients and branching ratios for the relevant reactions. Due to the size of the MCM and difficulties in extracting and importing the chemical schemes directly into Kintecus, the oxidation reactions added to the simulations for each VOC were limited. Reactions involving O<sub>3</sub> or NO<sub>3</sub> were not included and reactions involving OH or HO<sub>2</sub> with a branching ratio of less than 0.1 were ignored for brevity. Despite limiting the number of reactions added to the simulation, the monoterpenes mixture 1 model still numbered approximately 100 different reactions for the oxidation of *m*-xylene, *o*-xylene, isoprene, limonene and  $\alpha$ - and  $\beta$ -pinene. The other VOCs that made up the first monoterpenes mixture are not listed in the MCM and hence their oxidation schemes were not included.

The simulations were conducted with initial OH and HO<sub>2</sub> concentrations equal to  $3.1 \times 10^{11}$  molecules cm<sup>-3</sup>. O<sub>3</sub> and NO<sub>x</sub> concentrations were assumed to be zero and the impact of photolysis on the VOC oxidation was also assumed to be irrelevant. Simulations were performed at 298 K for 3 s, at which point the OH concentration was simulated to be negligible.

The following sections discuss the results of these simulations for the oxidation of each of the VOCs. Only products with a yield greater than 0.5% are included in the following discussion.

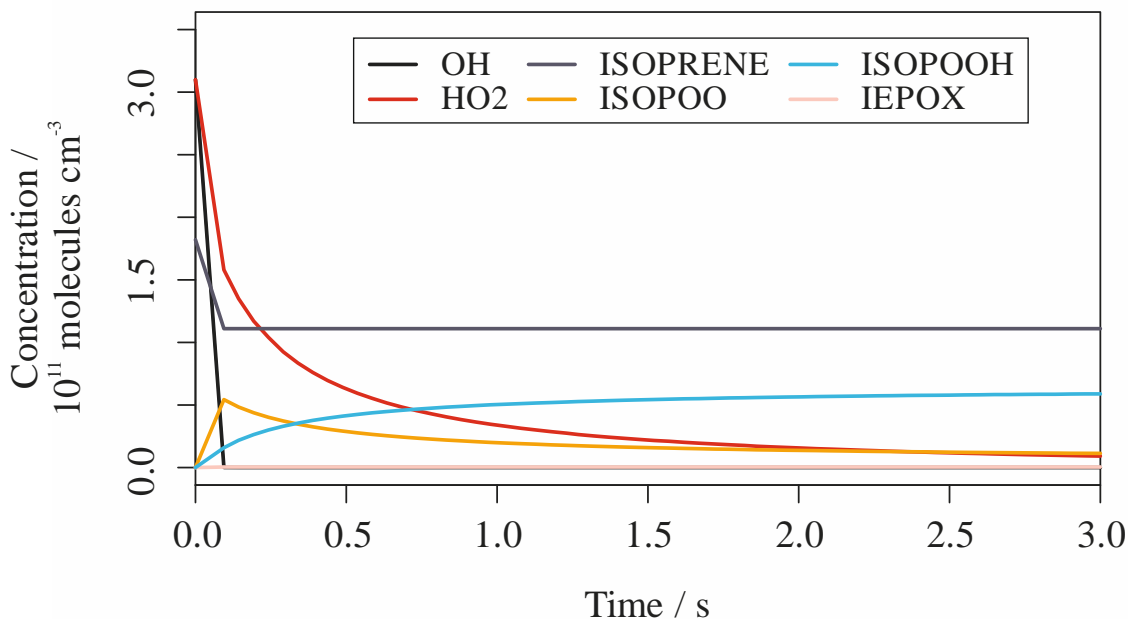
### 3.3.3.2 Isoprene

Figure 3.20 provides a time series for the simulated changes in the concentrations of OH, HO<sub>2</sub> and isoprene. The OH concentration decreased rapidly, falling from the initial concentration of  $3.1 \times 10^{11}$  molecules cm<sup>-3</sup> to zero in approximately 0.3 s. The complementary depletion in isoprene was also rapid but finished once the OH concentration was too low. The initial decrease in the HO<sub>2</sub> concentration was also fast, due presumably to the radical-radical reaction with OH. However, once the OH was depleted, the decrease in the HO<sub>2</sub> concentration slowed.

The simulation contained oxidation schemes for OH reaction at different carbon sites within the isoprene structure. The reactions therefore generated different isomers of ISOPOO in different proportions based on the branching ratios extracted from the MCM. However, for clarity, the total of the different ISOPOO concentrations are shown in Figure 3.20, alongside the sum of the different ISOPOOH and IEPOX concentrations.

The ISOPOO concentration initially increased rapidly, due to the reaction between OH and isoprene. The ISOPOOH concentration was also simulated to increase once oxidation began, but at a much slower rate. Once OH was consumed, the production of ISOPOO stopped and its concentration began to decrease as it reacted with HO<sub>2</sub>. This reaction continued, until ISOPOOH was the dominant reaction product at approximately 0.3 s. Whilst IEPOX was also produced in the reactor, its concentration was simulated to be several orders of magnitude lower than those for ISOPOO and ISOPOOH.

The simulated distribution of all the products from the OH initiated oxidation of isoprene is illustrated by Figure 3.21. The major products, in terms of percentage yield, were ISOPBOOH and ISOPA00H with yields of 29.6% and 29.4% respectively. These products, along with both ISOPCOOH and ISOPDOOH, resulted from OH addition to a double bond, followed by reaction with O<sub>2</sub> and then HO<sub>2</sub> to form C<sub>5</sub>O<sub>3</sub>H<sub>10</sub>.



**Figure 3.20** Time series showing the simulated changes in concentrations of OH, HO<sub>2</sub>, isoprene and the isoprene oxidation products, total ISOPOO, total ISOPOOH and total IEPOX.

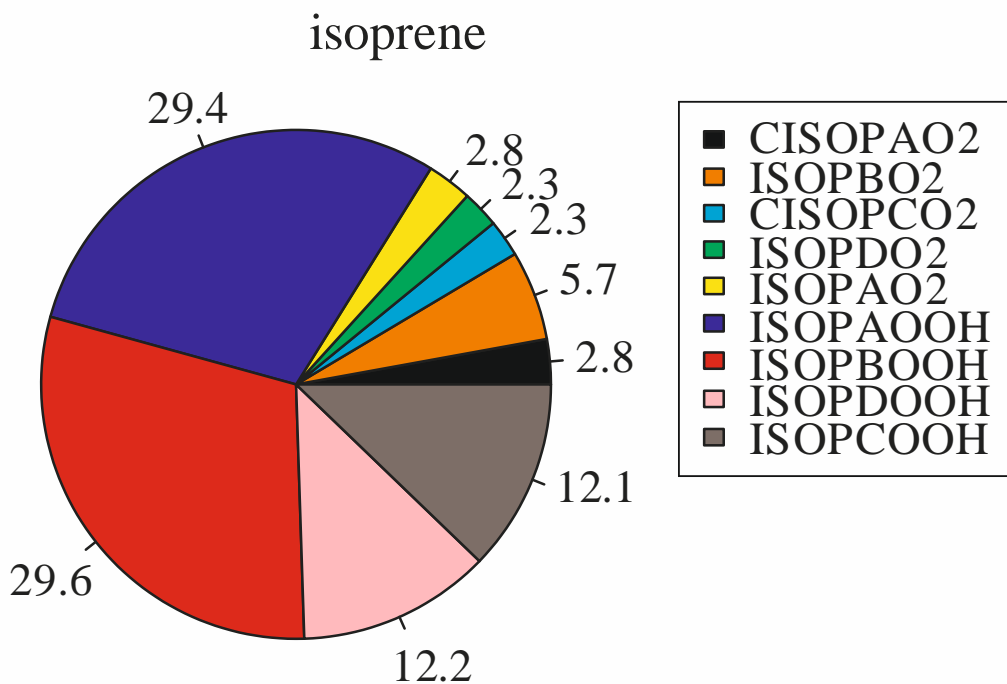


**Figure 3.21** Simulated distribution of products resulting from the OH-initiated oxidation of isoprene. Please refer to the MCM (Jenkin et al., 1997; Saunders et al., 2003; <http://mcm.leeds.ac.uk/MCM>; accessed 14/02/2018) for product structures.

### 3.2.3.1 Xylenes

The simulated distributions of products from the oxidation of *m*-xylene is shown in Figure 3.22.

The major product was predicted to be MXYBPEROOH, with a yield of 55.9%. This product resulted from OH addition to the carbon atom in the aromatic ring between the two methyl substituents, followed by reaction with O<sub>2</sub> and HO<sub>2</sub> to form C<sub>8</sub>O<sub>5</sub>H<sub>12</sub>. The next major product was MXYEPOXMUC, with a yield of 33.6%. This product does not retain the aromatic ring structure, with ring cleavage occurring to form C<sub>8</sub>O<sub>3</sub>H<sub>10</sub>. Six other minor products were also simulated, four of which are shown in Figure 3.22, with two excluded as they were produced with yields of less than 0.02%.

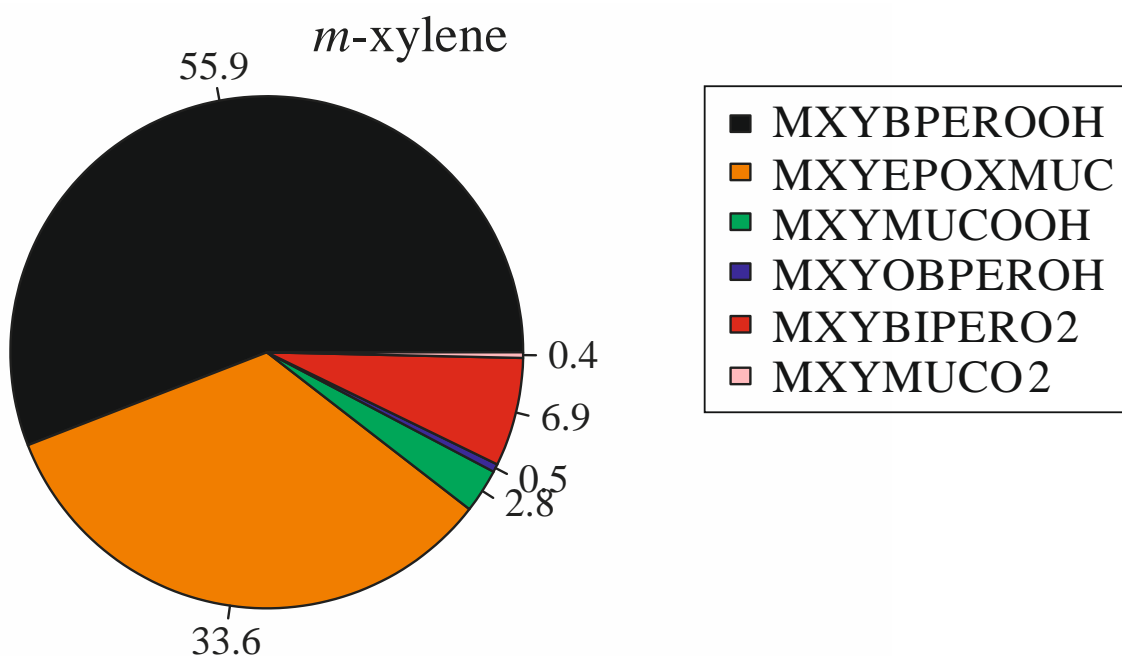


**Figure 3.22** Simulated distribution of products resulting from the OH-initiated oxidation of *m*-xylene. Please refer to the MCM (Jenkin et al., 1997; Saunders et al., 2003; <http://mcm.leeds.ac.uk/MCM>; accessed 14/02/2018) for product structures.

Figure 3.23 shows that the reaction between *o*-xylene and OH was simulated to have a very similar distribution of products to the oxidation of *m*-xylene, with the major products OXYBPEROOH (yield = 62.0%) and OXYEPOXMUC (yield = 27.8%). Seven minor products were produced, with the three not shown in Figure 3.23 possessing yields of 0.4%, 0.2% and 0.1%.

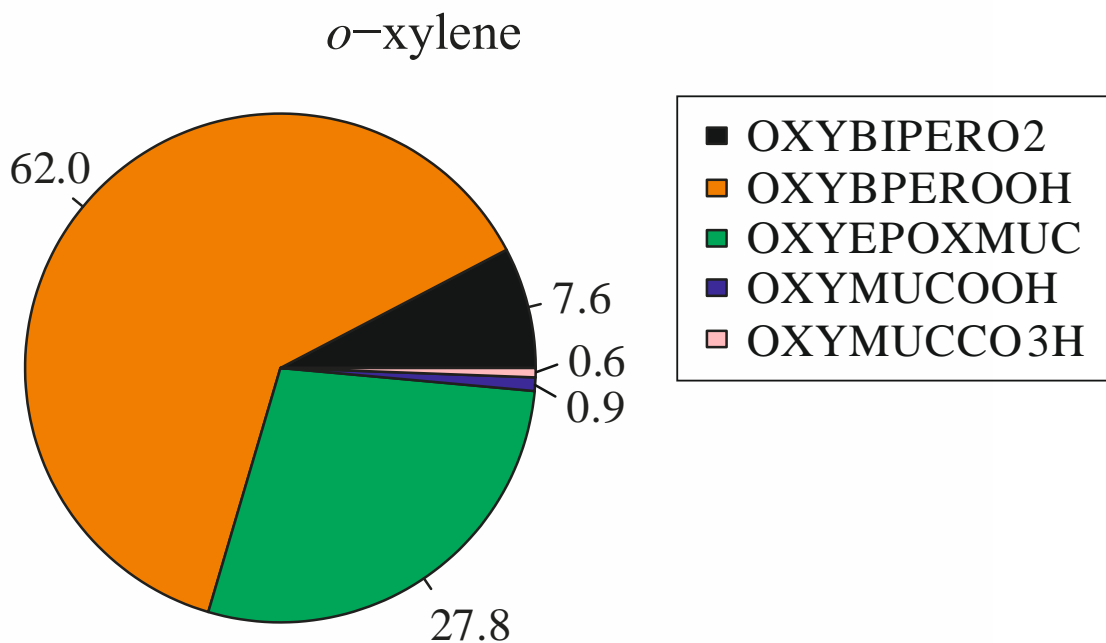


**Figure 3.23** Simulated distribution of products resulting from the OH-initiated oxidation of *o*-xylene. Please refer to the MCM (Jenkin et al., 1997; Saunders et al., 2003; <http://mcm.leeds.ac.uk/MCM>; accessed 14/02/2018) for product structures.

### 3.3.3.3 Monoterpenes

The simulated distributions of products from the oxidation of the three monoterpenes,  $\alpha$ - and  $\beta$ -pinene and limonene, are illustrated by Figure 3.24, Figure 3.25 and Figure 3.26 respectively. The oxidation of  $\alpha$ -pinene was simulated to result in four products, two of which accounted for over 90% of the product concentrations. These two products, APINAOOH and APINBOOH, resulted from OH addition to the double bond, followed by reaction with  $O_2$  and  $HO_2$  to form  $C_{10}O_3H_{18}$ . The two minor products, APINAO2 and APINBO2, resulted from the lack of availability of  $HO_2$ . The reaction scheme for  $\beta$ -pinene had only two simulated products due to a much larger branching ratio forming predominantly BPINAO2 and BPINAOOH. Again, the major product was formed by OH addition to the double bond followed by reaction with  $O_2$  and  $HO_2$  whilst the minor product was simulated to exist due to the lack of availability of  $HO_2$ .

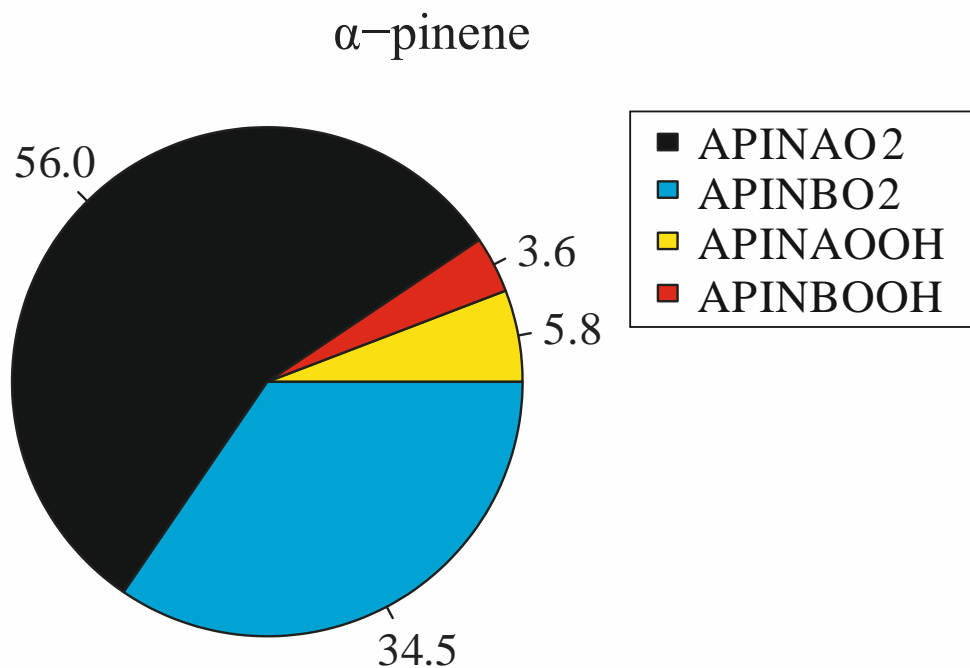


**Figure 3.24** Simulated distribution of products resulting from the OH-initiated oxidation of  $\alpha$ -pinene. Please refer to the MCM (Jenkin et al., 1997; Saunders et al., 2003; <http://mcm.leeds.ac.uk/MCM>; accessed 14/02/2018) for product structures.

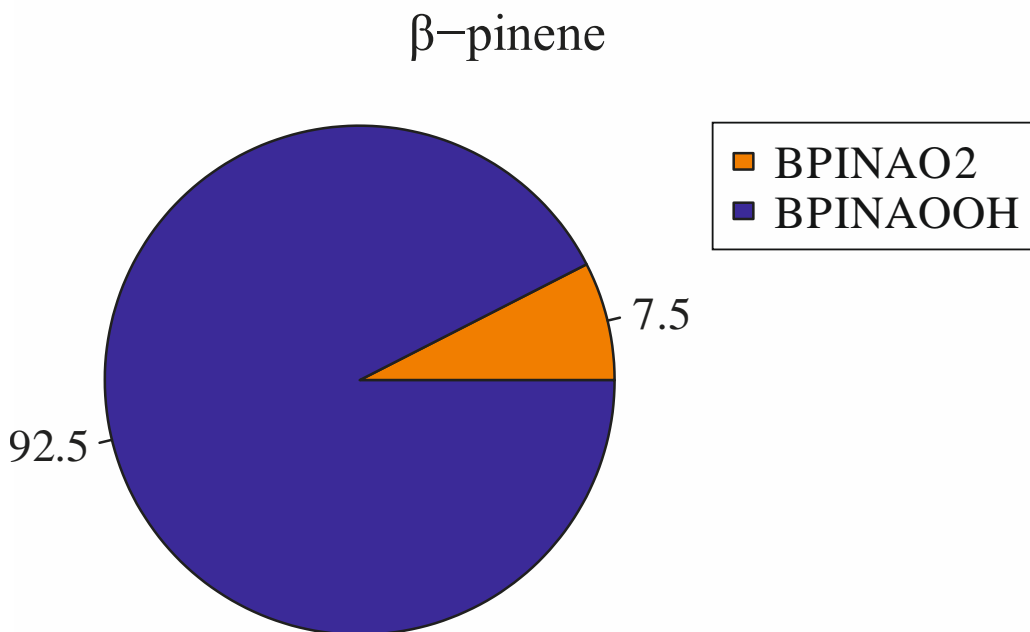


**Figure 3.25** Simulated distribution of products resulting from the OH-initiated oxidation of  $\beta$ -pinene. Please refer to the MCM (Jenkin et al., 1997; Saunders et al., 2003; <http://mcm.leeds.ac.uk/MCM>; accessed 14/02/2018) for product structures.

The oxidation of limonene resulted in six simulated products, as shown in Figure 3.26. Much like for the other monoterpenes, the products were separated into two categories; those that underwent extra oxidation via reaction with  $O_2$  and  $HO_2$ , and those that didn't. The products that underwent reaction with  $O_2$  and  $HO_2$  were the major products, as for the oxidation of  $\alpha$ - and  $\beta$ -pinene.

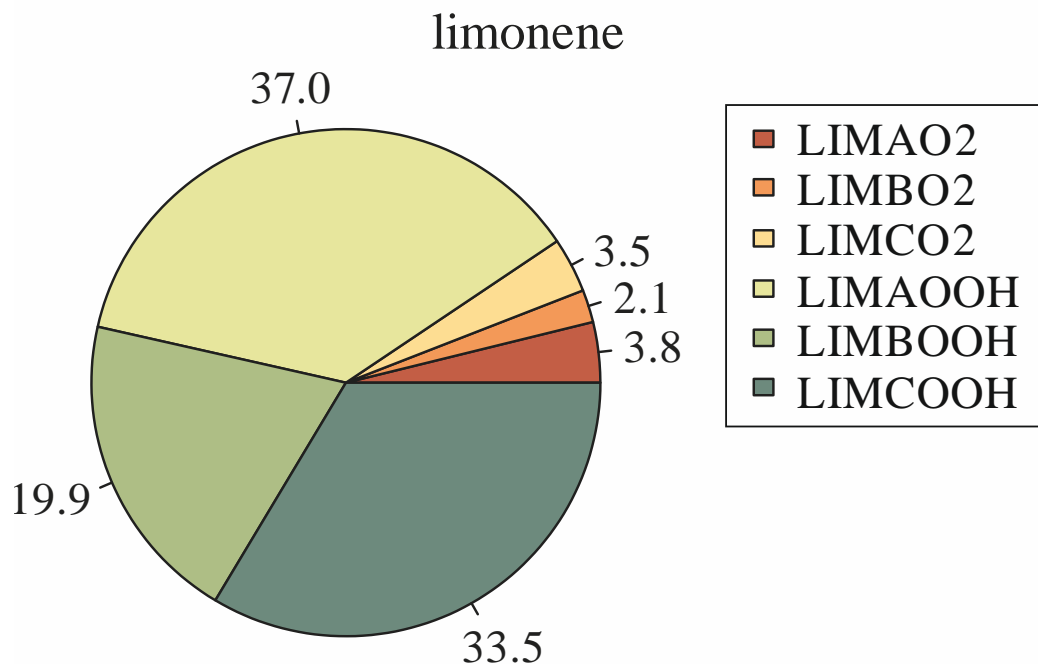


**Figure 3.26** Simulated distribution of products resulting from the OH-initiated oxidation of limonene. Please refer to the MCM (Jenkin et al., 1997; Saunders et al., 2003; <http://mcm.leeds.ac.uk/MCM>; accessed 14/02/2018) for product structures.

### 3.3.3.4 Summary

The major products simulated to result from the OH-initiated oxidation of the VOCs were generally highly oxidised species containing multiple oxygen atoms, of the form ROOH. These species were not detected via GC-MS. The only identified potential products all contained a single oxygen atom; methyl vinyl ketone and methacrolein ( $C_4H_6O$ ), 2-methylfuran ( $C_5H_6O$ ) and 3-methylpentan-2-one ( $C_6H_{12}O$ ; see Sections 3.1.1.8 and 3.1.3.5).

The simulations indicated that some  $RO_2$  species were still present within the reactor after 3 s. This was presumably due to a lack of time to react with the remaining  $HO_2$ . It may also be due to a lack of  $NO_x$  within the simulation, with which  $RO_2$  would be expected to react under normal atmospheric conditions.  $RO_2 + RO_2$  reactions were also not included within the simulation. These reactions therefore represent other possible routes for product formation which were not assessed.

## Conclusions

In conclusion, the multivariate relative rate technique was successfully applied to measure the rate coefficients for the reactions between 24 VOCs and OH in three different synthetic gas mixtures. Many of the results represent only the second or third measurements of their kind. The rate coefficient for the reaction between 2,3-dimethylpent-1-ene and OH, of  $57 (\pm 3) \times 10^{-12} \text{ cm}^3 \text{ molecule}^{-1} \text{ s}^{-1}$ , was measured for the first time. The correlation between depletion factor due to reaction with OH and rate coefficient was shown to be linear in most cases, although significant deviation from linearity did occur in some situations. A curved relationship was shown to be more prominent for mixtures exhibiting low OH reactivity resulting from low concentrations of VOCs. Kinetic simulations assisted in assessing the reliability of the curved data, and, whilst the observed curvature made the calculation of rate coefficients more difficult, it was shown to only limit the conditions in which ideal experimental results could be obtained. Kinetic simulations also aided in understanding the product distribution of the VOC + OH reactions, with the major products expected to be highly oxidised ROOH, containing multiple oxygen atoms, which were unlikely to be observed considering the chromatographic mode of separation used. The few products observed experimentally were only accounted for by assuming that  $\text{NO}_x$ , and possibly  $\text{O}_3$ , were present in the reactor.

## References

- Aschmann, S. M. and Atkinson, R.: Rate constants for the gas-phase reactions of OH radicals with *E*-7-tetradecene, 2-methyl-1-tridecene and C<sub>7</sub>-C<sub>14</sub> 1-alkenes at 295 ± 1 K, *Phys. Chem. Chem. Phys.*, 10, 4159-4164, <https://doi.org/10.1039/B803527J>, 2008.
- Aschmann, S. M., Arey, J. and Atkinson, R.: Kinetics and products of the reactions of OH radicals with cyclohexene, 1-methyl-1-cyclohexene, *cis*-cyclooctene, and *cis*-cyclodecene, *J. Phys. Chem. A*, 116, 9507-9515, <https://doi.org/10.1021/jp307217m>, 2012.
- Atkinson, R., Aschmann, S. M. and Carter, W. P.: Effects of ring strain on gas-phase rate constants 2. OH radical reactions with cycloalkenes, *Int. J. Chem. Kinet.*, 15, 1161-1177, <https://doi.org/10.1002/kin.550151105>, 1983.
- Atkinson, R. and Aschmann, S. M.: Rate constants for the reaction of OH radicals with a series of alkanes and dialkenes at 295 ± 1 K, *Int. J. Chem. Kinet.*, 16, 10, 1175-1186, <https://doi.org/10.1002/kin.550161002>, 1984.
- Atkinson, R. and Aschmann, S. M.: Rate constants for the gas-phase reactions of the OH radical with a series of aromatic hydrocarbons at 296 ± 2 K, *Int. J. Chem. Kinet.*, 21, 355-365, <https://doi.org/10.1002/kin.550210506>, 1989.
- Atkinson, R. and Arey, J.: Atmospheric degradation of volatile organic compounds, *Chem. Rev.*, 103, 4605-4638, <https://doi.org/10.1021/cr0206420>, 2003.
- Atkinson, R., Baulch, D. L., Cox, R. A., Crowley, J. N., Hampson, R. F., Hynes, R. G., Jenkin, M. E., Rossi, M. J. and Troe, J.: Evaluated kinetic and photochemical data for atmospheric chemistry: Volume II – gas phase reactions of organic species, *Atmos. Chem. Phys.*, 6, 3265-4055, 2006. Also at <http://iupac.pole-ether.fr/index.html>.
- Barnes, I., Bastian, V., Becker, K. H., Fink, E. H. and Zabel, F.: Reactivity studies of organic substances towards hydroxyl radicals under atmospheric conditions, *Atmos. Environ.*, 16, 545-550, [https://doi.org/10.1016/0004-6981\(82\)90163-9](https://doi.org/10.1016/0004-6981(82)90163-9), 1982.
- Burke, S.: Missing values, outliers, robust statistics & non-parametric methods. LC.GC Europe Online Supplement, statistics and data analysis, 19-24, 1998.

- Braure, T., Bedjanian, Y., Romanias, M. N., Morin, J., Riffault, V., Tomas, A. and Coddeville, P.: Experimental study of the reactions of limonene with OH and OD radicals: kinetics and products, *J. Phys. Chem. A*, **118**, 9482-9490, <https://doi.org/10.1021/jp507180g>, 2014.
- Calvert, J. G., Atkinson, R., Kerr, J. A., Madronich, S., Moortgat, G. K., Wallington, T. J. and Yarwood, G.: *The mechanisms of atmospheric oxidation of the alkenes*, Oxford University Press, New York, 2000.
- Calvert, J. G., Atkinson, R., Becker, K. H., Kamens, R. M., Seinfeld, J. H., Wallington, T. J. and Yarwood, G.: *The mechanisms of atmospheric oxidation of aromatic hydrocarbons*, Oxford University Press, New York, 2002.
- Ciccioli, P., Brancaleoni, E., Frattoni, M., Cecinato, A. and Pinciarelli, L.: Determination of volatile organic compounds (VOCs) emitted from biomass burning of Mediterranean vegetation species by GC-MS, *Anal. Lett.*, **34**, 6, 937-955, <https://doi.org/10.1018/AL-100103604>, 2001.
- Chuong, B. Davis, M., Edwards, M. and Stevens, P. S.: Measurements of the kinetics of the OH +  $\alpha$ -pinene and OH +  $\beta$ -pinene reactions at low pressure, *Int. J. Chem. Kinet.*, **34**, 5, 300-308, <https://doi.org/10.1002/kin.10058>, 2002.
- Cox, R. A., Derwent, R. G. and Williams, M. R.: Atmospheric photooxidation reactions. Rates, reactivity, and mechanism for reaction of organic compounds with hydroxyl radicals, *Environ. Sci. Technol.*, **14**, 57-61, <https://doi.org/10.1021/es60161a007>, 1980.
- Cryer, D. R.: Measurements of hydroxyl radical reactivity and formaldehyde in the atmosphere, PhD thesis, University of Leeds, 2016.
- Darnall, K. R., Winer, A. M., Lloyd, A. C. and Pitts Jr., J. N.: Relative rate constants for the reaction of OH radicals with selected C<sub>6</sub> and C<sub>7</sub> alkanes and alkenes at 305 ± 2 K, *Chem. Phys. Lett.*, **44**, 415-418, [https://doi.org/10.1016/0009-2614\(76\)80695-1](https://doi.org/10.1016/0009-2614(76)80695-1), 1976.
- Dash, M. R. and Rajakumar, B.: Experimental and theoretical rate coefficients for the gas phase reaction of  $\beta$ -pinene with OH radical, *Atmos. Environ.*, **79**, 161-171, <https://doi.org/10.1016/j.atmosenv.2013.05.039>, 2013.

- Dash, M. R., Balaganesh, M. and Rajakumar, B.: Rate coefficients for the gas-phase reaction of OH radical with  $\alpha$ -pinene: an experimental and computational study, *Mol. Phys.*, 112, 11, 1495-1511, <https://doi.org/10.1080/00268976.2013.840395>, 2014.
- Davis, M. E. and Stevens, P. S.: Measurements of the kinetics of the OH-initiated oxidation of  $\alpha$ -pinene: radical propagation in the OH +  $\alpha$ -pinene + O<sub>2</sub> + NO reaction system, *Atmos. Environ.*, 39, 1765-1774, <https://doi.org/10.1016/j.atmosenv.2004.09.068>, 2005.
- Dillon, T. J., Dulitz, K., Groß, C. B. M. and Crowley, J. N.: Temperature-dependent rate coefficients for the reactions of the hydroxyl radical with the atmospheric biogenics isoprene, alpha-pinene and delta-3-carene, *Atmos. Chem. Phys.*, 17, 15137-15150, <https://doi.org/10.5194/acp-17-15137-2017>, 2017.
- Doyle, G. J., Lloyd, A. C., Darnall, K. R., Winer, A. M., Pitts Jr., J. N.: Gas phase kinetic study of relative rates of reaction of selected aromatic compounds with hydroxyl radicals in an environmental chamber, *Environ. Sci. Technol.*, 9, 3, 237-241, <https://doi.org/10.1021/es60101a002>, 1975.
- Figueira, J., Câmara, H., Pereira, J. and Câmara, J. S.: Evaluation of volatile metabolites as markers in *Lycopersicon esculentum* L. cultivars discrimination by multivariate analysis of headspace solid phase microextraction and mass spectrometry data, *Food Chem.*, 145, 653-663, <https://doi.org/10.1016/j.foodchem.2013.08.061>, 2014.
- Gaona-Colmán, E., Blanco, M. B., Barnes, I. and Teruel, M. A.: Effect of NO<sub>x</sub> on product yields and Arrhenius parameters of gas-phase oxidation of  $\beta$ -ocimene initiated by OH radicals, *RSC Adv.*, 6, 92795-92803, <https://doi.org/10.1039/C6RA20321C>, 2016.
- Hites, R. A. and Turner, A. M.: Rate constants for the gas-phase  $\beta$ -myrcene + OH and isoprene + OH reactions as a function of temperature, *Int. J. Chem. Kinet.*, 41, 6, 407-413, <https://doi.org/10.1002/kin.20413>, 2009.
- Ianni, J. C.: Kintecus, Windows Version 5.20, 2017, [www.kintecus.com](http://www.kintecus.com)
- Jenkin, M. E., Saunders, S. M. and Pilling, M. J.: The tropospheric degradation of volatile organic compounds: a protocol for mechanism development, *Atmos. Environ.*, 31, 1, 81-104, [https://doi.org/10.1016/S1352-2310\(96\)00105-7](https://doi.org/10.1016/S1352-2310(96)00105-7), 1997.

- Jenkin, M. E., Valorso, R., Aumont, B., Rickard, A. R. and Wallington, T. J. Estimation of rate coefficients and branching ratios for gas-phase reactions of OH with aliphatic organic compounds for use in automated mechanism construction, *Atmos. Chem. Phys. Discuss.*, <https://doi.org/10.5194/acp-2018-145>, in review. 2018.
- Kim, D., Stevens, P. S. and Hites, R. A.: Rate constants for the gas-phase reactions of OH and O<sub>3</sub> with  $\beta$ -ocimene,  $\beta$ -myrcene, and  $\alpha$ - and  $\beta$ -farnesene as a function of temperature, *J. Phys. Chem. A*, 115, 500-506, <https://doi.org/10.1021/jp111173s>, 2011.
- Kleindienst, T. E., Harris, G. W. and Pitts Jr., J. N.: Rates and temperature dependences of the reaction of OH with isoprene, its oxidation products, and selected terpenes, *Environ. Sci. Technol.*, 16, 844-846, <https://doi.org/10.1021/es00106a004>, 1982.
- Kwok, E. S. C. and Atkinson, R.: Estimation of hydroxyl radical reaction rate constants for gas-phase organic compounds using a structure-reactivity relationship: an update, *Atmos. Environ.*, 29, 1685-1695, [https://doi.org/10.1016/1352-2310\(95\)00069-B](https://doi.org/10.1016/1352-2310(95)00069-B), 1995.
- Kramp, F. and Paulson, S. E.: On the uncertainties in the rate coefficients for OH reactions with hydrocarbons, and the rate coefficients of the 1,3,5-trimethylbenzene and *m*-xylene reactions with OH radicals in the gas phase, *J. Phys. Chem. A*, 102, 2685-2690, <https://doi.org/10.1021/jp973289o>, 1998.
- Li, R., Palm, B. B., Ortega, A. M., Hlywiak, J., Hu, W., Peng, Z., Day, D. A., Knote, C., Brune, W. H., de Gouw, J. A. and Jimenez, J. L.: Modelling the radical chemistry in an oxidation flow reactor: radical formation and recycling, sensitivities, and the OH exposure estimation equation, *J. Chem. Phys. A*, 199, 4419-4432, <https://doi.org/10.1021/jp509534k>, 2015.
- McGillen, M. R., Percival, C. J., Shallcross, D. E. and Harvey, J. N.: Is hydrogen abstraction an important pathway in the reaction of alkenes with the OH radical?, *Phys. Chem. Chem. Phys.*, 9, 4349-4356, <https://doi.org/10.1039/B703035E>, 2008.
- Montenegro, A., Ishibashi, J. S. A., Lam, P. and Li, Z.: Kinetics study of reactions of  $\alpha$ -pinene and  $\beta$ -pinene with hydroxyl radical at 1-8 Torr and 230-340 K using the relative rate/discharge flow/mass spectrometry method, *J. Phys. Chem. A*, 116, 12096-12103, <https://doi.org/10.1021/jp307718m>, 2012.

- Nielsen, O. J., Jørgensen, O., Donlon, M., Sidebottom, H. W., O'Farrel, D. J. and Treacy, J.: Rate constants for the gas-phase reactions of OH radicals with nitroethene, 3-nitropropene and 1-nitrocyclohexene at 298 K and 1 atm, *Chem. Phys. Lett.*, 168, 319-323, [https://doi.org/10.1016/0009-2614\(90\)85618-M](https://doi.org/10.1016/0009-2614(90)85618-M), 1990.
- Nishino, N., Arey, J. and Atkinson, R.: Rate constants for the gas-phase reactions of OH radicals with a series of C6-C14 alkenes at  $299 \pm 2$  K, *J. Phys. Chem. A*, 113, 852-857, <https://doi.org/10.1021/jp809305w>, 2009.
- Ohta, T.: Rate constants for reactions of diolefins with hydroxyl radicals in the gas-phase. Estimate of the rate constants from those for monoolefins, *J. Phys. Chem.*, 87, 1209-1213, <https://doi.org/10.1021/j100230a023>, 1983.
- Peeters, J. Vandenberk, S., Piessens, E. and Pultau, V.: H-atom abstraction in reactions of cyclic polyalkenes with OH, *Chemosphere*, 38, 1189-1195, [https://doi.org/10.1016/S0045-6535\(98\)00505-0](https://doi.org/10.1016/S0045-6535(98)00505-0), 1999.
- Peeters, J., Boullart, W., Pultau, V., Vandenberk, S. and Vereecken, L.: Structure-activity relationships for the addition of OH to (poly)alkenes: site specific and total rate constants, *J. Phys. Chem. A*, 111, 1618-1631, <https://doi.org/10.1021/jp066973o>, 2007.
- Peng, Z., Day, D. A., Ortega, A. M., Palm, B. B., Hu, W., Stark, H., Li, R., Tsigaridis, K., Brune, W. H. and Jimenez, J. L.: Non-OH chemistry in oxidation flow reactors for the study of atmospheric chemistry systematically examined by modelling, *Atmos. Chem. Phys. Discuss.*, 15, 23543-23586, doi:10.5194/acp-16-4283-2016, 2015.
- Poppe, D., Brauers, T., Dorn, H. -P., Karl, M., Mentel, T., Schlosser, E., Tillmann, R., Wegener, R. and Wahner, A.: OH-initiated degradation of several hydrocarbons in the atmosphere simulation chamber SAPHIR, *J. Atmos. Chem.*, 57, 203-214, <https://doi.org/10.1007/s10874-007-9065-y>, 2007.
- Rogers, J. D.: Rate constant measurements for the reaction of the hydroxyl radical with cyclohexene, cyclopentane, and glutaraldehyde, *Environ. Sci. Technol.*, 23, 177-181, <https://doi.org/10.1021/es00179a006>, 1989.
- Saunders, S. M., Jenkin, M. E., Derwent, R. G. and Pilling, M. J.: Protocol for the development of the Master Chemical Mechanism, MCM v3 (Part A): tropospheric degradation of non-

aromatic volatile organic compounds, *Atmos. Chem. Phys.*, 3, 161-180,  
<https://doi.org/10.5194/acp-3-161-2003>, 2003.

Singh, S. and Li, Z.: Kinetics investigation of OH reaction with isoprene at 240-340 K and 1-3 Torr using the relative rate/discharge flow/mass spectrometry technique, *J. Phys. Chem. A*, 111, 11843-11851, <https://doi.org/10.1021/jp074148h>, 2007.

Wu, C. H., Japar, S. M. and Niki, H.: Relative reactivities of HO-hydrocarbon reactions from smog reactor studies, *J. Environ. Sci. Health, Part A*, 11, 191-200,  
<https://doi.org/10.1080/10934527609385765>, 1976.



## Chapter 4

# Kinetic studies of aromatic VOC + OH reactions

## 4 Overview

This chapter describes the work undertaken to measure the rate coefficients for the reactions between OH and various aromatic VOCs (please refer to Chapter 1 Sections 1.2.2.3 and 1.3.4 for more information on the nature of, and importance of, aromatic VOCs). Two distinct synthetic mixtures, containing 22 different VOCs, were tested with the modified experimental setup described in Chapter 2 Section 2.2.1. The results for these reactions were compared with the available literature to determine the applicability of this technique for the simultaneous measurement of multiple rate coefficients for aromatic VOC + OH reactions. Numerical simulations were also performed to expand on the experimental results.

A new room temperature rate coefficient for the reaction between OH and *n*-pentylbenzene is provided in Table 4.2. New recommended room temperature rate coefficients for the reactions of OH with the three diethylbenzene isomers can be found in Table 4.6.

## 4.1 Results and discussion

The following section outlines the results from multiple mixtures containing aromatic VOCs. Results from two different synthetic mixtures, measured at room temperature (approximately 295 K) are presented.

### 4.1.1 Small aromatic VOCs mixture

This mixture contained 11 VOCs. The aromatic VOCs were small, comprising a single benzene ring and up to two alkyl substituents. Six of the VOCs had a single alkyl substituent, ranging in size from one methyl group to a five-carbon chain. The other five aromatic VOCs had two alkyl substituents, with a maximum chain length of just two carbon atoms each. 10 of the 11 aromatic VOCs in this mixture had rate coefficients available in the literature; data for the reaction between OH and *n*-pentylbenzene was not currently available at the time of writing.

Table 4.1 gives a full list of the 11 VOCs included in this mixture, along with the reference rate coefficient used for their reaction with OH and the number of measurements which could be found in the literature at the time of writing.

There was only a small range in OH rate coefficients for this mixture. The slowest reacting VOC was *t*-butylbenzene, which had a recommended rate coefficient for reaction with OH of  $4.5 (\pm 2) \times 10^{-12} \text{ cm}^3 \text{ molecule}^{-1} \text{ s}^{-1}$ . The fastest reacting VOC was *m*-xylene, which had a recommended rate coefficient for reaction with OH of  $23 (\pm 3) \times 10^{-12} \text{ cm}^3 \text{ molecule}^{-1} \text{ s}^{-1}$ . The estimated total OH reactivity of this mixture at STP was  $106 \text{ s}^{-1}$  (this value excludes the unknown contribution from *n*-pentylbenzene). This mixture was diluted with N<sub>2</sub> in differing amounts to inject gaseous samples into the reactor with a range of OH reactivities of between approximately 9 and  $27 \text{ s}^{-1}$ .

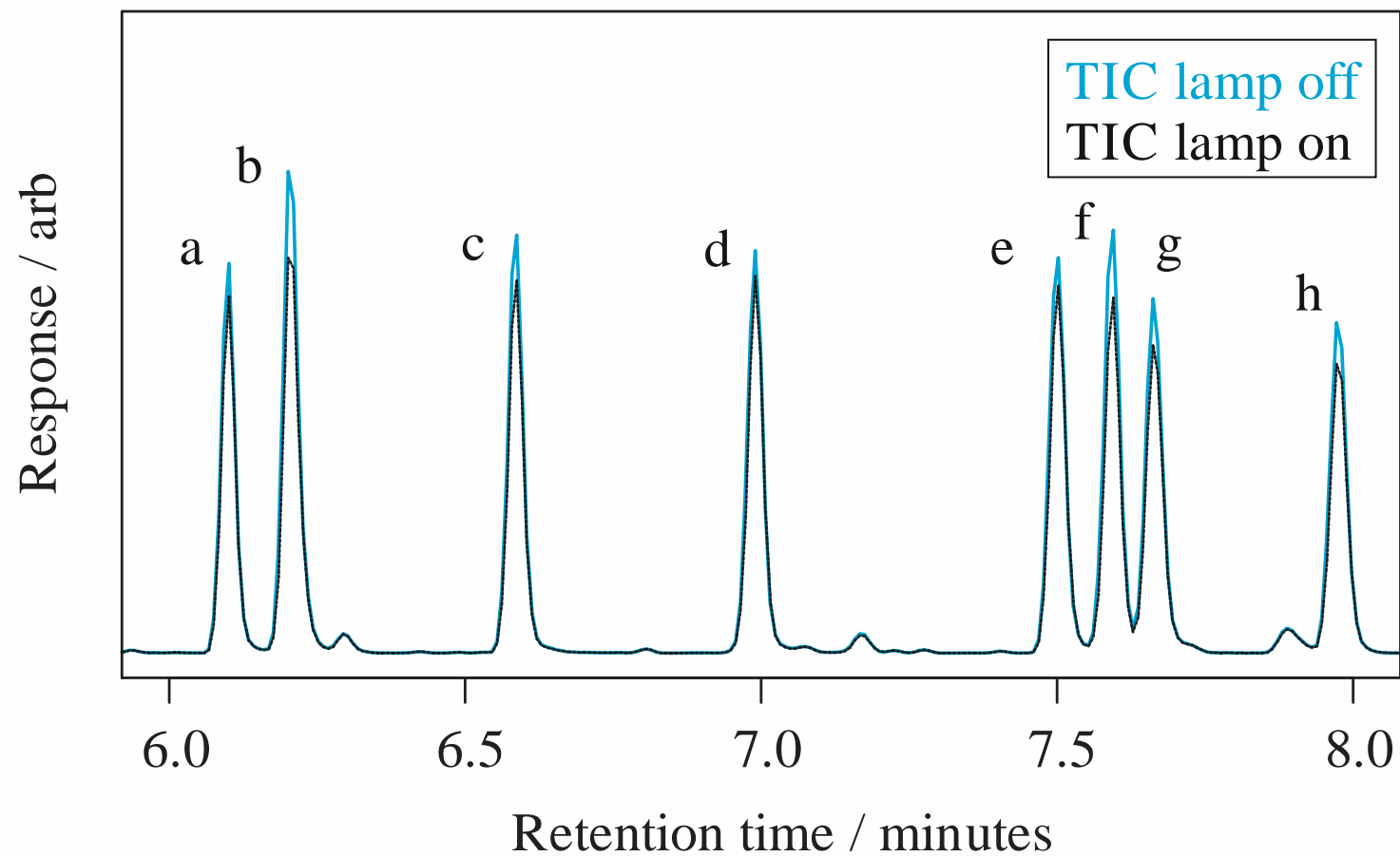
**Table 4.1** List of VOCs, in descending order of evaluated literature  $k$  value, in the small aromatic VOCs mixture along with their evaluated literature  $k$  value, reference and the number of measurements found in the literature at the time of writing.

Name	Evaluated literature $k$ (298 K) / $10^{-12}$ cm <sup>3</sup> molecule <sup>-1</sup> s <sup>-1</sup>	Reference used	Number of literature measurements
<i>m</i> -xylene	23 ± 3	Calvert et al., 2002	15
3-ethyltoluene	19 ± 7	Calvert et al., 2002	2
<i>o</i> -xylene	13 ± 3	Calvert et al., 2002	10
4-ethyltoluene	12 ± 4	Calvert et al., 2002	2
2-ethyltoluene	12 ± 4	Calvert et al., 2002	2
ethylbenzene	7.0 ± 2	Calvert et al., 2002	3
isopropylbenzene	6.3 ± 2	Calvert et al., 2002	3
<i>n</i> -propylbenzene	5.8 ± 1.5	Calvert et al., 2002	3
toluene	5.6 ( <sup>+1.5</sup> <sub>-1.2</sub> )	Atkinson et al., 2006	18
<i>t</i> -butylbenzene	4.5 ± 2	Calvert et al., 2002	2
<i>n</i> -pentylbenzene			0

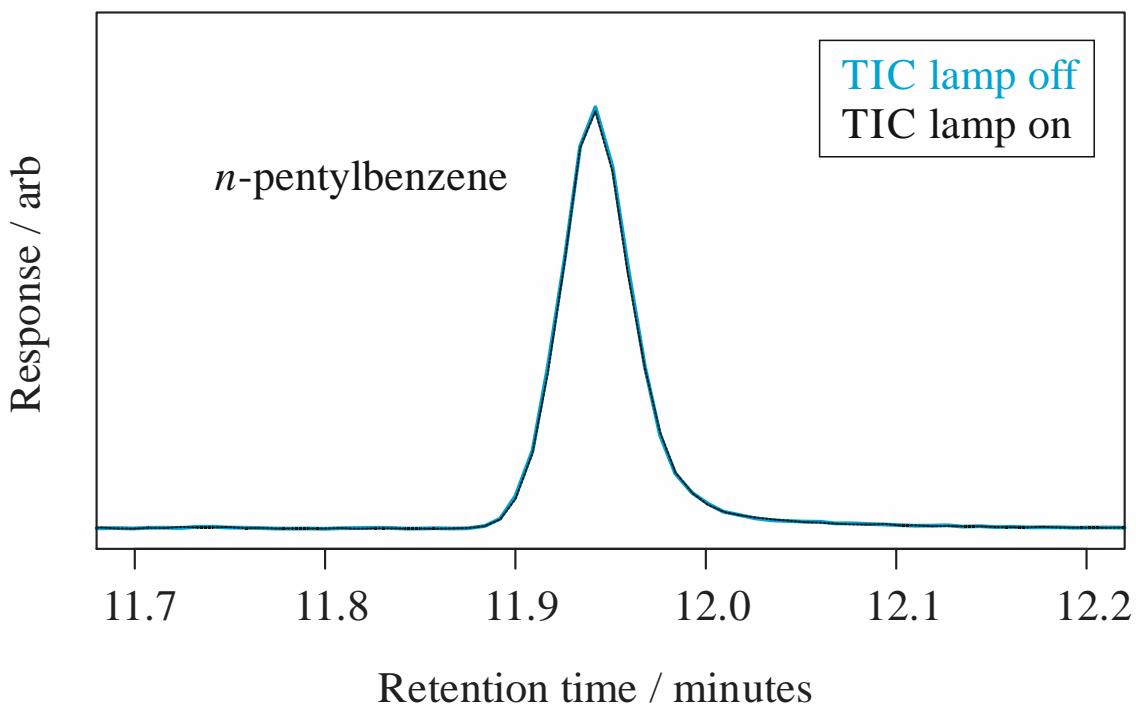
#### 4.1.1.1 Typical chromatogram data

Figure 4.1 shows sections of typical total ion chromatograms (TIC) obtained for this mixture with the reactor lamp turned off (blue) and the reactor lamp turned on (black). There was a reduction in the peak area for all the compounds shown when the lamp was turned on.

Figure 4.2 shows the same TICs but for the peak identified to be due to the elution of *n*-pentylbenzene. The y-axis on this plot has been magnified by up to five times relative to the same axis on Figure 4.1. Whilst all the VOCs in Figure 4.1 showed appreciable depletions in their peak areas when the lamp was switched on, an observable depletion in the *n*-pentylbenzene peak area was not easily distinguished. The two peaks, for lamp off and lamp on, were almost identical. This led to larger errors in the calculated depletion factor for *n*-pentylbenzene, relative to the other VOCs.



**Figure 4.1** Typical TIC sections obtained for the small aromatics mixture showing the peaks observed with the lamp off (blue) and the lamp on (black). The peaks were identified as: a, ethylbenzene; b, *m*-xylene; c, *o*-xylene; d, isopropylbenzene; e, *n*-propylbenzene; f, 3-ethyltoluene; g, 4-ethyltoluene; h, 2-ethyltoluene.

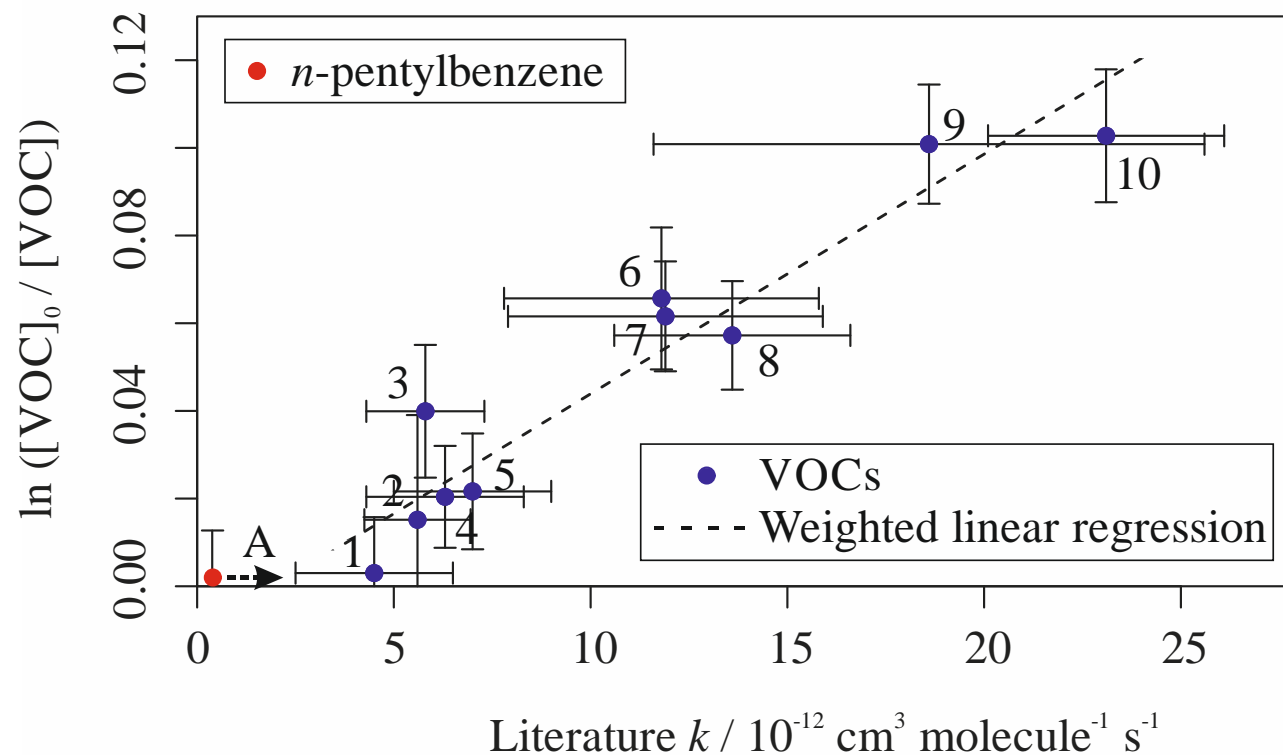


**Figure 4.2** TIC sections for the small aromatics mixture showing the peaks observed for *n*-pentylbenzene with the lamp turned off (blue) and the lamp turned on (black).

#### 4.1.1.2 Relative rate plots

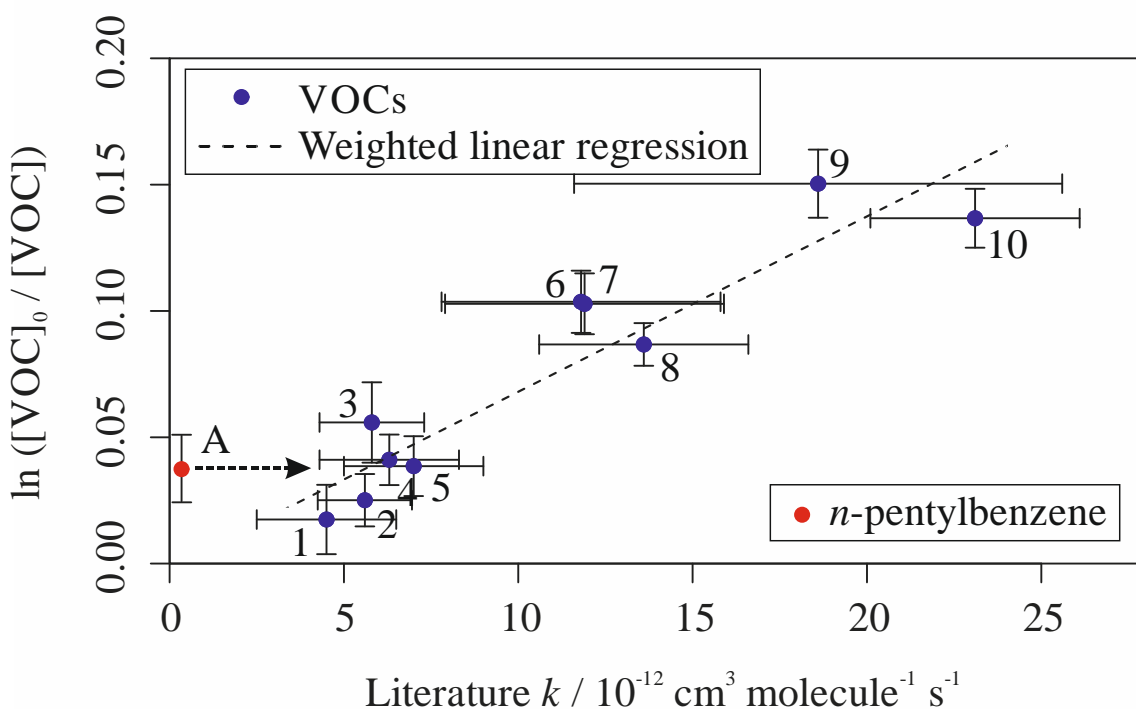
The depletion factor for each VOC was plotted against their evaluated literature rate coefficients for reaction with OH as discussed in Chapter 2 Section 2.1.8. Linear regression, weighted to the uncertainty in the depletion factors, was then used to obtain the  $OH_{exp}$  as per Eq. 2.19.

Figure 4.3 shows the relative rate plot for this mixture with an OH reactivity in the reactor of approximately  $18 \text{ s}^{-1}$  and in the absence of any NO. A linear relationship between depletion factor and  $k$  was clearly observed. However, the scale of the depletion factor for the compounds was relatively low when compared with the depletion factors observed when using more reactive mixtures, which were typically greater than 0.1 for all VOCs (see Chapter 3 Sections 3.1.1.3, 3.1.2.1 and 3.1.3.2). The depletion factors measured for most of the VOCs in this mixture were equivalent to percentage depletions of less than a few percent. For example, under these conditions, *t*-butyl- and *n*-pentylbenzene recorded depletions of just 0.3% and 0.2% respectively.



**Figure 4.3** Relative rate plot for the small aromatic VOCs mixture with an OH reactivity of approximately  $18 \text{ s}^{-1}$ , at 295 K. Compounds with a reference rate coefficient for reaction with OH were plotted using evaluated literature values as references. Error bars on the y-axis, equal to one standard error, were calculated by combining the standard error in peak areas for six lamp-off samples and six lamp-on samples. Error bars on the x-axis were typically large (approximately  $\pm 20\text{-}30\%$ ) and accounted for deviations from the trend for most VOCs. A weighted (to the uncertainty in the y-axis) linear fit was used to generate the slope with a value of  $OH_{exp} = 5.5 (\pm 0.6) \times 10^9 \text{ molecules cm}^{-3}$  and  $R^2$  of 0.899. Data for *n*-pentylbenzene (A), which had no literature  $k$  value, was not used in the calculation of the fit. The VOCs can be identified as follows: 1, *t*-butylbenzene; 2, toluene; 3, *n*-propylbenzene; 4, isopropylbenzene; 5, ethylbenzene; 6, 2-ethyltoluene; 7, 4-ethyltoluene; 8, *o*-xylene; 9, 3-ethyltoluene; 10, *m*-xylene.

Two different flows of NO (20 sccm and 40 sccm) were used to augment the observed depletion factors for the VOCs (see Chapter 2 Section 2.2.1). These flows of NO were equivalent to initial reactor concentrations of approximately 30 ppb for the smaller flow and 70 ppb for the greater flow. Figure 4.4 and Figure 4.5 show the relative rate plots for this mixture with 30 ppb and 70 ppb of NO respectively.



**Figure 4.4** Relative rate plot for the small aromatic VOCs mixture with an OH reactivity of approximately  $18 \text{ s}^{-1}$  measured with 20 ppb NO, at 295 K. Compounds with a reference rate coefficient for reaction with OH were plotted using evaluated literature values as references. Error bars on the y-axis, equal to one standard error, were calculated by combining the standard error in peak areas for six lamp-off samples and six lamp-on samples. Error bars on the x-axis were typically large (approximately  $\pm 20\text{-}30\%$ ) and accounted for deviations from the trend for most VOCs. A weighted (to the uncertainty in the y-axis) linear fit was used to generate the slope with a value of  $OH_{exp} = 6.9 (\pm 0.9) \times 10^9 \text{ molecules cm}^{-3}$  and  $R^2$  of 0.853. Data for *n*-pentylbenzene (A), which had no literature  $k$  value, was not used in the calculation of the fit. The VOCs can be identified as follows: 1, *t*-butylbenzene; 2, toluene; 3, *n*-propylbenzene; 4, isopropylbenzene; 5, ethylbenzene; 6, 2-ethyltoluene; 7, 4-ethyltoluene; 8, *o*-xylene; 9, 3-ethyltoluene; 10, *m*-xylene.

There was an observed increase in average depletion factor for the aromatic VOCs with increasing concentration of NO in the reactor. This was to be expected if NO was converting HO<sub>2</sub> to OH and limiting the extent of reactions between OH and HO<sub>2</sub>. The actual depletions in the VOCs increased from a maximum of 10% for *m*-xylene to 13%. The depletions in *t*-butyl- and *n*-pentylbenzene increased from 0.3% and 0.2% to 2.3% and 3.0% respectively.

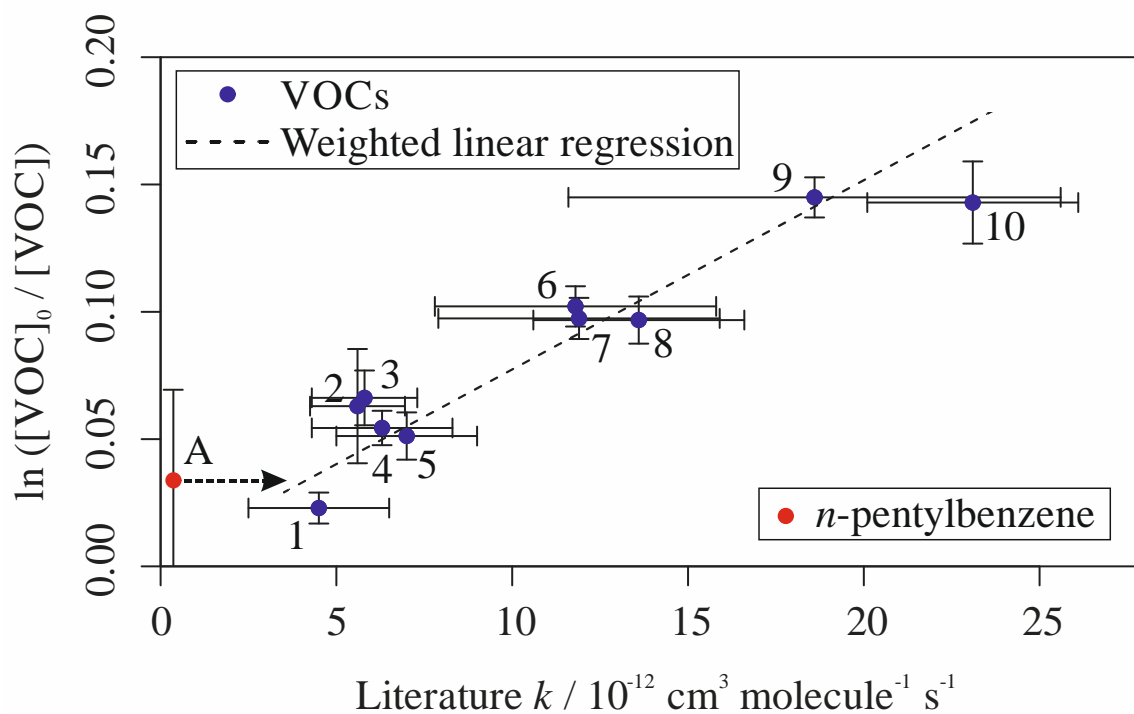


**Figure 4.5** Relative rate plot for the small aromatic VOCs mixture with an OH reactivity of approximately  $18 \text{ s}^{-1}$  measured with 40 ppb NO, at 295 K. Compounds with a reference rate coefficient for reaction with OH were plotted using evaluated literature values as references. Error bars on the y-axis, equal to one standard error, were calculated by combining the standard error in peak areas for six lamp-off samples and six lamp-on samples. Error bars on the x-axis were typically large (approximately  $\pm 20\text{-}30\%$ ) and accounted for deviations from the trend for most VOCs. A weighted (to the uncertainty in the y-axis) linear fit was used to generate the slope with a value of  $OH_{exp} = 7.5 (\pm 0.8) \times 10^9 \text{ molecules cm}^{-3}$  and  $R^2$  of 0.909. Data for *n*-pentylbenzene (A), which had no literature  $k$  value, was not used in the calculation of the fit. The VOCs can be identified as follows: 1, *t*-butylbenzene; 2, toluene; 3, *n*-propylbenzene; 4, isopropylbenzene; 5, ethylbenzene; 6, 2-ethyltoluene; 7, 4-ethyltoluene; 8, *o*-xylene; 9, 3-ethyltoluene; 10, *m*-xylene.

Figure 4.6 shows an overlay of Figure 4.3, Figure 4.4 and Figure 4.5 which demonstrates the increased OH exposure observed with increasing concentration of NO.  $OH_{exp}$  increased from  $5.5 (\pm 0.6) \times 10^9$  molecules  $\text{cm}^{-3}$  s without NO, to  $7.4 (\pm 0.8) \times 10^9$  molecules  $\text{cm}^{-3}$  s with 70 ppb NO. This corresponded to an increase in OH exposure of approximately 35%.

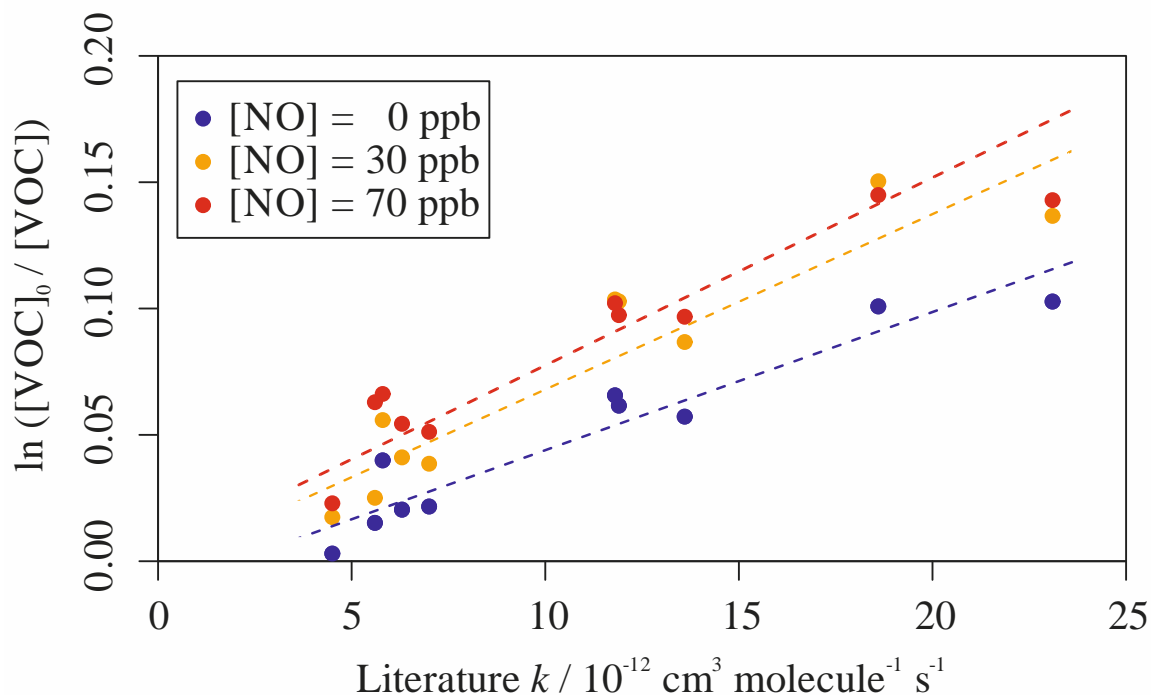


**Figure 4.6** Relative rate plots for the small aromatics mixture with an OH reactivity of  $18 \text{ s}^{-1}$ , at 295 K. Different concentrations of NO in the reactor are shown by the different coloured data.  $OH_{exp}$ , calculated from the weighted linear regressions, increased with increasing [NO].

#### 4.1.1.3 Calculation of rate coefficients

$k$  values for all the VOC + OH reactions in the mixture were calculated by combining the observed OH exposure with the depletion factor for each VOC (see Eq. 2.19). This was performed at each of the individual OH reactivities tested in the reactor, and a weighted average taken to yield the final result. Table 4.2 displays the measured values for each of the VOC + OH reactions at each of the different concentrations of NO in the reactor.

It was difficult to quantify exactly which concentration of NO gave the more reliable results overall. Whilst the measured depletion factors and observed depletions for the VOCs did increase with added NO, this did not transfer to a tangibly improved correlation with reference literature values. This was clearly evidenced by the  $R^2$  values, which did not significantly increase with increasing [NO]. In fact, the  $R^2$  values for this mixture with an OH reactivity of  $9 \text{ s}^{-1}$  actually

decreased with increasing [NO] (from 0.946 to 0.867). This resulted in little-to-no significant differences in the errors quoted on the measured values at different concentrations of NO.

On an individual reaction basis, different concentrations of NO did perform slightly better. For example, the measured value for the toluene + OH reaction with [NO] = 30 ppb was negative; the value in best agreement with the literature was measured when using [NO] = 0 ppb. However, for isopropylbenzene, the result at [NO] = 30 ppb was in best agreement with the literature, albeit not by any significant margin.

**Table 4.2** List of VOCs, in descending order of evaluated literature  $k$  value, in the small aromatics mixture along with their measured  $k$  value at each concentration of NO, average (weighted to the errors) measured  $k$  value and evaluated literature  $k$  value.

Name	Measured $k$ (295 K) / $10^{-12}$ cm <sup>3</sup> molecule <sup>-1</sup> s <sup>-1</sup>				Evaluated literature $k$ / $10^{-12}$ cm <sup>3</sup> molecule <sup>-1</sup> s <sup>-1</sup>
	[NO] = 0 ppb	[NO] = 30 ppb	[NO] = 70 ppb	Weighted average	
<i>m</i> -xylene	20.6 ± 0.7	19.6 ± 0.4	19.8 ± 1.3	19.9 ± 0.5	23 ± 3
3-ethyltoluene	19.7 ± 0.9	21.7 ± 0.4	19.4 ± 1.0	21.1 ± 1.2	19 ± 7
<i>o</i> -xylene	12.3 ± 1.3	12.4 ± 0.4	12.3 ± 0.6	12.4 ± 0.1	13 ± 3
4-ethyltoluene	14 ± 2	14.8 ± 0.5	14.1 ± 1.2	14.6 ± 0.3	12 ± 4
2-ethyltoluene	13.4 ± 1.0	15.0 ± 1.1	12.65 ± 0.06	12.7 ± 0.2	12 ± 4
ethylbenzene	4.9 ± 1.6	6.0 ± 0.3	6.7 ± 0.5	6.1 ± 0.4	7.0 ± 2
isopropylbenzene	6.5 ± 0.5	6.4 ± 0.4	6.5 ± 0.6	6.45 ± 0.02	6.3 ± 2
<i>n</i> -propylbenzene	8.9 ± 0.7	8.7 ± 0.6	7.4 ± 1.5	8.7 ± 0.5	5.8 ± 1.5
toluene	5 ± 2	0 ± 2	7 ± 2	4 ± 4	5.6 ( <sup>+1.5</sup> / <sub>-1.5</sub> )
<i>t</i> -butylbenzene	3.5 ± 1.1	3.4 ± 0.5	3.1 ± 0.7	3.31 ± 0.13	4.5 ± 2
<i>n</i> -pentylbenzene	3 ± 5	5.4 ± 0.4	1 ± 4	5.3 ± 0.7	

The measured values for the reaction between OH and *m*-xylene were in good agreement with those measured earlier in this work, in monoterpenes mixtures 1 and 2, of 22 (± 6) and 23.4 (± 1.4) × 10<sup>-12</sup> cm<sup>3</sup> molecule<sup>-1</sup> s<sup>-1</sup> respectively (see Chapter 3 Sections 3.1.1.4 and 3.1.2.2). The same was not true for the measurements of the *o*-xylene + OH reaction, which were in much better agreement with the literature than the result in Chapter 3 Section 3.1.1.4. *o*-xylene was the slowest reacting compound in the first monoterpenes mixture and was measured to have a rate coefficient for its reaction with OH of  $k = 5 (\pm 7) \times 10^{-12}$  cm<sup>3</sup> molecule<sup>-1</sup> s<sup>-1</sup>. It was proposed that its low reactivity relative to everything else in that mixture led to the large uncertainties in its measured value. The low reactivity of *o*-xylene wasn't a problem in the small aromatics mixture

and the measured value can be seen to be in much better agreement with the literature because of this.

#### 4.1.1.4 Determination of a new rate coefficient for the *n*-pentylbenzene + OH reaction

A reference literature rate coefficient for the reaction between OH and *n*-pentylbenzene could not be found at the time of writing. However, it is emitted from a variety of sources with National Atmospheric Emissions Inventory (NAEI) values of 0.013% from decorative paint, 0.016% from white spirits and between 0.19% and 0.23% from commercial, general and military aircraft landing and take-off procedures (Passant, 2002). These values were roughly similar to those for *n*-heptane and C<sub>13</sub> alkanes and approximately a third of those for naphthalene. The POCP value for *n*-pentylbenzene was 67.3 which was roughly equivalent to those for the ethyltoluenes and greater than that for ethylbenzene (see Chapter 1 Section 1.2.2.3).

Three measurements of the rate coefficient for the *n*-pentylbenzene + OH reaction were presented in this work; each used the same method but with different concentrations of NO. The three measurements were  $k = 3.3 (\pm 5)$ ,  $5.4 (\pm 0.4)$  and  $1.2 (\pm 0.4) \times 10^{-12} \text{ cm}^3 \text{ molecule}^{-1} \text{ s}^{-1}$  when using [NO] = 0, 30 and 70 ppb respectively. These three values were all quite different from one another. The results at [NO] = 0 and 70 ppb had large uncertainties placed upon them and the result at [NO] = 70 ppb was very small, even when compared with the other aromatic species. The derivation of a rate coefficient for the *n*-pentylbenzene + OH reaction was made more difficult by the apparent low reactivity of *n*-pentylbenzene relative to everything else in the mixture. Ideally, when deriving a new rate coefficient, the rate coefficient for the targeted reaction should lie in the middle of the calibrated reactivity spectrum for the mixture. Hence, a mixture where compounds with rate coefficients of approximately  $5.0 \times 10^{-12} \text{ cm}^3 \text{ molecule}^{-1} \text{ s}^{-1}$  were in the middle would be more appropriate for the derivation of a rate coefficient for *n*-pentylbenzene + OH.

As discussed in Section 4.1.2.3, it was difficult to quantify which concentration of NO provided the best overall results, in terms of agreement with reference literature values. Rather, individual VOCs performed differently at different [NO]. A mean of the three recorded measurements was deemed most appropriate in the absence of a clear preferential value. The average value, weighted using the errors at each [NO], for the rate coefficient for the reaction between *n*-pentylbenzene and OH was  $k = 5.3 (\pm 0.7) \times 10^{-12} \text{ cm}^3 \text{ molecule}^{-1} \text{ s}^{-1}$  at 295 K.

## 4.1.1.5 Comparison to SARs

Structure activity relationships (SARs) were used to estimate the rate coefficients for reactions between the aromatic VOCs in this mixture and OH. The SARs used were outlined in Kwok and Atkinson (1995) and Jenkin et al. (2018). The method described by Kwok and Atkinson (1995) used estimated H-atom abstraction and OH-addition rate coefficients. Generally, the contribution from H-atom abstraction from the substituent group(s) was minimal. The rate coefficients for OH-addition to the aromatic ring were estimated using the sum of the electrophilic substituent constants ( $\Sigma\sigma^+$ ).  $\Sigma\sigma^+$  has been shown to have a good correlation with OH-radical addition to aromatic rings, with the relationship given by Eq. 4.1 (Zetzsch, 1982). Values for  $\Sigma\sigma^+$  differ depending on the substituent positions on the aromatic ring (Brown and Okamoto, 1958; Ziemann and Atkinson, 2012).

$$\log_{10} k_{\text{add}} = -11.71 - 1.34 \Sigma\sigma^+ \quad \text{Eq. 4.1}$$

The SAR described by Jenkin et al. (2018) differed from that in Kwok and Atkinson (1995) in that parameters for OH-addition were determined directly from experimental rate coefficient measurements, rather than indirectly through correlation with electrophilic substituent constants. The results of the SAR estimated rate coefficients are given in Table 4.3.

**Table 4.3** List of VOCs, in descending order of evaluated literature  $k$  value, in the small aromatics mixture along with their SAR derived  $k$  values, average experimentally measured  $k$  value and evaluated literature  $k$  value.

Name	Rate coefficient for reaction with OH / $10^{-12} \text{ cm}^3 \text{ molecule}^{-1} \text{ s}^{-1}$			
	This work	Kwok and Atkinson (1995) SAR	Jenkin et al. (2018) SAR	Evaluated literature
<i>m</i> -xylene	$19.9 \pm 0.5$	$13 \pm 7$	$23 \pm 9$	$23 \pm 3$
3-ethyltoluene	$21.1 \pm 1.2$	$14 \pm 7$	$24 \pm 10$	$19 \pm 7$
<i>o</i> -xylene	$12.4 \pm 0.1$	$6.2 \pm 3.1$	$14 \pm 6$	$13 \pm 3$
4-ethyltoluene	$14.6 \pm 0.3$	$7.3 \pm 3.7$	$14 \pm 6$	$12 \pm 4$
2-ethyltoluene	$12.7 \pm 0.2$	$7.3 \pm 3.7$	$14 \pm 6$	$12 \pm 4$
ethylbenzene	$6.1 \pm 0.4$	$5.9 \pm 3.0$	$6.2 \pm 2.5$	$7.0 \pm 2$
isopropylbenzene	$6.45 \pm 0.02$	$5.9 \pm 3.0$	$7.1 \pm 2.8$	$6.3 \pm 2$
<i>n</i> -propylbenzene	$8.7 \pm 0.5$	$6.9 \pm 3.5$	$7.2 \pm 2.9$	$5.8 \pm 1.5$
toluene	$4 \pm 4$	$5.1 \pm 2.6$	$5.6 \pm 2.2$	$5.6 (^{+1.5}_{-1.2})$
<i>t</i> -butylbenzene	$3.31 \pm 0.13$	$8.7 \pm 4.4$	$5.7 \pm 2.3$	$4.5 \pm 2$
<i>n</i> -pentylbenzene	$5.3 \pm 0.7$	$8.7 \pm 4.4$	$9.3 \pm 3.7$	

The same information is shown graphically in Figure 4.7, alongside recommended literature values and the experimental values derived in this work. For the monosubstituted aromatics, especially those with three or fewer carbons in the alkyl chain, the SARs did a relatively good job of emulating the evaluated literature rate coefficients. The experimental data derived in this work for both ethylbenzene and *n*-propylbenzene correlated well with both the literature and the SARs. The experimental data for toluene differed considerably depending on the concentration of NO used in the reactor but appeared to be more in line with both the literature and the SARs when using 0 ppb of NO, and to a lesser extent, 70 ppb of NO.

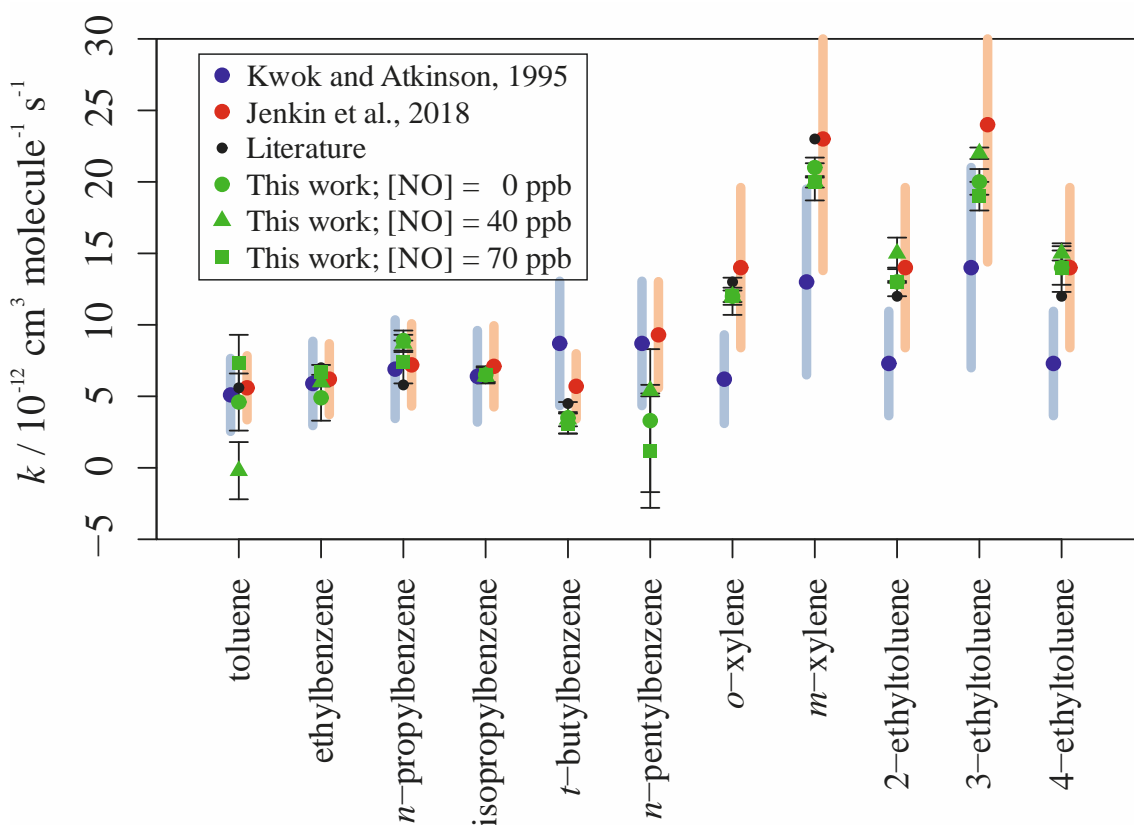


**Figure 4.7** Comparison of two different SAR methods (Kwok and Atkinson (1995), blue; Jenkin et al. (2018), red) for the prediction of rate coefficients for the reactions between aromatic VOCs and OH, alongside the experimental results derived in this work (green) and the recommended literature values (black).

The Kwok and Atkinson (1995) SAR overestimated the rate coefficient for the reaction between *t*-butylbenzene and OH, although the recommended literature rate coefficient was based off just two experimental studies. The Jenkin et al. (2018) SAR did a much better job of estimating the *k* value for this reaction.

The two SARs correlated well for the prediction of the rate coefficient for reaction between *n*-pentylbenzene and OH, with values of  $8.7$  and  $9.3 \times 10^{-12} \text{ cm}^3 \text{ molecule}^{-1} \text{ s}^{-1}$  for the Kwok and

Atkinson (1995) and Jenkin et al. (2018) relationships respectively. The experimental values derived in this work were smaller than these, indicating that either the SARs were unable to replicate experimental data for monosubstituted aromatics with C<sub>5</sub> substituents, or that the experimental data in this work for that reaction was poor. The large spread in experimentally measured values for the rate coefficient, suggest that the latter is more likely although the SARs did appear to increasingly deviate from the literature with an increasing number of alkyl carbon atoms.

Whilst the two SARs did a relatively good job of matching the literature rate coefficients for reactions of OH with monosubstituted aromatics, they both performed quite poorly for the polysubstituted aromatics. The SAR in Jenkin et al. (2018) reproduced the literature very well for the *o*- and *m*-xylene reactions but gave rate coefficients approximately 20% greater than the literature for the reactions of the three ethyltoluene isomers with OH. The SAR in Kwok and Atkinson underestimated all the rate coefficients for the polysubstituted aromatics + OH reactions by an average of 40%. The measurements provided in this work for the rate coefficients for the ethyltoluene + OH reactions were somewhere between the evaluated literature values and the SAR by Jenkin et al. (2018).

## 4.1.2 Large aromatic VOCs mixture

This mixture contained 13 VOCs. Ten of these had aromatic structures (see Chapter 1 Sections 1.2.2.3 and 1.3.4). The aromatic VOCs were generally larger than those in the mixture described in Section 4.1.2 and therefore generally reacted faster with OH. They comprised a single polyalkyl-substituted aromatic ring with up to four substituents. Two of the VOCs, *o*- and *m*-xylene, were also present in the mixture in Section 4.1.2. Three VOCs were tri-substituted and two VOCs were tetra-substituted aromatics, with just single carbon methyl substituents. The remaining three aromatic structures were the isomers of diethylbenzene, none of which had literature measurements for their rate coefficients for reaction with OH at the time of writing. The remaining three VOCs in the mixture were the alkenes, isoprene and  $\alpha$ - and  $\beta$ -pinene. These were included as they benefitted from multiple literature measurements for reaction with OH and therefore provided reliable reference rate coefficients, whereas many of the aromatic VOCs with rate coefficients greater than  $30 \times 10^{-12} \text{ cm}^3 \text{ molecule}^{-1} \text{ s}^{-1}$  had fewer than 5 available literature measurements. Table 4.4 gives a full list of the 13 VOCs included in this mixture, along with the reference rate coefficients for their reaction with OH.

There was only a small range in OH rate coefficients in this mixture. The slowest reacting VOC, was *o*-xylene, which had a recommended rate coefficient for reaction with OH of  $13 (\pm 3) \times 10^{-12} \text{ cm}^3 \text{ molecule}^{-1} \text{ s}^{-1}$ . The fastest reacting VOC was isoprene, which had a recommended rate coefficient for reaction with OH of  $100 \left( \begin{smallmatrix} +15 \\ -13 \end{smallmatrix} \right) \times 10^{-12} \text{ cm}^3 \text{ molecule}^{-1} \text{ s}^{-1}$ . The estimated OH reactivity of this mixture, excluding those with no literature measurements, was  $380 \text{ s}^{-1}$ .

**Table 4.4** List of VOCs, in descending order of evaluated literature  $k$  value, in the large aromatic mixture, along with their evaluated literature rate coefficient, reference and the number of measurements found in the literature at the time of writing.

Name	Evaluated literature $k$ (298 K) / $10^{-12} \text{ cm}^3$ molecule $^{-1} \text{ s}^{-1}$	Reference used	Number of literature measurements
Isoprene	100 ( $^{+15}$ / $_{-13}$ )	Atkinson et al., 2006	25+
$\beta$ -pinene	$79 \pm 20$	Atkinson and Arey, 2003	10
1,2,3,5-tetramethylbenzene	$62.4 \pm 0.8$	Alarcón et al., 2015	1
1,3,5-trimethylbenzene	$57 \pm 11$	Calvert et al., 2002	5
1,2,4,5-tetramethylbenzene	$55.5 \pm 3.4$	Aschmann et al., 2013	2
$\alpha$ -pinene	53 ( $^{+22}$ / $_{-15}$ )	Atkinson et al., 2006	9
1,2,4-trimethylbenzene	$33 \pm 8$	Calvert et al., 2002	5
1,2,3-trimethylbenzene	$33 \pm 8$	Calvert et al., 2002	5
<i>m</i> -xylene	$23 \pm 3$	Calvert et al., 2002	15
<i>o</i> -xylene	$13 \pm 3$	Calvert et al., 2002	10
1,2-diethylbenzene			0
1,3-diethylbenzene			0
1,4-diethylbenzene			0

## 4.1.2.1 Typical chromatogram data

Figure 4.8 shows sections of typical TICs obtained for this mixture with the reactor lamp turned off (blue) and the reactor lamp turned on (black). There was a reduction in the measured peak area for all of the compounds shown when the lamp was turned on.

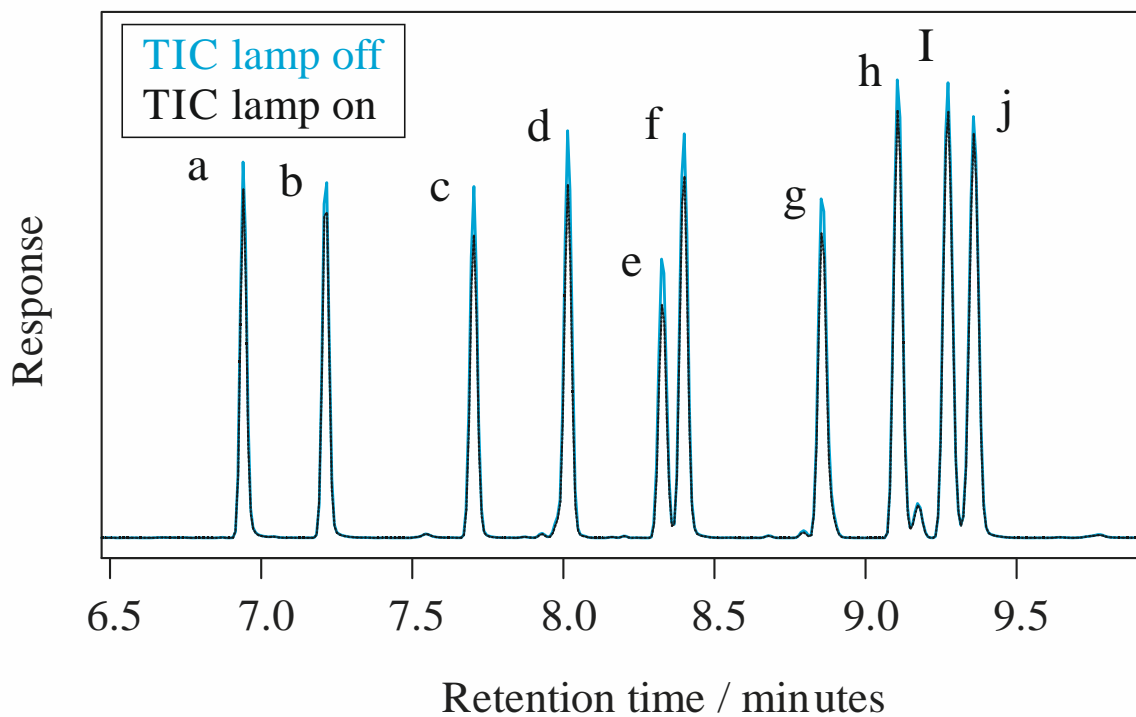
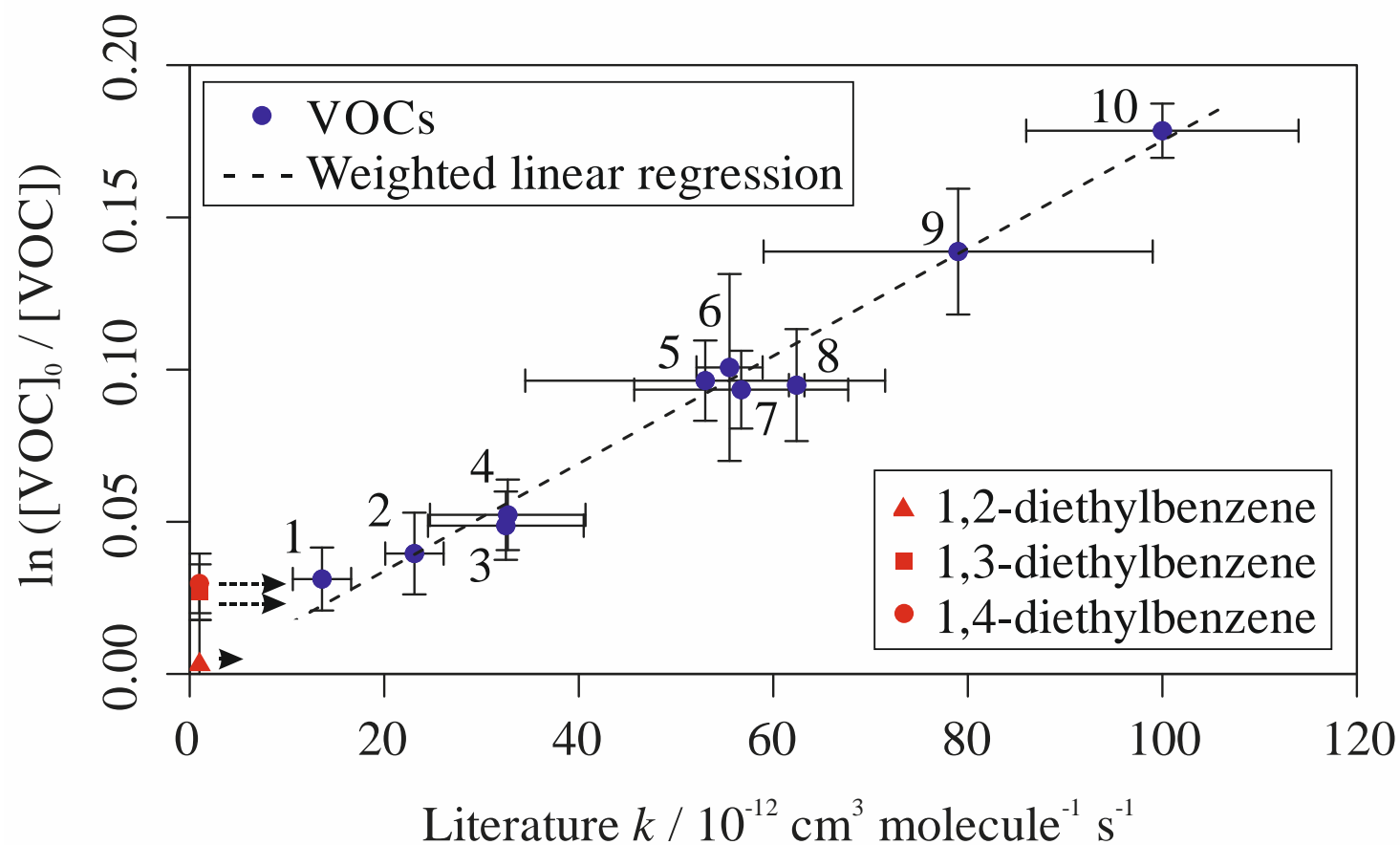


**Figure 4.8** Typical TIC sections obtained for the large aromatics mixture showing the peaks observed with the lamp off (blue) and the lamp on (black). The peaks were identified as: a, *m*-xylene; b, *o*-xylene; c,  $\alpha$ -pinene; d, 1,3,5-trimethylbenzene; e,  $\beta$ -pinene; f, 1,2,4-trimethylbenzene; g, 1,2,3-trimethylbenzene; h, 1,3-diethylbenzene; I, 1,4-diethylbenzene; j, 1,2-diethylbenzene.

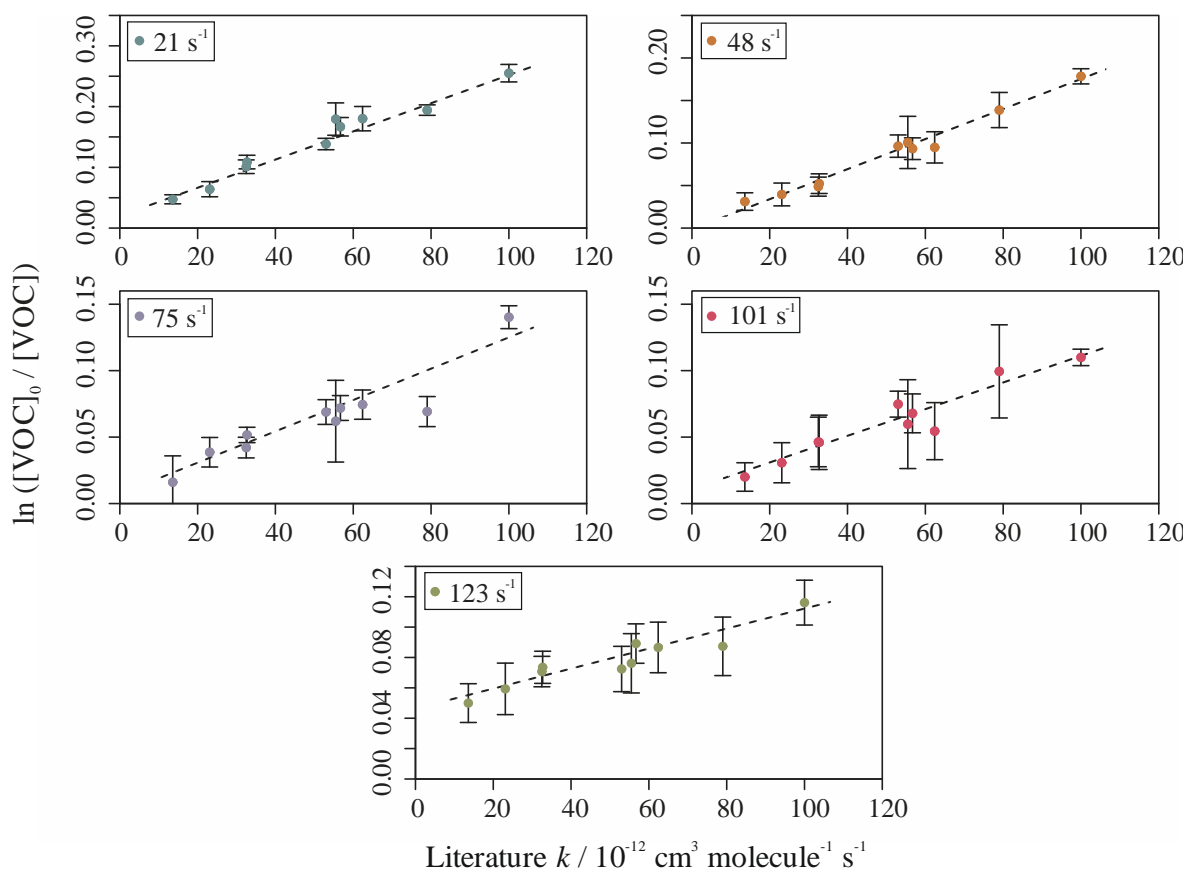
#### 4.1.2.2 Relative rate plots

Figure 4.9 shows the relative rate plot for this mixture with an OH reactivity of  $48 \text{ s}^{-1}$  and no NO in the reactor. A clear linear relationship between depletion factor and literature  $k$  value was observed. The depletion factors were all fairly large when compared with the small aromatic VOCs mixture and were equivalent to percentage depletions of between 3.1% and 17%. The adjusted  $R^2$  for the linear regression in this plot was 0.980 and the value of the  $OH_{exp}$ , given by the linear regression was  $1.8 (\pm 0.1) \times 10^9 \text{ molecules cm}^{-3} \text{ s}$ .

Figure 4.10 shows the relative rate plots for this mixture with OH reactivities of 21, 48, 75, 101 and  $123 \text{ s}^{-1}$ . They were all linear with adjusted  $R^2$  values of 0.958, 0.980, 0.907, 0.967 and 0.829 respectively. The  $OH_{exp}$  values for these plots were  $2.3 (\pm 0.1)$ ,  $1.8 (\pm 0.1)$ ,  $1.2 (\pm 0.2)$ ,  $1.0 (\pm 0.1)$  and  $0.7 (\pm 0.1) \times 10^9 \text{ molecules cm}^{-3} \text{ s}$  for OH reactivities of 21, 48, 75, 101 and  $123 \text{ s}^{-1}$  respectively.



**Figure 4.9** Relative rate plot for the large aromatics mixture with an OH reactivity of approximately  $48 \text{ s}^{-1}$ , at 295 K. Compounds with a reference rate coefficient for reaction with OH were plotted using evaluated reference values. Error bars on the y-axis, equal to one standard error, were calculated by combining the standard error in peak areas for eight lamp-off and eight lamp-on samples. Error bars on the x-axis were typically large (approximately  $\pm 20\text{-}30\%$ ) and accounted for deviations from the trend for all VOCs. A weighted (to the uncertainty in the y-values) linear fit was used to generate the slope, with a value of  $OH_{exp} = 1.8 (\pm 0.1) \times 10^9 \text{ molecules cm}^{-3} \text{ s}$  and  $R^2 = 0.980$ . Data for 1,2-, 1,3- and 1,4-diethylbenzene, which had no literature  $k$  values for their reaction with OH, were not used in the calculation of the fit. The VOCs can be identified as follows: 1, *o*-xylene; 2, *m*-xylene; 3, 1,2,4-trimethylbenzene; 4, 1,2,3-trimethylbenzene; 5,  $\alpha$ -pinene; 6, 1,2,4,5-tetramethylbenzene; 7, 1,3,5-trimethylbenzene; 8, 1,2,3,5-tetramethylbenzene; 9,  $\beta$ -pinene; 10, isoprene.



**Figure 4.10** Relative rate plots for the large aromatic VOCs mixture with OH reactivities of 21, 48, 75, 101 and 123  $\text{s}^{-1}$ . The  $R^2$  for the weighted linear fits were 0.958, 0.980, 0.907, 0.967 and 0.829 respectively. The values of  $OH_{exp}$  were  $2.3 (\pm 0.1)$ ,  $1.8 (\pm 0.1)$ ,  $1.2 (\pm 0.2)$ ,  $1.0 (\pm 0.1)$  and  $0.7 (\pm 0.1) \times 10^9 \text{ molecules cm}^{-3} \text{ s}$  respectively.

## 4.1.2.3 Calculation of rate coefficients

Table 4.5 gives the final measured rate coefficient values for the reactions between OH and the VOCs included as part of this mixture. All of the measured values were in excellent correlation with the evaluated literature rate coefficients, with only minor discrepancies between the two values for each of the VOCs. The measured values in this work were well within the margins of error placed upon the recommended literature values.

**Table 4.5** List of VOCs, in descending order of evaluated literature  $k$  value, in the large aromatics mixture along with their range of depletion due to reaction with OH, measured  $k$  value and evaluated literature  $k$  value.

Name	Range of depletion / %	Measured $k$ (295 K) / $10^{-12} \text{ cm}^3 \text{ molecule}^{-1} \text{ s}^{-1}$	Evaluated literature $k$ / $10^{-12} \text{ cm}^3 \text{ molecule}^{-1} \text{ s}^{-1}$
Isoprene	10 - 23	$102 \pm 4$	$100 (^{+15}_{-13})$
$\beta$ -pinene	7 - 18	$74 \pm 8$	$79 \pm 20$
1,2,3,5-tetramethylbenzene	5 - 16	$62 \pm 9$	$62.4 \pm 0.8$
1,3,5-trimethylbenzene	7 - 15	$60 \pm 5$	$57 \pm 11$
1,2,4,5-tetramethylbenzene	6 - 16	$59 \pm 12$	$55.5 \pm 3.4$
$\alpha$ -pinene	7 - 13	$53 \pm 8$	$53 (^{+22}_{-15})$
1,2,4-trimethylbenzene	4 - 10	$34 \pm 3$	$33 \pm 8$
1,2,3-trimethylbenzene	5 - 10	$38 \pm 4$	$33 \pm 8$
<i>m</i> -xylene	3 - 6	$21 \pm 3$	$23 \pm 3$
<i>o</i> -xylene	2 - 5	$10 \pm 4$	$13 \pm 3$
1,2-diethylbenzene	0.3 - 3	$-9 \pm 20$	
1,3-diethylbenzene	2 - 5	$5 \pm 30$	
1,4-diethylbenzene	1 - 7	$7 \pm 30$	

The rate coefficient for the OH + isoprene reaction measured here was in excellent agreement with the others presented in this work, of  $104 (\pm 6)$  and  $103 (\pm 5) \times 10^{-12} \text{ cm}^3 \text{ molecule}^{-1} \text{ s}^{-1}$  for monoterpenes mixture 1 and the alkenes mixture respectively (see Chapter 3). The same was also true of the  $\alpha$ - and  $\beta$ -pinene + OH measurements, with results of  $56 (\pm 6)$  and  $78 (\pm 11)$ , and  $53 (\pm 4)$  and  $75 (\pm 12) \times 10^{-12} \text{ cm}^3 \text{ molecule}^{-1} \text{ s}^{-1}$  for monoterpenes mixture 1 and the alkenes mixture respectively. The results presented here for the two xylene isomers were also in good agreement with others in this work, both in this Chapter in the small aromatic VOCs mixture, and in Chapter 3.

#### 4.1.2.4 Calculation of new rate coefficients

The three diethylbenzene isomers included as part of this mixture had no available measurements of their rate coefficients for reaction with OH in the literature at the time of writing. The values reported in this work therefore represent the first measurements.

Unfortunately, the measured rate coefficients for the reactions of OH with all three diethylbenzene isomers were unreliable. The values were all low and appeared to be inconsistent with other rate coefficients for reactions between similarly sized aromatic compounds and OH. The values all had large uncertainties placed upon them, owing mostly to the observed depletions in their concentrations after reaction with OH being highly inconsistent and varying to a large extent with the OH reactivity of the tested mixture. In some cases, their observed depletions were much less than a couple of percent and their calculated depletion factors were the lowest for all the compounds within the mixture. This resulted in the calculation of some negative  $k$  values when the  $y$ -intercept of the linear regression was greater than the observed depletion factors.

Removing the values with  $k$  less than zero before averaging gave a more sensible final rate coefficient for the reactions of 1,2-diethylbenzene, 1,3-diethylbenzene and 1,4-diethylbenzene with OH, of  $6.2 (\pm 4)$ ,  $16 (\pm 8)$  and  $22 (\pm 5) \times 10^{-12} \text{ cm}^3 \text{ molecule}^{-1} \text{ s}^{-1}$  respectively. Whilst the uncertainties were significantly reduced by removing the negative  $k$  values, there was no valid reason for doing so.

In the absence of any literature experimental results for comparison, it was difficult to come to a meaningful conclusion on the certainty of the data presented here for the diethylbenzene isomers. It may therefore be more appropriate to recommend rate coefficients for their reactions with OH that are smaller than the extent of the errors in their measured values; this yields estimates of less than  $30 \times 10^{-12} \text{ cm}^3 \text{ molecule}^{-1} \text{ s}^{-1}$ .

**Table 4.6** Recommended  $k$  values for the reactions between OH and the diethylbenzene stereoisomers, given the uncertainty in their measured values.

Name	Measured $k$ (295 K) / $10^{-12} \text{ cm}^3 \text{ molecule}^{-1} \text{ s}^{-1}$
1,2-diethylbenzene	< 30
1,3-diethylbenzene	< 30
1,4-diethylbenzene	< 30

### 4.1.2.5 Comparison to SARs

Rate coefficients estimated using SARs by Kwok and Atkinson (1995) and Jenkin et al. (2018) were used as comparisons for the measured rate coefficients for the reactions of compounds in the small aromatics mixture with OH in Section 4.1.2.5. The same two SARs were applied to estimate the rate coefficients for the reactions of the larger aromatics with OH, the results of which are given in Table 4.7.

**Table 4.7** List of VOCs, in descending order of evaluated literature  $k$  value, in the large aromatics mixture along with their SAR derived  $k$  values, average experimentally measured  $k$  value and evaluated literature  $k$  value.

Name	Rate coefficient for reaction with OH / $10^{-12} \text{ cm}^3 \text{ molecule}^{-1} \text{ s}^{-1}$			
	This work	Kwok and Atkinson (1995) SAR	Jenkin et al. (2018) SAR	Evaluated literature
1,2,3,5-tetramethylbenzene	$62 \pm 9$	$43 \pm 22$	$60 \pm 24$	$62.4 \pm 0.8$
1,3,5-trimethylbenzene	$60 \pm 5$	$35 \pm 18$	$60 \pm 25$	$57 \pm 11$
1,2,4,5-tetramethylbenzene	$59 \pm 12$	$20 \pm 10$	$57 \pm 23$	$55.5 \pm 3.4$
1,2,4-trimethylbenzene	$34 \pm 3$	$16 \pm 8$	$31 \pm 12$	$33 \pm 8$
1,2,3-trimethylbenzene	$38 \pm 4$	$16 \pm 8$	$31 \pm 12$	$33 \pm 8$
<i>m</i> -xylene	$21 \pm 3$	$13 \pm 7$	$23 \pm 9$	$23 \pm 3$
<i>o</i> -xylene	$10 \pm 4$	$6.2 \pm 3$	$14 \pm 6$	$13 \pm 3$
1,2-diethylbenzene	$-9 \pm 20$	$8.1 \pm 4$	$15 \pm 6$	
1,3-diethylbenzene	$5 \pm 30$	$14 \pm 7$	$25 \pm 10$	
1,4-diethylbenzene	$7 \pm 30$	$8.1 \pm 4$	$15 \pm 6$	

Figure 4.11 shows a comparison between the two SARs, the experimentally derived values in this work and the literature reference rate coefficients. It was quite clear that the SAR by Jenkin et al. (2018), the experimental measurements and the literature reference values were in excellent agreement for all but the diethylbenzene isomers. The SAR method in Kwok and Atkinson (1995) consistently underpredicted the rate coefficients for reaction between OH and all the aromatic VOCs, with the discrepancy increasing with the increasing size and number of substituent groups.

The results for the diethylbenzene stereoisomers were in poor agreement. Not only did the SAR estimated values by Jenkin et al. (2018) disagree strongly with the experimentally derived results (unless accounting for the disproportionately large uncertainties), but the experimental results were also smaller than those estimated by the SAR in Kwok and Atkinson (1995).

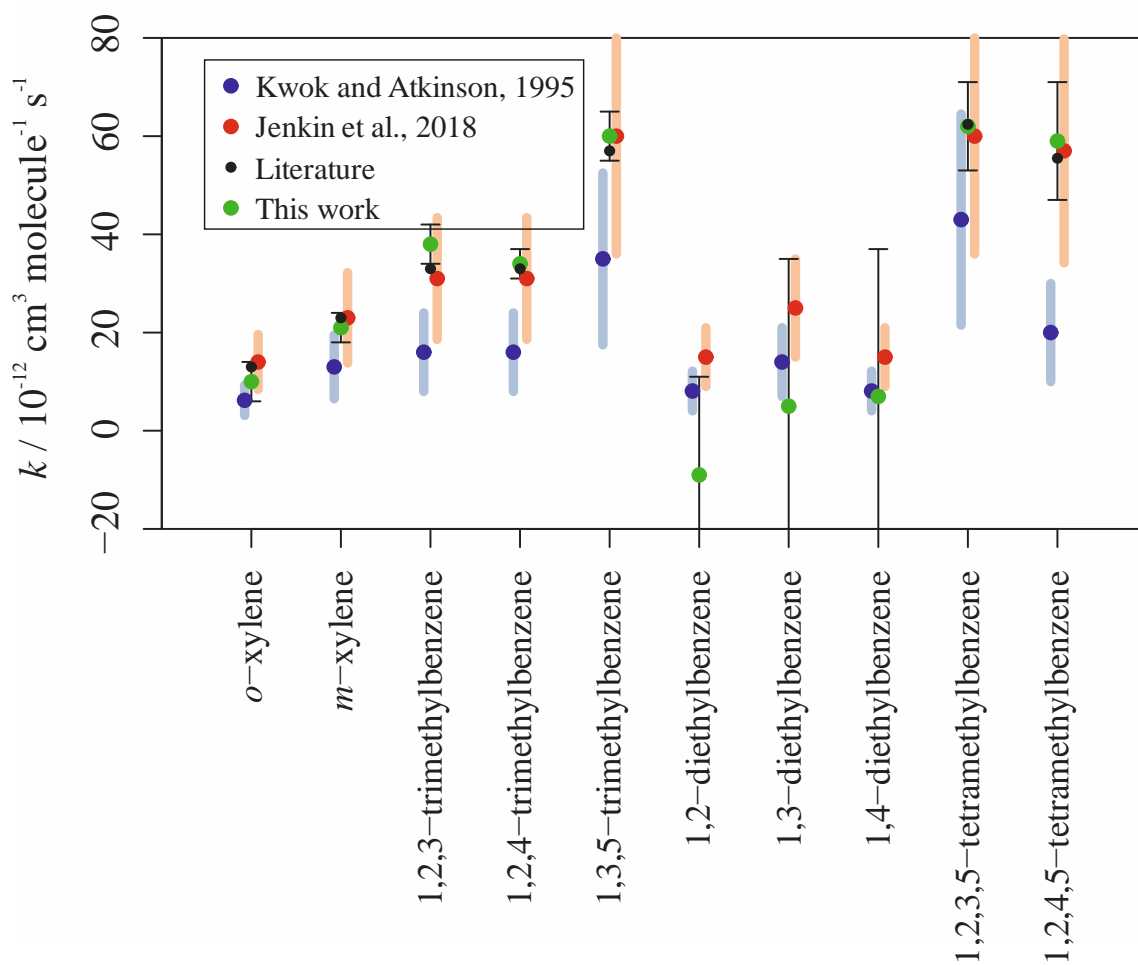


**Figure 4.11** Comparison of two different SAR methods (Kwok and Atkinson (1995), blue; Jenkin et al. (2018), red) for the prediction of rate coefficients for the reaction between aromatic VOCs and OH, alongside the experimental results derived in this work (green) and the recommended literature values (black).

## 4.2 Numerical simulations

### 4.2.1 Understanding the fate of the OH-aromatic adduct

It is currently thought that the OH-aromatic adduct, produced by OH addition onto an aromatic ring, is thermally unstable and can undergo back-decomposition to the original aromatic species (see Chapter 1 Section 1.3.4). The reversibility of the OH + aromatic reactions, shown in Figure 4.12, may result in complications in the relative rate studies of these species, particularly at elevated temperatures where the decay is faster. The measured final concentration of each VOC may be perturbed if the original aromatic species is regenerated. This would mean that the final VOC concentrations, as measured by the GC-MS, were no longer proportional to their rate coefficients for reaction with OH. Rather, they would be proportional to some ratio of the forwards ( $k$ ) and backwards ( $k_d$ ) rate coefficients for reaction with OH.

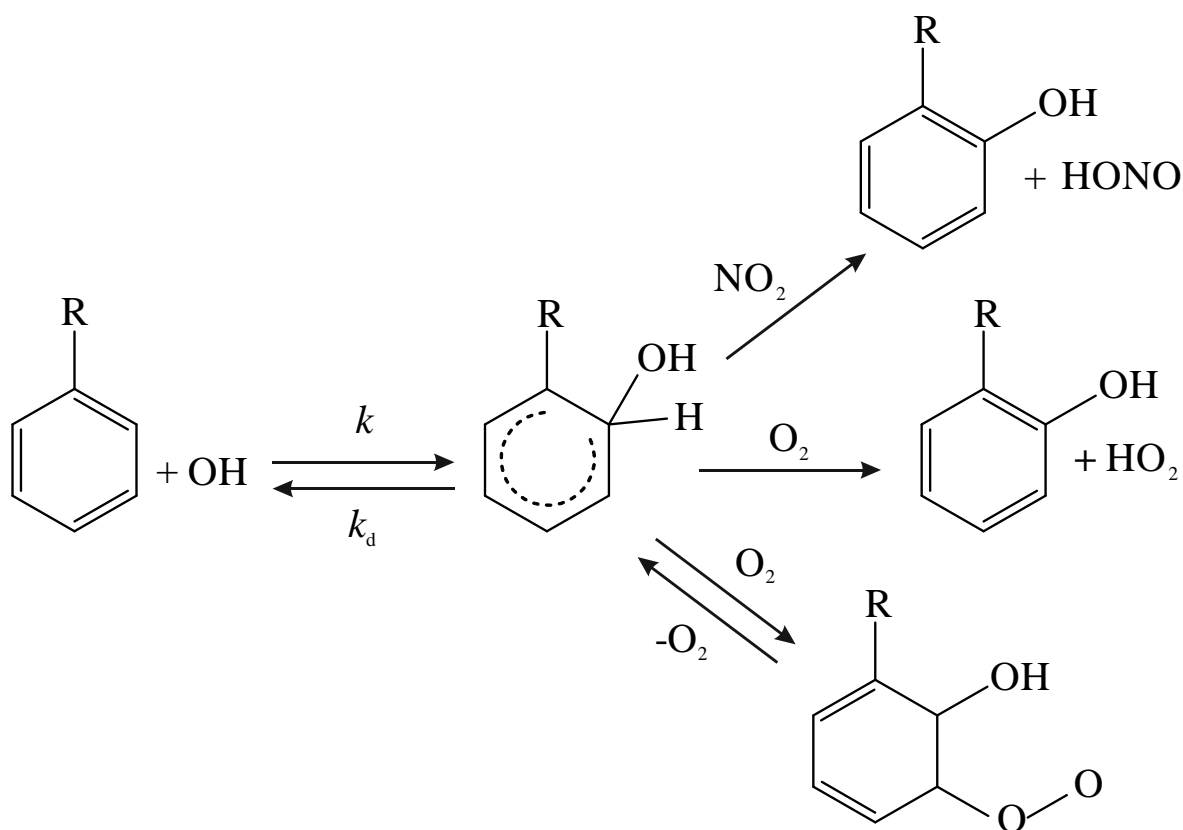


**Figure 4.12** Schematic showing the proposed decay of the OH-aromatic adduct back to the original aromatic reactant and OH. Other potential OH-aromatic adduct reactions are also shown. Schematic adapted from Newland et al., 2017.

Wahner and Zetsch (1983) measured the decay rate coefficient for the OH-benzene adduct as  $k_d = 1.95 (\pm 0.2) \text{ s}^{-1}$  at 298 K, and  $11.5 (\pm 1) \text{ s}^{-1}$  at 312 K. Knispel et al. (1990) measured thermal decomposition rate coefficients at different temperatures for the OH-benzene and OH-toluene adducts. They were able to derive Arrhenius expressions of  $k_d = 9.0 \times 10^{12} \text{ e}^{-8570/T}$  and  $1.5 \times 10^{12} \text{ e}^{-7880/T} \text{ s}^{-1}$  for OH-benzene and OH-toluene decomposition respectively. The expression for OH-benzene decay was in good agreement with that recommended by Atkinson (1989) of  $k_d = 9.4 \times 10^{12} \text{ e}^{-8540/T} \text{ s}^{-1}$ . Perry et al. (1977) reported rate parameters for the thermal decomposition of several OH-aromatic adducts allowing for the derivation of Arrhenius expressions for the decays of OH-aromatic adducts of benzene, toluene, *o*-, *m*- and *p*-xylene and 1,2,3-, 1,2,4- and 1,3,5-trimethylbenzene (Calvert et al., 2002).

The thermal decay of the OH-aromatic adduct is in direct competition with reaction with  $\text{O}_2$  and  $\text{NO}_2$ . Reaction with  $\text{NO}_2$  is unlikely, both in the atmosphere and in the experimental reactive system. However, it is possible that some amount of  $\text{O}_2$  was present in the reactor, owing to impurities in the  $\text{N}_2$  bath gas. If the  $\text{N}_2$  (zero-grade, BOC) was assumed to be 99.998% pure, the concentration of  $\text{O}_2$  in the reactor could have been as much as  $10^{16} \text{ molecules cm}^{-3}$ .

Knispel et al. (1990) measured the reactivity of the OH-benzene adduct towards  $\text{O}_2$  as  $2 \times 10^{-16} \text{ cm}^3 \text{ s}^{-1}$ , and that for the OH-toluene adduct as  $5 \times 10^{-16} \text{ cm}^3 \text{ s}^{-1}$ . More recently, Koch et al. (2007) measured the rate coefficients for the  $\text{O}_2$  addition reactions to the OH-aromatic adducts of benzene, toluene, and *m*- and *p*-xylene across the temperature range 298-354 K (benzene,  $3.5 \times 10^{-14} \text{ e}^{-1600/T}$ ; toluene,  $5.9 \times 10^{-16} \text{ e}^{-20/T}$ ; *m*-xylene,  $2.7 \times 10^{-16} \text{ e}^{580/T}$ ; *p*-xylene,  $3.8 \times 10^{-16} \text{ e}^{250/T}$ ).

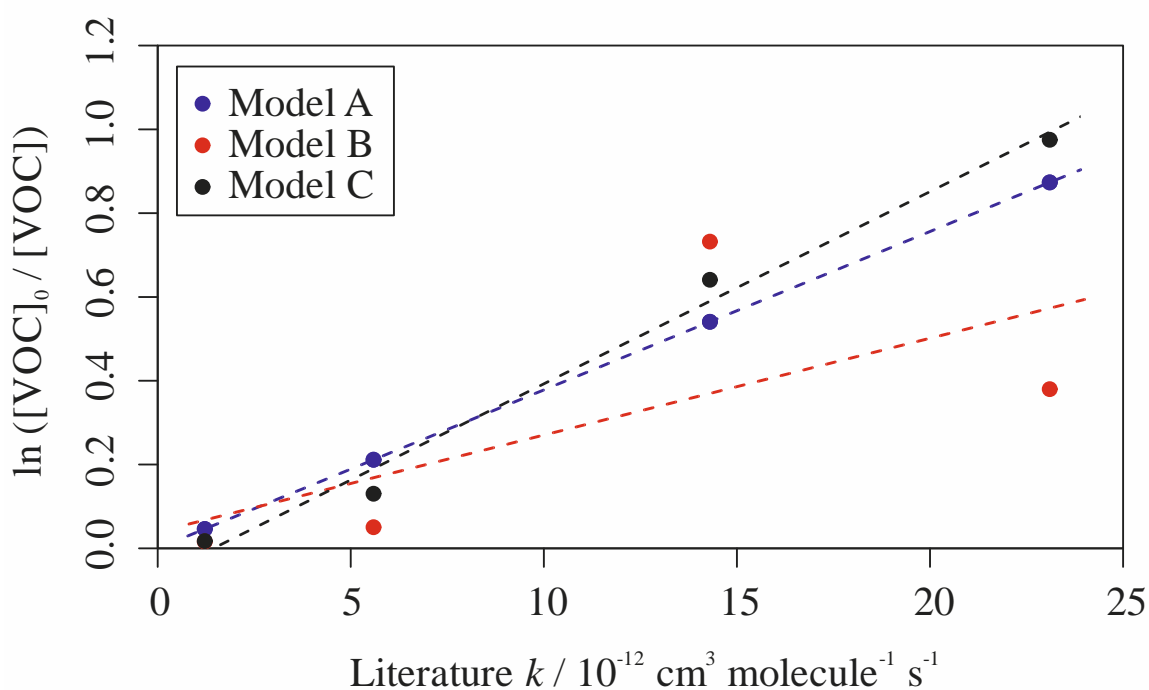
### 4.2.1.1 Simulating the decomposition of the OH-aromatic adducts

A simple kinetic simulation was built in Kintecus (Ianni, 2017; <http://kintecus.com/>) to model the impact that the back-decomposition of the OH-aromatic adduct might have had on the relative rate experiments under the conditions reported in this work. The model included Arrhenius expressions for the reactions between OH and benzene, toluene and *m*- and *p*-xylene. The products of these reactions were assumed to be exclusively OH-aromatic adducts due to the relatively minor importance of the H-abstraction reaction pathway (e.g. as little as 7% for the toluene + OH reaction). The OH-aromatic adducts could then react in two ways; decay back into the original aromatic species, or react with O<sub>2</sub>. Arrhenius expressions for both of these reactions for each of the four aromatic species were incorporated into the model. The decay of the OH-aromatic adducts and the reaction between O<sub>2</sub> and the OH-aromatic adducts could be turned off. Table 4.8 displays the different scenarios investigated and the reactions simulated under different modelling conditions. For all simulations, the initial OH concentration was kept at  $2 \times 10^{11}$  molecules cm<sup>-3</sup> and for Model C, the initial O<sub>2</sub> concentration was set to  $1 \times 10^{16}$  molecules cm<sup>-3</sup>.

**Table 4.8** Different simulation scenarios.

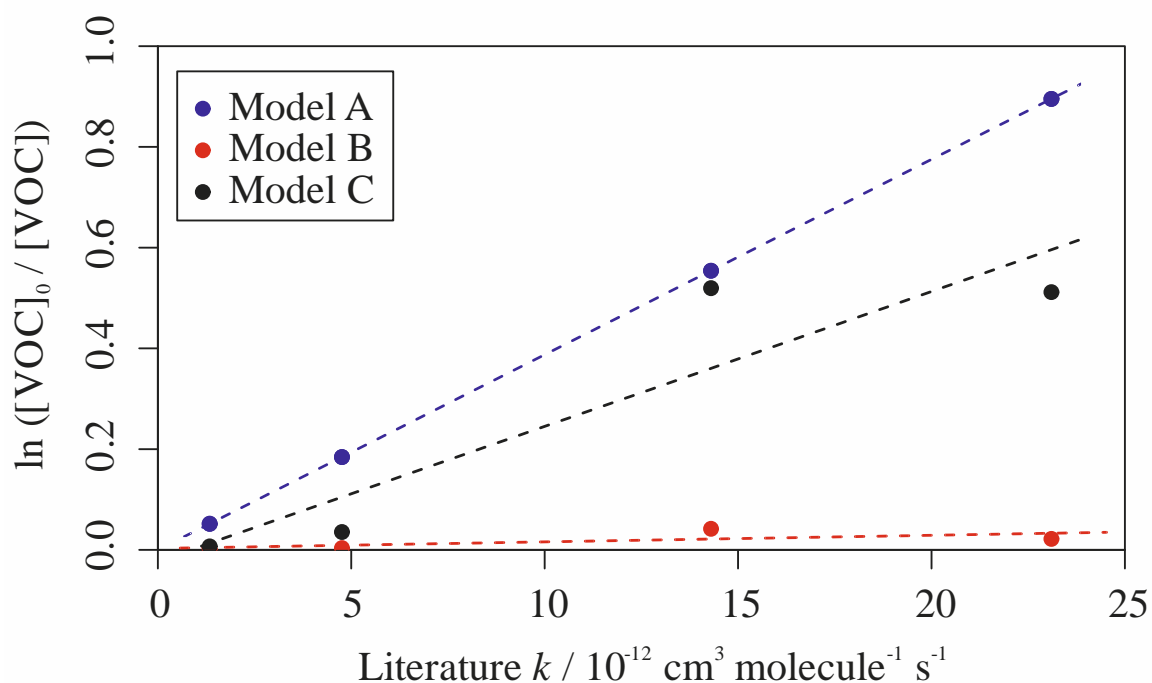
Model name	OH + aromatic	OH-aromatic adduct decay	OH-aromatic adduct + O <sub>2</sub>
Model A	Yes	No	No
Model B	Yes	Yes	No
Model C	Yes	Yes	Yes

Figure 4.13 shows the simulated relationships at 300 K. Model A resulted in the correct relationship between depletion factor and literature  $k$  value, with an  $R^2$  value of 1.0. However, Models B and C did not yield the correct relationship, although Model C gave a  $OH_{exp}$  result similar to that given by Model A. Model B, in which the OH-aromatic adducts could decay back to the original aromatic species, yielded a particularly bad result, with an adjusted  $R^2$  value of just 0.173. Whilst Model C did not simulate an  $R^2$  equal to 1, the adjusted  $R^2$  value of 0.981 was high enough that it could be assumed to. In this case, at 300 K, the  $O_2 + OH$ -aromatic reaction proceeded at a rate fast enough to prevent significant amounts of the OH-aromatic adducts undergoing back-decomposition to the original aromatic species.



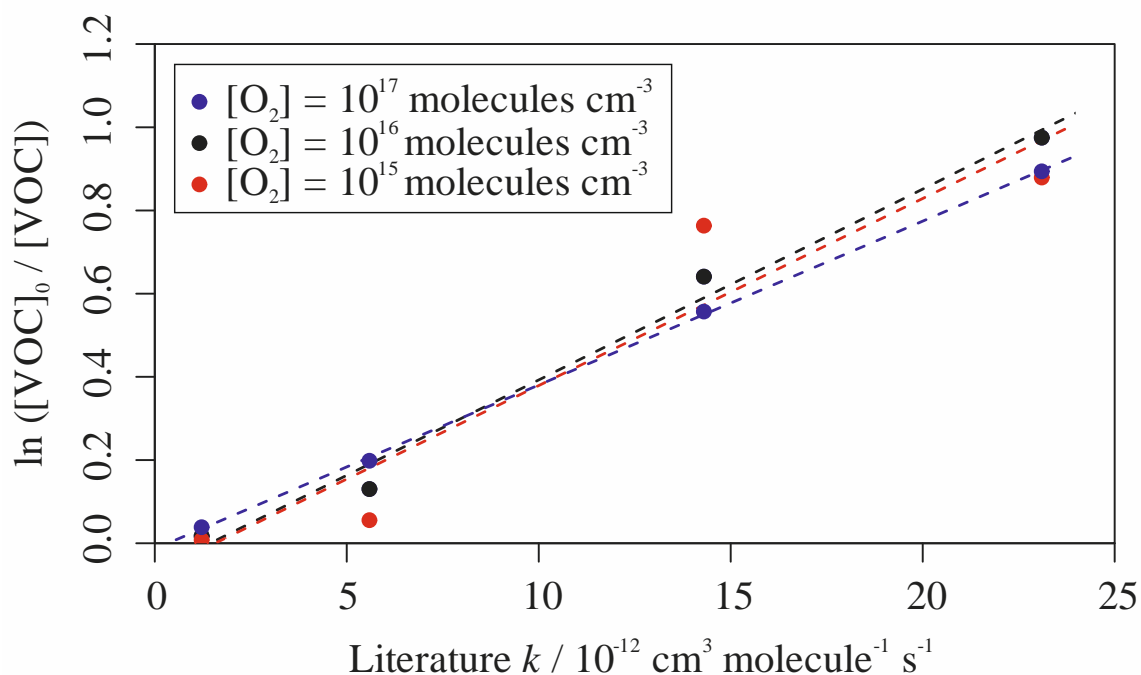
**Figure 4.13** Simulated relative rate plot for the four aromatic VOCs incorporated in the numerical simulations under different modelling scenarios at 300 K. From left to right the points can be identified as; benzene, toluene, *p*-xylene and *m*-xylene. The adjusted  $R^2$  values for the linear fits were: Model A, 1.00; Model B, 0.173; Model C, 0.981.

Figure 4.14 shows the same simulation but at 350 K. Again, the correct relationship was simulated when using Model A, with an  $R^2$  equal to 1.00. However, when using Model B, not only was the  $R^2$  value exceptionally low (0.187) but the simulated depletion factors for the four species were also very small. This is consistent with the proposed theory; the decay of the OH-aromatic adduct is highly temperature dependent and proceeds rapidly at temperatures exceeding 325 K. The temperature dependence of the back-decomposition at 350 K was to the extent that the equilibrium between the aromatic species and the OH-aromatic adducts moved towards the aromatic species. Hence, the aromatic VOCs showed little-to-no depletion after exposure to OH. Even with the inclusion of  $10^{16}$  molecules  $\text{cm}^{-3}$   $\text{O}_2$  in Model C, the relationship between depletion factor and literature  $k$  remained inconsistent with an adjusted  $R^2$  value of 0.771.



**Figure 4.14** Simulated relative rate plot for the four aromatic VOCs incorporated in the kinetic simulations under different modelling scenarios at 350 K. From left to right the points can be identified as; benzene, toluene, *p*-xylene and *m*-xylene. The adjusted  $R^2$  values for the linear fits were: Model A, 1.00; Model B, 0.187; Model C, 0.771.

The concentration of  $O_2$  in the reactor had not been measured; the  $[O_2]$  used for the simulations above was estimated using the purity of the  $N_2$  carrier gas, but is potentially misleading. For this reason, simulations using Model C were performed with different concentrations of  $O_2$ . Figure 4.15 shows the impact of higher and lower concentrations of  $O_2$ , of  $10^{15}$  and  $10^{17}$  molecules  $cm^{-3}$  respectively, at 300 K. As expected, the relationship between depletion factor and literature  $k$  improved when using a greater simulated  $[O_2]$  but reduced when using a lower  $[O_2]$ . The adjusted  $R^2$  values for the linear relationships are 0.856, 0.981 and 1.00 (0.9995 to 4 sf) for the simulations with  $10^{15}$ ,  $10^{16}$  and  $10^{17}$  molecules  $cm^{-3}$  of  $O_2$  respectively. Therefore, if the estimated reactor  $[O_2]$  (of  $10^{16}$  molecules  $cm^{-3}$ ) was an underestimation of the concentration in the real system, then the assumption that the OH-aromatic adducts did not undergo back decomposition is only improved. However, if the estimate of  $[O_2]$  in the reactor was an overestimation, then it was likely that the OH-aromatic adducts underwent some back-decomposition and the measured relationship between depletion factor and literature  $k$  is therefore less reliable.



**Figure 4.15** Comparison of the impact that different concentrations of  $O_2$  had on the simulated relative rate plots for four aromatic VOCs at 300 K. The  $R^2$  values were 0.856, 0.981 and 1.00 for  $[O_2] = 10^{15}$ ,  $10^{16}$  and  $10^{17}$  molecules  $cm^{-3}$  respectively.

$O_2$  is not the only species that may prevent the OH-aromatic adducts undergoing back decomposition. Other chemicals, such as NO,  $NO_2$ ,  $HO_2$  and  $RO_2$ , may perform a similar role but it is unlikely that they were present in the reactor in any significant concentration.

For Model B, as the temperature increased it becomes less appropriate to plot depletion factor against literature rate coefficient for the reaction with OH. The depletion in the VOCs instead became proportional to the ratio of the forwards and backwards rate coefficient for reaction with OH, as in Eq. 4.2.

$$\ln\left(\frac{[\text{VOC}]_0}{[\text{VOC}]}\right) \propto \frac{k_{\text{OH+aromatic}}}{k_d} \quad \text{Eq. 4.2}$$

This relationship is supported by Figure 4.16, where plotting depletion factor against literature  $k/k_d$  resulted in an adjusted  $R^2$  for the linear regression of 1.00. Hence, at higher temperatures ( $T > 325$  K) and very low  $[\text{O}_2]$ , it may be more appropriate to use this type of plot to yield an estimate of the ratio between  $k$  and  $k_d$  for aromatic VOC + OH reactions.

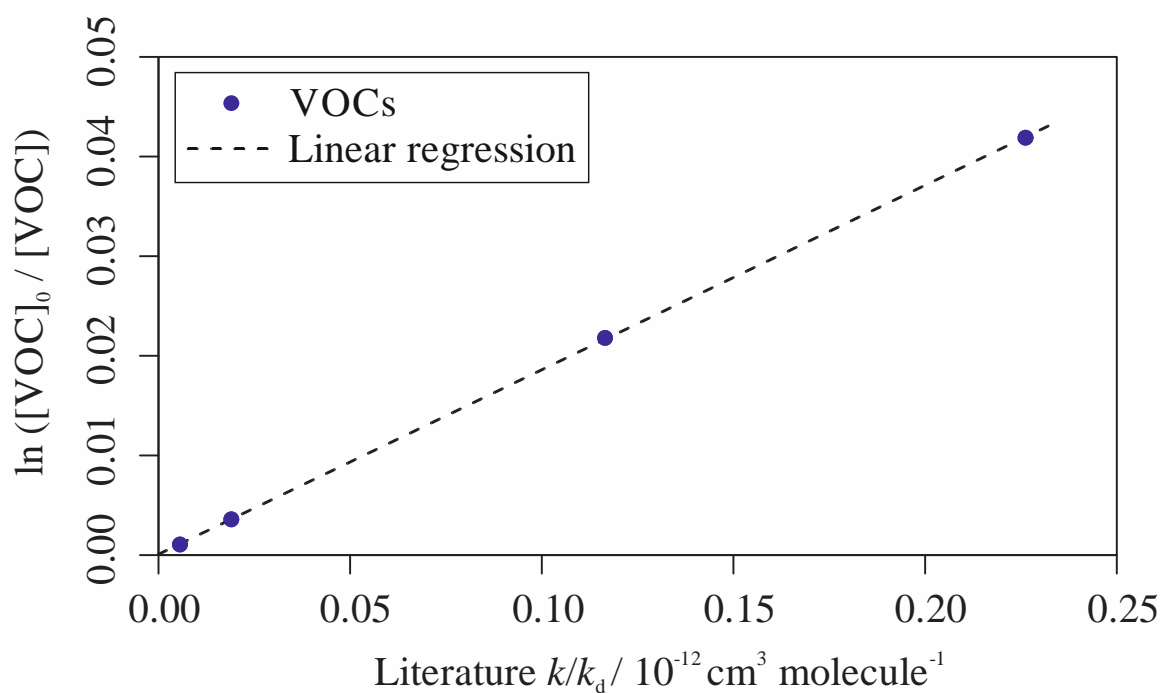


**Figure 4.16** Simulated relative rate plot for the four aromatic VOCs at 350 K. Rather than plotting depletion factor against  $k$ , as in typical relative rate plots, the depletion factor was plotted against the ratio of  $k$  to  $k_d$ , to account for the thermal back-decomposition of the aromatic-OH adducts. The adjusted  $R^2$  value for the linear regression was equal to 1.00 showing that aromatic VOC depletions at higher temperatures are proportional to this ratio.

For Model C, the simulated relative rate relationship was most appropriate when also incorporating the rate coefficient for the reaction between the OH-aromatic adduct and O<sub>2</sub>, as in Eq. 4.3 and demonstrated in Figure 4.17.

$$\ln\left(\frac{[\text{VOC}]_0}{[\text{VOC}]}\right) \propto \frac{k_{\text{OH+aromatic}} \times k_{\text{adduct+O}_2}}{k_d} \quad \text{Eq. 4.3}$$

Hence, at high temperatures ( $T > 325$  K) and high [O<sub>2</sub>], the depletion in aromatic VOCs is no longer proportional to just the rate coefficient for the forwards reaction with OH, but a balance of the rate coefficients for the various reactions involved in the photochemical oxidation scheme for the aromatic VOC.

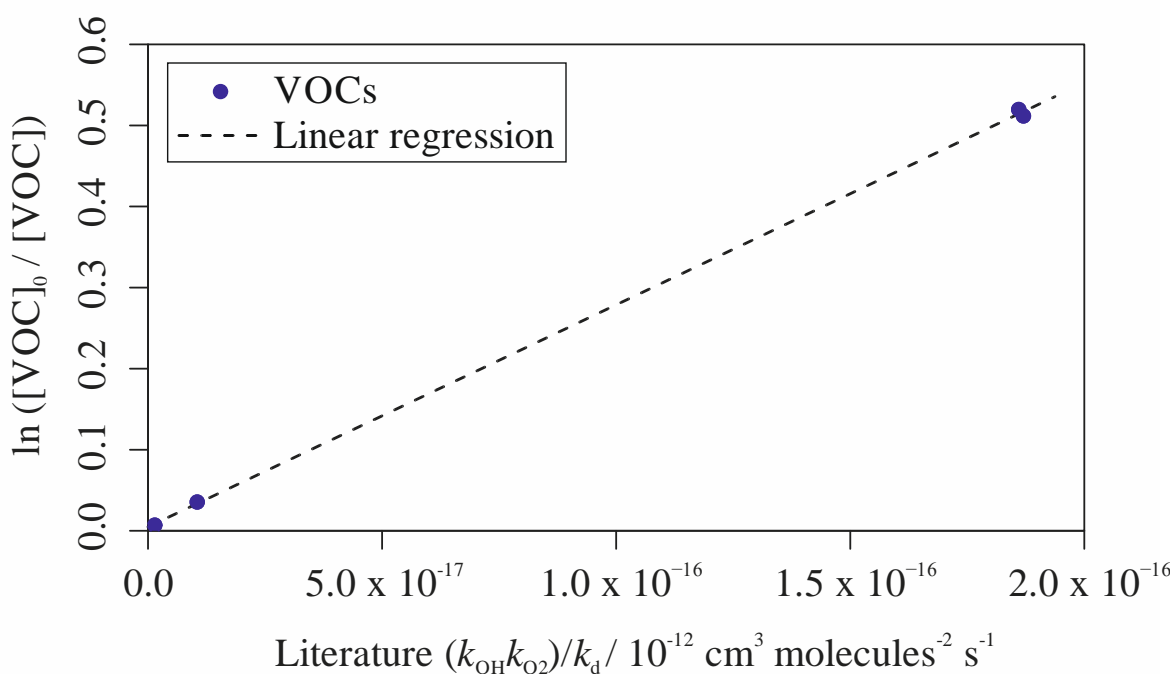


**Figure 4.17** Model C simulated depletion factor at 350 K for four aromatic VOCs plotted against a different parameter to the normal relative rate plots. Here, simulated depletion factor was plotted against the ratio between the forwards rate coefficient for the reaction forming the OH-aromatic adduct and the rate coefficient for the decay of the OH-aromatic, or  $k \times k_{\text{O}_2} / k_d$ . The adjusted R<sup>2</sup> value for the linear regression was equal to 1.00.

### 4.2.1.2 Summary

The thermal instability of the primary product of the OH initiated oxidation of aromatic species may complicate the relative rate nature of experiments conducted at  $T > 300$  K. The potential decay of the OH-aromatic adducts formed via these reactions back into the original aromatic compound and the OH radical, meant that the experimentally measured concentrations of each aromatic species may not have been totally consistent with their relative rates of reaction.

At temperatures below 300 K, and with  $O_2$  concentrations of greater than  $10^{16}$  molecules  $cm^{-3}$ , the decomposition reaction was shown to not significantly affect the results during simulations. At  $T < 300$  K, the decay of the OH-aromatic adduct is relatively slow, with the reaction between the adduct and  $O_2$  proceeding at a much quicker rate. The OH-aromatic adduct +  $O_2$  reaction dominated to the point that the decay could be ignored. Therefore, at these temperatures, the measured depletions of the aromatic species should be relative to their rate coefficients with OH.

As the reactions in this work were conducted at temperatures below 300 K, and with a large enough estimated  $[O_2]$  concentration, it was assumed that the back-decomposition did not affect the experimental results.

However, the back-decomposition of the OH-aromatic is highly dependent on temperature. At elevated temperatures, where  $T > 300$  K, the relationship between simulated depletion factor and literature  $k$  value was shown to become increasingly inappropriate. The concentration of  $O_2$  estimated to be present in the reactor was not significant enough to prevent decay of the OH-aromatic adducts back into the original species. For this reason, the simulated depletions for the aromatic species were not relative to their rate coefficients for reaction with OH. Instead, the relationship between depletion factors was better modelled by plotting against  $k_{OH+aromatic} \times k_{OH-aromatic+O_2} / k_d$ . However, values of  $k_{OH-aromatic+O_2}$  and  $k_d$  for many OH-aromatic adducts were not available in the literature at the time of writing.

## 4.2.2 Simulating the impact of NO

A numerical simulation was built using the Kintecus package to assess the impact of NO on the oxidation of aromatic VOCs. The simulation contained oxidation schemes for nine small aromatic compounds (toluene, ethylbenzene, *n*-propylbenzene, isopropylbenzene, *m*- and *o*-xylene and 2-, 3- and 4-ethyltoluene) which were adapted from the MCM (Jenkin et al., 2003; Bloss et al., 2005; <http://mcm.leeds.ac.uk/MCM>; accessed 14/02/2018). The oxidation schemes input into the numerical simulation did not include any reactions involving O<sub>3</sub> or NO<sub>3</sub>, which should not be present in the reactor in any significant quantities and did not include reactions involving RO<sub>2</sub> as a reactant.

The model comprised a total of 160 reactions between 88 different species and incorporated some basic HO<sub>x</sub>/NO<sub>x</sub> chemistry, the reactions of which are outlined in Table 4.9. Reaction 4.2 involved the formation of secondary OH, which was indicated by *sOH* in the simulation. OH present at the start of the simulation was indicated by *pOH*. Reaction products which were preceded by either an α or β were modelled separately, so that the impact of primary and secondary OH could be assessed individually.



**Table 4.9** List of HO<sub>x</sub>/NO<sub>x</sub> reactions included in the numerical simulation testing the impact of NO on the oxidation of aromatic VOCs.

Reaction	$k / 10^{-12} \text{ cm}^3 \text{ molecule}^{-1} \text{ s}^{-1}$	Reference
$\text{pOH} + \text{HO}_2 \rightarrow \alpha\text{H}_2\text{O} + \text{O}_2$	110	Atkinson et al. (2006)
$\text{sOH} + \text{HO}_2 \rightarrow \beta\text{H}_2\text{O} + \text{O}_2$	110	Atkinson et al. (2006)
$\text{HO}_2 + \text{NO} \rightarrow \text{sOH} + \text{NO}_2$	8.8	Atkinson et al. (2006)
$\text{pOH} + \text{NO} \rightarrow \alpha\text{HONO}$	9.7	Atkinson et al. (2006)
$\text{sOH} + \text{NO} \rightarrow \beta\text{HONO}$	9.7	Atkinson et al. (2006)
$\text{pOH} + \text{NO}_2 \rightarrow \alpha\text{HNO}_3$	65	Atkinson et al. (2006)
$\text{sOH} + \text{NO}_2 \rightarrow \beta\text{HNO}_3$	65	Atkinson et al. (2006)

Nine different scenarios were simulated, with varying concentrations of both individual VOCs and initial NO. The different scenarios are shown in Table 4.10. The small changes in the concentrations of the individual VOCs across the three different [NO] scenarios arose due to the inclusion of the extra diluting flow of NO, which increased the total flow rate through the reactor. In all nine scenarios, initial [*pOH*] and [HO<sub>2</sub>] was set to  $2.0 \times 10^{11} \text{ molecules cm}^{-3}$ , as a rough estimate of the initial *pOH* and HO<sub>2</sub> concentrations, as determined in Chapter 3, Section 3.2.1.

**Table 4.10** List of the nine different [VOC] and [NO] scenarios simulated.

Simulation No.	[VOC] / $10^{11}$ molecules $\text{cm}^{-3}$	OH reactivity / $\text{s}^{-1}$	[NO] / $10^{11}$ molecules $\text{cm}^{-3}$	[NO] / ppb
1	0.82	8.50	0	0
2	1.64	17.0	0	0
3	2.46	25.5	0	0
4	0.81	8.45	7.38	30
5	1.63	16.9	7.38	30
6	2.44	25.3	7.38	30
7	0.81	8.39	17.2	70
8	1.62	16.8	17.2	70
9	2.43	25.2	17.2	70

The following sections compare the simulated impacts of increasing the amount of NO on the concentrations of other species with respect to simulation numbers 2, 5 and 8.

4.2.2.1 Impact on  $[pOH]$ 

Figure 4.18 shows the simulated impact that different  $[NO]$  had on the concentration of  $pOH$  in the reactor. As expected, adding  $NO$  to the reactor in increasingly greater concentrations increased the rate at which  $pOH$  was removed from the reactor. This was due to the reactions between  $NO$  and  $pOH$  and  $NO_2$  and  $pOH$  acting as extra sinks for  $pOH$ , in addition to the sinks already present due to the VOCs and  $HO_2$ . At 70 ppb of  $NO$ ,  $pOH$  was removed almost entirely from the reactor within 0.94 s. This was 1.02 s quicker than when 0 ppb of  $NO$  was simulated in the reactor.

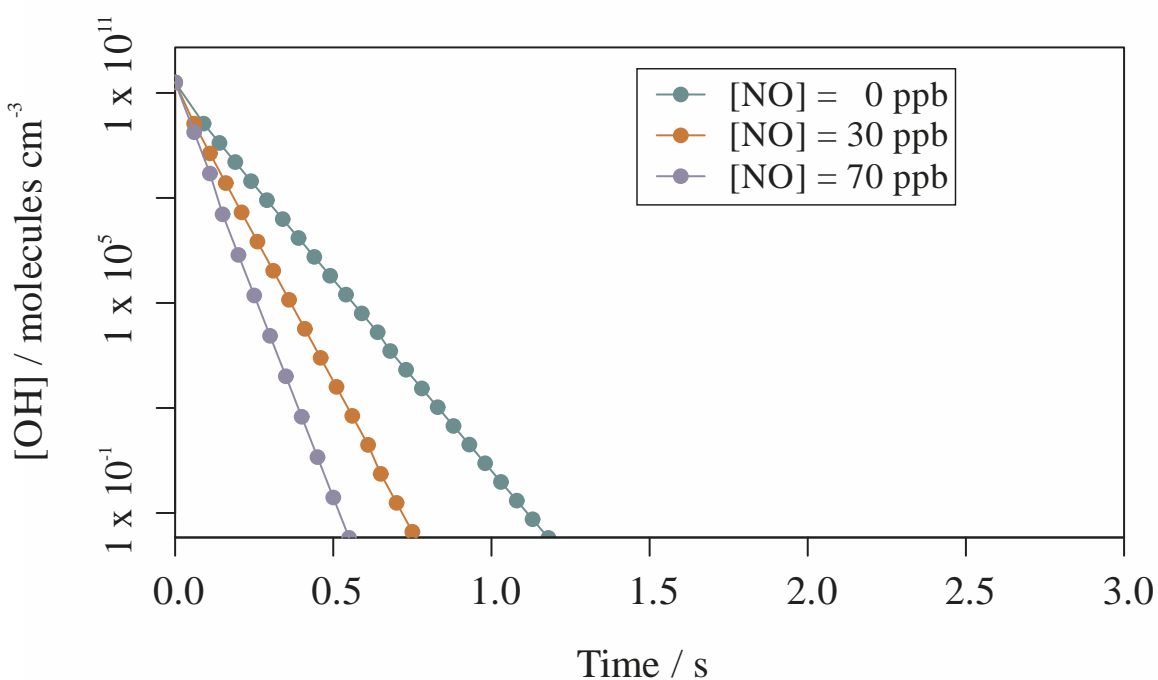


**Figure 4.18** Simulated impact of different initial concentrations of  $NO$  on the concentration of  $pOH$  over time. The concentration of  $pOH$  decreased more rapidly with an increased concentration of  $NO$ .

4.2.2.2 Impact on  $[\text{HO}_2]$ 

The impact of NO on the concentration of  $\text{HO}_2$  over time is illustrated by Figure 4.19. The rate of depletion of  $\text{HO}_2$  increased with increasing concentrations of NO, as expected, due to the reaction between NO and  $\text{HO}_2$ . In the scenario where no NO was present, the  $\text{HO}_2$  concentration initially reduced rapidly, due to the relatively quick reaction with *pOH*, but then stabilised at approximately  $4 \times 10^{10}$  molecules  $\text{cm}^{-3}$ . With NO present in the reactor, the initial rapid decrease in  $[\text{HO}_2]$  was still observed, but the  $[\text{HO}_2]$  continued to decrease beyond this due to the relatively slow reaction with NO. When simulating conditions with 70 ppb of NO, the concentration of  $\text{HO}_2$  was reduced to less than 1000 molecules  $\text{cm}^{-3}$  after 3 s.

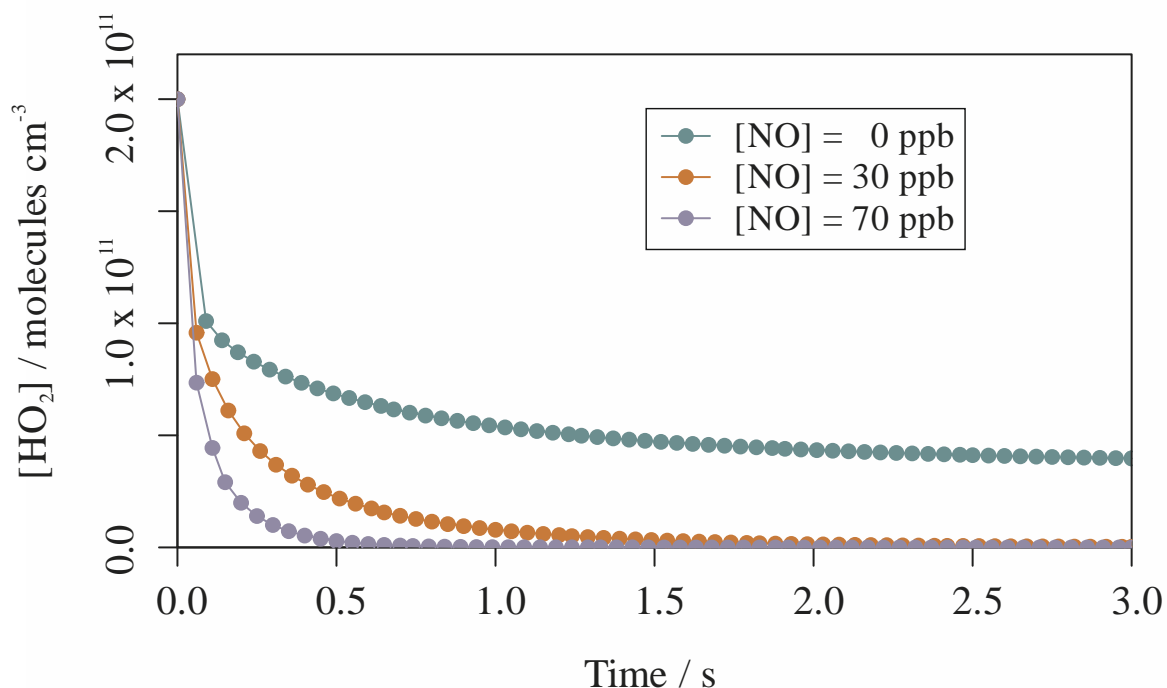


**Figure 4.19** Simulated impact of different initial concentrations of NO on the concentration of  $\text{HO}_2$  over time. The concentration of  $\text{HO}_2$  decreased more rapidly with increasing concentration of NO and was reduced to a concentration of less than 1000 molecules  $\text{cm}^{-3}$  within 3 s with a NO concentration of 70 ppb.

### 4.2.2.3 Impact on [sOH]

Secondary OH was produced by the reaction between NO and HO<sub>2</sub> (R. 4.2). Figure 4.20 shows the simulated impact that different [NO] had on the concentration of sOH. Clearly, in the simulation without NO, the formation of sOH didn't occur. However, with NO in the reactor, the concentration of sOH immediately rapidly increased, up to a value of approximately  $2 \times 10^{10}$  molecules cm<sup>-3</sup> (roughly equivalent to 1 ppb). This concentration was equal to approximately 10% of the initial primary OH concentration thought to be generated via the VUV photolysis of H<sub>2</sub>O.

After the initial rapid increase in concentration, [sOH] began to decrease rapidly. The initial decrease was much quicker with 70 ppb than with 30 ppb of NO. This was likely due to the increased sink for both pOH and sOH with respect to NO. The concentration of sOH settled after approximately 3 s in both scenarios, as it presumably reached some form of equilibrium between formation (via R. 4.1) and destruction (via reactions with VOCs, HO<sub>2</sub>, NO and NO<sub>2</sub>).

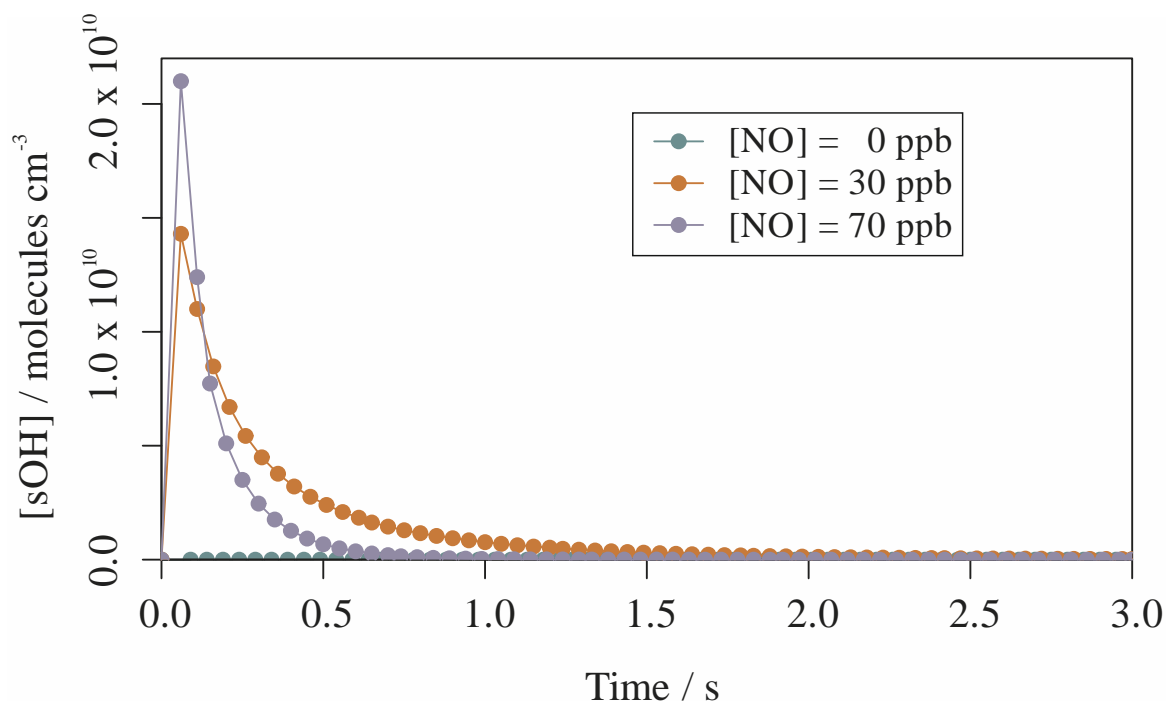


**Figure 4.20** Simulated impact of different initial concentrations of NO on the concentration of secondary OH (sOH) over time. sOH was not produced when NO wasn't present in the reactor. When NO was added to the reactor, sOH was generated rapidly, peaking at approximately  $2 \times 10^{10}$  molecules cm<sup>-3</sup> with 70 ppb NO. The concentration of sOH then decreased with time, due to reactions with VOCs, HO<sub>2</sub>, NO and NO<sub>2</sub>.

Evidence for the continued production of *sOH* is shown by Figure 4.21. The production of *sOH* continued past the peak in concentration shown in Figure 4.20 at approximately 0.1 s. *sOH* was continually produced up until approximately 1.5 s for an NO concentration of 30 ppb, and approximately 0.7 s for an NO concentration of 70 ppb, where the rate of production of *sOH* became less appreciable. The total *sOH* produced was approximately  $1.81$  and  $1.96 \times 10^{11}$  molecules  $\text{cm}^{-3}$  for NO concentrations of 30 and 70 ppb respectively, showing that many of the  $2.0 \times 10^{11}$  molecules  $\text{cm}^{-3}$  of initial  $\text{HO}_2$  were converted to secondary OH via reaction with NO.

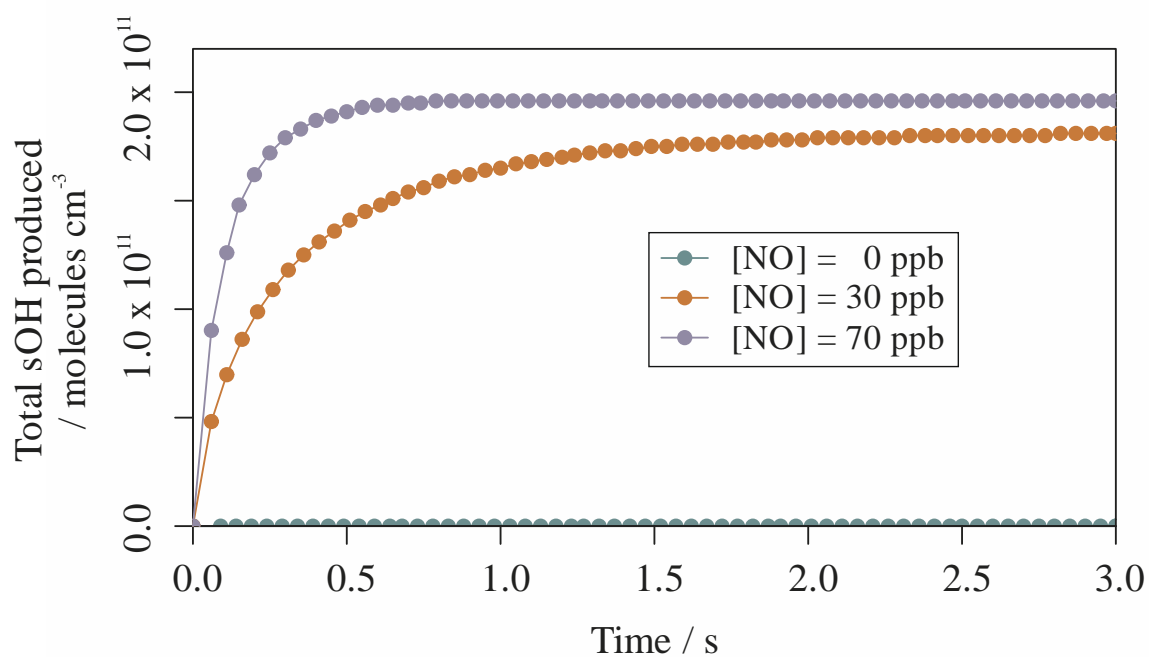


**Figure 4.21** Simulated impact of different initial concentrations of NO on the total *sOH* produced over time. *sOH* was not produced when NO wasn't present in the reactor.

4.2.2.4 Impact on [NO] and [NO<sub>2</sub>]

Figure 4.22 illustrates the simulated impact of different initial NO concentrations on the NO and NO<sub>2</sub> concentrations as a function of time. Clearly, the initial concentration of NO had an impact on the total amount of NO reacted. For an initial [NO] of 30 ppb, approximately half the initial amount of NO reacted, leaving around 15 ppb of NO in the reactor after 3 s. For an initial [NO] of 70 ppb, only approximately 26% of the initial NO was used up during reactions, although this was equivalent to 18 ppb of NO, somewhat more than in the case with less initial NO. The depletion in NO can be seen to be roughly similar to the depletion in HO<sub>2</sub>; once the HO<sub>2</sub> was used up (Figure 4.19) the [NO] stabilised, showing that HO<sub>2</sub> was the major sink for NO in the reactor.

NO<sub>2</sub> was the by-product of the OH producing reaction between HO<sub>2</sub> + NO (R. 4.2). As such, it displayed a similar temporal profile to *sOH*. For initial NO concentrations of 30 and 70 ppb, the [NO<sub>2</sub>] at 3 s was simulated to be 2.09 and 2.16 × 10<sup>11</sup> molecules cm<sup>-3</sup> (approximately 8.5 and 8.7 ppb) respectively.

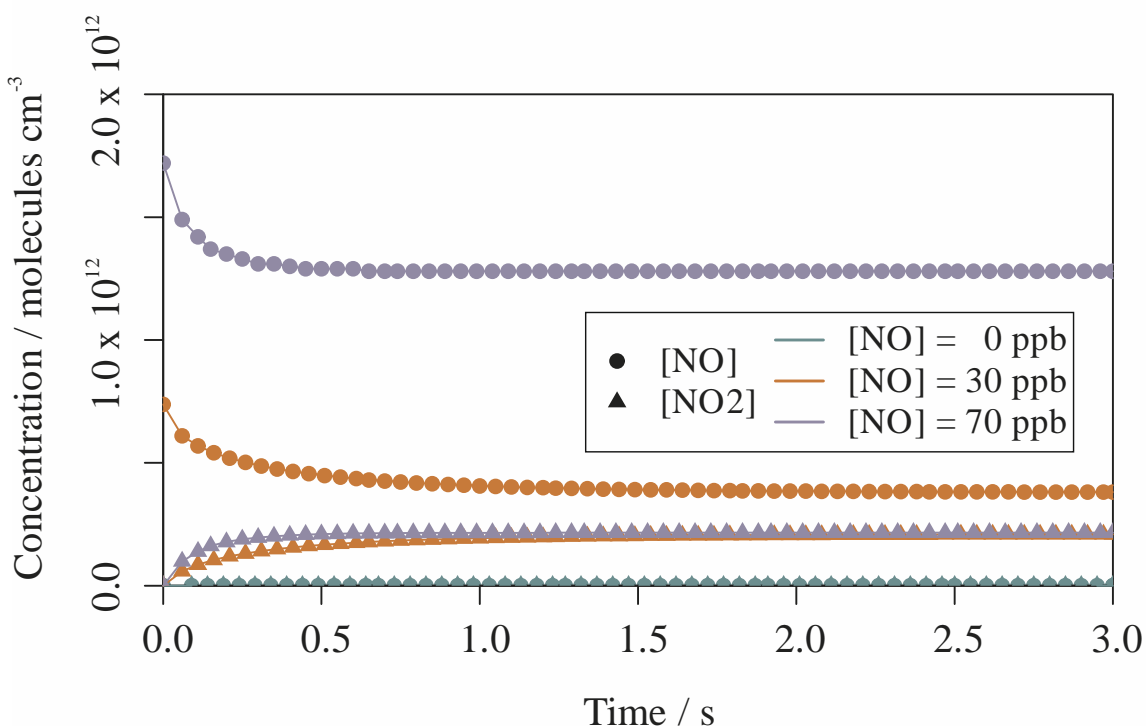


**Figure 4.22** Simulated impact of different initial concentrations of NO on the NO and NO<sub>2</sub> concentrations over time.

#### 4.2.2.5 Impact on *pOH* sinks

Figure 4.23 illustrates the impact that changing the concentration of NO had on the simulated sinks for *pOH*. The sinks for *pOH* included in the model were: reaction with HO<sub>2</sub>, reaction with primary aromatic VOCs and secondary VOCs (*sVOCs*) and reaction with NO and NO<sub>2</sub>. *sVOCs* refer to the products of initial radical + VOC reactions.

In the absence of NO, less than half of the available *pOH* reacted with the aromatic VOCs - the intended target. Over half (52.3%) of the *pOH* was simulated to react with HO<sub>2</sub>. This simulation suggested that the HO<sub>2</sub> sink was responsible for the small observed depletions in VOC concentrations during the experimental work.

However, upon addition of NO, the fraction of *pOH* reacting with VOCs actually decreased, to 30.8 and 22.2% for [NO] = 30 and 70 ppb respectively. The proportion of the *pOH* simulated to react with HO<sub>2</sub> showed a similar reduction, to 36.3% and 25.6% for [NO] = 30 and 70 ppb respectively. The additional sink to NO accounted for much of this reduction in the sinks towards reaction with VOCs and HO<sub>2</sub>, with NO<sub>2</sub> and secondary VOCs also having a minor contribution.

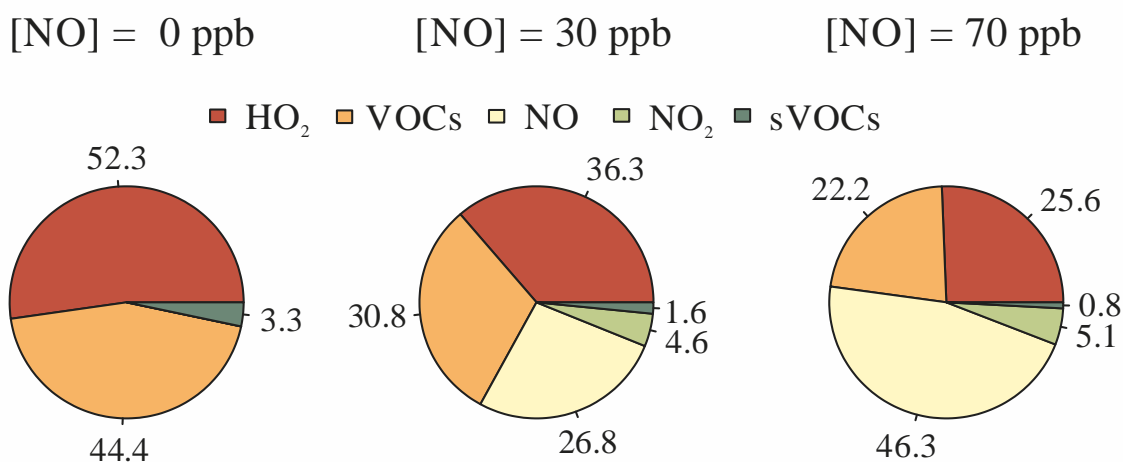


**Figure 4.23** Simulated impact of different initial concentrations of NO on the sinks for *pOH*; reaction with HO<sub>2</sub>, reaction with primary VOCs, reaction with NO, reaction with NO<sub>2</sub> and reaction with secondary VOCs (*sVOCs*).

#### 4.2.2.6 Impact on *sOH* sinks

The simulated impacts of different NO concentrations on the sinks for secondary OH are shown in Figure 4.24. Clearly, no *sOH* existed when NO was absent from the reactor, as *sOH* was not produced. When the concentration of NO in the reactor was 30 ppb, the primary aromatic VOCs were simulated to be the largest sink, accounting for 32.4% of the reacted *sOH*. NO and HO<sub>2</sub> represented the next largest sinks, accounting for 22.7% and 15.7% of the reacted *sOH* respectively.

When the concentration of NO in the reactor was increased to 70 ppb, the proportion of *sOH* reacting with VOCs decreased and NO became the dominant sink. This suggests that there may be some optimum reactor concentration of NO above which the amount of NO reacting with *sOH* actually decreases the amount of *sOH* available for reaction with the VOCs.

The sinks to NO<sub>2</sub> and *sVOCs* were much larger for *sOH* than the equivalent sinks for the primary OH. This was likely due to the delay in the formation of these species; by the time they were present in an appreciable quantity much of the primary OH had already reacted away.

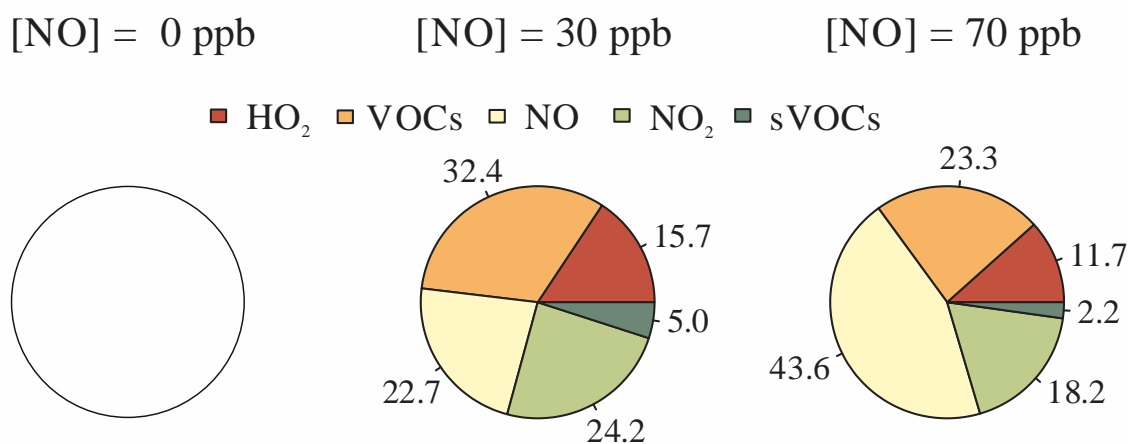


**Figure 4.24** Simulated impact of different initial concentrations of NO on the sinks for *sOH*; reaction with HO<sub>2</sub>, reaction with primary VOCs, reaction with NO, reaction with NO<sub>2</sub> and reaction with secondary VOCs (*sVOCs*).

#### 4.2.2.7 Impact on VOCs

NO was added to the reactor to increase the depletion in the VOCs' concentrations. This appeared to work during experimental studies, with larger depletion factors observed for the majority of VOCs with increasing concentrations of NO. **Figure 4.25** shows the simulated impacts of different concentrations of NO on the VOC depletions.

In the absence of NO, the total amount of VOCs simulated to react with OH was just 6.1%; the remaining 93.9% of the VOCs were left unreacted. Adding NO with a concentration of 30 ppb increased the simulated amount of reacted VOC, to a total of approximately 8.2%. 4.0% of this was due to reaction with the secondary OH, and 4.2% due to reaction with the primary OH. The proportion of VOCs reacting with primary OH was therefore reduced, compared with the case without NO. This was, however, mitigated by a similar proportion of VOCs reacting with the *sOH*, produced as a result of the added NO. The percentage of VOCs left unreacted was simulated to be approximately 91.8%, a reduction of just over 2%. This provides further evidence that the addition of NO increased the overall depletion in the VOC concentrations.

Increasing the [NO] to 70 ppb reduced both the amount of VOC reacting with OH and the amount of VOC reacting with *sOH*. Whilst the unreacted VOC was still less than in the case without NO in the simulation (93.8% with 70 ppb NO and 93.9% without NO), this did not represent a significant change in the simulated depletions in the VOCs. This result was not reproduced experimentally, where the depletion factors continued to increase with increasing [NO], but does suggest that there may be an upper limit to the amount of NO that can be added into the reactor without negating the positive impact. As observed in Figure 4.23 and Figure 4.24 the sinks of *pOH* and *sOH* to NO and NO<sub>2</sub> were much larger when the initial concentration of NO was 70 ppb.

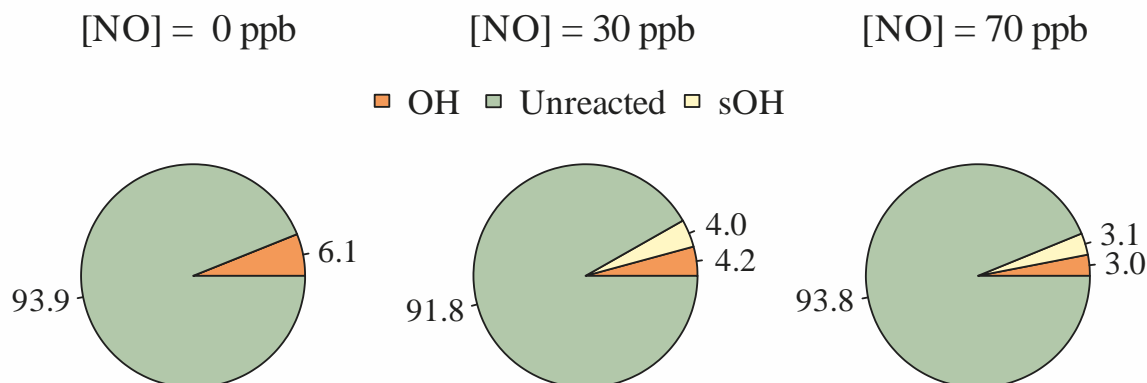


**Figure 4.25** Simulated impact of different initial concentrations of NO on the VOC sinks.

## Conclusions

Aromatic VOCs are prevalent in the atmosphere due primarily to vehicle fuel emissions. Their oxidation within the atmosphere represents a significant source of tropospheric ozone and is therefore important for air quality control. Unfortunately, measurements of the rate coefficients for reactions between aromatic VOCs and OH are sparse, especially for aromatics with multiple, or large, alkyl chain substituents. The multivariate relative rate technique was therefore successfully applied to two mixtures containing a suite of different aromatic VOCs, resulting in the measurement of 19 rate coefficients for reactions between aromatic VOCs and OH. Four of the measured results represent the first measurements of those reactions at the time of writing.

Unfortunately, the measurement of rate coefficients for aromatic VOC + OH reactions proved difficult and required additional chemistry to achieve the desired results. The procedure for generating OH radicals within the reactive system resulted in the production of significant concentrations of HO<sub>2</sub>. The HO<sub>2</sub> was found to act as a large sink for OH, meaning that, for low reactivity VOC mixtures, the observed depletions in the VOC concentrations were small and potentially within the noise of the experiment. Adding NO in different concentrations to the reactive system was shown to increase the depletion in the VOCs through the production of secondary OH via the NO + HO<sub>2</sub> reaction. This was demonstrated both experimentally and through numerical simulations.

Three of the four novel rate coefficients measured in this work were poorly defined, likely due to their minimal observed depletions. Rate coefficients for the reactions of the three diethylbenzene isomers with OH were therefore not specified; an upper limit, of  $k < 3 \times 10^{-11} \text{ cm}^3 \text{ molecule}^{-1} \text{ s}^{-1}$  was provided instead. This estimate was found to be in relatively good agreement with recent SAR estimations by Jenkin et al. (2018).

Work studying aromatic VOC + OH reactions is recommended to continue. The three diethylbenzene isomers should be measured in a less reactive mixture, perhaps with the addition of NO, to improve the extent of their depletion measurements. Many other alkyl-substituted aromatic structures also exist, some of which are likely to be present in the atmosphere in trace concentrations. Furthermore, the multivariate relative rate technique could potentially be expanded to study other functionalities, such as aromatic aldehydes and polyaromatic hydrocarbons, which are also commonly observed in the atmosphere.

## References

- Alarcón, P., Bohn, B. and Zetzsch, C.: Kinetic and mechanistic study of the reaction of OH radicals with methylated benzene: 1,4-dimethyl-, 1,3,5-trimethyl-, 1,2,4,5-, 1,2,3,5- and 1,2,3,4-tetramethyl-, pentamethyl-, and hexamethylbenzene, *Phys. Chem. Chem. Phys.*, **17**, 19, 13053-13065, <https://doi.org/10.1039/C5CPoo253B>, 2015.
- Aschmann, S. M., Arey, J. and Atkinson, R.: Rate constants for the reactions of OH radicals with 1,2,4,5-tetramethylbenzene, pentamethylbenzene, 2,4,5-trimethylbenzaldehyde, 2,4,5-trimethylphenol, and 3-methyl-3-hexene-2,5-dione and products of OH + 1,2,4,5-tetramethylbenzene, *J. Phys. Chem. A*, **117**, 12, 2556-2568, <https://doi.org/10.1021/jp400323n>, 2013.
- Atkinson, R.: Kinetics and mechanisms of the gas phase reactions of the hydroxyl radical with organic compounds, *J. Phys. Chem. Ref. Data*, 1-246, 1989.
- Atkinson, R. and Arey, J.: Atmospheric degradation of volatile organic compounds, *Chem. Rev.*, **103**, 4605-4638, <https://doi.org/10.1021/cr0206420>, 2003.
- Atkinson, R., Baulch, D. L., Cox, R. A., Crowley, J. N., Hampson, R. F., Hynes, R. G., Jenkin, M. E., Rossi, M. J. and Troe, J.: Evaluated kinetic and photochemical data for atmospheric chemistry: Volume II – gas phase reactions of organic species, *Atmos. Chem. Phys.*, **6**, 3625-4055, 2006. Also at <http://iupac.pole-ether.fr/index.html>.
- Bloss, C., Wagner, V., Jenkin, M. E., Volkamer, R., Bloss, W. J., Lee, J. D., Heard, D. E., Wirtz, K., Martin-Reviejo, M., Rea, G., Wenger, J. C. and Pilling, M. J.: Development of a detailed chemical mechanism (MCMv3.1) for the atmospheric oxidation of aromatic hydrocarbons, *Atmos. Chem. Phys.*, **5**, 641-664, <https://doi.org/10.5194/acp-5-641-2005>, 2005.
- Brown, H. C. and Okamoto, Y.: Electrophilic substituent constants, *J. Am. Chem. Soc.*, **80**, 18, 4979-4987, <https://doi.org/10.1021/ja01551a055>, 1958.
- Calvert, J. G., Atkinson, R., Becker, K. H., Kamens, R. M., Seinfeld, J. H., Wallington, T. J. and Yarwood, G.: The mechanisms of atmospheric oxidation of aromatic hydrocarbons, Oxford University Press, New York, 2002.
- Ianni, J. C.: Kintecus, Windows Version 5.20, 2017, [www.kintecus.com](http://www.kintecus.com)

- Jenkin, M. E., Saunders, S. M., Wagner, V. and Pilling, M. J.: Protocol for the development of the Master Chemical Mechanism, MCM v3 (Part B): Tropospheric degradation of aromatic volatile organic compounds, *Atmos. Chem. Phys.*, 3, 181-193, <https://doi.org/10.5194/acp-3-182-2003>, 2003.
- Jenkin, M. E., Valorso, R., Aumont, B., Rickard, A. R. and Wallington, T. J.: Estimation of rate coefficients and branching ratios for gas-phase reactions of OH with aromatic organic compounds for use in automated mechanism construction, *Atmos. Chem. Phys. Discuss.*, <https://doi.org/10.5194/acp-2018-146>, in review, 2018.
- Knispel, R., Koch, R., Siese, M. and Zetsch, C.: Adduct formation of OH radicals with benzene, toluene, and phenol and consecutive reactions of the adducts with NO<sub>x</sub> and O<sub>2</sub>, *Ber. Bunsenges. Phys. Chem.*, 94, 1375-1379, <https://doi.org/10.1002/bbpc.199000036>, 1990.
- Koch, R., Knispel, R., Elend, M., Siese, M. and Zetsch, C.: Consecutive reactions of aromatic-OH adducts with NO, NO<sub>2</sub> and O<sub>2</sub>: benzene, naphthalene, toluene, *m*- and *p*-xylene, hexamethylbenzene, phenol, *m*-cresol and aniline, *Atmos. Chem. Phys.*, 7, 2057-2071, <https://doi.org/10.5194/acp-7-2057-2007>, 2007.
- Kwok, E. S. C. and Atkinson, R.: Estimation of hydroxyl radical reaction rate constants for gas-phase organic compounds using a structure-reactivity relationship: an update, *Atmos. Environ.*, 29, 14, 1685-1695, [https://doi.org/10.1016/1352-2310\(95\)00069-B](https://doi.org/10.1016/1352-2310(95)00069-B), 1995.
- Mehta, D., Nguyen, A., Montenegro, A. and Li, Z.: A kinetic study of the reaction of OH with xylenes using the relative rate/discharge flow/mass spectrometry technique, *J. Phys. Chem. A*, 113, 12942-12951, <https://doi.org/10.1021/jp905074j>, 2009.
- Newland, M. J., Jenkin, M. E. and Rickard, A. R.: Elucidating the fate of the OH-adduct in toluene oxidation under tropospheric boundary layer conditions, *P. Natl. Acad. Sci. USA*, <https://doi.org/10.1073/pnas.1713678114>, 2017.
- Nicovich, J. M., Thompson, R. L. and Ravishankara, A. R.: Kinetics of the reactions of the hydroxyl radical with xylenes, *J. Phys. Chem.*, 85, 2913-2916, <https://doi.org/10.1021/j150620a012>, 1981.
- Passant, N. R.: Speciation of UK emissions of non-methane volatile organic compounds, Issue 1, AEAT/ENV/R/0545, 2002.

Perry, R. A., Atkinson, R. and Pitts Jr., J. N.: Kinetics and mechanism of the gas phase reaction of OH radicals with aromatic hydrocarbons over the temperature range 296-473 K, *J. Phys. Chem.*, 81, 296-304, <https://doi.org/10.1021/j100519a004>, 1977.

Ravishankara, A. R., Wagner, S., Fischer, S., Smith, G., Schiff, R., Watson, R. T., Tesi, G. and Davis, D. D.: A kinetics study of the reactions of OH with several aromatic and olefinic compounds, 10, 783-804, <https://doi.org/10.1002/kin.550100802>, 1978.

Wahner, A. and Zetzsch, C.: Rate constants for the addition of OH to aromatics (benzene, *p*-chloroaniline, and *o*-, *m*-, and *p*-dichlorobenzene) and the unimolecular decay of the adduct, *J. Phys. Chem.*, 87, 4945-4951, <https://doi.org/10.1021/j150642a036>, 1983.

Zetzsch, C.: Predicting the rate of OH-addition to aromatics using  $\sigma^+$ -electrophilic substituent constants for mono- and polysubstituted benzene, 15th Informal Conference on Photochemistry, Stanford, California, 1982.

Ziemann, P. J. and Atkinson, R.: Kinetics, products, and mechanisms of secondary organic aerosol formation, *Chem. Soc. Rev.*, 41, 6582-6605, <https://doi.org/10.1039/C2CS35122F>, 2012.



## Chapter 5

# Kinetic studies of alkane oxidation reactions

## 5 Overview

This chapter describes the work undertaken to investigate the atmospheric oxidation of an important class of VOCs; the alkanes (please refer to Chapter 1 Sections 1.2.2.1 and 1.3.2 for more information on alkanes as VOCs). Alkanes react slowly with OH relative to many of the VOCs studied as part of the mixtures discussed in previous chapters. Two modifications to the basic ensemble relative rate technique were made for the measurements of the reactions of these VOCs. The first involved heating the reactor to determine rate coefficients for the alkane + OH reactions at different temperatures, allowing for the estimation of Arrhenius parameters. The second involved the substitution of the radical oxidant for Cl, with which alkanes react much quicker than with OH. The following chapter will discuss the results obtained from these experiments.

New room temperature rate coefficients for the reactions of OH with 2-methylheptane, 2-methylnonane and ethylcyclohexane can be found in Table 5.2. A new room temperature rate coefficient for the reaction between Cl and 2-methylheptane is provided in Table 5.9.

## 5.1 Temperature-dependent alkane + OH reactions

The rate coefficient for the gas-phase reactions between VOCs and OH are dependent on temperature. The temperature of the atmosphere can vary substantially depending on the time of day, season, geographic location and height above the surface. Many gas-phase reactions also occur in high temperature environments such as those found in fires or in combustion engines.

The rate coefficient for the reaction between methane (CH<sub>4</sub>) and OH varies by approximately 25 times, across a temperature range of 200 – 323 K, a conservative estimate of the range of temperatures observed throughout the Earth's atmosphere. This value increases to around 400 times when accounting for the range of temperatures than can occur inside a combustion engine (which can be up to 2000 K in diesel engines). Clearly, rate coefficient measurements made at, or close to, room temperature may not be entirely adequate for describing the kinetics of such reactions in the many varied environments present in the Earth system.

The Arrhenius equation, shown in Eq. 5.1, provides a useful expression for  $k(T)$ . The pre-exponential factor ( $A$ ) is defined, by collision theory, as the frequency of collisions;  $E_a$  is the activation energy and  $R$  is the universal gas constant.

$$k = Ae^{-\frac{E_a}{RT}} \quad \text{Eq. 5.1}$$

By making a range of rate coefficient measurements at different temperatures it was possible to derive values for both  $A$  and  $E_a$  for a suite of reactions simultaneously. This was done using Arrhenius plots, in which  $\ln k$  for a particular reaction was plotted against the reciprocal of temperature, yielding  $\ln A$  as the intercept and  $-E_a/R$  as the slope of the plot, via Eq. 5.2.

$$\ln k = \ln A - \frac{E_a}{R} \frac{1}{T} \quad \text{Eq. 5.2}$$

### 5.1.1 Alkane mixture

The alkanes mixture used in the temperature-dependency experiments contained 12 VOCs. Four of the VOCs were the linear alkanes *n*-octane, *n*-nonane, *n*-decane and *n*-undecane. Five of the VOCs were branched alkanes; 2- and 3-methylpentane, 2-methylheptane, 2-methylnonane and 2,2,3-trimethylbutane. The remaining three VOCs were cyclic in nature; cycloheptane, cyclooctane and the branched cyclic alkane, ethylcyclohexane. The reaction of 11 of these VOCs

with OH had been the subject of previous kinetic studies. 10 of these had been extensively reviewed in Atkinson (2003), in which recommended literature rate coefficients (at 298 K) were provided for all, and recommended Arrhenius expressions, across varying temperature ranges, were provided for just six. 2-methylheptane and ethylcyclohexane had just one rate coefficient measurement for their reactions with OH, at 323 K (Shaw et al., 2018) and 2-methylnonane was notable in that it had no available literature rate coefficient for its reaction with OH at any temperature, at the time of writing. Table 5.1 gives a full list of the 12 VOCs, along with the 298 K literature rate coefficient used for their reaction with OH, their recommended Arrhenius expressions, where available, and the number of available  $k$  value measurements in the literature at the time of writing.

There was a small range in the  $k$  values across the VOCs in this mixture. The estimated total OH reactivity of this mixture, at standard temperature and pressure (STP), was  $110 \text{ s}^{-1}$ , not counting the alkane without a literature room temperature rate coefficient for its reaction with OH. At all temperatures, this mixture was injected into the reactor with an approximate OH reactivity of  $4.3 \text{ s}^{-1}$ . As in Chapter 4, for the measurement of aromatic VOC + OH reactions with rate coefficients less than  $20 \times 10^{-12} \text{ cm}^3 \text{ molecule}^{-1} \text{ s}^{-1}$ , NO (approximately 50 ppb) was also injected into the reactor to augment the observed OH depletions.

### 5.1.2 Room temperature measurements

Figure 5.1 shows the relative rate plot for this mixture recorded at room temperature (297 K). The relationship between depletion factor and  $k$  value was linear, with an adjusted  $R^2 = 0.971$  and  $OH_{exp} = 3.8 (\pm 0.2) \times 10^9 \text{ molecules cm}^{-3} \text{ s}$ . The resulting room temperature rate coefficients are provided in Table 5.2, along with their evaluated room temperature literature equivalents.

All the rate coefficient measurements for the alkane + OH reactions were in excellent agreement with the evaluated literature equivalents, within errors. The rate coefficients for the reaction between three alkanes and OH were measured for the first time at room temperature: 2-methylheptane + OH,  $k = 9.1 (\pm 0.3) \times 10^{-12} \text{ cm}^3 \text{ molecule}^{-1} \text{ s}^{-1}$ ; 2-methylnonane + OH,  $k = 11 (\pm 0.3) \times 10^{-12} \text{ cm}^3 \text{ molecule}^{-1} \text{ s}^{-1}$ ; ethylcyclohexane + OH,  $k = 14.4 (\pm 0.3) \times 10^{-12} \text{ cm}^3 \text{ molecule}^{-1} \text{ s}^{-1}$ .

**Table 5.1** List of VOCs, in descending order of evaluated literature  $k$  (298 K) value, in the alkane mixture along with their evaluated literature  $k$  (298 K) value, recommended Arrhenius expression (where available), reference and the number of experimental studies found in the literature at the time of writing.

Name	Evaluated literature $k$ (298 K) / $10^{-12} \text{ cm}^3$ molecule $^{-1} \text{ s}^{-1}$	Recommended Arrhenius expression / $\text{cm}^3 \text{ molecule}^{-1} \text{ s}^{-1}$	Temperature range / K	Reference used	Number of studies
Cyclooctane	$13 \pm 7$	$k = 5.91 \times 10^{17} T^2 e^{(276 \pm 143)/T}$	290 - 390	Atkinson, 2003	2
<i>n</i> -undecane	$12 \pm 2$			Atkinson, 2003	2
Cycloheptane	$12 \pm 3$	$k = 3.99 \times 10^{17} T^2 e^{(373 \pm 119)/T}$	290 - 390	Atkinson, 2003	3
<i>n</i> -decane	$11 \pm 2$	$k = 3.17 \times 10^{17} T^2 e^{(406 \pm 56)/T}$	290 - 1100	Atkinson, 2003	6
<i>n</i> -nonane	$10 \pm 2$	$k = 2.53 \times 10^{17} T^2 e^{(436 \pm 54)/T}$	290 - 1100	Atkinson, 2003	9
<i>n</i> -octane	$8 \pm 2$	$k = 2.72 \times 10^{17} T^2 e^{361/T}$	290 - 1080	Atkinson, 2003	6
2-methylpentane	$5.2 \pm 1.3$			Atkinson, 2003	4
3-methylpentane	$5.2 \pm 1.3$			Atkinson, 2003	3
2,2,3-trimethylbutane	$3.8 \pm 1.0$	$k = 9.20 \times 10^{18} T^2 e^{459/T}$	290 - 760	Atkinson, 2003	6
2-methylheptane					1*
2-methylnonane					0
Ethylcyclohexane					1*

\* Shaw et al. (2018) did not include any measurements at room temperature for these compounds hence no literature  $k$  can be provided at 298 K.

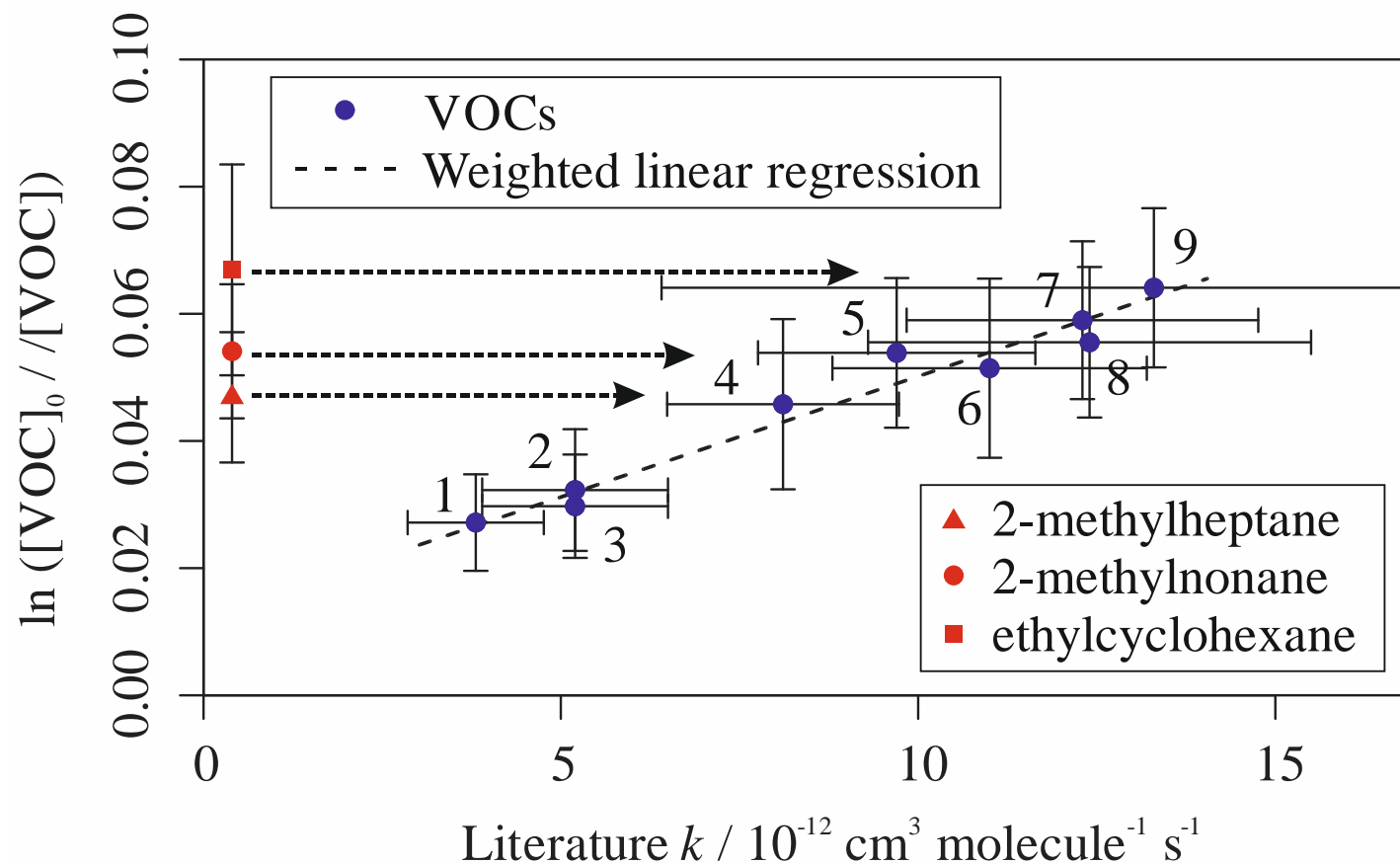


**Figure 5.1** Relative rate plot for the alkane mixture with an OH reactivity of  $4.3 \text{ s}^{-1}$ , at 295 K. Compounds with a reference rate coefficient were plotted using evaluated literature values. Error bars on the y-axis, equal to one standard error, were calculated by combining the standard error in peak areas for six lamp-off and six lamp-on samples. Error bars on the x-axis were typically large (approximately  $\pm 20\text{-}30\%$ ) and accounted for deviations from the lines for all VOCs. A weighted (to the uncertainty in the y-values) linear fit was used to generate the slope, with a value of  $OH_{exp} = 3.8 (\pm 0.2) \times 10^9 \text{ molecules cm}^{-3}$  and  $R^2 = 0.971$ . Data for 2-methylheptane, 2-methylnonane and ethylcyclohexane, which had no literature  $k$  (298 K) values, were not used in the calculation of the fit. The VOCs can be identified as follows; 1, 2,2,3-trimethylbutane; 2, 2-methylpentane; 3, 3-methylpentane; 4, *n*-octane; 5, *n*-nonane; 6, *n*-decane; 7, *n*-undecane; 8, cycloheptane; 9, cyclooctane.

**Table 5.2** List of VOCs, in descending order of evaluated literature  $k$  (298 K) value, in the alkanes mixture along with their measured  $k$  (297 K) value and evaluated literature  $k$  (298 K) value.

Name	Measured $k$ (297 K) / $10^{-12} \text{ cm}^3 \text{ molecule}^{-1} \text{ s}^{-1}$	Evaluated literature $k$ (298 K) / $10^{-12} \text{ cm}^3 \text{ molecule}^{-1} \text{ s}^{-1}$
cyclooctane	$13.7 \pm 0.3$	$13 \pm 7$
<i>n</i> -undecane	$12.3 \pm 0.3$	$12 \pm 2$
cycloheptane	$11.4 \pm 0.3$	$12 \pm 3$
<i>n</i> -decane	$10.3 \pm 0.3$	$11 \pm 2$
<i>n</i> -nonane	$11.0 \pm 0.3$	$10 \pm 2$
<i>n</i> -octane	$8.8 \pm 0.3$	$8 \pm 2$
2-methylpentane	$4.6 \pm 0.3$	$5.2 \pm 1.3$
3-methylpentane	$5.3 \pm 0.3$	$5.2 \pm 1.3$
2,2,3-trimethylbutane	$3.9 \pm 0.3$	$3.8 \pm 1.0$
2-methylheptane	$9.1 \pm 0.3$	
2-methylnonane	$11.0 \pm 0.3$	
ethylcyclohexane	$14.4 \pm 0.3$	

### 5.1.3 Elevated temperature measurements

A suite of relative rate experiments was conducted with the temperature of the reactor set to greater than room temperature using the equipment set up described in Chapter 2 Section 2.2.3. The literature rate coefficients used as reference values for the experiments were calculated using the recommended Arrhenius expressions provided by Atkinson (2003; see Table 5.1). These Arrhenius expressions were limited to specific temperature ranges, and as such, the number of reference compounds available decreased with increasing temperature. At temperatures greater than 390 K (117 °C), only four VOCs were used as reference compounds, somewhat limiting the fitting of the  $OH_{exp}$  linear regression and thereby leading to increased uncertainty.

Regardless, measurements of the depletions in concentration due to the reactions of the VOCs in the alkanes mixture with OH were made at a number of temperatures up to 466 K (193 °C). The depletion factors were plotted against the available literature rate coefficients at each temperature, using the methods outlined in earlier chapters, and final measured relative rate coefficients estimated at each temperature for each species. Table 5.3 provides the  $OH_{exp}$  and  $R^2$  values derived from the weighted linear regressions made at each temperature.

**Table 5.3** List of temperatures at which relative rate experiments were conducted on the alkanes mixture. The estimated  $OH_{exp}$ , as derived from the weighted linear regressions for the relative rate plots, are provided, along with the  $R^2$  value and the number of reference compounds used at each temperature.

T / K	$OH_{exp} / 10^9$ molecules $cm^{-3}$	$R^2$	Number of reference compounds
297 ± 1.4	3.8 ± 0.2	0.971	9
323 ± 5	3.8 ± 0.5	0.914	6
326 ± 5	2.1 ± 0.6	0.710	6
326 ± 5	2.9 ± 0.5	0.858	6
329 ± 5	1.5 ± 1.0	0.204	6
351 ± 6	3.7 ± 0.8	0.790	6
373 ± 6	2.8 ± 1.0	0.573	6
373 ± 6	3.0 ± 0.6	0.803	6
390 ± 6	4.3 ± 0.5	0.924	6
397 ± 6	5.9 ± 0.8	0.952	4
419 ± 7	5.2 ± 0.5	0.976	4
422 ± 7	5.4 ± 0.5	0.972	4
441 ± 7	5.0 ± 0.7	0.945	4
466 ± 7	6.1 ± 0.6	0.945	4

The following sections describe the Arrhenius plots for each of the VOCs in this mixture, along with the estimated Arrhenius expression calculated using the data from this work. The corresponding literature for each of the VOC + OH reactions in the mixture is also provided.

## 5.1.4 Arrhenius expressions

### 5.1.4.1 OH + 2,2,3-trimethylbutane

2,2,3-trimethylbutane was one of the few alkanes in the mixture with a recommended Arrhenius expression for reaction with OH which continued outside of the experimental range for this work. However, the recommended expression for the rate coefficient at temperatures greater than 500 K was based on a single data point (Baldwin et al., 1981). Figure 5.2 shows the Arrhenius plot for this compound, along with the available literature and both the recommended Arrhenius trend and the Arrhenius trend that was estimated using the results derived in this work.

The vast majority of the rate coefficient measurements for the 2,2,3-trimethylbutane + OH reaction were in good agreement with the recommended Arrhenius expression provided in Atkinson (2003). This was to be expected, as the Arrhenius expression provided the data which was used to calculate the relative rate values. Several data points were anomalous and sat away from the line, particularly those measured at lower temperatures where more evaluated rate coefficients were available for the derivation of the  $OH_{exp}$  constant. In previous chapters, the VOCs at the extreme ends (both lower and upper) of the OH reactivity scale within a mixture have been shown to be subject to greater uncertainties. Therefore, the discrepancy of much of the data at the lower temperatures was attributed to this.

The following Arrhenius expression for the temperature dependence of the rate coefficient for the reaction between 2,2,3-trimethylbutane and OH was derived from this work (Eq. 5.3).

$$k_{2,2,3\text{-trimethylbutane+OH}}(290 - 470 \text{ K}) = (0.60 \pm 0.10) \times 10^{-12} e^{(100 \pm 100)/T}$$

Eq. 5.3

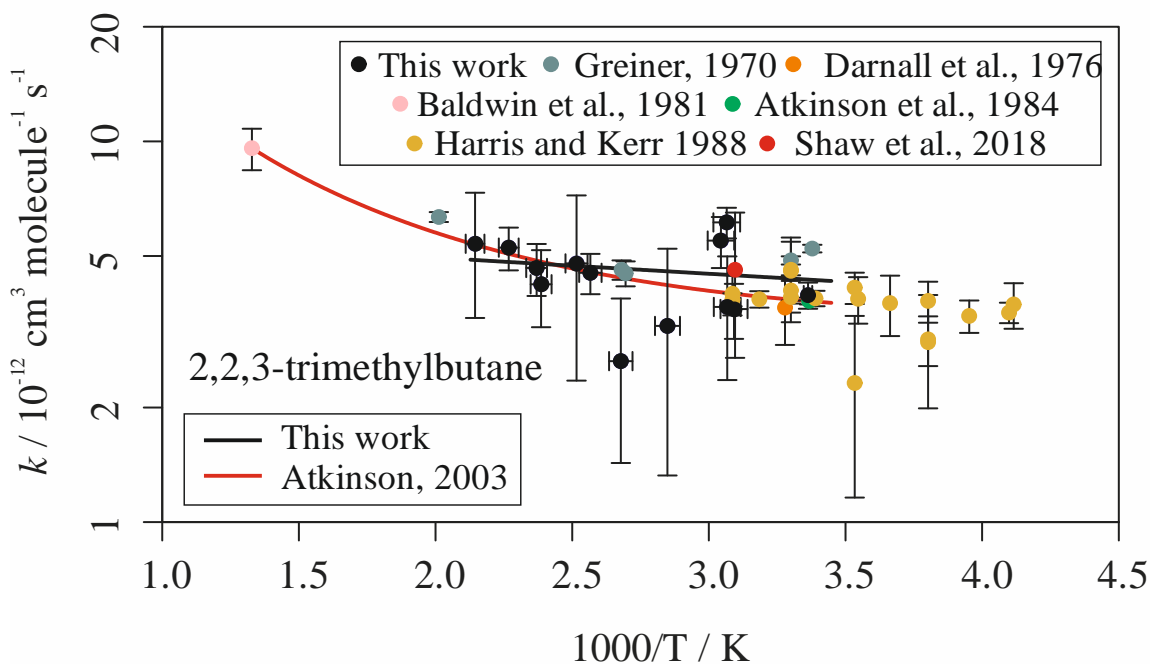


**Figure 5.2** Arrhenius plot showing the observed temperature dependence of the rate coefficient for the reaction between 2,2,3-trimethylbutane and OH. Rate coefficients derived as part of this work are shown alongside the available literature. Two Arrhenius expressions are also shown; one derived in this work (black) and the other as recommended by Atkinson, 2003 (red).

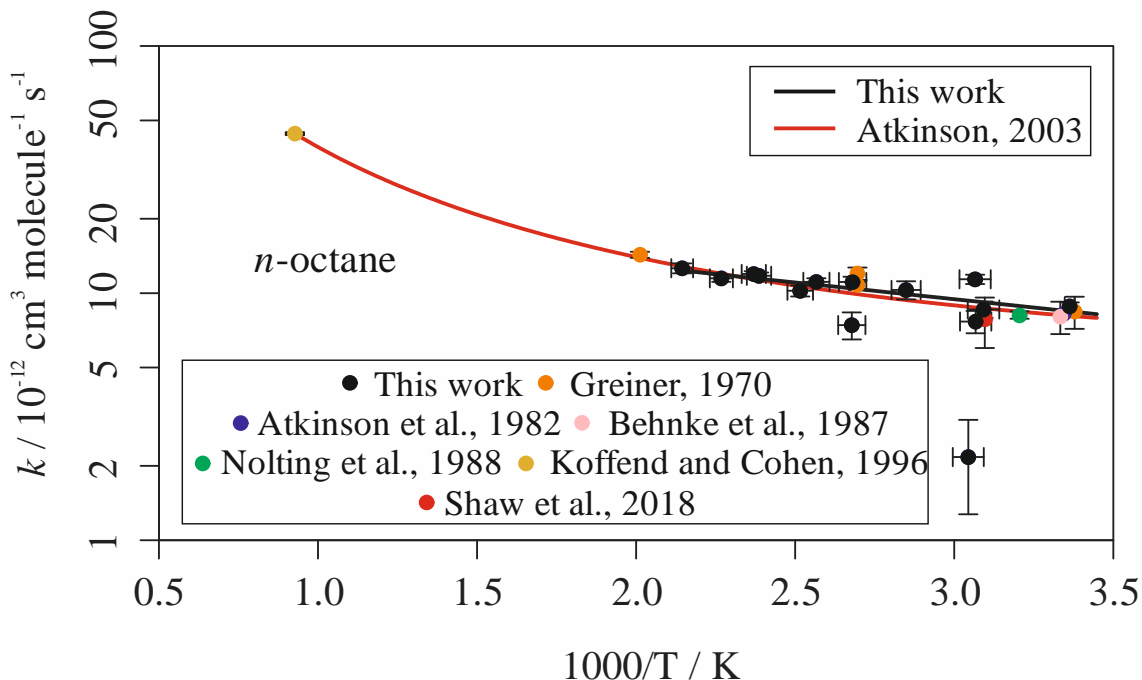


**Figure 5.3** Arrhenius plot showing the observed temperature dependence of the rate coefficient for the reaction between *n*-octane and OH. Rate coefficients derived as part of this work are shown alongside the available literature. Two Arrhenius expressions are also shown; one derived in this work (black) and the other as recommended by Atkinson, 2003 (red).

#### 5.1.4.2 OH + *n*-octane, OH + *n*-nonane and OH + *n*-decane

These three linear alkanes also benefited from having recommended Arrhenius expressions which continued outside of the experimental range of this work. As for 2,2,3-trimethylbutane, the Arrhenius expressions for each of these compounds above approximately 500 K was based on a single data point (Koffend and Cohen, 1996).

Figure 5.3 shows that the vast majority of the data for the reaction between *n*-octane and OH was in excellent agreement with the literature, and with the recommended Arrhenius expression. A single point, measured at around 327 K, was approximately 75 % smaller than the other data at that temperature but that can be assumed to be an anomaly. The Arrhenius expression derived from the results in this work was therefore almost identical to the recommended Arrhenius expression across the temperature range 290 – 470 K (Eq. 5.4).

$$k_{n\text{-octane}+\text{OH}}(290 - 470 \text{ K}) = (2.40 \pm 0.03) \times 10^{-12} e^{(310 \pm 130)/T} \quad \text{Eq. 5.4}$$

Similar observations were made for the temperature dependence of the *n*-nonane + OH (Figure 5.4) and *n*-decane + OH (Figure 5.5) reactions, with the vast majority of the data in excellent agreement with both the literature and with the recommended Arrhenius expressions. The Arrhenius expressions for these reactions derived in this work were also both in excellent agreement with the recommended Arrhenius expressions across the temperature range 290 – 470 K (Eq. 5.5 and 5.6).

$$k_{n\text{-nonane}+\text{OH}}(290 - 470 \text{ K}) = (1.81 \pm 0.02) \times 10^{-12} e^{(130 \pm 80)/T} \quad \text{Eq. 5.5}$$

$$k_{n\text{-decane}+\text{OH}}(290 - 470 \text{ K}) = (3.37 \pm 0.05) \times 10^{-12} e^{(320 \pm 140)/T} \quad \text{Eq. 5.6}$$

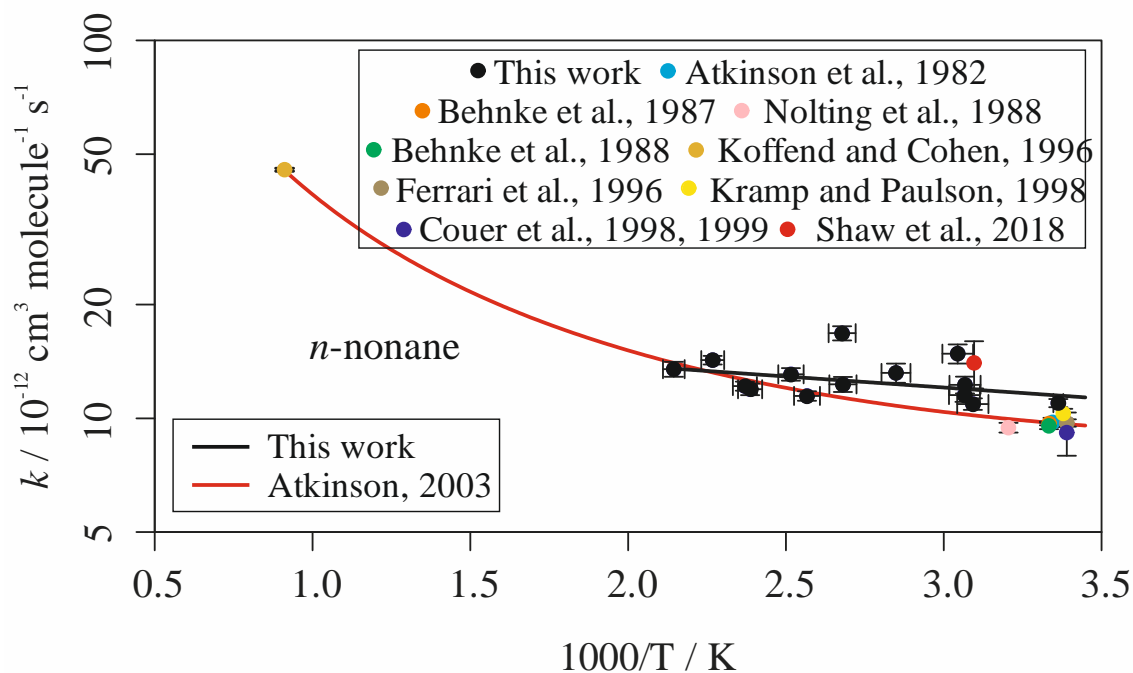


**Figure 5.4** Arrhenius plot showing the observed temperature dependence of the rate coefficient for the reaction between *n*-nonane and OH. Rate coefficients derived as part of this work are shown alongside the available literature. Two Arrhenius expressions are also shown; one derived in this work (black) and the other as recommended by Atkinson, 2003 (red).

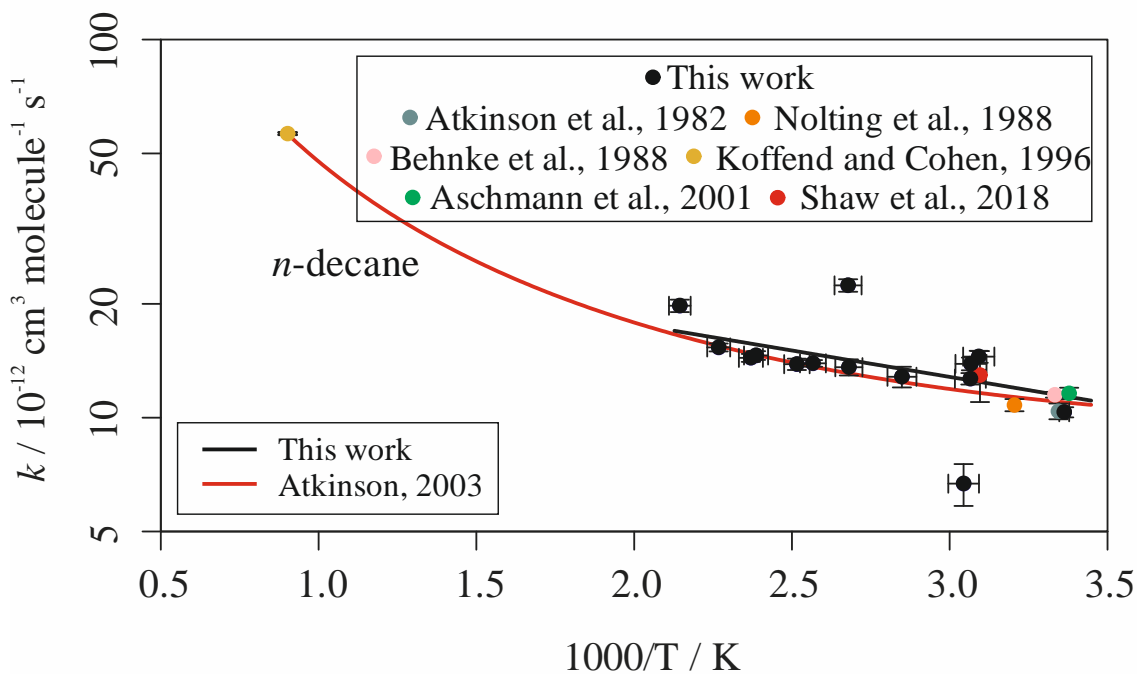


**Figure 5.5** Arrhenius plot showing the observed temperature dependence of the rate coefficient for the reaction between *n*-decane and OH. Rate coefficients derived as part of this work are shown alongside the available literature. Two Arrhenius expressions are also shown; one derived in this work (black) and the other as recommended by Atkinson, 2003 (red).

### 5.1.4.3 OH + cycloheptane and OH + cyclooctane

These two cyclic alkanes also had recommended Arrhenius expressions for reaction with OH provided in Atkinson (2003), albeit as the result of a single temperature dependent study by Donahue et al. (1998). The range for the recommended Arrhenius expressions was limited to between 290 and 390 K.

The measurements made in this work, whilst in good agreement with the literature, suggested that the rate coefficients for the reactions of OH with cycloheptane (Figure 5.6) and cyclooctane (Figure 5.7) were largely independent of temperature, across the range 290 – 470 K.

The Arrhenius expressions derived from the data in this work are given by Eq. 5.7 and Eq. 5.8.

$$k_{\text{cycloheptane+OH}}(290 - 470 \text{ K}) = (1.24 \pm 0.03) \times 10^{-12} e^{(40 \pm 200)/T} \quad \text{Eq. 5.7}$$

$$k_{\text{cyclooctane+OH}}(290 - 470 \text{ K}) = (2.36 \pm 0.02) \times 10^{-12} e^{(150 \pm 70)/T} \quad \text{Eq. 5.8}$$

### 5.1.4.4 OH + 2-methylpentane and OH + 3-methylpentane

Literature measurements of the rate coefficients for the reactions of 2- and 3-methylpentane with OH were limited mainly to room temperature measurements, with only one study performed at an elevated temperature (Shaw et al., 2018). The rate coefficient measurements for these reactions between 290 and 470 K therefore represent the first extensive studies of their kind.

Whilst the data for the reaction between 2-methylpentane and OH at the lower temperatures was in good agreement with the available literature, the data at the higher temperatures were somewhat scattered (Figure 5.8). It was unknown as to why this occurred but interferences with other C<sub>6</sub> hydrocarbons, such as *n*-hexane (a common laboratory solvent), had been observed previously. The four measurements at approximately 325 K were in exceptionally poor agreement with each other, spanning a whole order of magnitude, with values between 1.5 and 14 × 10<sup>-12</sup> cm<sup>3</sup> molecule<sup>-1</sup> s<sup>-1</sup>. The derived Arrhenius expression, which shows little to no temperature dependence, was therefore subject to a large amount of uncertainty (Eq. 5.9).

$$k_{\text{2-methylpentane+OH}}(290 - 470 \text{ K}) = (3.2 \pm 0.2) \times 10^{-12} e^{(470 \pm 430)/T} \quad \text{Eq. 5.9}$$

The results for the reaction between 3-methylpentane and OH were also in good agreement with the available literature at the lower temperatures. The data at the higher temperatures were less scattered than those for the 2-methylpentane + OH reaction but were still in poor agreement. The estimated rate coefficient at 467 K also had an abnormally large uncertainty placed upon it. The Arrhenius expression derived from this data, for the temperature dependence of the rate coefficient for the reaction between 3-methylpentane and OH, is given by Eq. 5.10.

$$k_{3\text{-methylpentane+OH}}(290 - 470 \text{ K}) = (9.9 \pm 0.5) \times 10^{-12} e^{(820 \pm 450)/T} \quad \text{Eq. 5.10}$$

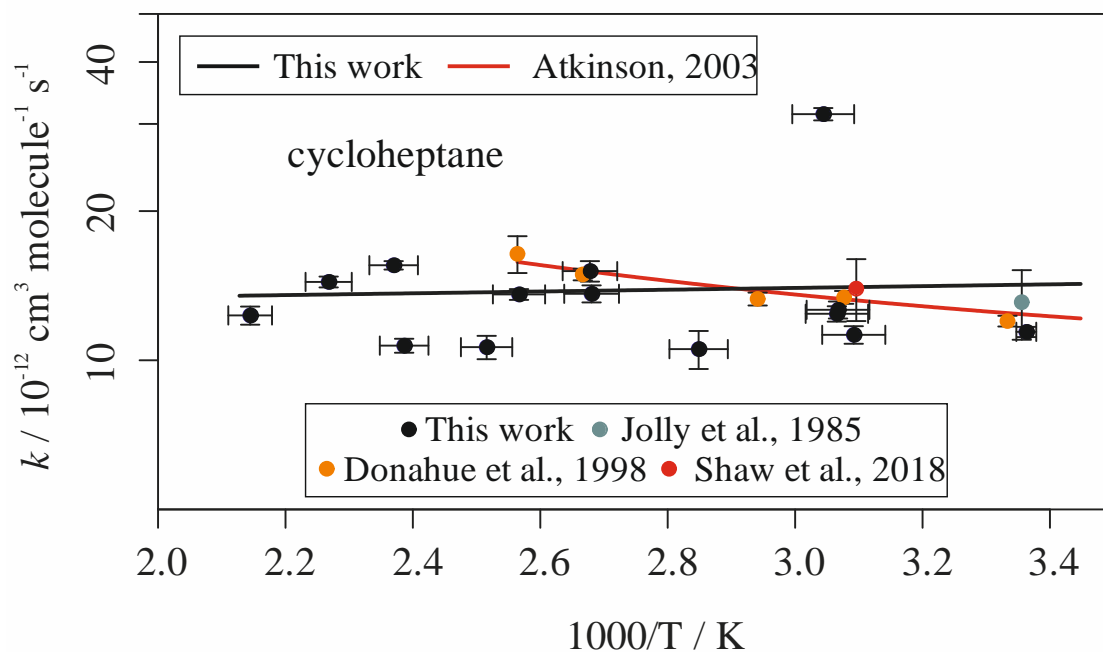


**Figure 5.6** Arrhenius plot showing the observed temperature dependence of the rate coefficient for the reaction between cycloheptane and OH. Rate coefficients derived as part of this work are shown alongside the available literature. Two Arrhenius expressions are also shown; one derived in this work (black) and the other as recommended by Atkinson, 2003 (red).

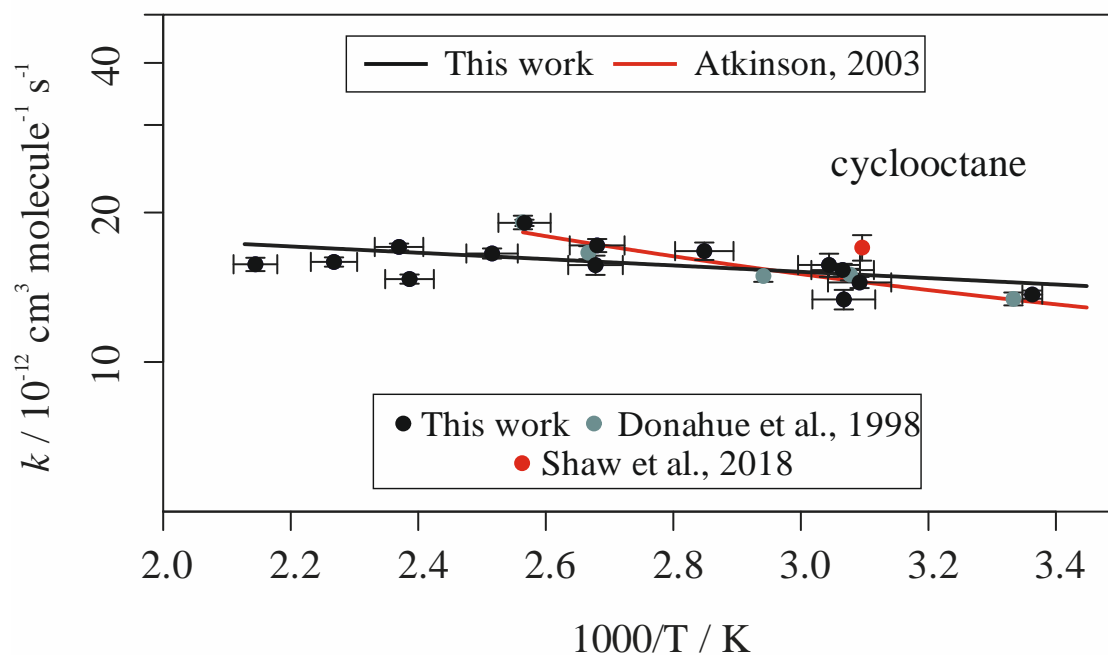


**Figure 5.7** Arrhenius plot showing the observed temperature dependence of the rate coefficient for the reaction between cyclooctane and OH. Rate coefficients derived as part of this work are shown alongside the available literature. Two Arrhenius expressions are also shown; one derived in this work (black) and the other as recommended by Atkinson, 2003 (red).

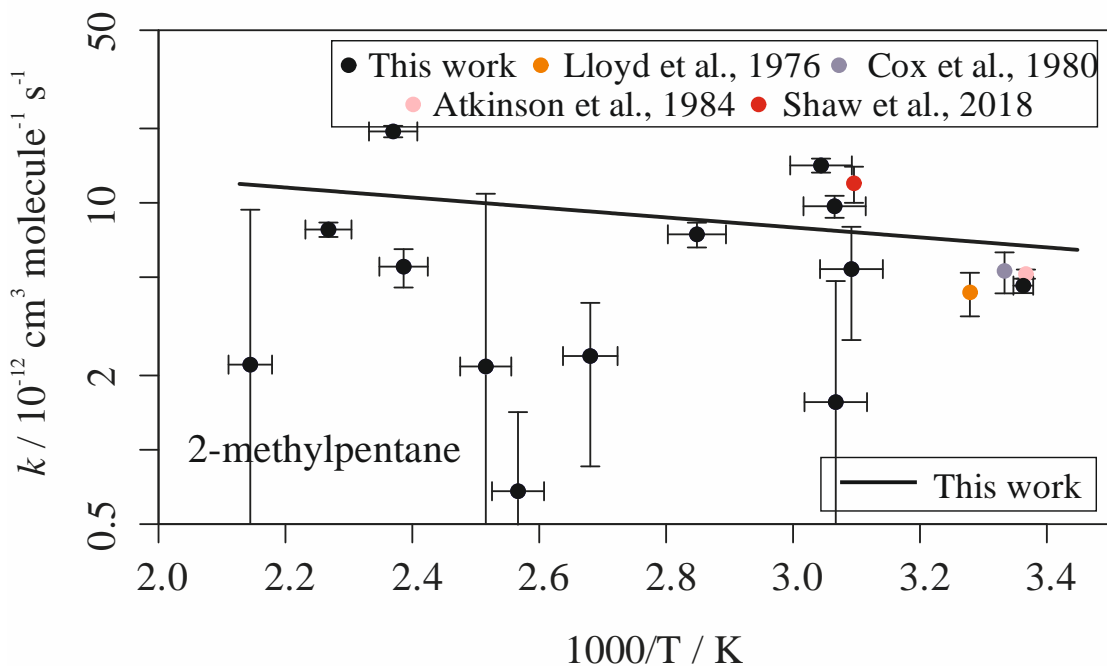


**Figure 5.8** Arrhenius plot showing the observed temperature dependence of the rate coefficient for the reaction between 2-methylpentane and OH. Rate coefficients derived as part of this work are shown alongside the available literature. The Arrhenius expression derived in this work is also shown.

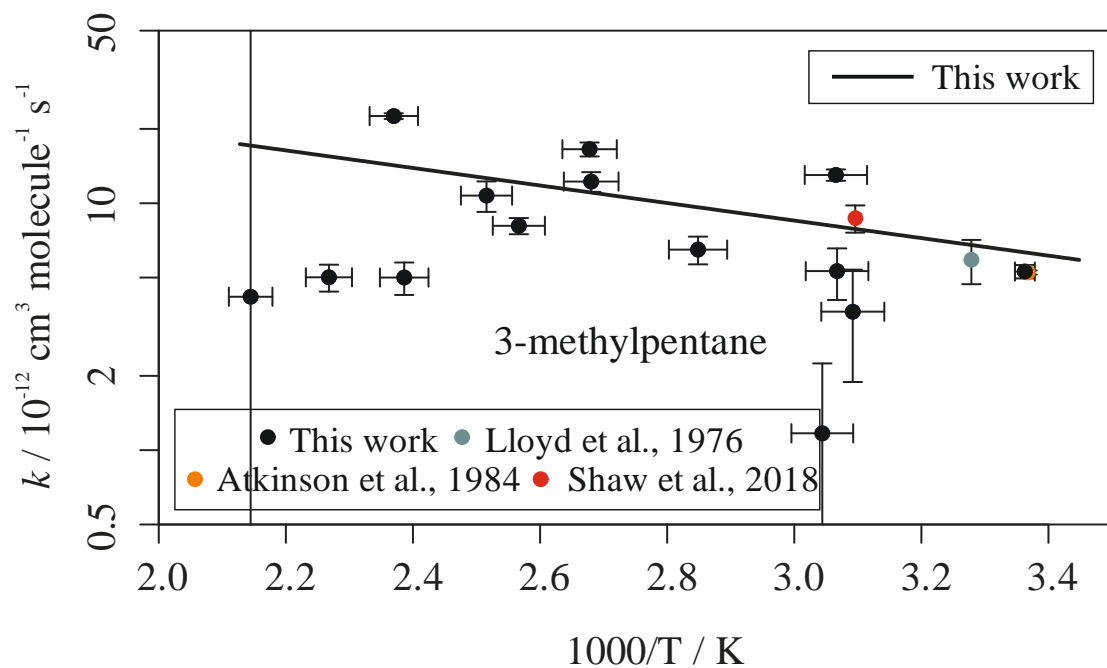


**Figure 5.9** Arrhenius plot showing the observed temperature dependence of the rate coefficient for the reaction between 3-methylpentane and OH. Rate coefficients derived as part of this work are shown alongside the available literature. The Arrhenius expression derived in this work is also shown.

#### 5.1.4.5 OH + *n*-undecane

There were only two literature measurements for the reaction between the C<sub>11</sub> linear alkane *n*-undecane and OH at the time of writing (Behnke et al. 1988; Nolting et al., 1988). Both of these were made at close to room temperature. The temperature dependent measurements of the rate coefficient for the reaction between *n*-undecane and OH made in this work therefore represent the first of their kind.

Figure 5.10 shows the measurements of the relative rate coefficient for the *n*-undecane + OH reaction made at different temperatures. There was some scatter in the data but the trend showed an overall independence of the rate coefficient with temperature. However, the lower temperature measurements, below 320 K, were poorly represented by the estimated Arrhenius expression (Eq. 5.11) despite the fact that they were in considerable agreement with each other.

$$k_{n\text{-undecane+OH}}(290 - 470 \text{ K}) = (1.65 \pm 0.04) \times 10^{-12} e^{(-30 \pm 200)/T} \quad \text{Eq. 5.11}$$

#### 5.1.4.6 OH + 2-methylheptane

There was only a single measurement, at 323 K, for the reaction between 2-methylheptane and OH at the time of writing (Shaw et al., 2018). Some of the data from this work at approximately 323 K was in good agreement with that study, as shown by Figure 5.11. The Arrhenius expression derived from this work is given by Eq. 5.12.

$$k_{2\text{-methylheptane+OH}}(290 - 470 \text{ K}) = (1.25 \pm 0.02) \times 10^{-12} e^{(90 \pm 100)/T} \quad \text{Eq. 5.12}$$

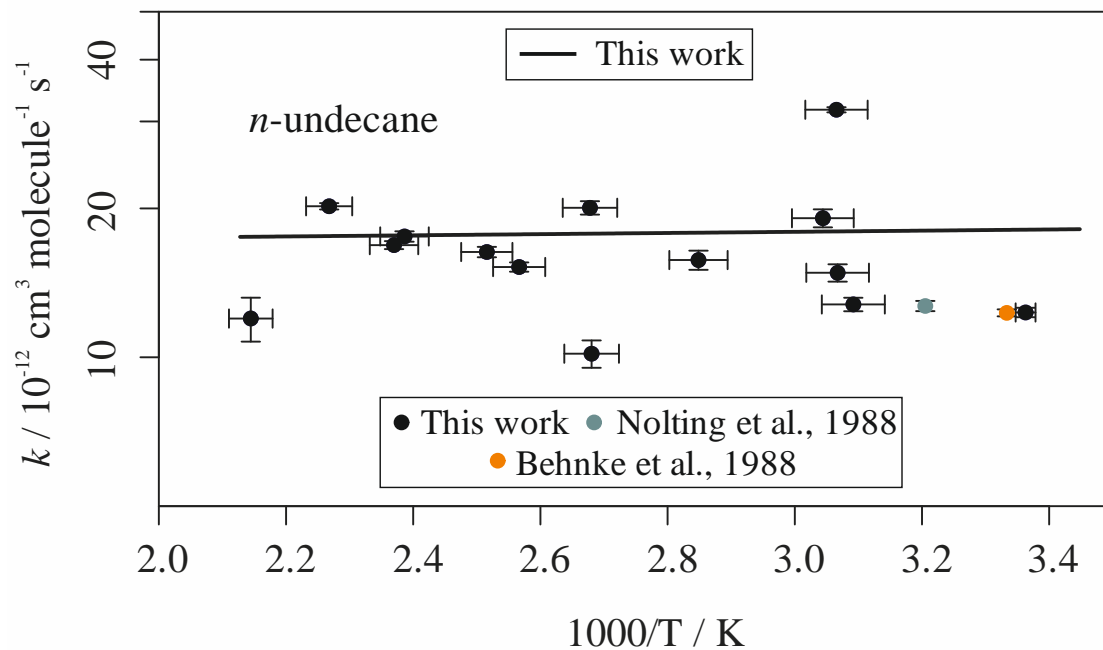


**Figure 5.10** Arrhenius plot showing the observed temperature dependence of the rate coefficient for the reaction between *n*-undecane and OH. Rate coefficients derived as part of this work are shown alongside the available literature. The Arrhenius expression derived in this work is also shown.

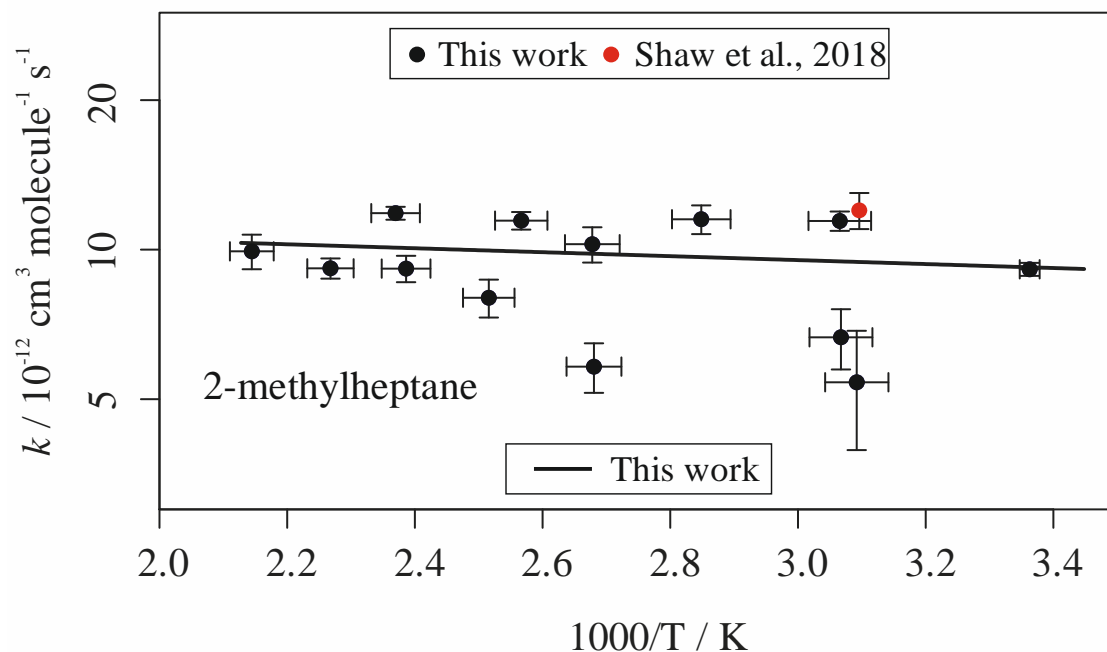


**Figure 5.11** Arrhenius plot showing the observed temperature dependence of the rate coefficient for the reaction between 2-methylheptane and OH. Rate coefficients derived as part of this work are shown alongside the available literature. The Arrhenius expression derived in this work is also shown.

#### 5.1.4.7 OH + 2-methylnonane

This work represents the first study of the rate coefficient for the reaction between 2-methylnonane and OH, at any temperature. In the absence of any literature to compare it to, it was difficult to assess the validity of the data. Whilst some of the data points appeared to be outliers from the general trend (at 326 and 440 K), the majority of the data was in good agreement with the estimated Arrhenius expression (Eq. 5.13).

$$k_{2\text{-methylnonane+OH}}(290 - 470 \text{ K}) = (2.09 \pm 0.03) \times 10^{-12} e^{(150 \pm 140)/T} \quad \text{Eq. 5.13}$$

#### 5.1.4.8 OH + ethylcyclohexane

The results for the ethylcyclohexane + OH reaction measured at around 323 K were in poor agreement with the value provided in Shaw et al. (2018) despite being in excellent agreement with each other. The average measurement in this work at 326 ( $\pm 5$ ) K, of  $11.2 (\pm 0.6) \times 10^{-12} \text{ cm}^3 \text{ molecule}^{-1} \text{ s}^{-1}$ , was approximately 25 % smaller than the value provided in Shaw et al. (2018), of  $15 (\pm 1) \times 10^{-12} \text{ cm}^3 \text{ molecule}^{-1} \text{ s}^{-1}$ , at 323 K.

Regardless, the measurement in Shaw et al. (2018) was the only available measurement of the rate coefficient for the ethylcyclohexane + OH reaction, at the time of writing. The derived Arrhenius expression from this work is given by Eq. 5.14.

$$k_{\text{ethylcyclohexane+OH}}(290 - 470 \text{ K}) = (1.50 \pm 0.02) \times 10^{-12} e^{(-50 \pm 90)/T} \quad \text{Eq. 5.14}$$

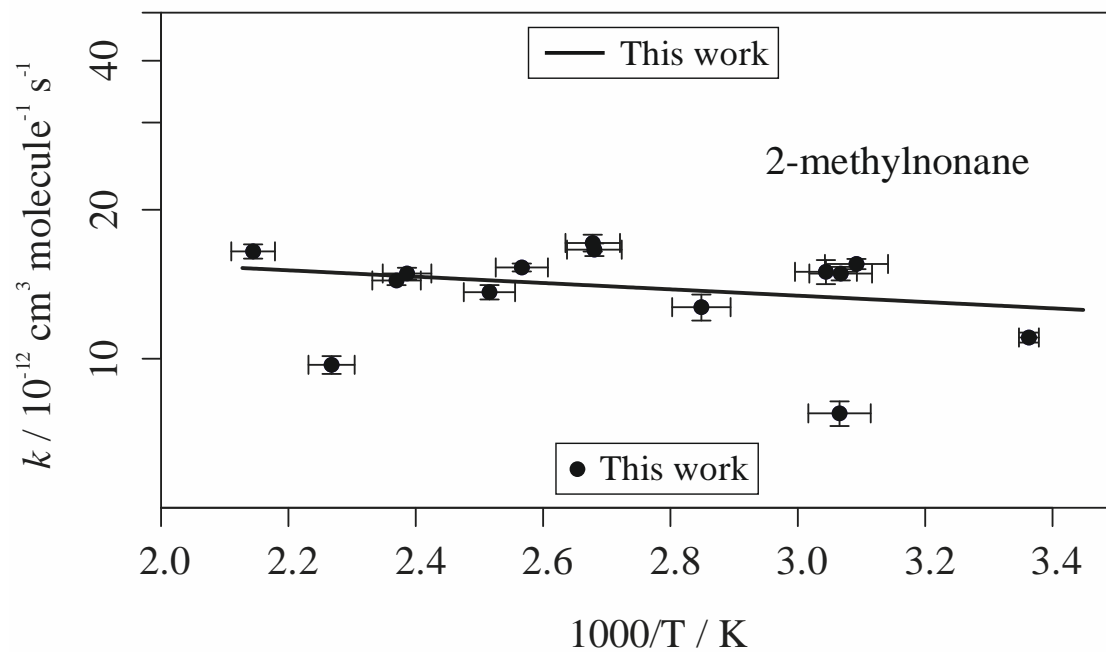


**Figure 5.12** Arrhenius plot showing the observed temperature dependence of the rate coefficient for the reaction between 2-methylnonane and OH. The Arrhenius expression derived in this work is also shown.

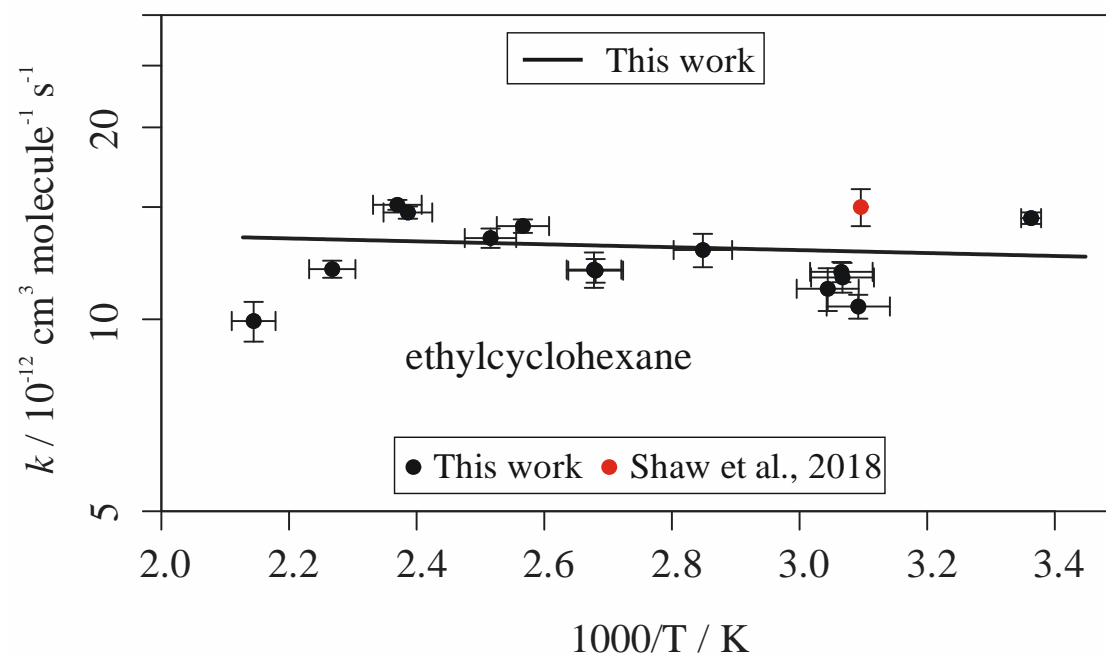


**Figure 5.13** Arrhenius plot showing the observed temperature dependence of the rate coefficient for the reaction between ethylcyclohexane and OH. Rate coefficients derived as part of this work are shown alongside the available literature. The Arrhenius expression derived in this work is also shown.

## 5.1.4.9 Summary

Table 5.4 provides a summary of the Arrhenius parameters derived from the temperature dependent relative rate measurements in this work. The recommended literature Arrhenius expressions, provided in Atkinson (2003), are also given as a means of comparison.

**Table 5.4** Summary of Arrhenius parameters derived from this work alongside those recommended in Atkinson (2003).

Name	This work*		Atkinson (2003)			
	A / 10 <sup>-12</sup> cm <sup>3</sup> molecule <sup>-1</sup> s <sup>-1</sup>	E <sub>a</sub> /R / K	A / 10 <sup>-17</sup> cm <sup>3</sup> molecule <sup>-1</sup> s <sup>-1</sup>	E <sub>a</sub> /R / K	n	T <sub>range</sub> / K
cyclooctane	2.36 ± 0.02	150 ± 67	5.91	276 ± 143	2	290 - 390
undecane	1.65 ± 0.04	-30 ± 200				
cycloheptane	1.24 ± 0.03	40 ± 200	3.99	373 ± 119	2	290 - 390
decane	3.37 ± 0.05	320 ± 140	3.17	406 ± 56	2	290 - 1100
n-nonane	1.81 ± 0.02	130 ± 82	2.53	436 ± 34	2	290 - 1100
n-octane	2.40 ± 0.03	310 ± 130	2.72	361	2	290 - 1080
2-methylpentane	3.2 ± 0.2	470 ± 430				
3-methylpentane	9.9 ± 0.5	820 ± 450				
2,2,3-trimethylbutane	0.60 ± 0.10	100 ± 100	0.92	459	2	290 - 760
2-methylheptane	1.25 ± 0.02	90 ± 100				
2-methylnonane	2.09 ± 0.03	150 ± 140				
ethylcyclohexane	1.50 ± 0.02	-50 ± 90				

\* The Arrhenius parameters derived in this work were measured for the temperature range 290 – 470 K.

In summary, the ensemble relative rate technique developed in this work was successfully modified to accommodate temperature dependent measurements of relative rate coefficients for the reactions of VOCs with OH. Multivariate relative rate measurements were performed on a mixture of 12 alkanes at temperatures varying between 297 K (considered to be room temperature) and 466 K. Recommended Arrhenius expressions from Atkinson (2003) were used to place these measurements on an absolute basis to derive Arrhenius expressions for a number of alkane + OH reactions.

The Arrhenius expressions derived for six of the compounds were in good agreement with the available literature across the temperature range 290 to 470 K. The expressions derived for the remaining six compounds represent the first of their kind, thereby showing that this method can be used to rapidly generate *k* vs *T* relationships for multiple compounds simultaneously, albeit

with large uncertainty, especially when fewer reactions are available for use as reference reactions. The multivariate relative rate technique may therefore be better suited for assessing existing Arrhenius parameters for suites of reactions, rather than for the derivation of novel parameters where no previous measurements exist for comparison.

## 5.2 Alkanes + Cl reaction rate coefficient measurements

The hydroxyl radical (OH) is widely acknowledged to be the most important atmospheric oxidant, particularly during the daytime. However, the relative importance of Cl radical chemistry in the oxidation of VOCs has gained more attention in recent years. Recent observations of Cl-precursor compounds in mid-continental locations, far removed from the sea (historically thought to be the primary source of Cl radicals) has led to renewed interest (e.g. Thornton et al., 2010). Despite this, measurements of Cl + VOC rate coefficients remain relatively sparse compared with OH.

Several methods have been used to monitor the reactions between VOCs and chlorine radicals (see Chapter 1 Section 1.4 for an overview of methods for measuring gas-phase rate coefficients). Some of the first measurements of the rates of reactions between Cl and VOCs were published in Pritchard et al. (1955). Cl was generated via the photolysis of Cl<sub>2</sub> using a tungsten filament lamp. Rates for the reaction of Cl with methane and some short chain, branched and cyclic alkanes were measured relative to the rate of reaction between Cl and H<sub>2</sub>. Manning and Kurylo (1977) used flash photolysis to investigate the temperature dependencies of the reactions between Cl and some halogenated hydrocarbons. Cl was generated via the photolysis of CCl<sub>4</sub>, yielding initial Cl atom concentrations of approximately 10<sup>11</sup> cm<sup>-3</sup>. A discharge flow technique was used by Lin et al. (1978) to measure the rate of reaction between Cl and methane. The decay of methane due to reaction with Cl was monitored using mass spectrometry. The relative rate method was employed by Atkinson and Aschmann (1985) to measure the rates of reaction between Cl and some alkenes and aromatic VOCs for the first time. A series of reactions between Cl and aldehydes were studied for the first time using the relative rate method by Rodríguez et al. (2005) whilst biogenic monoterpenes have been studied by Canosa-Mas et al. (1999), Finlayson-Pitts et al. (1999) and Timerghazin and Ariya (2001). The sources referenced here represent some of the first studies of their kind but are by no means a comprehensive review of Cl + VOC reaction rate measurements.

Figure 5.14 shows rate coefficient values for VOC + Cl reactions ( $k_{Cl}$ ) plotted against rate coefficient values for VOC + OH reactions ( $k_{OH}$ ). There is evidently a wide range in  $k_{Cl}:k_{OH}$  ratios. Biogenic compounds (blue), which include isoprene and various monoterpenes, have Cl rate coefficients which are approximately five times greater than their OH counterparts.  $k_{Cl}$  values for the linear alkenes (red) are approximately 10 times greater than the same values for reactions with OH. The branched and cyclic alkenes (purple) have an average ratio somewhere between that for the linear alkenes and biogenics. The ratio for many of the smaller aromatics (benzene,

toluene, ethylbenzene and *o*- and *p*-xylene) is around an order of magnitude whilst the ratio for larger aromatics (*m*-xylene, styrene, 1,3,5-trimethylbenzene) is somewhat smaller, at approximately half that. The alkanes, both linear (yellow) and branched (green), react with Cl around 50 times faster than they do with OH; a significant difference. There are also some compounds, notably oxygenated VOCs such as acids, which react quicker with OH than Cl, but they are not shown here.

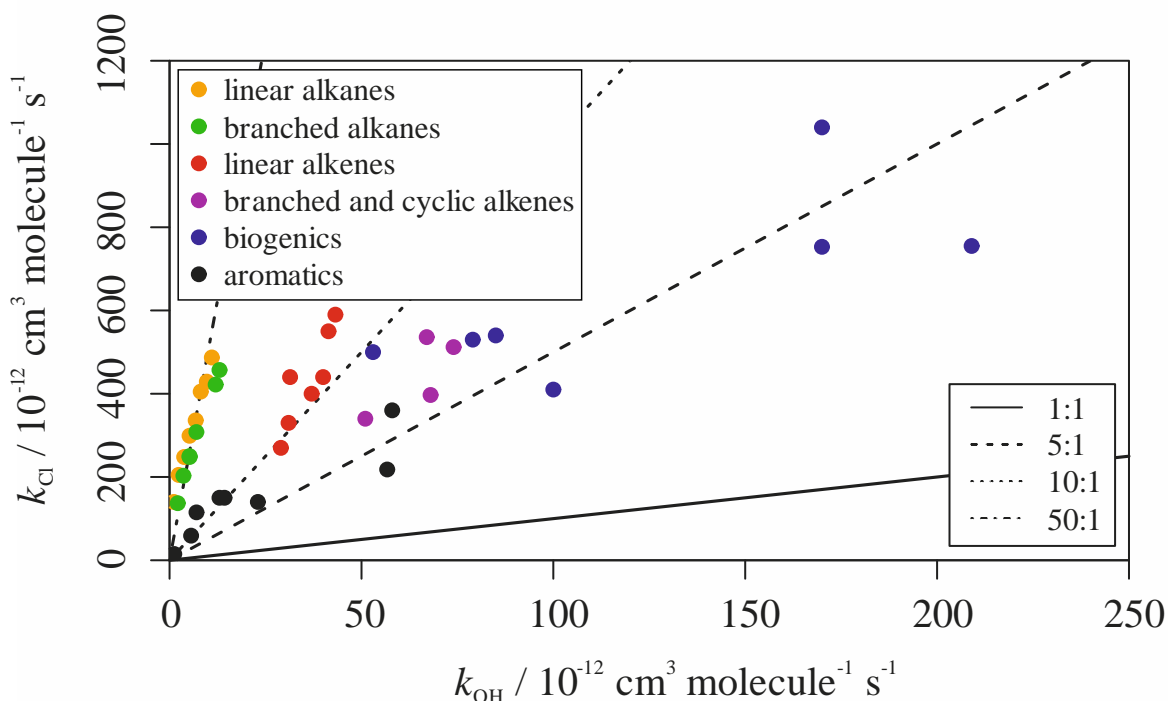


**Figure 5.14**  $k_{\text{Cl}}$  values plotted against  $k_{\text{OH}}$  value for multiple VOC reactions. Linear and branched alkanes are shown in yellow and green respectively. Linear alkenes are shown in red, branched and cyclic alkenes are in purple and biogenic compounds (comprising mainly monoterpenes) are in blue. Aromatic VOCs are shown in black.

Whilst Figure 5.14 demonstrates the stark contrast in the reactivity of OH and Cl radicals, particularly with respect towards alkanes, it does little to illustrate the relative importance of each radical. Cl is thought to be present in the troposphere in a much lower concentration than OH. OH is generally considered to have a daytime concentration of approximately  $10^6 \text{ cm}^{-3}$  (Krol et al., 1998). This concentration is a global average but, due to the nature of its formation OH is considered to be fairly ubiquitous throughout the troposphere. The sources of Cl radicals are not fully understood and hence the concentration of Cl in the troposphere is debated. The global average concentration in the marine boundary layer is estimated to be about  $10^3 \text{ cm}^{-3}$ , three orders of magnitude lower than that for OH. However, reports of Cl concentrations near Texas, USA approaching  $10^6 \text{ cm}^{-3}$  have been made through measurements of  $\text{ClNO}_2$  concentrations

(Osthoff et al., 2008) and estimated concentrations of  $0.6$  to  $4.7 \times 10^4 \text{ cm}^{-3}$  have been made on the island of Crete using NMHC ratios (Arsene et al., 2007).

### 5.2.1 Control experiments

Minor modifications were made to the equipment to allow for the measurement of VOC + Cl rate coefficients (see Chapter 2 Section 2.2.2). To ensure that these modifications had no impact on the experimental results, it was deemed necessary to run several control experiments in the absence of Cl<sub>2</sub>, the Cl atom precursor. These experiments were conducted using the large aromatics mixture described in Chapter 4 Section 4.1.2.

The first of these experiments attempted to quantify the impact of extracting the excess Cl<sub>2</sub> using the chemiresistant diaphragm pump. The large aromatics mixture was injected into the reactor at a constant flow of 400 sccm. Six samples were collected without the pump running and six samples were collected with the pump running. All other conditions were kept constant i.e. the lamp was kept off for all samples. Small depletions in the average peak areas, of up to 5%, were observed for 12 of the 13 VOCs when the pump was switched on, presumably due to a small drop in the pressure in the reactor. The peak areas for a single compound (1,2,3,5-tetramethylbenzene) were the only ones to increase with the pump switched on. It is unknown why this might have occurred. The average depletion in each VOC with the pump on was 2.0% ( $\pm$  3%) when including 1,2,3,5-tetramethylbenzene, or 2.9% ( $\pm$  1%) when excluding 1,2,3,5-tetramethylbenzene. Fortunately, the depletions in the observed peak areas due to the inclusion of the pump should not affect the results of the relative rate experiment so long as all VOCs experience a consistent depletion from lamp-off to lamp-on samples.

A second experiment was conducted to determine the effects of the 330 nm UV light on the VOCs in the large aromatics mixture. Four samples were collected with the lamp off and four with the lamp on. All other conditions were kept constant. Five compounds exhibited small increases in average peak area with the lamp on, whereas eight compounds experienced small decreases with the lamp on. The largest depletion in peak area, of 1.9%, was observed for *m*-xylene. The largest increase in peak area, of 2.4%, was observed for 1,2,3,5-tetramethylbenzene. The average change in peak area for a VOC was -0.1% ( $\pm$  1%). This change was insignificant and was therefore unlikely to be a result of the photolytic effects of the lamp. Deviations of this amount were more likely to be due to small, random fluctuations that occurred during the sampling and subsequent analysis.

For this reason, the impact of 330 nm UV light on the concentrations of VOCs was assumed to be negligible.

#### 5.2.1.1 Cl<sub>2</sub> chromatogram

Figure 5.15 shows the TIC obtained when a flow of Cl<sub>2</sub> (0.3 ppm) was injected into the reactor with the lamp off and in the absence of any VOCs. The large peak observed at approximately 3.5 minutes was identified as Cl<sub>2</sub>. The smaller peaks for compounds that eluted after Cl<sub>2</sub> were identified as; acetyl chloride (CH<sub>3</sub>COCl; 4.1 mins), acetic acid (CH<sub>3</sub>COOH; 4.7 mins), carbon tetrachloride (CCl<sub>4</sub>; 6.4 mins) and chloroacetyl chloride (CH<sub>2</sub>ClCOCl; 7.0 mins). These compounds may represent significant interferences for Cl atom exposure, if their rate coefficient for reaction with Cl are sufficiently high.

The rate coefficient for reaction between Cl and acetic acid has been measured twice. IUPAC recommends a  $k$  value of  $2.65 \left( {}^{+1.6}_{-1.0} \right) \times 10^{-14} \text{ cm}^3 \text{ molecule}^{-1} \text{ s}^{-1}$  at 298 K for their reaction (Atkinson et al., 2006). Rate coefficients for the reaction between Cl and acetyl chloride, carbon tetrachloride (CCl<sub>4</sub>) and chloroacetyl chloride did not exist in the literature at the time of writing. However, the rates coefficients for the reactions between these compounds and OH had been measured. The rate coefficient for the OH + acetyl chloride reaction was recommended to be  $1.7 \left( {}^{+2}_{-1} \right) \times 10^{-14} \text{ cm}^3 \text{ molecule}^{-1} \text{ s}^{-1}$  and that for the CCl<sub>4</sub> + OH to be  $< 1 \times 10^{-19} \text{ cm}^3 \text{ molecule}^{-1} \text{ s}^{-1}$  (Atkinson et al., 2006). These values are many orders of magnitude smaller than the rate coefficients for the reaction between most VOCs and OH so it is unlikely that they will have a significant impact on the relative rate kinetics occurring within the reactor for Cl reactions.

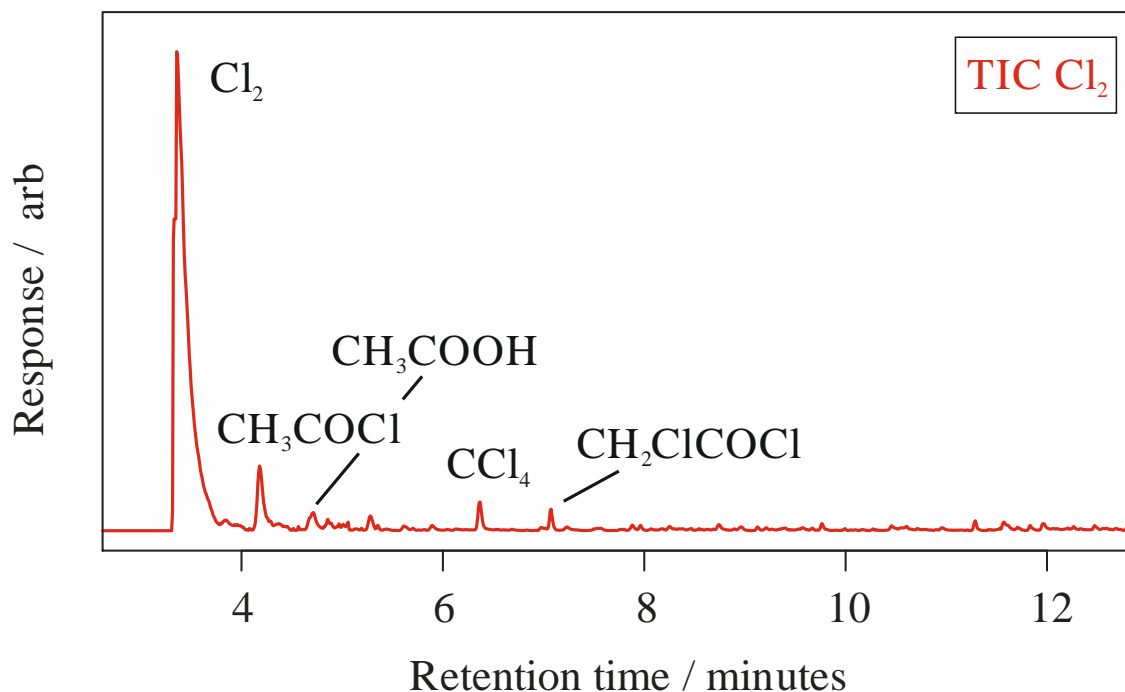


**Figure 5.15** TIC observed for a flow of  $\text{Cl}_2$  (0.3 ppm) in  $\text{N}_2$  injected into the reactor. The peaks were identified as molecular chlorine ( $\text{Cl}_2$ ), acetyl chloride ( $\text{CH}_3\text{COCl}$ ), acetic acid ( $\text{CH}_3\text{COOH}$ ), carbon tetrachloride ( $\text{CCl}_4$ ) and chloroacetyl chloride ( $\text{CH}_2\text{ClCOCl}$ ).

#### 5.2.1.2 Potential losses of VOCs due to $\text{Cl}_2$

Molecular chlorine ( $\text{Cl}_2$ ) was used as the precursor for the generation of Cl radicals.  $\text{Cl}_2$  was expected to be unreactive towards most VOCs (alkanes and aromatics) in the gas phase. The rate coefficient for the reaction between  $\text{Cl}_2$  and OH is several orders of magnitude less than those for reactions between OH and VOCs;  $k = 6.5 \left( \begin{smallmatrix} +1.3 \\ -1.1 \end{smallmatrix} \right) \times 10^{-14} \text{ cm}^3 \text{ molecule}^{-1} \text{ s}^{-1}$  (Atkinson et al., 2006). In the atmosphere, photolysis, rather than chemical reaction, represents the major loss process for  $\text{Cl}_2$ .

Figure 5.16 shows the TICs obtained for the large aromatics mixture with  $\text{Cl}_2$  (red; 66 ppm) and without  $\text{Cl}_2$  (blue) in the reactor. In both cases, the lamp was kept off to prevent the generation of any radicals via photolysis. In the absence of atomic Cl radicals, and with the assumed non-reactivity of gas-phase  $\text{Cl}_2$  towards VOCs, both chromatograms were expected to be essentially identical. This was clearly not the case.

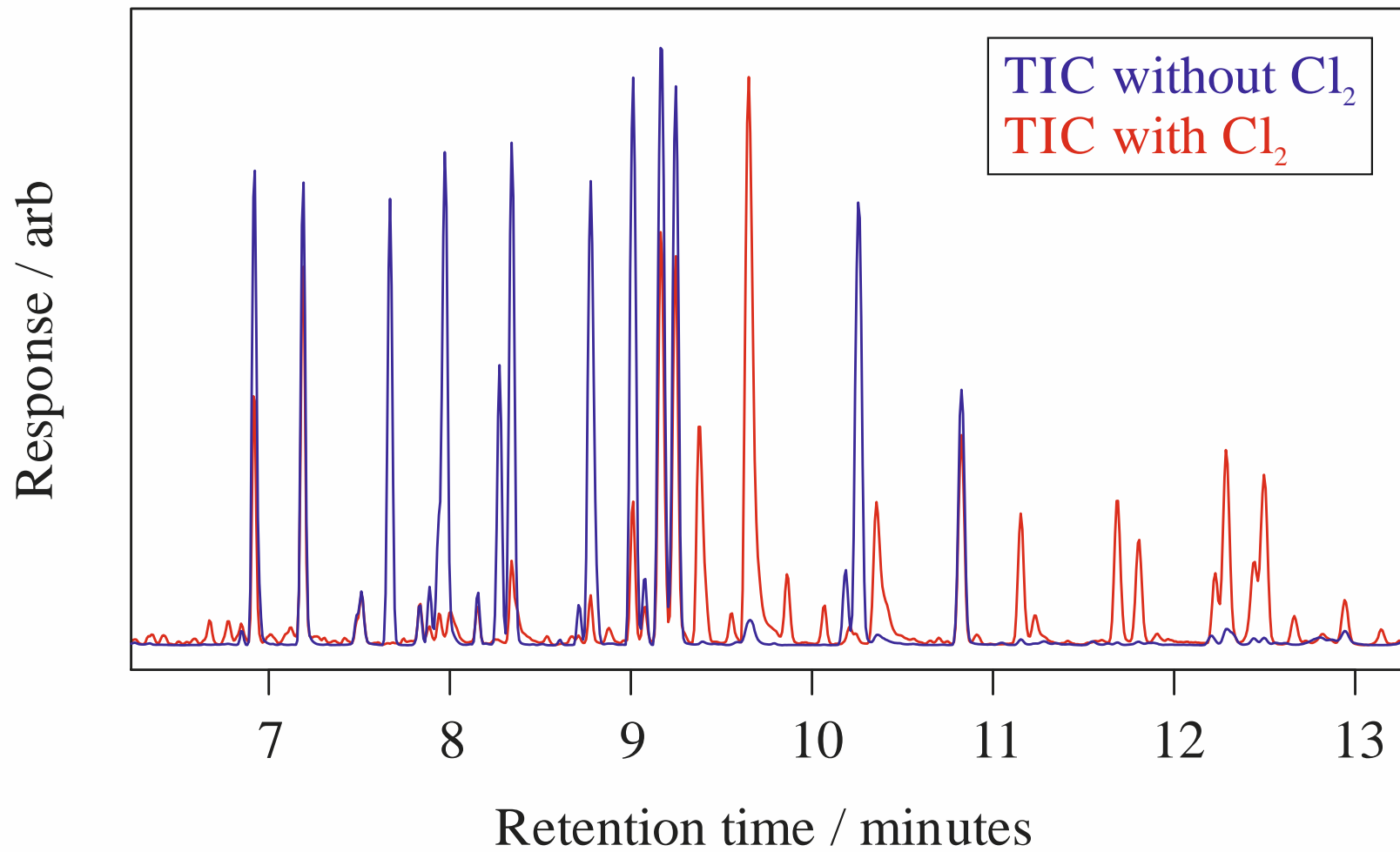


**Figure 5.16** TICs for the large aromatics mixture with Cl<sub>2</sub> (red; 66 ppm) and without Cl<sub>2</sub> (blue) in the reactor. See Table 5.5 for a list of peak identities.

In the case without Cl<sub>2</sub> (blue), the peaks appearing earlier in the chromatograms were due to the VOCs included in the mixture. The peak at 9.7 mins was identified as benzoyl chloride; this was likely left over from the previous GC sample, shown by the red chromatogram.

In the case with Cl<sub>2</sub> (red), many of the peaks due to the large aromatic VOCs disappeared entirely, or were significantly reduced. The amount of reduction, or suppression, varied from compound to compound. The two xylenes showed the least amount of suppression, with *o*-xylene remaining largely unchanged upon addition of Cl<sub>2</sub>.  $\alpha$ - and  $\beta$ -pinene were reduced almost entirely, so that their peaks were unidentifiable in the red chromatograph. Suppression occurred to a large extent for *n*-propylbenzene and the three trimethylbenzene isomers but less so for the three diethylbenzene isomers. The peak areas for the two tetramethylbenzene isomers were also significantly suppressed.

New peaks were also present in the TIC obtained with Cl<sub>2</sub> in the reactor. These peaks were identified as; 2-chloro-1,3-*m*-xylene ((CH<sub>3</sub>)<sub>2</sub>C<sub>6</sub>H<sub>3</sub>Cl; 9.4 mins), benzoyl chloride (C<sub>6</sub>H<sub>5</sub>COCl; 9.7 mins), 5-chloro-*m*-xylene ((CH<sub>3</sub>)<sub>2</sub>C<sub>6</sub>H<sub>3</sub>Cl; 9.9 mins), benzoic acid ((C<sub>6</sub>H<sub>5</sub>COOH; 10.4 mins), 2-chloro-1,3,5-trimethylbenzene, or isomers of C<sub>9</sub>H<sub>11</sub>Cl (11.2, 11.7, 11.8 and 12.5 mins) and 2-chloro-*p*-cymene, or isomers of C<sub>10</sub>H<sub>13</sub>Cl (12.2, 12.3, 12.5 and 12.9 mins). Many of these compounds are aromatic in nature but also incorporate one, or more, chlorine atoms. This suggests that they were the products of some aromatic VOC + Cl reactions which were presumably also responsible for the observed suppression in the primary aromatic VOC's peaks.

As mentioned previously, Cl<sub>2</sub> was expected to be generally unreactive towards the VOCs in the gas phase. It is therefore unlikely that gas phase VOC + Cl<sub>2</sub> reactions were responsible for the formation of these products. In the absence of a photolytic source for Cl, the potential presence of these reactions therefore suggests an alternative mechanism may be resulting in the formation of Cl radicals within the reactor.

**Table 5.5** List of compounds identified in the TICs obtained with and without Cl<sub>2</sub> in the presence of the large aromatics mixture (see Figure 5.16). Compounds which are underlined were present in the synthetic large aromatics mixture standard (see Chapter 4 Section 4.1.2).

Compound	Retention time / mins	Without Cl <sub>2</sub>	With Cl <sub>2</sub>
<u>m-xylene</u>	6.9	Yes	Yes
<u>o-xylene</u>	7.2	Yes	Yes
octamethylcyclotetrasiloxane	7.5	Yes	Yes
<u>α-pinene</u>	7.7	Yes	No
propylbenzene	7.8	Yes	Yes
3-ethyltoluene	7.9	Yes	Yes
<u>1,2,3-trimethylbenzene</u>	8.0	Yes	No
<u>β-pinene</u>	8.3	Yes	No
<u>1,2,4-trimethylbenzene</u>	8.4	Yes	Yes
<u>1,3,5-trimethylbenzene</u>	8.8	Yes	Yes
<u>1,3-diethylbenzene</u>	9.0	Yes	Yes
<u>1,4-diethylbenzene</u>	9.2	Yes	Yes
<u>1,2-diethylbenzene</u>	9.3	Yes	Yes
2-chloro- <i>m</i> -xylene	9.4	No	Yes
benzoyl chloride	9.7	Yes	Yes
5-chloro- <i>m</i> -xylene	9.9	No	Yes
<u>1,2,3,4-tetramethylbenzene</u>	10.2	Yes	No
<u>1,2,3,5-tetramethylbenzene</u>	10.3	Yes	No
benzoic acid	10.4	No	Yes
n-pentylbenzene	10.8	Yes	Yes
C <sub>9</sub> H <sub>11</sub> Cl	11.2, 11.7, 11.8, 12.5	No	Yes
C <sub>10</sub> H <sub>13</sub> Cl	12.2, 12.3, 12.5, 12.9	No	Yes

### 5.2.2 Cl mixture 1

This mixture contained five VOCs, of which all had at least one  $k$  measurement available in the literature at the time of writing. All five VOCs were alkanes with between six and nine carbon atoms. The alkanes were; 2-methylpentane, *n*-hexane, *n*-octane, cyclooctane and *n*-nonane. Table 5.6 gives a full list of the five alkanes in this mixture, along with the reference rate coefficient used.

There was only a small range in Cl rate coefficients in this mixture. The estimated total Cl reactivity of this mixture at STP was  $1400 \text{ s}^{-1}$ . The OH reactivity of the mixture was also estimated as  $31 \text{ s}^{-1}$ , at STP. This large discrepancy in reactivity clearly highlights the disparity between alkane + Cl and alkane + OH reactivity. This mixture was diluted with  $\text{N}_2$  in a ratio of approximately 1:60, to yield an estimated Cl reactivity in the reactor of  $23 \text{ s}^{-1}$  (OH reactivity of  $0.5 \text{ s}^{-1}$ ). Different flows of  $\text{Cl}_2$  were injected into the reactor to vary the number of radicals available for reaction with the VOCs; these flows resulted in estimated  $\text{Cl}_2$  concentrations in the reactor of between 30 and 100 ppm.

**Table 5.6** List of VOCs, in descending order of evaluated literature  $k$  value, in Cl mixture 1 along with their literature  $k$  value used as a reference and the total number of measurements found in the literature at the time of writing.

Name	Reference literature $k$ (298 K) / $10^{-12} \text{ cm}^3$ molecule $^{-1} \text{ s}^{-1}$	Reference used	Number of literature measurements
Cyclooctane	$457 \pm 15$	Aschmann and Atkinson, 2012	2
<i>n</i> -nonane	$453 \pm 28$	Aschmann and Atkinson, 1995	1
<i>n</i> -octane	$428 \pm 26$	Aschmann and Atkinson, 1995	3
<i>n</i> -hexane	$316 \pm 10$	Aschmann and Atkinson, 1995	3
2-methylpentane	$264 \pm 11$	Aschmann and Atkinson, 1995	2

## 5.2.2.1 Typical chromatogram data

Figure 5.17 shows sections of typical TICs obtained for this mixture with the reactor lamp turned off (blue) and the reactor lamp turned on (black). There is a clear reduction in the peak area for the two compounds shown (*n*-nonane and cyclooctane) when the lamp is switched on.

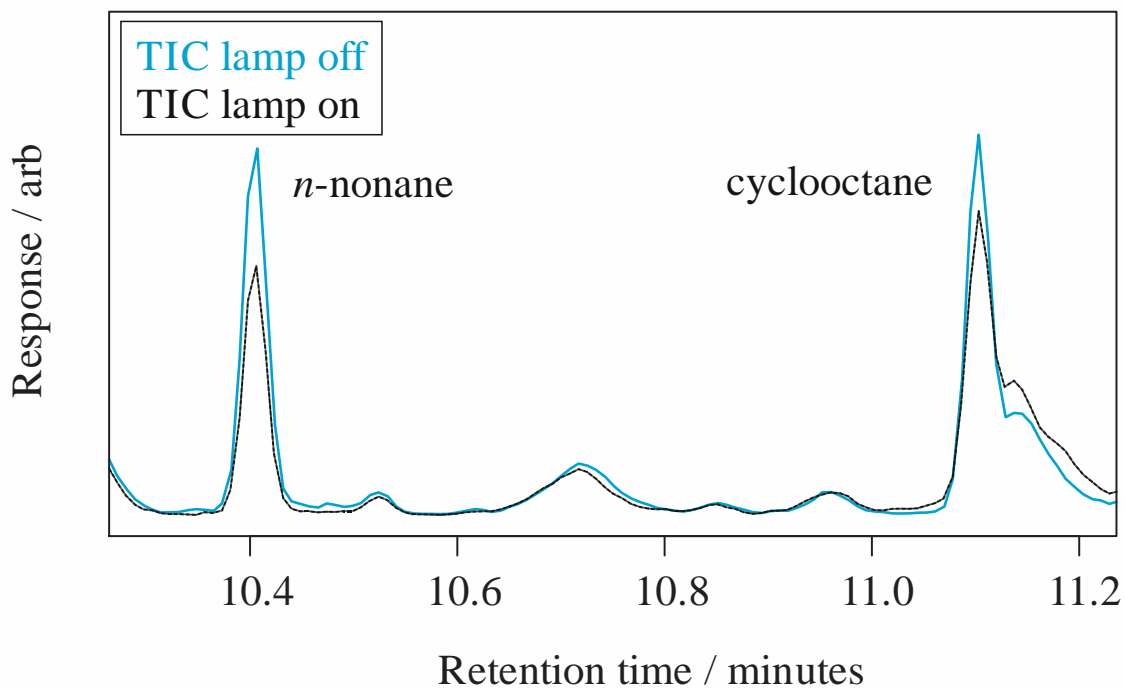


**Figure 5.17** Typical TIC sections obtained for Cl mixture 1 with the lamp turned off (blue) and the lamp turned on (black). Greater differences in peak areas were observed for VOCs which have a larger rate coefficient for their reaction with Cl. Literature rate coefficients (in units of  $10^{-12} \text{ cm}^3 \text{ molecule}^{-1} \text{ s}^{-1}$ ) for these alkane + OH reactions are: *n*-nonane,  $453 (\pm 28)$ ; cyclooctane,  $457 (\pm 15)$  (see Table 5.6).

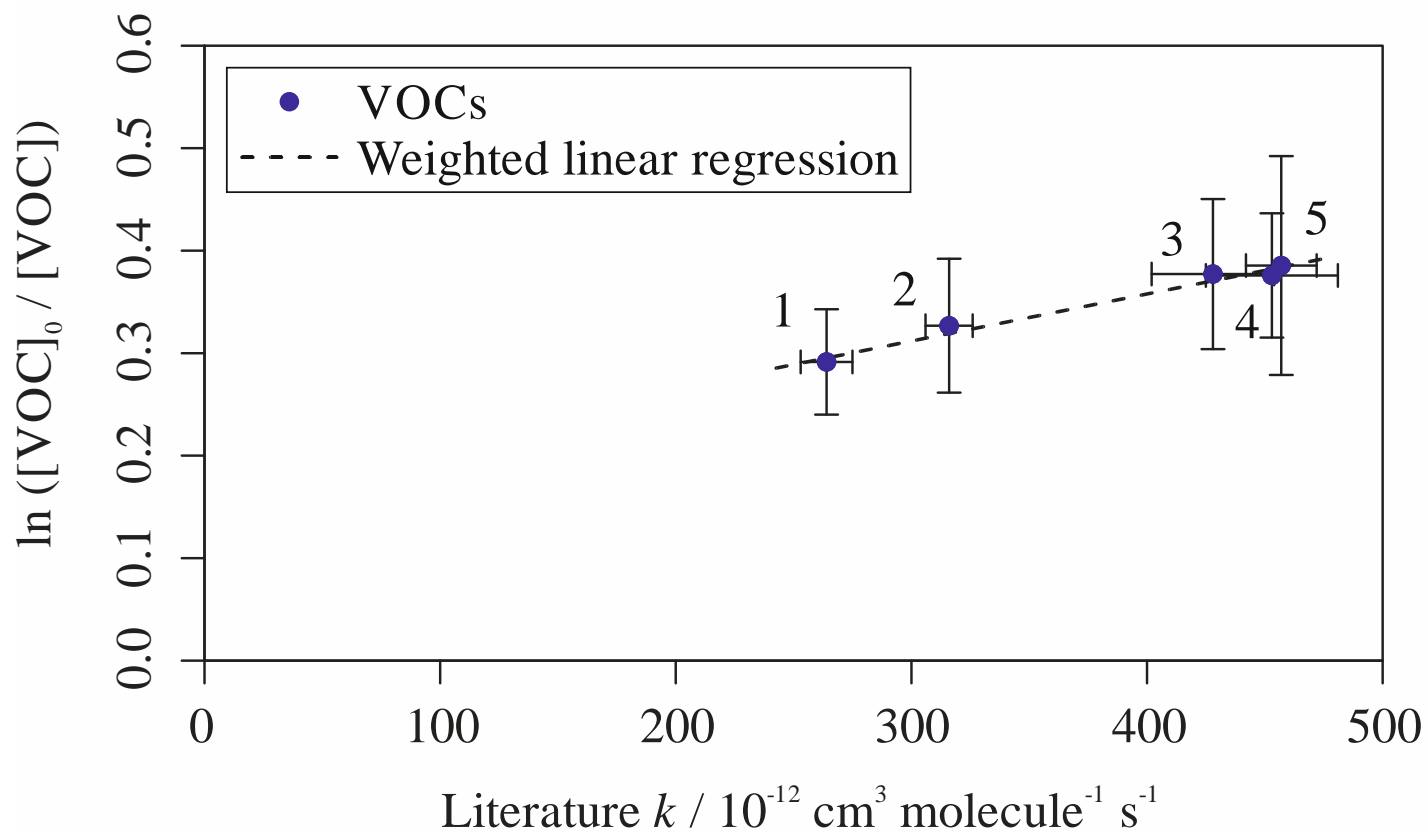
### 5.2.2.2 Relative rate plots

Figure 5.18 shows the relative rate plot for this mixture with an estimated  $\text{Cl}_2$  concentration in the reactor of 60 ppm. There was a clear linear correlation between the extent of depletion and the literature  $k$  value for each VOC. VOCs with a larger rate coefficient were observed to deplete more than VOCs with a smaller rate coefficient for reaction with Cl. The  $Cl_{exp}$  obtained using weighted linear regression had a value of  $0.5 (\pm 0.04) \times 10^9$  molecules  $\text{cm}^{-3}$  s. The  $R^2$  value for the fit was 0.96.

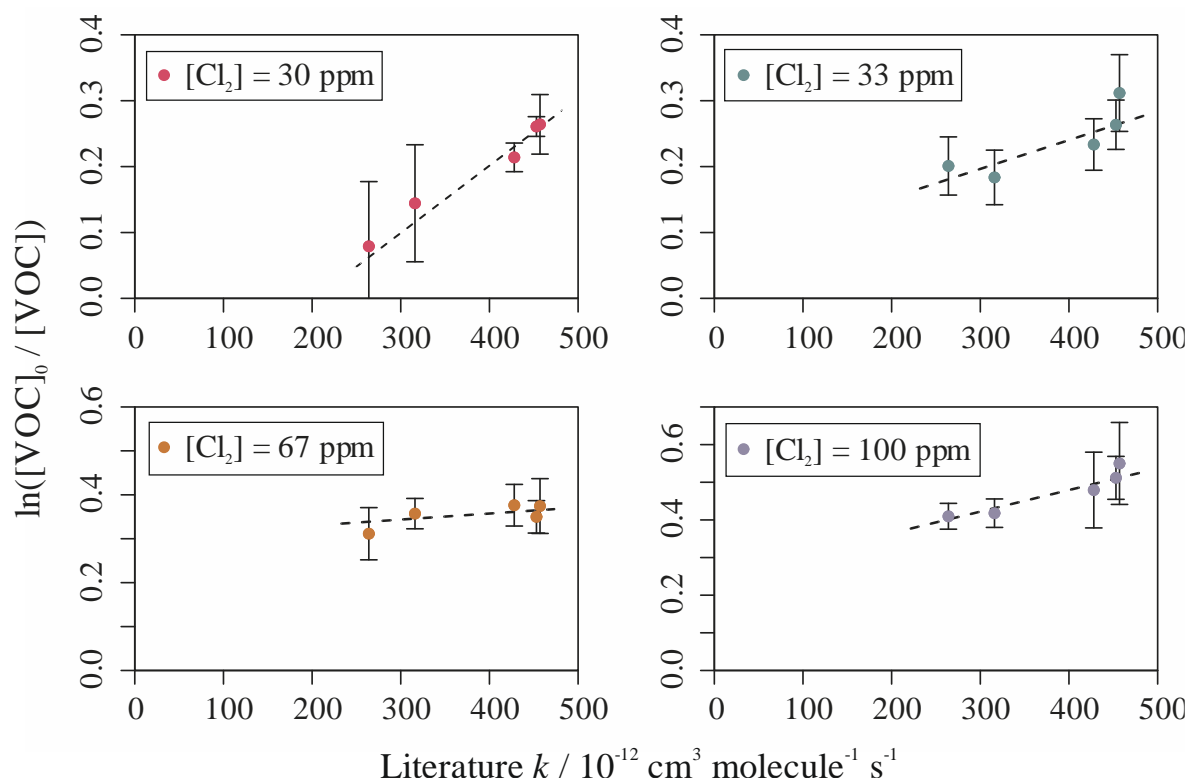
Figure 5.19 illustrates that similar trends were observed for this mixture when using different  $\text{Cl}_2$  concentrations. For estimated  $\text{Cl}_2$  concentrations of 30, 33 and 100 ppm, the  $Cl_{exp}$  values were  $1.0 (\pm 0.2)$ ,  $0.4 (\pm 0.2)$  and  $0.6 (\pm 0.1) \times 10^9$  molecules  $\text{cm}^{-3}$  s respectively. The  $R^2$  values of the linear fits were 0.83, 0.69 and 0.91 respectively.

Figure 5.19 also shows the relative rate plot for this mixture with a  $\text{Cl}_2$  concentration in the reactor of 67 ppm. There was only a small increase in depletion factor with increasing  $k$  value observed at this  $\text{Cl}_2$  concentration. The weighted linear regression at this  $\text{Cl}_2$  concentration was therefore almost flat, with a calculated slope of  $0.14 (\pm 0.12) \times 10^9$  molecules  $\text{cm}^{-3}$  s. It was still possible to extract relative rate data from this plot but the uncertainties in the estimated relative rate  $k$  values were much larger.

Whilst many of the measurements for this mixture gave results with a reasonably well-defined relationship between depletion factors and  $k$  values across the range of Cl reactivities tested, the limited range in VOC + Cl reactions meant that the relationship across a broader range of reactivities was not evaluated. Results earlier in this work have shown that the relationship between depletion factor and  $k$  value may not always be linear, especially over large reactivity ranges and when involving relatively fast reactions. In the absence of measurements for VOC + Cl reactions with  $k < 200 \times 10^{-12}$   $\text{cm}^3$  molecule $^{-1}$  s $^{-1}$ , it was impossible to determine if the broader relationship was linear or curved.



**Figure 5.18** Relative rate plot for Cl mixture 1 with a Cl reactivity of  $23 \text{ s}^{-1}$  and  $\text{Cl}_2$  (60 ppm) injected into the reactor, at 295 K. Compounds with a reference rate coefficient for reaction with Cl were plotted using literature values as references. Error bars on the y-axis, equal to one standard error, were calculated by combining the standard error in peak areas for four lamp-off and four lamp-on samples. Error bars on the x-axis were typically large and accounted for deviations from the trend for all VOCs. A weighted (to the uncertainty in the y-values) linear fit was used to generate the slope, with a value of  $Cl_{exp} = 0.5 (\pm 0.04) \times 10^9 \text{ molecules cm}^{-3} \text{ s}$  and  $R^2 = 0.96$ . The VOCs can be identified as follows; 1, 2-methylpentane; 2, *n*-hexane; 3, *n*-octane; 4, *n*-nonane; 5, cyclooctane.



**Figure 5.19** Relative rate plots for Cl mixture 1 with a Cl reactivity of  $23 \text{ s}^{-1}$  and estimated  $[Cl_2]$  of 30, 33, 67 and 100 ppm. The  $R^2$  values for the weighted linear fits were 0.83, 0.69, 0.09 and 0.91 respectively. The values of  $Cl_{exp}$  were  $1.0 (\pm 0.2)$ ,  $0.4 (\pm 0.2)$ ,  $0.14 (\pm 0.12)$  and  $0.6 (\pm 0.1) \times 10^9 \text{ molecules cm}^{-3} \text{ s}$  respectively. Error bars on the x-axis are not shown for reasons of clarity.

### 5.2.2.3 Calculation of rate coefficients

Rate coefficients for reaction with Cl for each of the VOCs in the mixture, relative to each of the other VOC + Cl reactions, were calculated using Eq. 2.30 and the  $Cl_{exp}$  values approximated using linear regression. This was performed at each of the different  $Cl_2$  concentrations injected into the reactor. An average value, weighted to the uncertainties, was then calculated, resulting in a single rate coefficient for each VOC + Cl reaction, relative to all the others. The final results are given in Table 5.7, along with the literature reference  $k$  values used.

**Table 5.7** List of VOCs, in descending order of literature  $k$  value, in Cl mixture 1 along with their range of depletion due to reaction with Cl, measured  $k$  value and literature  $k$  value used as a reference.

Name	Range of depletion / %	Measured $k$ (295 K) / $10^{-12} \text{ cm}^3 \text{ molecule}^{-1} \text{ s}^{-1}$	Literature $k$ / $10^{-12} \text{ cm}^3 \text{ molecule}^{-1} \text{ s}^{-1}$
cyclooctane	23 - 42	$496 \pm 41$	$457 \pm 15$
<i>n</i> -nonane	23 - 40	$443 \pm 21$	$453 \pm 28$
<i>n</i> -octane	19 - 38	$430 \pm 34$	$428 \pm 26$
<i>n</i> -hexane	13 - 34	$316 \pm 29$	$316 \pm 10$
2-methylpentane	8 - 34	$262 \pm 39$	$264 \pm 11$

The measured  $k$  values for all the VOC + Cl reactions were in good agreement with the literature reference values used.

### 5.2.2.4 Comparisons to the literature

In terms of other literature results, the measurement for the 2-methylpentane + Cl reaction in this work was in excellent agreement with the measurement by Hooshiyar and Niki (1995), of  $258 (\pm 8) \times 10^{-12} \text{ cm}^3 \text{ molecule}^{-1} \text{ s}^{-1}$ . The measurement for the *n*-hexane + Cl reaction also agreed well with previous measurements by Atkinson and Arey (1985) and Hooshiyar and Niki (1995). However, the measurement for the cyclooctane + Cl reaction was in poor agreement with that by Aranda et al. (2007), who reported a  $k$  value for that reaction of  $263 (\pm 54) \times 10^{-12} \text{ cm}^3 \text{ molecule}^{-1} \text{ s}^{-1}$ . The measurement for *n*-octane + Cl was also in somewhat poor agreement with another recent measurement by Li and Piresteh (2006), of  $322 (\pm 36) \times 10^{-12} \text{ cm}^3 \text{ molecule}^{-1} \text{ s}^{-1}$  but agreed well with the measurement in Hooshiyar and Niki (1995), of  $409 (\pm 12) \times 10^{-12} \text{ cm}^3 \text{ molecule}^{-1} \text{ s}^{-1}$ .

### 5.2.3 Cl mixture 2

This mixture contained seven VOCs, of which all but one had at least one  $k$  measurement available in the literature at the time of writing. Five of the VOCs were alkanes with between six and nine carbon atoms; 2-methylpentane, *n*-octane, cyclooctane, 2-methylheptane and *n*-nonane. Two of the VOCs were simple alkyl substituted aromatic compounds (toluene and ethylbenzene). Table 5.8 gives a full list of the VOCs in this mixture, along with the reference rate coefficients used.

There was a larger range in Cl rate coefficient in this mixture, when compared with the pure alkanes mixture in Section 5.2.2. The addition of two aromatic compounds to the mixture, with  $k$  values for reaction with Cl of less than  $150 \times 10^{-12} \text{ cm}^3 \text{ molecule}^{-1} \text{ s}^{-1}$ , allowed for a broader evaluation of the relationship between depletion factor and rate coefficient. The estimated total Cl reactivity of this mixture, excluding the compound with an unknown  $k$  value, was approximately  $1600 \text{ s}^{-1}$  at STP. The OH reactivity of the mixture was also estimated to be  $61 \text{ s}^{-1}$  at STP. This mixture was diluted with  $\text{N}_2$  in a ratio of approximately 1:60, to yield an estimated Cl reactivity of  $27 \text{ s}^{-1}$  (OH reactivity of  $1.0 \text{ s}^{-1}$ ) in the reactor. Different flows of  $\text{Cl}_2$  were injected into the reactor to vary the number of radicals available for reaction with the VOCs; these flows resulted in estimated  $\text{Cl}_2$  concentrations in the reactor of between 50 and 300 ppm.

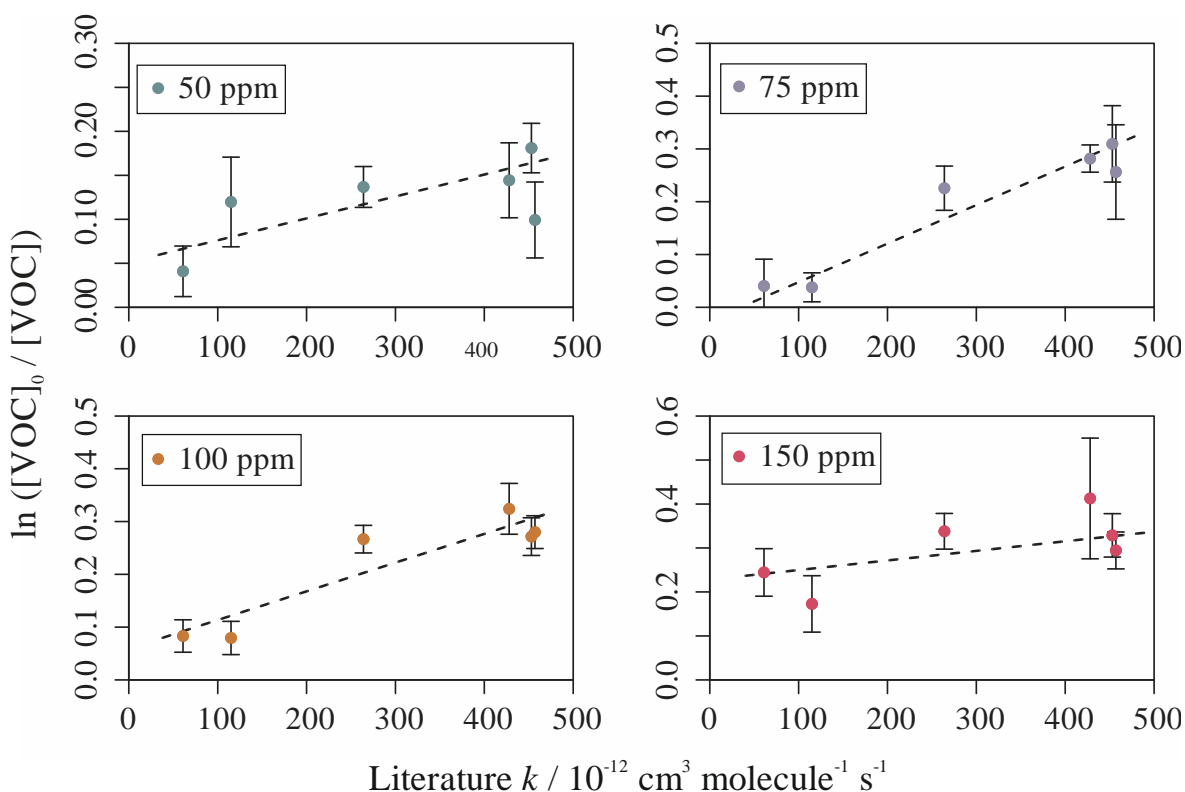
**Table 5.8** List of VOCs, in descending order of literature  $k$  value, in Cl mixture 2 along with their literature  $k$  value used as a reference and the total number of measurements found in the literature at the time of writing.

Name	Reference literature $k$ (298 K) / $10^{-12} \text{ cm}^3$ molecule $^{-1} \text{ s}^{-1}$	Reference used	Number of literature measurements
Cyclooctane	$457 \pm 15$	Aschmann and Atkinson, 2012	2
<i>n</i> -nonane	$453 \pm 28$	Aschmann and Atkinson, 1995	1
<i>n</i> -octane	$428 \pm 26$	Aschmann and Atkinson, 1995	3
2-methylpentane	$264 \pm 11$	Aschmann and Atkinson, 1995	2
Ethylbenzene	$115 \pm 4$	Anderson et al., 2007	1
Toluene	$61 \pm 1.1$	Atkinson and Aschmann, 1985	4
2-methylheptane			0

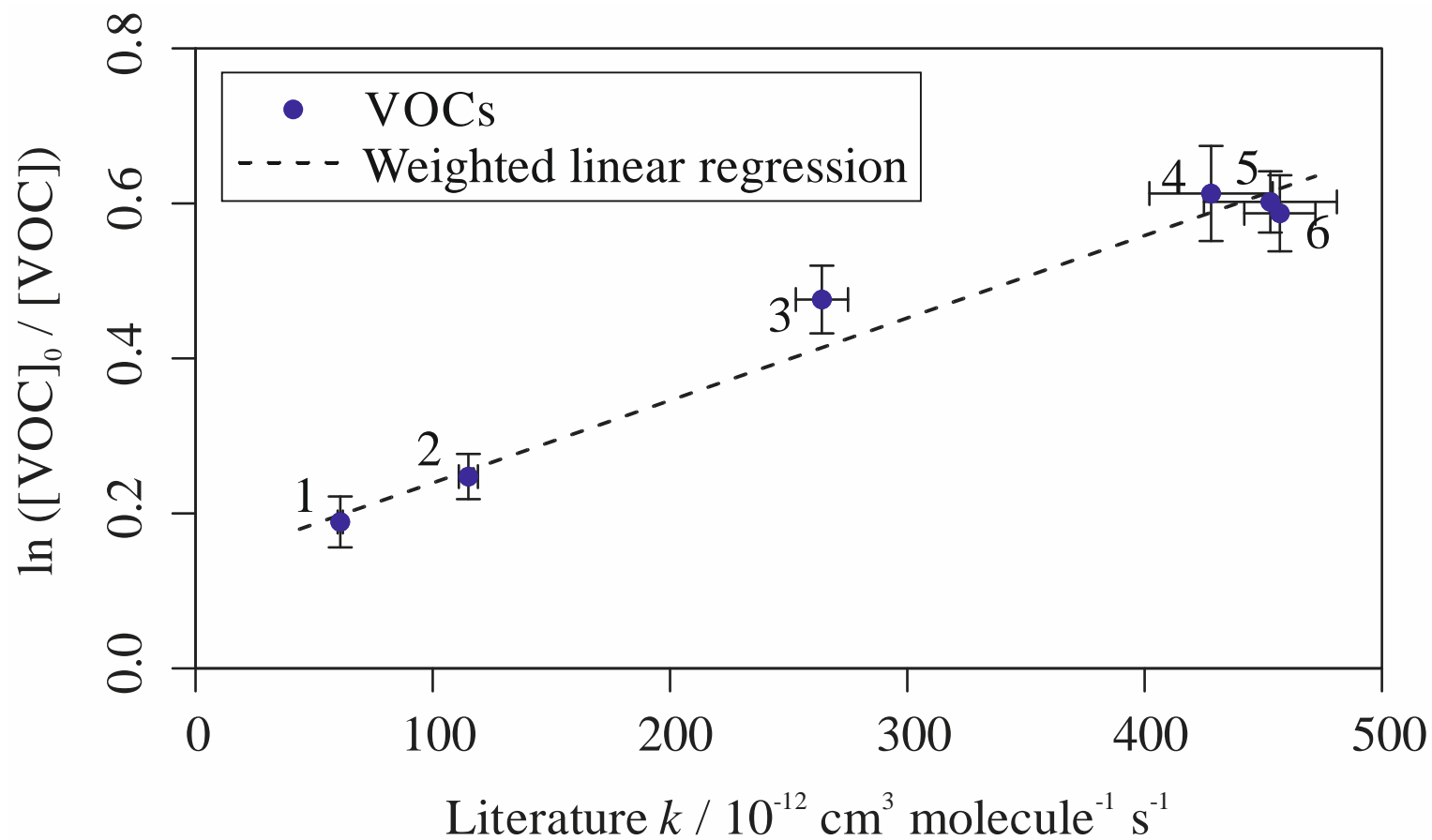
## 5.2.3.1 Relative rate plots

Figure 5.21 shows a relative rate plot for this mixture when using 300 ppm  $\text{Cl}_2$ . The figure shows that there was a linear correlation between the depletion factors for each compound due to reaction with Cl and the reference rate coefficients used. Unlike the first Cl mixture, where there were no data below  $200 \times 10^{-12} \text{ cm}^3 \text{ molecule}^{-1} \text{ s}^{-1}$ , this mixture contained two aromatic compounds with reference  $k$  values of  $61 (\pm 1.1)$  and  $115 (\pm 4) \times 10^{-12} \text{ cm}^3 \text{ molecule}^{-1} \text{ s}^{-1}$ . The depletion factors in both aromatic VOCs were related linearly to the depletions in the faster reacting alkanes, confirming that a linear relationship between depletion factor and  $k$  was observed across the reactivity spectrum, as opposed to a potential curved relationship. The  $Cl_{exp}$  of the mixture, using 300 ppm of  $\text{Cl}_2$ , was  $1.1 (\pm 0.1) \times 10^9 \text{ molecules cm}^{-3} \text{ s}$ . The  $R^2$  value was 0.97.

Similar trends were observed when using  $\text{Cl}_2$  with concentrations of 50, 75, 100 and 150 ppm. Relative rate plots for these  $\text{Cl}_2$  concentrations are shown in Figure 5.20. The  $Cl_{exp}$  at these concentrations were  $0.3 (\pm 0.1)$ ,  $0.5 (\pm 0.1)$ ,  $0.7 (\pm 0.1)$  and  $0.2 (\pm 0.1)$ , with  $R^2$  values of 0.54, 0.76, 0.93 and 0.21 respectively.



**Figure 5.20** Relative rate plots for Cl mixture 2 with a Cl reactivity of  $27 \text{ s}^{-1}$  and estimated  $[\text{Cl}_2]$  of 50, 75, 100 and 150 ppm. The  $R^2$  values for the weighted linear fits were 0.54, 0.76, 0.93 and 0.21 respectively. The values of  $Cl_{exp}$  were  $0.3 (\pm 0.1)$ ,  $0.5 (\pm 0.1)$ ,  $0.7 (\pm 0.1)$  and  $0.2 (\pm 0.1) \times 10^9 \text{ molecules cm}^{-3} \text{ s}$  respectively. Error bars on the x-axis are not shown for reasons of clarity.



**Figure 5.21** Relative rate plot for Cl mixture 2 with a Cl reactivity of  $27 \text{ s}^{-1}$  and  $\text{Cl}_2$  (300 ppm) injected into the reactor, at 295 K. Compounds with a reference rate coefficient for reaction with Cl were plotted using literature values as references. Error bars on the y-axis, equal to one standard error, were calculated by combining the standard error in peak areas for four lamp-off and four lamp-on samples. Error bars on the x-axis were typically large and accounted for deviations from the trend for all VOCs. A weighted (to the uncertainty in the y-values) linear fit was used to generate the slope, with a value of  $Cl_{exp} = 1.1 (\pm 0.1) \times 10^9 \text{ molecules cm}^{-3} \text{ s}$  and  $R^2 = 0.97$ . The VOCs can be identified as follows; 1, toluene; 2, ethylbenzene; 3, 2-methylpentane; 4, *n*-octane; 5, *n*-nonane; 6, cyclooctane.

### 5.2.3.2 Calculation of rate coefficients

It was possible to calculate measured  $k$  values for the compounds in this mixture using their depletion factors and the measured  $Cl_{exp}$ , derived from the weighted linear fits. This calculation was performed for each  $Cl_2$  concentration before a weighted average of the five derived rate coefficients was used to result in a final experimental value for each VOC + Cl reaction. These values are shown in Table 5.9.

**Table 5.9** List of VOCs, in descending order of literature  $k$  value, in Cl mixture 2 along with their range of depletion due to reaction with Cl, measured  $k$  value and literature  $k$  value used as a reference.

Name	Range of depletion / %	Measured $k$ (295 K) / $10^{-12}$ $cm^3$ molecule $^{-1}$ s $^{-1}$	Literature $k$ / $10^{-12}$ $cm^3$ molecule $^{-1}$ s $^{-1}$
cyclooctane	16 - 44	410 ± 51	457 ± 15
<i>n</i> -nonane	18 - 45	442 ± 27	453 ± 28
<i>n</i> -octane	9 - 46	455 ± 76	428 ± 26
2-methylpentane	13 - 39	339 ± 42	264 ± 11
ethylbenzene	6 - 22	96 ± 96	115 ± 4.0
toluene	0 - 22	49 ± 24	61 ± 1.12
2-methylheptane	9 - 45	426 ± 77	

The results for five of the six VOC + Cl reactions were in agreement with the literature, within errors.

### 5.2.3.4 Comparisons to the literature

The measured  $k$  value for toluene was in excellent agreement with the literature, although it did have a much larger uncertainty placed upon it. Other  $k$  values for the toluene + Cl reaction have been measured to be 59 (± 5), 56 and 55.7 (± 1.5) × 10<sup>-12</sup> cm<sup>3</sup> molecule<sup>-1</sup> s<sup>-1</sup> (Shi and Bernhard, 1997; Fantechi et al., 1998; Ryzhkov et al., 2008). These are all in good agreement with that measured in this work.

The measured value for the Cl + ethylbenzene was also in good agreement with its reference literature counterpart. However, the measured value in this work had a large uncertainty placed upon it. The literature measurement, provided by Anderson et al. (2007), was the only previous measurement of the rate coefficient for this reaction at the time of writing.

Measured values for the reactions of the four alkanes (2-methylpentane, cyclooctane, *n*-octane and *n*-nonane) with Cl, were compared with the literature previously. However, the values derived using this mixture differed for some compounds to those derived earlier. All results were in agreement within errors but the *k* value for the 2-methylpentane + Cl reaction was approximately 30 % larger than that derived in the previous mixture and was therefore in poor agreement with the reference literature value. The value for the cyclooctane + Cl reaction was also almost 25 % smaller than the value measured previously (of  $496 (\pm 41) \times 10^{-12} \text{ cm}^3 \text{ molecule}^{-1} \text{ s}^{-1}$ ). The results for the linear *n*-alkanes in the two mixtures were in excellent agreement however.

### 5.2.3.3 Determination of a new rate coefficient for the 2-methylheptane + Cl reaction

2-methylheptane had no recorded rate coefficient for its reaction with Cl in the literature at the time of writing. The measurement provided in this work, of  $426 (\pm 77) \times 10^{-12} \text{ cm}^3 \text{ molecule}^{-1} \text{ s}^{-1}$  therefore represents the first experimental measurement of its kind.

Several structure activity relationships (SARs) for estimating the rate coefficient for reaction between alkanes and Cl exist in the literature. Estimated *k* values for the 2-methylheptane + Cl reaction are 410, 416, 398 and  $407 \times 10^{-12} \text{ cm}^3 \text{ molecule}^{-1} \text{ s}^{-1}$  for the SARs provided by Aschmann and Atkinson (1995, 2012), Hooshiyar and Niki (1995), Tyndall et al. (1997) and Qian et al. (2002). The SAR provided in Aschmann and Atkinson (2012) was an update to that published in Aschmann and Atkinson (1995) in which the rate coefficients were updated relative to  $k_{n\text{-butane}+\text{Cl}} = 2.05 \times 10^{-10} \text{ cm}^3 \text{ molecule}^{-1} \text{ s}^{-1}$ . The same update of reference values was applied to the rate coefficients used to derive the SARs provided in the other works, in order to make a fair comparison.

In all cases, the SARs estimated a slightly smaller rate coefficient than that measured experimentally for the Cl + 2-methylheptane reaction. However, the uncertainty placed upon the measured value meant that it did not differ significantly from the SAR estimated values. Figure 5.22 shows experimentally derived *k* values, alongside theoretical SAR derived *k* values, for a homologous series of 2-methylalkanes with between four and eight total carbon atoms. All four SARs were able to reproduce the measured values across the series exceptionally well. The only experimental *k* value that did not fit the anticipated trend was that observed for the 2-methylpentane + Cl reaction as part of this mixture. The result obtained for 2-methylpentane + Cl in the previous mixture was in excellent agreement with all other data, however.

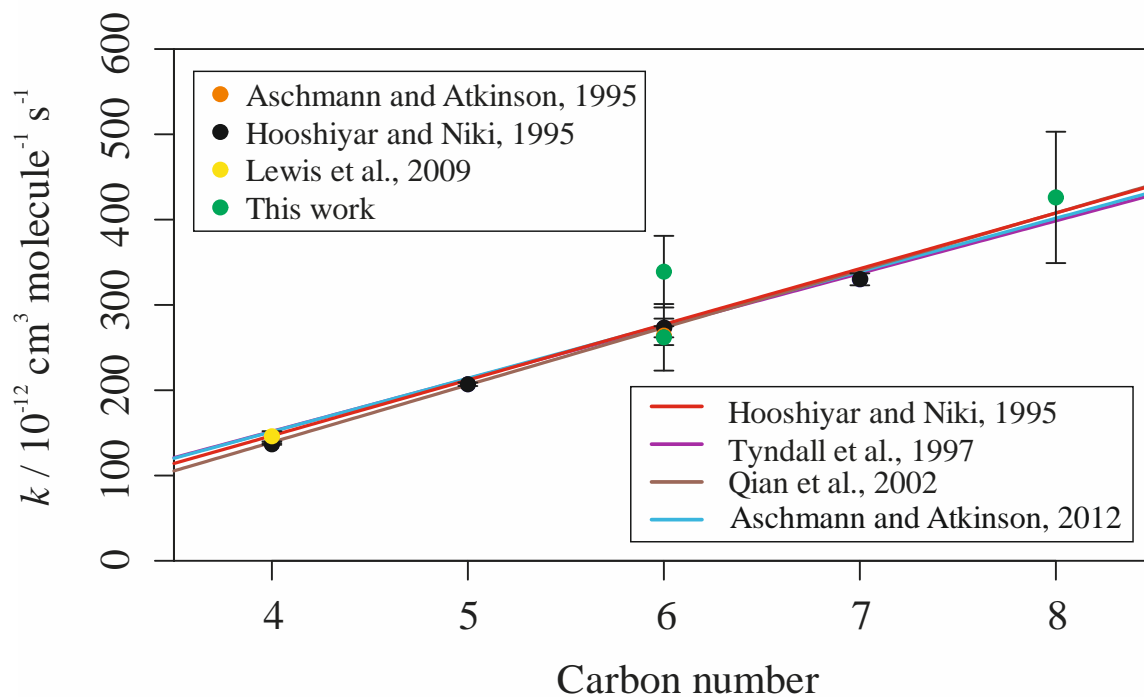


**Figure 5.22** Experimentally derived (data points) and predicted SAR derived (lines)  $k$  values for the homologous series of 2-methylalkane + Cl reactions. Data from this study are shown in green and were in good agreement with both previous experimentally measured values and theoretical predictions.

## 5.2.4 Numerical simulations

Numerical simulations were used to complement the experimental studies and to further aid in the comprehension of the experimental results. Most of the simulations were performed using Kintecus V5.20 (Ianni, 2017; <http://kintecus.com/>).

### 5.2.4.1 Estimated Cl concentration and Cl<sub>2</sub> to Cl conversion

The concentration of Cl in the reactor was approximated by summing the losses in all the VOCs in the mixture. As previously, when estimating [OH] in the reactor (see Chapter 3 Section 3.2.1 for more information), a few assumptions were made for this method to generate an estimate of the [Cl] available for reaction. First, it was assumed that all the Cl atoms reacted only with VOCs i.e. no other reactions took place. This was unlikely to be true however, as the Cl + Cl recombination reaction (R. 5.1) was likely to occur, with an approximate second-order rate coefficient at room temperature and close-to-atmospheric pressure, of  $k = 1.7 (\pm 0.2) \times 10^{-13} \text{ cm}^3 \text{ molecule}^{-1} \text{ s}^{-1}$  (Donohoue et al., 2005). The measured peak area of each VOC with the lamp off was also assumed to be representative of its anticipated concentration in the reactor. This assumption should be correct if the estimated concentration of the VOCs in the cylinder, and therefore the reactor, were accurate.



Figure 5.23 shows the relationship between the estimated [Cl] and approximate [Cl<sub>2</sub>] in the reactor for the two mixtures tested. There was a distinct linear relationship for each mixture; as the amount of Cl<sub>2</sub> in the reactor increased, the estimated concentration of Cl radicals also increased. However, there did appear to be a discrepancy between the two mixtures; there was an apparently greater yield in Cl for Cl mixture 1 relative to Cl mixture 2 when using the same concentrations of Cl<sub>2</sub>. It's possible that the difference in the Cl reactivity of the mixtures was the cause of this; a mixture with a higher reactivity towards Cl will typically reduce the amount of Cl-Cl recombination reactions taking place.

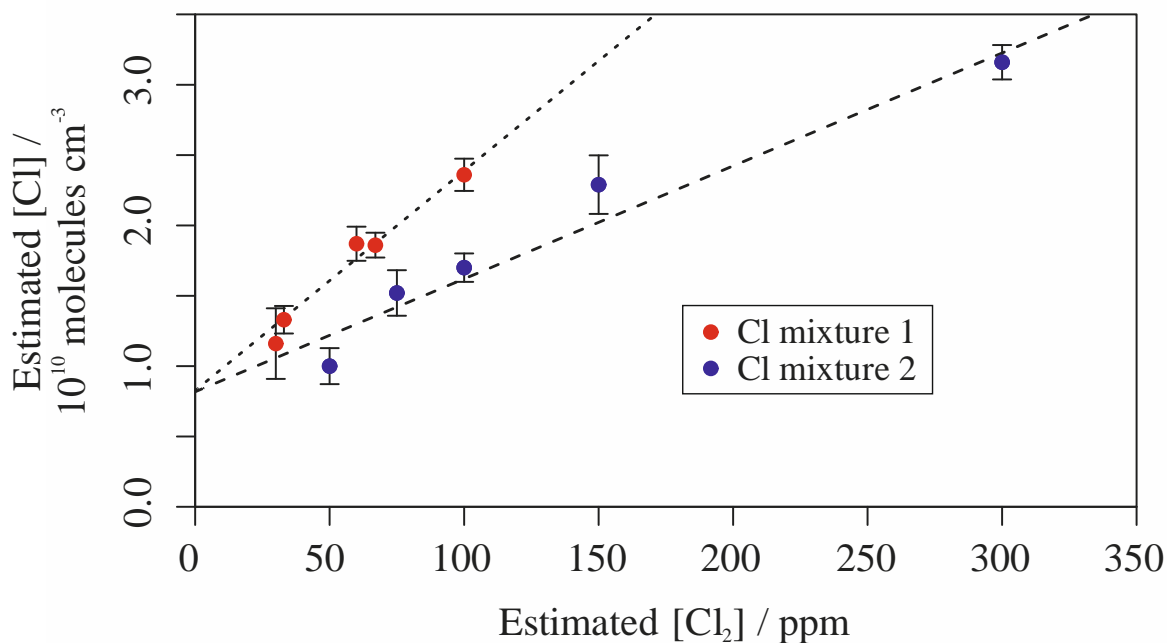


**Figure 5.23** The estimated concentrations of Cl radicals resulting from the photolysis of different concentrations of Cl<sub>2</sub> injected into the reactor.

The concentration of Cl in the reactor ranged from approximately  $1.0 \times 10^{10}$  molecules cm<sup>-3</sup>, when [Cl<sub>2</sub>] = 30 ppm, to approximately  $3.2 \times 10^{10}$  molecules cm<sup>-3</sup>, when [Cl<sub>2</sub>] = 300 ppm. This radical concentration was somewhat lower than the estimated concentration of OH, which was approximated to be on the order of  $10^{11}$  molecules cm<sup>-3</sup> depending on the OH reactivity of the mixture used (see Chapter 3 Section 3.2.1). The average yield of Cl, in units of Cl atoms per million Cl<sub>2</sub> molecules, was  $12 (\pm 0.7)$  and  $6.6 (\pm 0.4)$  for the mixture 1 and 2 respectively.

## Conclusions

The multivariate relative rate technique was successfully adapted to allow for the measurement of rate coefficients for VOC + OH reactions at carefully controlled temperatures. A mixture containing a series of alkanes was used to test the new apparatus. Results for this mixture at room temperature were in exceptional agreement with the available evaluated literature rate coefficients used as references for 9 alkane + OH reactions. The room temperature measurements of the reactions of 2-methylheptane, 2-methylnonane and ethylcyclohexane with OH represented the first measurements of their kind at the time of writing.

Relative rate measurements of the rate coefficients at elevated temperatures were less convincing. Whilst Arrhenius parameters were derived for the reaction of all 12 compounds with OH across the range of temperatures explored (290 – 470 K), much of the data were subject to significant scatter. However, for alkane + OH reactions with more comprehensive temperature dependent studies, the Arrhenius parameters derived in this work were in good agreement with those derived elsewhere. It is therefore suggested that the multivariate relative rate technique is better suited for the assessment of existing Arrhenius parameters, rather than for the derivation of new Arrhenius parameters, for which a more precise technique may be more applicable.

The multivariate relative rate technique was also successfully adapted to accommodate Cl radical reaction rate coefficient measurements. Two mixtures, comprising mainly alkanes alongside some aromatic VOCs, were tested with the Cl experimental method at room temperature. Most of the results for VOC + Cl reactions were in good agreement with the literature, although the extent of literature available to use as references was limited. A new rate coefficient for the 2-methylheptane + Cl reaction, of  $426 (\pm 77) \times 10^{-12} \text{ cm}^3 \text{ molecule}^{-1} \text{ s}^{-1}$ , was derived for the first time.

Experiments involving Cl were potentially complicated by the observed interaction of the Cl radical precursor, Cl<sub>2</sub>, with the VOCs. The mechanism by which Cl<sub>2</sub> interacted with VOCs was not explored but was identified as a potential source of interference if it could not be accounted for.

## References

- Anderson, R. S., Huang, L., Iannone, R. and Rudolph, J.: Laboratory measurements of the  $^{12}\text{C}/^{13}\text{C}$  kinetic isotope effects in the gas-phase reactions of unsaturated hydrocarbons with Cl atoms at  $298 \pm 3$  K, *J. Atmos. Chem.*, 56, 275-291, <https://doi.org/10.1007/s10874-006-9056-4>, 2007.
- Arsene, C., Bougiatioti, A., Kanakidou, M., Bonsang, B. and Mihalopoulos, N.: Tropospheric OH and Cl levels deduced from non-methane hydrocarbon measurements in a marine site, *Atmos. Chem. Phys.*, 7, 4661-4673, <https://doi.org/10.5194/acp-7-4661-2007>, 2007.
- Aschmann, S. M. and Atkinson, R.: Rate constants for the gas-phase reactions of alkanes with Cl atoms at  $296 \pm 2$  K, *Int. J. Chem. Kinet.*, 27, 613-622, <https://doi.org/10.1002/kin.550270611>, 1995.
- Aschmann, S. M., Arey, J. and Atkinson, R.: Atmospheric chemistry of three  $\text{C}_{10}$  alkanes, *J. Phys. Chem. A*, 105, 7598-7606, <https://doi.org/10.1021/jp010909j>, 2001.
- Aschmann, S. M. and Atkinson, R.: Rate constants for the reactions of Cl atoms with a series of  $\text{C}_6$ - $\text{C}_{10}$  cycloalkanes and cycloketones at  $297 \pm 2$  K, *Int. J. Chem. Kinet.*, 45, 52-58, <https://doi.org/10.1002/kin.20743>, 2012.
- Atkinson, R., Aschmann, S. M., Carter, W. P. L., Winer, A. M. and Pitts Jr., J. N.: Kinetics of the reactions of OH radicals with *n*-alkanes at  $299 \pm 2$  K, *Int. J. Chem. Kinet.*, 14, 781-788, <https://doi.org/10.1002/kin.550140706>, 1982.
- Atkinson, R., Carter, W. P. L., Aschmann, S. M., Winer, A. M. and Pitts Jr., J. N.: Kinetics of the reactions of OH radicals with a series of branched alkanes at  $297 \pm 2$  K, *Int. J. Chem. Kinet.*, 16, 469-481, <https://doi.org/10.1002/kin.550160413>, 1984.
- Atkinson, R. and Aschmann, S. M.: Kinetics of the gas phase reaction of Cl atoms with a series of organics at  $296 \pm 2$  K and atmospheric pressure, *Int. J. Chem. Kinet.*, 17, 33-41, <https://doi.org/10.1002/kin.550170105>, 1985.
- Atkinson, R.: Kinetics of the gas-phase reactions of OH radicals with alkanes and cycloalkanes, *Atmos. Chem. Phys.*, 3, 2233-2307, <https://doi.org/10.5194/acp-3-2233-2003>, 2003.

- Atkinson, R., Baulch, D. L., Cox, R. A., Crowley, J. N., Hampson, R. F., Hynes, R. G., Jenkin, M. E., Rossi, M. J. and Troe, J.: Evaluated kinetic and photochemical data for atmospheric chemistry: Volume II – gas phase reactions of organic species, *Atmos. Chem. Phys.*, 6, 3265-4055, 2006. Also at <http://iupac.pole-ether.fr/index.html>.
- Baklanov, A. V. and Krasnoperov, L. N.: Oxalyl chloride – a clean source of chlorine atoms for kinetic studies, *J. Phys. Chem. A*, 105, 97-103, <https://doi.org/10.1021/jp0019456>, 2001.
- Baldwin, R. R., Walker, R. W. And Walker, R. W.: Addition of 2,2,3-trimethylbutane to slowly reacting mixtures of hydrogen and oxygen at 480 °C, *J. Chem. Soc. Faraday Trans. 1*, 77, 2157-2173, <https://doi.org/10.1039/F19817702157>, 1981.
- Behnke, W., Nolting, F. and Zetzsch, C.: A smog chamber study of the impact of aerosols on the photodegradation of chemicals in the environment, *J. Aerosol. Sci.*, 18, 65-71, [https://doi.org/10.1016/0021-8502\(87\)90011-5](https://doi.org/10.1016/0021-8502(87)90011-5), 1987.
- Behnke, W., Holländer, W., Koch, W., Nolting, F. and Zetzsch, C.: A smog chamber for studies of the photochemical degradation of chemicals in the presence of aerosols, *Atmos. Environ.*, 22, 1113-1120, [https://doi.org/10.1016/0004-6981\(88\)90341-1](https://doi.org/10.1016/0004-6981(88)90341-1), 1988.
- Canosa-Mas, C. E., Hutton-Squire, H. R., King, M. D., Stewart, D. J., Thompson, K. C. and Wayne, R. P.: Laboratory kinetic studies of the reactions of Cl atoms with species of biogenic origin:  $\Delta$ -3-carene, isoprene, methacrolein and methyl vinyl ketone, *J. Atmos. Chem.*, 34, 1, 163-170, <https://doi.org/10.1023/A:1006214423298>, 1999.
- Coeur, C., Jacob, V., Foster, P. and Baussand, P.: Rate constant for the gas-phase reaction of hydroxyl radical with the natural hydrocarbon bornyl acetate, *Int. J. Chem. Kinet.*, 30, 497-502, [https://doi.org/10.1002/\(SICI\)1097-4601\(1998\)30:7<497::AID-KIN6>3.0.CO;2-N](https://doi.org/10.1002/(SICI)1097-4601(1998)30:7<497::AID-KIN6>3.0.CO;2-N), 1998.
- Coeur, C., Jacob, V. and Foster, P.: Gas-phase reaction of hydroxyl radical with the natural hydrocarbon bornyl acetate, *Phys. Chem. Earth (C)*, 24, 537-539, [https://doi.org/10.1016/S1464-1917\(99\)00087-2](https://doi.org/10.1016/S1464-1917(99)00087-2), 1999.
- Cox, R. A., Derwent, R. G. and Williams, M. R.: Atmospheric photooxidation reactions, reactivity, and mechanism for reaction of organic compounds with hydroxyl radicals, *Environ. Sci. Technol.*, 14, 57-61, <https://doi.org/10.1021/es60161a007>, 1980.

- Darnall, K. R., Winer, A. M., Lloyd, A. C. and Pitts Jr., J. N.: Relative rate constants for the reaction of OH radicals with selected C<sub>6</sub> and C<sub>7</sub> alkanes and alkenes at 305 ± 2 K, *Chem. Phys. Lett.*, 44, 415-418, [https://doi.org/10.1016/0009-2614\(76\)80685-1](https://doi.org/10.1016/0009-2614(76)80685-1), 1976.
- Donahue, N. M., Anderson, J. G. and Demerjian, K. L.: New rate constants for ten OH alkane reactions from 300 to 400 K: an assessment of accuracy, *J. Phys. Chem. A*, 102, 3121-3126, <https://doi.org/10.1021/jp980532q>, 1998.
- Donohoue, D. L., Bauer, D. and Hynes, A. J.: Temperature and pressure dependent rate coefficients for the reaction of Hg with Cl and the reaction of Cl with Cl: a pulsed laser photolysis-pulsed laser induced fluorescence study, *J. Phys. Chem. A*, 109, 7732-7741, <https://doi.org/10.1021/jp051354l>, 2005.
- Fantechi, G., Jensen, N. R., Saasted, O., Hjorth, J. and Peeters, J.: Reactions of Cl atoms with selected VOCs: Kinetics, products and mechanisms, *J. Atmos. Chem.*, 31, 3, 247-267, <https://doi.org/10.1023/A:1006033910014>, 1998.
- Ferrari, C., Roche, A., Jacob, V., Foster, P. and Baussand, P.: Kinetics of the reactions of OH radicals with a series of esters under simulated conditions at 295 K, *Int. J. Chem. Kinet.*, 28, 609-614, [https://doi.org/10.1002/\(SICI\)1097-4601\(1996\)28:8<609::AID-KIN6>3.0.CO;2-Z](https://doi.org/10.1002/(SICI)1097-4601(1996)28:8<609::AID-KIN6>3.0.CO;2-Z), 1996.
- Finlayson-Pitts, B. J., Keoshian, C. J., Buehler, B. and Ezell, A. A.: Kinetics of reaction of chlorine atoms with some biogenic organics, *Int. J. Chem. Kinet.*, 31, 491-499, [https://doi.org/10.1002/\(SICI\)1097-4601\(1999\)31:7<491::AID-KIN4>3.0.CO;2-E](https://doi.org/10.1002/(SICI)1097-4601(1999)31:7<491::AID-KIN4>3.0.CO;2-E), 1999.
- Greiner, N. R.: Hydroxyl radical kinetics by kinetic spectroscopy VI. Reactions with alkanes in the range 300-500 K, *J. Chem. Phys.*, 53, 1070-1076, <https://doi.org/10.1063/1.1674099>, 1970.
- Harris, S. J. and Kerr, J. A.: Relative rate measurements of some reactions of hydroxyl radicals with alkanes studied under atmospheric conditions, *Int. J. Chem. Kinet.*, 20, 939-955, <https://doi.org/10.1002/kin.550201203>, 1988.
- Hooshiyar, P. A. and Niki, H.: Rate constants for the gas-phase reactions of Cl-atoms with C<sub>2</sub>-C<sub>8</sub> alkanes at T = 296 ± 2 K, *Int. J. Chem. Kinet.*, 27, 1197-1206, <https://doi.org/10.1002/kin.550271206>, 1995.

Ianni, J. C.: Kintecus, Windows Version 5.20, 2017, [www.kintecus.com](http://www.kintecus.com)

Jolly, G. S., Paraskevopoulos, G. and Singleton, D. L.: Rates of OH radical reactions, XII. The reactions of OH with *c*-C<sub>3</sub>H<sub>6</sub>, *c*-C<sub>5</sub>H<sub>10</sub>, and *c*-C<sub>7</sub>H<sub>14</sub>. Correlation of hydroxyl rate constants with bond dissociation energies, *Int. J. Chem. Kinet.*, 17, 1-10, <https://doi.org/10.1002/kin.550170102>, 1985.

Koffend, J. B. and Cohen, N.: Shock tube study of OH reactions with linear hydrocarbons near 1100 K, *Int. J. Chem. Kinet.*, 28, 79-87, [https://doi.org/10.1002/\(SICI\)1097-4601\(1996\)28:2<79::AID-KIN2>3.0.CO;2-I](https://doi.org/10.1002/(SICI)1097-4601(1996)28:2<79::AID-KIN2>3.0.CO;2-I), 1996.

Kramp, F. and Paulson, S. E.: On the uncertainties in the rate coefficients for OH reactions with hydrocarbons, and the rate coefficients of the 1,3,5-trimethylbenzene and *m*-xylene reactions with OH radicals in the gas phase, *J. Phys. Chem. A*, 102, 2685-2690, <https://doi.org/10.1021/jp973289o>, 1998.

Krol M., van Leeuwen, P. J. and Lelieveld, J.: Global OH trend inferred from methylchloroform measurements, *J. Geophys. Res.*, 103, 10697-10711, <https://doi.org/10.1029/98JD00459>, 1998.

Lewis, R. S., Sander, S. P., Wagner, S. and Watson, R. T.: Temperature-dependent rate constants for the reaction of ground-state chlorine with simple alkanes, *J. Phys. Chem.*, 84, 2009-2015, <https://doi.org/10.1021/j100453a004>, 1980.

Lin, C. L., Leu, M. T. and DeMore, W. B.: Rate constant for the reaction of atomic chlorine with methane, *J. Phys. Chem.*, 82, 16, 1772-1777, <https://doi.org/10.1021/j100505a002>, 1978.

Lloyd, A. C., Darnall, K. R., Winer, A. M. and Pitts Jr., J. N.: Relative rate constants for reaction of the hydroxyl radical with a series of alkanes, alkenes, and aromatic hydrocarbons, *J. Phys. Chem.*, 80, 789-794, <https://doi.org/10.1021/j100549a003>, 1976.

Manning, R. G. and Kurylo, M. J.: Flash photolysis resonance fluorescence investigation of the temperature dependencies of the reactions of Cl(<sup>2</sup>P) atoms with CH<sub>4</sub>, CH<sub>3</sub>Cl, CH<sub>3</sub>F, and C<sub>2</sub>H<sub>6</sub>, *J. Phys. Chem.*, 81, 4, 291-296, <https://doi.org/10.1021/j100519a003>, 1977.

Nolting, F., Behnke, W. and Zetzsch, C.: A smog chamber for studies of the reactions of terpenes and alkanes with ozone and OH, *J. Atmos. Chem.*, 6, 47-59, <https://doi.org/10.1007/BF00048331>, 1988.

- Osthoff, H. D., Roberts, J. M., Ravishankara, A. R., Williams, E. J., Lerner, B. M., Sommariva, R., Bates, T. S., Coffman, D., Quinn, P. K., Dibb, J. E., Stark, H., Burkholder, J. B., Talukdar, R. K., Meagher, J., Fehsenfeld, F. and Brown, S. S.: High levels of nitryl chloride in the polluted subtropical marine boundary layer, *Nat. Geosci.*, **1**, 324-328, <https://doi.org/10.1038/ngeo177>, 2008.
- Pritchard, H. O., Pyke, J. B. and Trotman-Dickenson, A. F.: The study of chlorine atom reactions in the gas phase, *J. Am. Chem. Soc.*, **77**, 2629-2633, <https://doi.org/10.1021/ja01614a088>, 1955.
- Rodríguez, D., Rodríguez, A., Notario, A., Aranda, A., Díaz-de-Mera, Y. and Martínez, E.: Kinetic study of the gas-phase reaction of atomic chlorine with a series of aldehydes, *Atmos. Chem. Phys.*, **5**, 3433-3440, <https://doi.org/10.5194/acp-5-3433-2005>, 2005.
- Ryzhkov, A., Ariya, P. A., Raofie, F., Niki, H. and Harris, G. W.: Chapter 13 – Theoretical and experimental studies of the gas-phase Cl-atom initiated reactions of benzene and toluene, *Adv. Quantum Chem.*, **55**, 275-295, [https://doi.org/10.1016/S0065-3276\(07\)00213-4](https://doi.org/10.1016/S0065-3276(07)00213-4), 2008.
- Shaw, J.T., Lidster, R. T., Cryer, D. R., Ramirez, N., Whiting, F. C., Boustead, G. A., Whalley, L. K., Ingham, T., Rickard, A. R., Dunmore, R. E., Heard, D. E., Lewis, A. C., Carpenter, L. J., Hamilton, J. F. and Dillon, T. J.: A self-consistent, multivariate method for the determination of gas-phase rate coefficients applied to reactions of atmospheric VOCs and the hydroxyl radical, *Atmos. Chem. Phys.*, **18**, 4039-4054, <https://doi.org/10.5194/acp-18-4039-2018>, 2018.
- Shi, J. and Bernhard, M. J.: Kinetic studies of Cl-atom reactions with selected aromatic compounds using the photochemical reactor-FTIR spectroscopy technique, *Int. J. Chem. Kinet.*, **29**, 349-358, [https://doi.org/10.1002/\(SICI\)1097-4601\(1997\)29:5<349::AID-KIN5>3.0.CO;2-U](https://doi.org/10.1002/(SICI)1097-4601(1997)29:5<349::AID-KIN5>3.0.CO;2-U), 1997.
- Thornton, J. A., Kercher, J. P., Riedel, T. P., Wagner, N. L., Cozic, J., Holloway, J. S., Dubé, W. P., Wolfe, G. M., Quinn, P. K., Middlebrook, A. M., Alexander, B. and Brown, S. S.: A large atomic chlorine source inferred from mid-continental reactive nitrogen chemistry, *Nature*, **464**, 271-274, <https://doi.org/10.1038/nature08905>, 2010.

- Timerghazin, Q. K. and Ariya, P. A.: Kinetics of the gas-phase reaction of atomic chlorine with selected monoterpenes, *Phys. Chem. Chem. Phys.*, 3, 3981-3986, <https://doi.org/10.1039/B101380G>, 2001.
- Tyndall, G. S., Orlando, J. J., Wallington, T. J., Dill, M. and Kaiser, E. W.: Kinetics and mechanisms of the reactions of chlorine atoms with ethane, propane, and *n*-butane, *Int. J. Chem. Kinet.*, 29, 43-55, [https://doi.org/10.1002/\(SICI\)1097-4601\(1997\)29:1::AID-KIN6<3.0.CO;2-L](https://doi.org/10.1002/(SICI)1097-4601(1997)29:1::AID-KIN6<3.0.CO;2-L), 1997.
- Qian, H.-B., Turton, D., Seakins, P. W., Pilling, M. J.: A laser flash photolysis/IR diode laser absorption study of the reaction of chlorine atoms with selected alkanes, *Int. J. Chem. Kinet.*, 34, 86-94, <https://doi.org/10.1002/kin.10025>, 2002.

# Concluding remarks

The multivariate relative rate technique has been used to assess existing, and determine novel, rate coefficients for multiple gas-phase reactions between atmospheric VOCs and radicals. Throughout this body of work, various synthetic mixtures containing a large array of different VOCs and different organic functionalities were evaluated using this method. In most cases, the derived results were in excellent agreement with the evaluated literature rate coefficients used as references. Novel rate coefficients for the reactions of eight VOCs with OH, and for the reaction of a single compound with Cl, were derived using a suite of the kinetic literature as a reference. Table 6.1 provides a summary of the measured results for all VOC + OH reactions explored in this work, allowing for an inter-comparison of values for the same reactions that were tested across different synthetic gas mixtures.

The technique was used across a wide variety of conditions. Deviations from the expected linear relationship between depletion factor and  $k$  value were observed for low reactivity mixtures containing fast reacting compounds. This experimental artefact was examined and accounted for using both mathematical theory and numerical simulations. Low reactivity mixtures containing compounds which react relatively slowly with OH were also observed to yield small depletions in VOC concentrations due to a competitive OH sink to HO<sub>2</sub>. The HO<sub>2</sub> problem was alleviated via the addition of NO, which was shown to improve the observed depletion factors for low reactivity samples containing these slow reacting compounds. The multivariate technique was also tested across a range of temperatures, and, whilst the results weren't always ideal, the temperature dependence of several alkane + OH reactions was measured for the first time. The large

uncertainty placed upon many of the newly derived Arrhenius parameters suggested that the multivariate technique is not suitable for the measurement of temperature dependent rate coefficients, particularly when many compounds do not have suitable reference values at elevated temperatures.

The technique described and evaluated in this work holds a huge potential for future measurements of gas-phase rate coefficients. This technique succeeds where the traditional relative rate technique fails; in the throughput of target reactions. The rate at which new rate coefficient results can be obtained and evaluated using this technique is its major advantage, especially when faced with the vast number of reactive species that have been observed to exist in the atmosphere. Whilst structure-activity relationships provide useful estimations of rate coefficient values, this technique is capable of rapidly generating experimental results for homologous series of compounds. This would be incredibly useful for SAR validation, development and improvement.

Future work using this technique could take a number of directions. Perhaps, most simply, it could be used to examine the kinetics of mixtures containing similar species to those measured here; for example, more diverse and branched alkanes and alkenes, different monoterpenes, or larger and more complicated alkyl substituted aromatic compounds. However, atmospheric VOCs are not limited to this range of compounds; a vast array of different functionalities have been detected in the atmosphere. This technique could therefore also be applied to the measurements of rate coefficients for reactions of oxygenated VOCs, of which there are many types, both aliphatic and aromatic. Measuring compounds with yet more functionalities may also be possible, for example, compounds that contain nitrogen or chlorine or bromine. The technique is also unlikely to be limited to using GC-MS as the method of detection. Using a different method of detection, such as PTR-MS or SIFT-MS, could be particularly useful for those compounds which are poorly resolved using traditional GC-MS techniques.

Beyond this, the multivariate relative rate technique could be used for reactions with other radicals and atmospheric oxidants. This work has already shown that it can be applied to reactions involving Cl, although those experiments were limited in scope. Utilising the NO<sub>3</sub> radical is also a big possibility. Kinetics for both Cl and NO<sub>3</sub> have been less extensively measured than those for OH. This is both advantageous, in that many results would be novel, but problematic, in that a smaller suite of suitable reference reactions exist.

**Table 6.1** Summary of all measured rate coefficients for VOC + OH reactions from all mixtures.

Name	Measured $k$ (297 ( $\pm$ 2) K) / $10^{-12}$ cm <sup>3</sup> molecule <sup>-1</sup> s <sup>-1</sup>						Evaluated literature
	Monoterpenes mixture 1	Monoterpenes mixture 2	Alkenes mixture	Aromatics mixture 1	Aromatics mixture 2	Alkanes mixture	
$\alpha$ -terpinene		348 $\pm$ 22					350 ( $^{+71}_{-59}$ )
$\alpha$ -phellandrene		269 $\pm$ 21					320 ( $^{+65}_{-54}$ )
$\beta$ -ocimene	223 $\pm$ 10						245 $\pm$ 49
terpinolene		198 $\pm$ 23					220 ( $^{+91}_{-64}$ )
myrcene	204 $\pm$ 8						209 $\pm$ 42
$\beta$ -phellandrene		270 $\pm$ 30					170 ( $^{+70}_{-50}$ )
$\gamma$ -terpinene	207 $\pm$ 6	221 $\pm$ 19					170 ( $^{+44}_{-35}$ )
limonene	152 $\pm$ 4	176 $\pm$ 19					170 $\pm$ 51
isoprene	104 $\pm$ 6	119 $\pm$ 36	103 $\pm$ 5		102 $\pm$ 4		100 ( $^{+15}_{-13}$ )
3-carene	97 $\pm$ 4						85 $\pm$ 17
$\beta$ -pinene	78 $\pm$ 11	59 $\pm$ 9	75 $\pm$ 12		74 $\pm$ 8		79 $\pm$ 20
cycloheptene			74 $\pm$ 10				74 $\pm$ 10
cyclohexene			71 $\pm$ 4				68 $\pm$ 17
cyclopentene			69 $\pm$ 9				67 $\pm$ 23
1,2,3,5-tetramethylbenzene					62 $\pm$ 9		62.4 $\pm$ 0.8
1,3,5-trimethylbenzene					60 $\pm$ 5		57 $\pm$ 11

Name	Measured $k$ (297 ( $\pm$ 2) K) / $10^{-12}$ cm <sup>3</sup> molecule <sup>-1</sup> s <sup>-1</sup>						Evaluated literature
	Monoterpenes mixture 1	Monoterpenes mixture 2	Alkenes mixture	Aromatics mixture 1	Aromatics mixture 2	Alkanes mixture	
1,2,4,5-tetramethylbenzene					59 $\pm$ 12		55.5 $\pm$ 3.4
$\alpha$ -pinene	56 $\pm$ 6	50 $\pm$ 3	53 $\pm$ 4		53 $\pm$ 8		53 ( <sup>22</sup> / <sub>15</sub> )
camphene		61 $\pm$ 5					53 $\pm$ 11
1-nonene			41 $\pm$ 3				43.2 $\pm$ 0.5
1-octene			44 $\pm$ 5				41.4 $\pm$ 0.8
1-heptene			36 $\pm$ 4				40 $\pm$ 12
1-hexene			46 $\pm$ 12				37 $\pm$ 11
1,2,3-trimethylbenzene					38 $\pm$ 4		33 $\pm$ 8
1,2,4-trimethylbenzene		39 $\pm$ 6			34 $\pm$ 3		33 $\pm$ 8
<i>m</i> -xylene	22 $\pm$ 6	23 $\pm$ 4		20 $\pm$ 1.3	21 $\pm$ 3		23 $\pm$ 4
3-ethyltoluene				19 $\pm$ 1.0			19 $\pm$ 7
cyclooctane						13.7 $\pm$ 0.3	13 $\pm$ 7
<i>o</i> -xylene	5 $\pm$ 7			12 $\pm$ 0.6	10 $\pm$ 4		13 $\pm$ 3
2-ethyltoluene				13 $\pm$ 0.06			12 $\pm$ 4
4-ethyltoluene				14 $\pm$ 1.2			12 $\pm$ 4
cycloheptane						11.4 $\pm$ 0.3	12 $\pm$ 3
<i>n</i> -undecane						12.3 $\pm$ 0.3	12 $\pm$ 2
<i>n</i> -decane						10.3 $\pm$ 0.3	11 $\pm$ 2
<i>n</i> -nonane						11.0 $\pm$ 0.3	10 $\pm$ 2

Name	Measured $k$ (297 ( $\pm$ 2) K) / $10^{-12}$ cm <sup>3</sup> molecule <sup>-1</sup> s <sup>-1</sup>						Evaluated literature
	Monoterpenes mixture 1	Monoterpenes mixture 2	Alkenes mixture	Aromatics mixture 1	Aromatics mixture 2	Alkanes mixture	
<i>n</i> -octane						8.8 $\pm$ 0.3	8 $\pm$ 2
ethylbenzene				6.7 $\pm$ 0.5			7.0 $\pm$ 2
isopropylbenzene				6.5 $\pm$ 0.6			6.3 $\pm$ 2
<i>n</i> -propylbenzene				7.4 $\pm$ 1.5			5.8 $\pm$ 1.5
toluene				7.3 $\pm$ 2			5.6 ( <sup>+1.5</sup> / <sub>-1.2</sub> )
2-methylpentane						4.6 $\pm$ 0.3	5.2 $\pm$ 1.3
3-methylpentane						5.3 $\pm$ 0.3	5.2 $\pm$ 1.3
<i>t</i> -butylbenzene				3.1 $\pm$ 0.7			4.5 $\pm$ 2
2,2,3-trimethylbutane						3.9 $\pm$ 0.3	3.8 $\pm$ 1.0
1,2-diethylbenzene					< 30		
1,3-diethylbenzene					< 30		
1,4-diethylbenzene					< 30		
2-methylheptane						9.1 $\pm$ 0.3	
2-methynonane						11.0 $\pm$ 0.3	
2,3-dimethylpent-1-ene			57 $\pm$ 3				
ethylcyclohexane						14.4 $\pm$ 0.3	
<i>n</i> -pentylbenzene				1.2 $\pm$ 4			



# Abbreviations

<b>CI</b>	Chemical ionisation
<b>CIA</b>	Canister interface accessory
<b>CFC</b>	Chlorofluorocarbon
<b>DCM</b>	Dichloromethane
<b>DRS</b>	Diffuse reflectance spectroscopy
<b>EI</b>	Electron ionisation
<b>EIC</b>	Extracted ion chromatogram
<b>FID</b>	Flame ionisation detector
<b>FTIR</b>	Fourier-transform infrared (spectroscopy)
<b>GC</b>	Gas chromatography
<b>HCFC</b>	Hydrochlorofluorocarbon
<b>ID</b>	Internal diameter
<b>IUPAC</b>	International Union of Pure and Applied Chemistry
<b>IVOC</b>	Intermediate volatility organic compound(s)
<b>LIF</b>	Laser-induced fluorescence
<b>MALDI</b>	Matrix assisted laser desorption ionisation
<b>MCM</b>	Master chemical mechanism
<b>MFC</b>	Mass flow controller
<b>MS</b>	Mass spectrometry
<b>MVK</b>	Methyl vinyl ketone
<b>NMHC</b>	Non-methane hydrocarbon
<b>OH</b>	Hydroxyl radical
<b><i>OH<sub>exp</sub></i></b>	OH exposure
<b>PID</b>	Proportional-integral-derivative
<b>PM</b>	Particulate matter
<b>POCP</b>	Photochemical ozone creation potential
<b>PTR-MS</b>	Proton-transfer reaction mass spectrometry
<b>SAR</b>	Structure-activity relationship
<b>sccm</b>	Standard cubic centimetre(s) per minute (cm <sup>3</sup> min <sup>-1</sup> )

## Abbreviations

<b>SIFT-MS</b>	Selected ion flow tube mass spectrometry
<b>slm</b>	Standard litre(s) per minute
<b>SOA</b>	Secondary organic aerosol
<b>STEL</b>	Short-term exposure limit
<b>STP</b>	Standard temperature and pressure
<b>TIC</b>	Total ion chromatogram
<b>ToF-MS</b>	Time-of-flight mass spectrometry
<b>TDU</b>	Thermal desorption unit
<b>VOC</b>	Volatile organic compound
<b>VUV</b>	Vacuum ultraviolet